THE ROLE OF THE PROLINE RICH HOMEODOMAIN TRANSCRIPTION FACTOR (PRH/HHex) IN CHOLANGIOCARCINOMA

By

KA YING LEE

A thesis submitted to University of Birmingham for the degree of DOCTOR OF PHILOSOPHY

Institute of Immunology and Immunotherapy
College of Medicinal and Dental Sciences
The University of Birmingham
October, 2020

UNIVERSITY OF BIRMINGHAM

University of Birmingham Research Archive

e-theses repository

This unpublished thesis/dissertation is copyright of the author and/or third parties. The intellectual property rights of the author or third parties in respect of this work are as defined by The Copyright Designs and Patents Act 1988 or as modified by any successor legislation.

Any use made of information contained in this thesis/dissertation must be in accordance with that legislation and must be properly acknowledged. Further distribution or reproduction in any format is prohibited without the permission of the copyright holder.

Abstract

Cholangiocarcinoma (CCA) is cancer of the bile duct that only has a few treatment options, typically with poor prognostic outcomes. The Proline-Rich Homeodomain protein (PRH), also known as haematopoietically expressed homeobox (Hhex), is a transcription factor that regulates liver and bile duct development. PRH is not expressed in normal bile duct cells but this protein is highly expressed in CCA cells. Using a combination of overexpression and knockdown experiments, PRH was shown to increase cell proliferation, migration and invasion in tumour cell lines. Similar results were obtained in immortalized AKN-1 cells and also in primary biliary epithelial cells. In these cells PRH overexpression also led to the initiation of epithelial to mesenchymal transition (EMT) and anoikis resistance as well as increased cell proliferation and invasion. Gene Ontology and Gene Set Enrichment Analysis of RNA-sequencing data from cells with altered PRH levels reveal that in all cell types PRH regulates multiple signaling pathways and that key genes involved in the Notch signaling pathway, the cell cycle and EMT are regulated by PRH.

CCA cells with elevated PRH expression were found to be more sensitive to the CDK4/6 inhibitor Palbociclib as PRH controls the cell cycle through regulation of multiple cell cycle genes including *CCND2*. Drug screening with a drug repurposing library was performed to identify novel drug treatments for CCA and several repurposed drugs that show a stronger cytotoxic effect when combined with Palbociclib were identified using cell viability assays. This thesis therefore reveals that PRH protein is an important oncoprotein in CCA and that this protein may play a role in initiating CCA and in driving cancer progression and identifies new drug treatment options.

Acknowledgement

First, I would like to thank my parents who set me off on the road to this PhD and always encouraged me to aim high and try my hardest. Without their financial support, I would not have completed this PhD. Second, I would like to express sincere gratitude to Dr. Padma Sheela Jayaraman for her guidance throughout the PhD and writing this thesis. I appreciate her contribution of time and patience. Next, I would like to thank Dr. Philip Kitchen for his supervision of my lab techniques when I started out in the lab. His patience, motivation, and immense knowledge was instrumental to my studies and it would be tremendously difficult for me to imagine a better mentor than he was. Following that, I would also like to thank Dr. Simon Afford and Ms. Laine Wallace on giving me the chance to access primary samples and assisting me with the isolation of primary cells. I would also like to thank the former members in Jayaraman lab who worked with me and colleagues I encountered in the IBR building. I would also like to thank Dr. Farhat Kanim for her kind donation of the repurposing drug library.

My time in Birmingham was enjoyable largely due to my friends and boyfriend and so finally, I would also like to thank them for their support and encouragement.

Table of Contents

ABSTRACT **1**

ACKNOWLEDGEMENT **2**

LIST OF FIGURES **7**

2. INTRODUCTION **14**

1.1 Transcriptional regulation **15**

1.2 PRH protein **19**
1.2.1 PRH/HHex protein 19
1.2.2 PRH structure and function 20
1.2.3 Regulation of PRH expression 22
1.2.4 PRH in endothelial cells 23
1.2.5 Phosphorylated PRH 24
1.2.6 PRH and cancer 24
1.2.7 PRH as a tumour suppressor gene 25
1.2.8 PRH as an oncogene 27

1.3 Cell Signaling pathways **28**
1.3.1 Growth factor signaling 29
1.3.2 PI3K/Akt/mTOR pathway 29
1.3.3 Wnt signaling 30
1.3.4 Notch signaling 32
1.3.5 TGFβ signaling 34

1.4 Cancer hallmarks **35**
1.4.1 Cell cycle and proliferation 36
1.4.2 Signaling pathways regulating cell proliferation 38
1.4.3 Apoptosis 39
1.4.4 Metastasis and epithelial-mesenthymal transition (EMT) 41
1.4.5 Metastasis and anoikis resistance 43
1.4.6 Immune evasion 44

1.5 Liver and bile duct development **45**
1.5.1 Initiation of liver development 45
1.5.2 Formation of liver bud 46
1.5.3 Liver expansion 47
1.5.4 Segregation of hepatobiliary lineage and bile duct formation 48
1.5.5 Bile acid synthesis and regulation 50

1.6 Liver cancers **51**
1.6.1 HCC 51
1.6.2 Cholangiocarcinoma 52
1.6.3 Risk factors for Cholangiocarcinoma 53
1.6.4 Treatment for CCA 55
1.6.5 CCA cells origin 56
1.6.6 Genomic heterogeneity and molecular pathogenesis in CCA 56

1.6.7 Notch and CCA development....58
1.6.8 Wnt signaling and CCA development....60
1.6.9 EMT and CCA....61

1.7 Cell lines used in this research....62

1.8 Aim of the research....65

3. MATERIALS AND METHODS....67

2.1 Cell Culture Protocols....67
2.1.1 Adherent Cell Culture....67
2.1.2 Cryopreservation of cells....68
2.1.3 Thawing cells....68
2.1.4 Mycoplasma Test....68
2.1.5 Primary biliary epithelial cells (BECs) isolation....69
2.1.6 Transient transfection of plasmid DNA....71
2.1.7 Generation of stable cell line....73
2.1.8 Adenoviral infection of cells....74
2.1.9 Agarose Gel Electrophoresis....75
2.1.10 Plasmid transformation into *E.Coli*....75
2.1.11 Plasmid Maxi Preparation....76
2.1.12 Plasmid Maps....77

2.2 Western blotting....84
2.2.1 Extraction of whole cell protein....84
2.2.2 Determining protein concentration....84
2.2.3 Protein separation....85
2.2.4 Transfer of protein....86
2.2.5 Protein detection by antibodies....86
2.2.6 Densitometry analysis....87

2.3 Biochemical fractionation....88
2.3.1 Nuclear and Cytoplasmic fractionation and protein extraction....88
2.3.2 Immunoprecipitation....89

2.4 Quantitative PCR....90
2.4.1 RNA extraction....90
2.4.2 Complementary DNA production....91
2.4.3 Quantitative PCR....92
2.4.4 RNA sequencing and bioinformatics....95

2.6 Chromatin Immunoprecipitation (ChIP)....97
2.6.1 Cross-linking....97
2.6.2 Optimization of sonication....97
2.6.3 ChIP-sequencing....102

2.7 Proliferation and apoptosis assay....104
2.7.1 Proliferation assay....104
2.7.2 Apoptosis assay....105
2.7.3 Flow cytometry....107

2.8 Colony formation assay....107

2.9 Migration and invasion assay **108**
2.9.1 Migration assay 108
2.9.2 Invasion assay 110

2.10 Cumulative growth curves **111**

2.11 MTT cell viability assay **111**

2.12 Statistical Analysis **112**

4. INVESTIGATING THE ROLE OF PRH IN CHOLANGIOCARCINOMA CELLS **115**

3.1 PRH expression is upregulated in CCA **115**

3.2 PRH KD in CCA inhibit cumulative cell growth **122**

3.3 PRH KD inhibits cell proliferation **124**

3.4 PRH knockdown changes cell morphology and inhibits cell migration and invasion **130**

3.5 PRH KD cells decreases colony formation and reduces tumour size and numbers in vivo **133**

3.6 RNA sequencing and Gene Set Enrichment Analysis to identify differential gene expression and altered pathways in PRH KD cells **135**

3.7 PRH overexpression increases cumulative cell number **145**

3.8 PRH overexpression increases cell proliferation **148**

3.9 PRH overexpression increases migration, invasion **152**

3.10 Identify differential gene expression by PRH overexpression by RNA-sequencing **153**

5. THE MECHANISM OF PRH REGULATING CELL CYCLE AND EMT GENES IN CCA TUMOUR CELL LINES **165**

4.1 The expression of Notch3, Cyclin D2, and E-cadherin in multiple CCA cell lines **165**

4.2 PRH forms positive feedback loop with Notch3 ..... **167**

4.3 PRH regulates proliferation, EMT and Cyclin D2 via Notch 3 ..... **169**

4.4 PRH regulation of endogenous Vimentin expression is influenced by cell confluency **172**

4.5 PRH directly regulate CDKN1B, CDKN2B and Vimentin through DNA binding **177**

4.6 Vimentin and PRH both promote proliferation **187**

4.7 PRH regulates Vimentin through protein-protein interaction **196**

6. INVESTIGATING THE ROLE OF PRH IN AKN-1 AND PRIMARY BECS **209**

5.1 PRH overexpression drives proliferation in AKN-1 and primary BECs **209**

5.2 PRH overexpression increases migration, invasion and colony formation in AKN-1 213

5.3 Identify differential gene expression in AKN-1 when PRH is overexpressed by RNA sequencing..216

5.4 PRH overexpression increases migration, invasion and colony formation in primary BECs 221

5.5 PRH overexpression increases migration, invasion and colony formation in primary BECs 224

5.6 Identify differential gene expression in primary BECs when PRH is overexpressed by RNA sequencing.....226

5.7 Investigation of the differentially regulated genes and pathways in primary BECs donors.....233

7. NOVEL DRUG TREATMENT FOR CCA 242

6.1 PRH overexpression increases sensitivity to Palbociclib 242

6.2 Drug repurposing screen to determine novel drug treatment for CCA 253

6.3 Drug combination 269

8. DISCUSSION 279

7.1 PRH is an oncoprotein in CCA 279

7.2 PRH increases tumour cell number and anoikis resistance in CCA 281

7.3 PRH regulates cell proliferation through Notch signaling 284
7.3.1 PRH regulates cell cycle genes independently and together with Notch3 286
7.3.2 PRH does not alter basal apoptosis in CCLP cells.....290
7.3.3 PRH regulates migration, invasion and EMT in CCA 291

7.4 PRH regulates EMT pathway 292
7.4.1 PRH regulates epithelial cell marker, E-cadherin.....292
7.4.2 PRH regulates EMT-related junction proteins 295
7.4.3 PRH regulates EMT-related Transcription Factors.....296
7.4.4 PRH regulates mesenchymal marker, Vimentin 297
7.4.5 PRH directly binds and interact with Vimentin.....298

7.5 Novel therapeutic agents for CCA 303
7.5.1 PRH increases CCLP cells sensitivity towards Palbociclib.....303
7.5.2 Drug screening 305
7.5.3 Drug combination experiments 308

7.6 Conclusion 310

9. REFERENCES..... 311

10. APPENDICES (SUPPLEMENTARY FIGURES) 333

List of Figures

Figure 1.1 Gene expression regulated by epigenetics 18
Figure 1.2 The structure of PRH protein. 19
Figure 1.3 Summary of PRH regulation of gene expression. 28
Figure 1.4 Cell signaling pathways including growth factor signaling, Wnt and TGFβ signaling. 32
Figure 1.5 The Notch signaling pathway. Ligand binding promotes two proteolytic cleavage events in the Notch receptor. 34
Figure 1.6 The cell cycle. 38
Figure 1.7 The anatomy of the liver and bile duct. 53
Figure 2.1 Diagram of PMUG1 Myc-PRH plasmid 77
Figure 2.2 Diagram of pMUG1 Myc-PRH 7-198 (NHD, with C-terminus deletion) 78
Figure 2.3 Diagram of pMUG1 Myc-PRH 136-270 (HDC, N-terminus deletion) 79
Figure 2.4 Diagram of pMUG1 Myc-PRH 50-270 80
Figure 2.5 Diagram of pEGFP-PRHMyc and pEGFP-PRH 81
Figure 2.6 Diagram of Hhex shRNA and scrambled control 82
Figure 2.7 Diagram of Adenoviral vector pDC515 83
Figure 2.8 Image of gel for optimization of sonication 98
Figure 2.9 Work-flow of ChIP. 102
Figure 2.10 Standard curve for Caspase-3 assay. 106
Figure 2.11 Diagram of migration assay 109
Figure 2.12 Standard curve of MTT signal against cell numbers. 112
Figure 3.1 Public TCGA data on *PRH/HHEX* mRNA expression and *PRH/HHEX* mutation profile. 118
Figure 3.2 GEPIA data of PRH expression. 119
Figure 3.3 Characterizing PRH expression in a range of CCA cell lines, immortalised cholangiocytes and primary BECs. 121
Figure 3.4 PRH KD inhibits cumulative cell number in CCLP. 124
Figure 3.5 PRH depletion decreases cell proliferation in CCLP. 126
Figure 3.6 PRH depletion does not change apoptotic activity in CCLP. 129
Figure 3.7 PRH KD leads to MET. 131
Figure 3.8 PRH KD inhibits cell migration and invasion. 132
Figure 3.9 PRH depletion inhibits colony formation in soft agar. 134
Figure 3.10 RNA-seq on PRH depleted and control CCLP cells. 136
Figure 3.11 The effect of PRH KD on cell cycle and EMT genes. 139
Figure 3.12 Gene ontology analysis on RNA seq data. 141
Figure 3.13 GSEA of PRH KD CCLP cells with the hallmark gene sets. 144
Figure 3.14 PRH expression in AdPRH and AdEmpty infected CCLP cells. 146
Figure 3.15 PRH overexpression increases cumulative cell number in CCSW. 147
Figure 3.16 PRH overexpression increases cell proliferation in CCLP and CCSW. 149
Figure 3.17 Exogenous PRH has no effect on apoptosis in CCLP cells. 151
Figure 3.18 PRH overexpression increases cell migration and invasion in CCLP and CCSW cells. 153
Figure 3.19 RNA-seq of PRH OE and control CCLP cells. 154

Figure 3.20 PRH overexpression effects on genes associated with proliferation in CCLP cells. 155
Figure 3.21 Gene ontology analysis of the PRH OE DEGs. 157
Figure 3.22 GSEA of PRH OE CCLP cells with the hallmark gene sets. 157
Figure 3.23 Expression of EMT related genes in PRH OE and control cells. 160
Figure 3.24 Identifying differential gene expression by PRH KD and OE by RNA-seq. 163
Figure 4.1 Endogenous PRH protein and potential PRH target proteins in CCA cell lines and primary cells. 166
Figure 4.2 PRH OE upregulates Notch3 and Cyclin D2 expression in CCSW. 167
Figure 4.3 Notch3 KD decreases cell proliferation and leads to MET in CCLP cells. 169
Figure 4.4 PRH regulates EMT and Cyclin D2 via Notch3. 172
Figure 4.5 Vimentin expression is dependent on cell confluency. 174
Figure 4.6 PRH expression is affected by cell confluency. 176
Figure 4.7 PRH regulates *CDKN1B* and *CDKN2B* through DNA binding. 181
Figure 4.8 CCLP ChIP-Seq GSEA. 182
Figure 4.9 ChIP-seq track from UCSC software on other PRH target genes. 186
Figure 4.10 Vimentin KD decreases cell proliferation and changes cell morphology in CCLP cells. 189
Figure 4.11 Vimentin KD regulates cell cycle genes in CCLP cells. 190
Figure 4.12 The effects of PRH and Vimentin double knockdown on proliferation in CCLP. 192
Figure 4.13 The effects of PRH and Vimentin double knockdown on proliferation in CCLP. 194
Figure 4.14 Vimentin KD impairs the DNA binding ability of PRH to CDKN1B and CDKN2B. 196
Figure 4.15 PRH interacts with Vimentin in both cytoplasm and nucleus in CCLP cells. 198
Figure 4.16 PRH interacts with Vimentin at N-terminal domain. 202
Figure 4.17 PRH interacts with Vimentin in both the cytoplasm and the nucleus in AKN-1 cells. 203
Figure 4.18 Mass spectrometry on Myc-PRH IP of CCLP. 206
Figure 4.19 The PRH/HHEX RNA expression correlate with VIM in the GEPIA dataset. 207
Figure 5.1 PRH OE increases cumulative cell number and change the cell morphology in AKN-1 cells. 212
Figure 5.2 PRH OE leads to EMT and increases Notch expression. 213
Figure 5.3 Stable PRH expression increases AKN-1 cell migration and invasion. 214
Figure 5.4 Stable PRH expression in AKN-1 promotes colony formation in soft agar. 215
Figure 5.5 PRH OE upregulates Notch3 and modulates EMT genes expression in AKN-1 cells. 217
Figure 5.6 GSEA of RNA-seq data of PRH OE AKN-1. 219
Figure 5.7 Overlap of genes regulated by PRH in CCA and cholangiocytes. 221
Figure 5.8 Characterization of primary BECs. 223
Figure 5.9 PRH OE increases proliferation in BECs. 224
Figure 5.10 PRH OE increases cell migration and invasion in primary BECs (Donor 1).225

Figure 5.11 AdPRH in BECs (Donor 1) promotes colony formation in soft agar. 226
Figure 5.12 PRH OE up-regulates Notch3 and modulates EMT genes expression in BECs donor 1. 228
Figure 5.13 GSEA of RNA-seq data of PRH OE BECs donor 1. 230
Figure 5.14 The effects of PRH OE in proliferation of primary BECs donor 2 and donor 3. 232
Figure 5.15 RNA seq data of BECs donor 3. 236
Figure 5.16 RNA seq and qPCR data from BECs donor 2. 237
Figure 5.17 GSEA of RNA-seq data from PRH overexpression in BECs donor 2. 239
Figure 5.18 GSEA of RNA-seq data of PRH OE BECs donor 3. 240
Figure 6.1 AdPRH expression increases sensitivity towards Palbociclib in the CCA cell lines. 244
Figure 6.2 The effect of Palbociclib on CCA cell lines. 245
Figure 6.3 Effect of Palbociclib on Rb and phosphor Rb. 248
Figure 6.4 The effect of Palbociclib in PRH OE and KD CCLP cells. 249
Figure 6.5 Palbociclib has apoptotic effect on CCA cell lines. 252
Figure 6.6 Repurposing drug screening by MTT assay. 255
Figure 6.7 Repurposing drug screening by MTT assay. 257
Figure 6.8 Dose response curves for selected drug candidates. 263
Figure 6.9 Effect of drug candidates on CCLP cells. 267
Figure 6.10 Niclosamide treatment downregulate PRH expression in CCA cell lines. 271
Figure 6.12 The survival rate of the drug combination treatment. 272
Figure 6.13 The survival rate of selected drug combination treatment. 274
Figure 6.14 Synergism of drug combination Niclosamide with Palbociclib in CCA cell lines. 276
Figure 6.15 Synergism of drug combination FiVE1 with Niclosamide in CCA cell lines. 277
Figure 7.1 Regulation of cell cycle by PRH. PRH directly represses p15 and p27 and hence causes cell arrests in G1 phase and S phase. 289
Figure 7.2 The overview of PRH in cancer hallmarks in CCA. 302

List of tables

Table 1 The cell lines used in this study 64
Table 2 SiRNA used in this study 73
Table 3 Buffers for Western Blotting..... 88
Table 4 Antibodies used in this study..... 90
Table 5 Primers used for PCR amplification for gene expression 95
Table 6 Buffers for ChIP 104
Table 7 Primers used for manual ChIP-qPCR..... 104
Table 8 PRH expression and the number of DEGs (q<0.05) from the RNA-seq data of AKN-1 and BECs donors. 234
Table 9 Effect of various compounds on CCLP, CCSW and immortalised cell line AKN-1 260
Table 10 Dose response curves for selected drug candidates. 264
Table 11 List of drug combinations that are shown to be 10 times more effective than single drug treatment in CCLP and CCSW cells 273

Part of the data in chapter 3, 4 and 5 are published in the following paper:

Kitchen, P.; **Lee, K.Y**.; Clark, D.; Lau, N.; Lertsuwan, J.; Sawasdichai, A.; Satayavivad, J.; Oltean, S.; Afford, S. Gaston, K.; et al. A runaway PRH/HHEX-Notch3 positive feedback loop drives cholangiocarcinoma anddetermines response to CDK4/6 inhibition. Cancer Res.2019.

List of abbreviations

Abbreviations	Definition
ALD	Alcohol Liver disease
APS	Ammonium persulphate
BECs	Biliary epithelial cells
BSA	Bovine serum albumin
CCA	Cholangiocarcinoma
CDKs	Cyclin-dependent kinases
cDNA	Complementary deoxyribonucleic acid
CH18	Chromosome 18
ChIP	Chromatin immunoprecipitation
ChIP-seq	Chromatin Immunoprecipitation – sequencing
CK2	Casein Kinase 2
DEG	Differentially regulated gene
DMEM	Dulbecco's Modified Eagle Medium
DMSO	Dimethyl Sulfoxide
EDTA	Ethylenediaminetetraacetic acid
Edu	5-Ethynyl-2'-deoxyuridine
EGF	Epidermal growth factor
EGFR	Epidermal growth factor receptor
EGTA	Ethylene glycol-bis (β-aminoethyl ether)-N,N,N',N'tetraacetic acid
eIF-4E	Eukaryotic translation initiation factor 4E
EMT	Epithelial to Mesenchymal Transition
ESM	Endothelial cell-specific molecule
F12	Nutrient Mixture F-12 (Ham's)
FACs	Fluorescense activated cell sorting
FBS	Foetal Bovine Serum
FDR	False discovery rate
FGF	Fibroblast growth factor
FITC	Fluorescein isothiocyanate
G1	Gap 1 phase
GAPDH	Glyceraldehyde 3-phosphate dehydrogenase
GEPIA	Gene Expression Profiling Interactive Analysis
GFP	Green fluorescent protein
GO	Gene Ontology
GSEA	GeneSet Enrichment analysis
GTEX	Genotype Tissue Expression
HCC	Hepatocellular Carcinomas
HD	Homeodomain
HHEX	Haematopoietically Expressed Homeobox
HNF3β	Hepatocyte Nuclear Factor 3 β
HRP	Horseradish peroxidase
IgG	Immunoglobulin G

IHC	Immunohistochemistry
IL	Interleukin
KD	Knockdown
KO	Knockout
LB	Lysogeny Broth
MET	Mesenchymal to Epithelial Transition
mRNA	Messenger Ribonucleic Acid
MSigDB	Molecular Signatures Database
MTT	3-(4,5-dimethylthiazol-2-yl)-2,5-diphenyltetrazolium bromide
OE	Overexpression
PANTHER	Protein analysis through evolutionary relationships
PBS	Phosphate buffered saline
PEI	Polyethylenimine
PI	Propidium Iodide
PRH	Proline rich homeodomain
qPCR	Quantitative Polymerase Chain Reaction
R110	Rhodamine 110
RNA-seq	Ribonucleic acid-sequencing
SDS	Sodium dodecyl sulphate
shRNA	Short hairpin RNA
siRNA	Small interfering RNA
TCGA	The Cancer Genome Atlas
TEMED	Tetramethylethylenediamine
TF	Transcription factor
TGF-β	Transforming Growth Factor β
TLE	Transducin-like enhancer
TNF	Tumour necrosis factor
VEGF	Vascular Endothelial Growth Factor

CHAPTER 1

Introduction

1. Introduction

This thesis investigates the role of the PRH/HHex transcription factor in the development of bile duct cancer, also known as cholangiocarcinoma (CCA). Adult bile duct cells maintain normal homeostasis by perceiving and responding to the microenvironment and rarely proliferate. Cell proliferation is however required during embryonic development and adult responses to pathological wound healing and signaling pathways are activated to allow increased cell proliferation (Cooper, 2000). During the pathogenesis of cancer, the dysregulation of embryonic and growth factor related cell signaling and pathways lead to uncontrolled cell proliferation and survival. These signaling pathways are able to alter the activity of transcription factors to execute gene expression alterations that allow these outcomes. Here we will describe transcription factors (TF) and transcriptional regulations, as well as key signaling pathways that are frequently dysregulated in cancer generally and those dysregulated in CCA in particular. We will also describe the characteristics of cancer cells often referred to as the “hallmarks of cancer” that are pertinent to bile duct cancer or the types of cancer that PRH concern. As previously mentioned, many embryonic processes are reinstated during the development of cancer. Hence, we will also describe some key features of liver and bile duct development with a focus on signaling processes altered in bile duct cancer.

1.1 Transcriptional regulation

Most signaling pathways culminate in the regulation of TFs. TFs regulate the process of transcription whereby an RNA copy is produced by transcription with the transfer of sequence information from a DNA template. This single stranded RNA copy is called messenger RNA (mRNA) when used as a template for protein synthesis in a process known as translation. Transcription is carried out by four RNA polymerases which are large and complex enzymes in eukaryotic cells (White, 2011). Transcription of protein encoding genes begins with an initiation step, in which the RNA polymerase II recognises the promoter region and binds to core promoter sequences around 30-100 base pairs upstream of the transcription start site (TSS). Transcription factors of three general types help to recruit the appropriate RNA polymerase: (i) the DNA binding TFs such as c-Myc, (ii) the non-DNA binding TFs that have co-activator or co-repressor activity and interact with sequence specific DNA binding proteins and finally (iii) the general or basal TFs that interact with RNA polymerase. The completed assembly of transcription factors and RNA polymerase II bind to the promoter and form a transcription pre-initiation complex (PIC) (Fuda et al., 2009). The most extensively studied core promoter sequence is 5'-TATAAA-3', known as the "TATA box" and is associated with the general TF complex TFIID (Lifton et al, 1978). Several other core promoter sequences also exist and they allow recruitment of RNA Polymerase II through general TFs. There are also other consensus sequences in DNA for TFs that are specifically bound by different families of DNA binding TFs. RNA polymerase II catalyses the synthesis of a new RNA strand in the 5' to 3' direction, adding new nucleotides to the 3' end of the growing RNA strand. RNA polymerases unwind the double stranded DNA ahead of them and allow the unwound

DNA behind them to rewind. Therefore, RNA strand synthesis appears as a transcription bubble of about 25 DNA base-pairs. When the RNA polymerase reaches the end of the gene, the process is terminated. The termination process occurs by polyadenylation (addition of adenosines on the 3' end of the mRNA). This allows the recruitment of termination factor proteins that destabilise the DNA:RNA interaction (Proudfoot, 2016). The DNA binding TFs are classified into different types according to the DNA-binding domain they contain. Examples of DNA binding TFs include homeodomain proteins, helix-turn helix proteins, zinc finger proteins and Leucine Zipper proteins. In terms of DNA binding, DNA–TF interactions *in vivo* are largely shaped by the chromatin landscape. Nucleosomes are the fundamental unit of DNA structure consisting of DNA wrapped around a core of histones and provide a hindrance to most TF-DNA binding (Cutter and Hayes, 2015). Histones are negatively charged basic proteins that associate with the positively charged DNA. As DNA is tightly bound in nucleosomes and condensed, TF binding to DNA is restricted as the DNA is not accessible. Therefore, most TFs preferentially bind to regions of open, accessible chromatin. The remodeling of chromatin is achieved by ATP-dependent chromatin remodelers and other chromatin remodeling proteins. Switch/sucrose-non-fermenting (SWI/SNF) is the most well-established chromatin remodeler family that activates gene transcription (Tyagi et al., 2016). To restructure the nucleosome, the ATP-dependent chromatin remodelers obtain energy from ATP hydrolysis; this disrupts DNA and histone binding and thereby regulates the dynamics of chromatin accessibility (Khorasanizadeh, 2004). A group of proteins termed the histone chaperones are responsible for collecting the histones after the disruption of DNA and histone binding by the chromatin remodelers. These two

group of proteins work together to alter the dynamics of chromatin accessibility (Das and Tyler, 2013). Apart from the chromatin remodelers, TFs themselves can regulate histone chaperones to open chromatin and allow binding of a secondary TF to the chromatin (Swinstead et al., 2016). For example, transcription factor *GATA3* can increase chromatin accessibility by recruiting the SWI/SNF complex to the chromatin (Takaku et al., 2016). Chromatin modulation is also achieved by post-translational modification of DNA and there are four types of DNA modification identified: (i) methylation, (ii) hydroxy-methylation, (iii) formylation and (iv) carboxylation. The key players involved in DNA and histone modifications are known as writers, erasers and readers. Writers refer to enzymes that are capable of modifying the nucleotide base and specific amino acid residues in histones; erasers refer to enzymes that can remove the modifications and readers refer to proteins that possess specific domains to recognize specific epigenetic marks in a locus (Biswas and Rao, 2018).

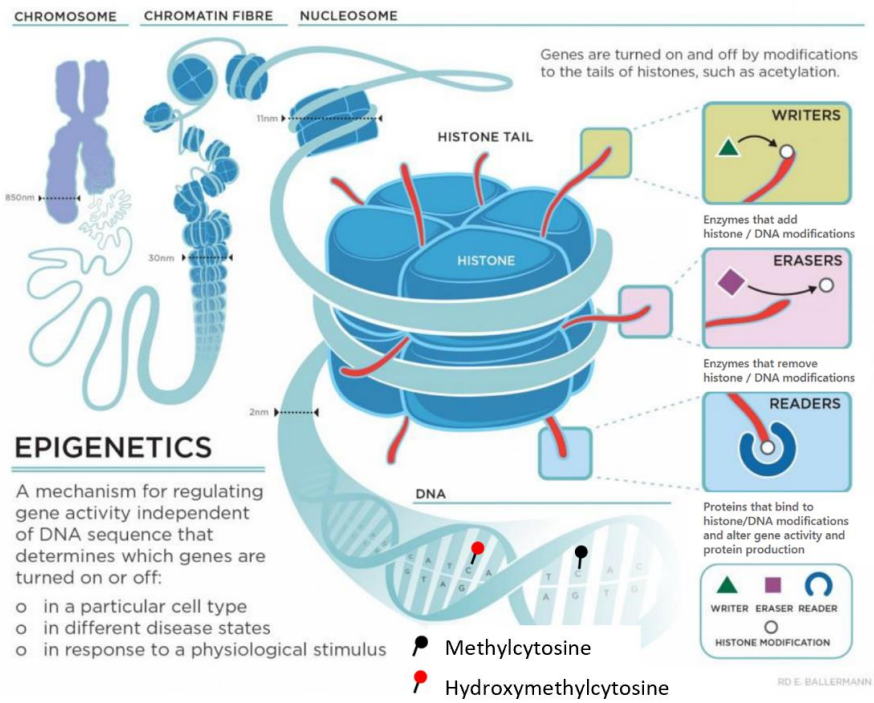

Figure 1.1 Gene expression regulated by epigenetics (adapted from R. Ballermann, 2012).

DNA binding TFs play an important role in contributing to the development of cancer. Gene expression is often altered during tumourigenesis and deregulation of TFs modifies gene expression that favors the development of cancer (Lee and Young, 2013). There are at least 19 signaling pathways known in regulating biological function and DNA binding TFs participate in regulating these pathways by activating or repressing transcription of specific genes in the pathways (Nebert, 2002). The genes that encode the DNA binding TFs that are involved in cancer development can be either oncogenes or tumour suppressor genes. Oncogenes refer to genes when mutated or upregulated to promote cancer development whereas tumour suppressor genes refer to genes when mutated or downregulated to promote cancer development.

1.2 PRH protein

1.2.1 PRH/HHex protein

Proline-rich homeodomain (PRH) protein, also known as human hematopoietically expressed homeodomain (HHex) is a TF that is crucial in liver development and is altered in liver cancer (Hunter et al., 2007). PRH expression was first identified in avian and human haematopoietic cells (Crompton et al., 1992). The homeodomain of PRH is highly conserved between different animal species; the human PRH homeodomain shares 97% homology with chicken PRH and with only one amino acid differing from that of mouse. As a TF, PRH can activate or repress transcription through direct and indirect pathways. It can directly bind to DNA to regulate transcription through the PRH consensus binding sequence 5' ATTAA on the DNA and recruit co-repressors such as the Transducin-like enhancer (TLE) (Gaston et al., 2016). Indirectly, PRH can alter the DNA binding or transcriptional activity of other TFs through transcriptional modulation (Soufi and Jayaraman, 2008).

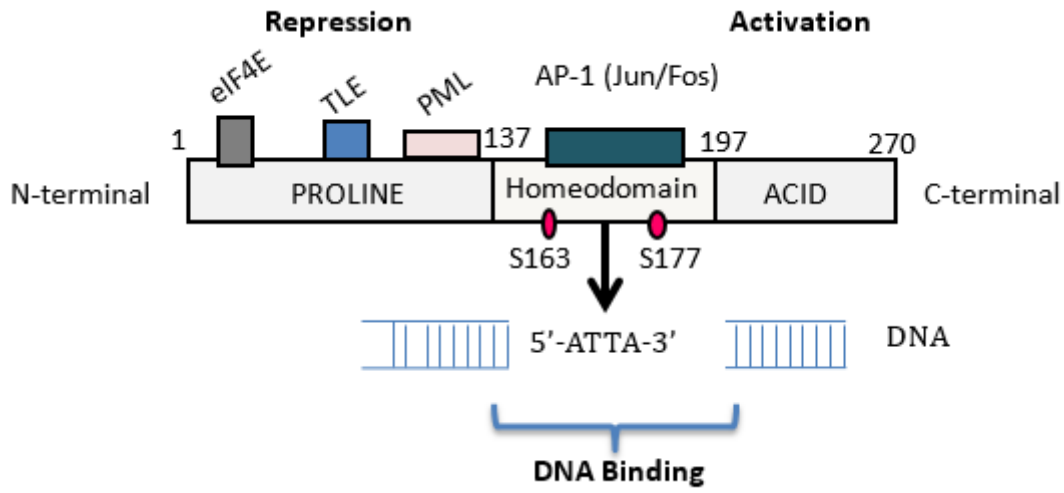

Figure 1.2 The structure of PRH protein. This diagram illustrates the N-terminal, homeodomain and C-terminal domain of PRH and the interaction sites of PRH with its interacting partners, adapted from (Kershaw et al., 2014).

1.2.2 PRH structure and function

The structure of PRH is well characterized and consists of 3 regions. The N-terminal region is approximately 20% proline-rich N-terminal region (amino acids 1-136) whereas the C-terminal region is highly acidic (197-270) **(Figure 1.3)** (Crompton et al., 1992; Soufi et al., 2006). The central PRH homeodomain is 60 amino acids long and consists of a short N-terminal arm and three alpha helices. The PRH DNA recognition binding site 5'-C/TA/TATTAAA/G-3' was identified by Systematic evolution of ligands by exponential enrichment (SELEX) experiments but those experiments used a truncated PRH comprising only the C-terminal fragment of PRH and homeodomain (Crompton et al., 1992). Further study using Electrophoretic mobility shift assay (EMSA) with the isolated PRH homeodomain showed that PRH binds to 5'-ATTAA-3' and 5'-CAAG-3' sequences and therefore PRH appears to have a relaxed DNA binding specificity (Pellizzari et al., 2000). The Goosecoid promoter contains 5'-C/TA/TATTAAA/G-3' sequences that the full length PRH protein binds to using the homeodomain (Williams et al., 2008). However, since no *in vivo* studies have used the entire PRH protein to characterize the PRH consensus binding sequence, the binding specificity of the full-length protein in cells is still not well defined. The PRH homeodomain can repress transcription without binding to DNA but rather by interacting with activator protein-1 (AP-1). AP-1 is a TF that promotes cell growth and consists of the proteins c-Fos and c-Jun heterodimer. AP-1 dependent activation of genes is repressed by helix 3 of the PRH homeodomain binding to the N-terminus of c-Jun, resulting in inhibition of Fos/Jun heterodimerization (Schaefer et al., 2001).

The PRH C-terminal domain is acidic and this is often a characteristic of transcription

activator proteins (Triezenberg, 1995). The C-terminal domain of PRH contains 4 times as many acidic residues as basic residues. It binds to the sodium-dependent bile acid co-transporter promoter (NTCP) and activates NTCP, a bile transporter gene (Kasamatsu et al., 2004). PRH also represses transcription by interacting with TBP (TATA box binding protein) (Guiral et al., 2001). In contrast, PRH can act as a co-activator with other TFs. For example, it has been shown that PRH binds to Hepatocyte nuclear factor-1α (HNF-1α) at the liver pyruvate kinase (L-PK) gene promoter region. This stimulates the transcription activity of HNF-1α by the C-terminus and homeodomain of PRH (Tanaka et al., 2005).

The N-terminal domain of PRH has key properties that determine PRH activity in the nucleus. The N-terminal domain of PRH appears to be split into 2 regions that have different roles. The first 50 amino acids are responsible for PRH dimerization. The second region, downstream of the first 50 amino acids of PRH, vital for collaborating with the PRH homeodomain (amino acids 132-270) to promote oligomerization. N-terminal dimerization is partially resistant to SDS unfolding and does not show either typical α-helical or β-sheet secondary structures (Soufi et al., 2006). The N-terminal domain can repress transcription independently of the homeodomain when fused to another DNA binding domain (Guiral et al., 2001). The N-terminal domain of PRH acts as a platform for protein-protein interactions including the HC8 proteasome unit (Bess et al., 2003), CK2β subunit (Soufi et al., 2009), Promyelocytic leukaemia protein (PML) (Topcu et al., 1999), eIf4E (Topisirovic et al., 2003) and members of the Groucho/TLE co-repressor family (Gaston et al., 2016; Swingler et al., 2004a). TLE proteins cannot function by binding to DNA directly but instead bind to DNA-binding proteins to modulate their

effects and also directly bind to histones (Kaul et al., 2014). The overexpression of TLE resulted in an increase in transcriptional repression by PRH while knockdown of TLE showed a decrease in transcriptional repression by PRH. These findings, together with evidence of direct protein-protein interaction suggest that TLE is a co-repressor with PRH (Swingler et al., 2004). PRH also interacts with Polycomb-repressive complex 2 (PRC2) and this leads to histone methylation (H3K27me3) and transcriptional repression. Loss of PRH leads to significant reactivation of PRC2 targets including *CDKN2A* encoding the p16 and p14 cell cycle inhibiting proteins (Shields et al., 2016).

The PRH N-terminal domain also interacts with eIF-4E (eukaryotic initiation factor 4E) causing conformational changes in the eIF-4E protein. Overexpressing eIF-4E leads to uncontrolled cell proliferation and malignant changes in T293 cell line by promoting mRNA transport and/or translation of mRNAs that are essential in cell growth. PRH can reverse these oncogenic transformations of immortalized cell lines by disrupting the eIF4E present in the nucleus, resulting in inhibition of eIF4E-dependent transport of these transcripts (Topisirovic et al., 2003).

Therefore, the structure of PRH is intensively studied and the regions of where PRH interacting or binding partners interact are also identified by using different PRH truncations.

1.2.3 Regulation of PRH expression

The expression of PRH is regulated by a number of proteins in different contexts. In liver development, PRH is required for early hepatogenesis and also the hepatoblast (hepatocytes precursors) differentiation; the expression of PRH needs to be activated by bone morphogenetic protein (BMP) (Zorn et al., 1999), fibroblast growth factor (FGF)

and Wnt for embryonic liver development (Zhang et al., 2004). Another example of regulatory factors that activate PRH expression is HNF3β and GATA-4 in the HepG2 hepatoblastoma (liver cancer) cell line (Denson et al., 2000). Collectively, the findings suggest that the activation of PRH expression in the liver is important in liver organogenesis and this will be discussed further in the liver development section. Interestingly, PRH also regulates its own gene promoter and forms a positive auto-regulatory feedback loop in thyroid cells (Puppin et al., 2004, 2003).

1.2.4 PRH in endothelial cells

PRH is important in the development of vascular endothelium as PRH knockout leads to abnormal vasculogenesis and it was identified that PRH represses endothelial cell-specific molecule (ESM) necessary for vascular development (Cong et al., 2006; Hallaq et al., 2004). It was also reported that PRH is required for angiogenesis in zebra fish experiments which revealed that PRH is an important upstream regulator for vascular endothelial growth factor C (VEGFC), its receptor FLT4 and Prospero homeobox protein 1 (PROX1) in regulating lymphangiogenesis (Gauvrit et al., 2018). PRH is important in development and the deregulation of signaling pathways by PRH can contribute to cancer development. PRH negatively regulates vascular endothelial growth factor receptor (VEGFR) 1 and 2 by direct binding and in turns control cell survival (Noy et al., 2010). In the leukemia cell line K562, PRH knockdown shows increase expression of the genes involved in the VEGF pathway leading to increased cell survival (Noy et al., 2010). The activation of these genes is likely to cause tumourigenesis. The association between PRH and malignancy will be described further in the PRH and cancer section.

1.2.5 Phosphorylated PRH

CK2 is an enzyme that regulates proteins involved in transcription, cell signaling and proliferation pathways. It consists of two α subunits forming a catalytic domain, and two regulatory β subunits (Litchfield, 2003). Aberrant CK2 expression is related to several cancers including non-small cell lung cancer (Daya-Makin et al., 1994), prostate cancer (Landesman-Bollag et al., 2001; Yenice et al., 1994) and breast cancer (Landesman-Bollag et al., 2001). PRH can be phosphorylated by protein kinase CK2 *in vivo* at Serine 163 and Serine 177 through binding to the β subunit of CK2 (casein kinase II) (Soufi et al., 2009). Phosphorylation at these sites inhibits the ability of PRH to bind DNA and to regulate transcription of its target genes. Furthermore, the pPRH protein is targeted for proteasomal processing resulting in formation of a truncated stable pPRH protein that lacks the C-terminal domain (PRHΔC). PRHΔC is a negative regulator of full-length PRH by sequestering TLE co-repressor proteins (Noy et al., 2012). Inhibition of CK2 activity through inhibition of upstream kinases that activate CK2 restore PRH function in cancers such as leukemia resulting in downregulation of pPRH in leukemic cells (Noy et al., 2010). For example, the SRC kinase inhibitor Dasatinib decreases the proliferation of K562 leukemic cells through an indirect effect on CK2 activity resulting in increased PRH activity. Therefore, phosphorylation of PRH by CK2 is an important mechanism for regulating PRH transcription activity in hematopoietic cells. Direct inhibition of CK2 activity in immortalized prostate cells also restores PRH activity in these cells and this alters their proliferation and migratory capacity (Siddiqui et al., 2017).

1.2.6 PRH and cancer

PRH is a regulator of cell proliferation, dysregulation of PRH expression and localization

are associated with cancer development. Downregulation of PRH protein expression and aberrant subcellular localization of PRH are related to liver (Djavani et al., 2005), breast (Kershaw et al., 2017), thyroid (Martinez Barbera et al., 2000) and prostate cancer (Kershaw et al., 2014). Although PRH acts as an oncogene in some subtypes of acute myeloid leukemia as described earlier, it also has tumour inhibiting effects in other subtypes of leukemia.

1.2.7 PRH as a tumour suppressor gene

PRH has been demonstrated to have tumour suppressive properties in various cancer types although the mechanisms that lead to downregulation of PRH are not well understood. There are a few examples that PRH acts as a tumour suppressor gene. It was described earlier that PRH disrupts eIF4E nuclear bodies by direct binding in leukemic cells (PML). The binding of PRH leads to inhibition of eIF4E mRNA transport activity and repression of the eIF4E downstream targets including Cyclin D1 and which leads to decreased cell proliferation (Topisirovic et al., 2003). Apart from proliferation, PRH has been shown to inhibit other cancer properties including cell migration, invasion and cell survival.

Goosecoid is an inducer of Epithelial Mesenchymal Transition (EMT) in breast cancer and PRH can directly repress the transcription of Goosecoid in breast cancer (Hartwell et al., 2006). EMT refers to the process of epithelial cells losing cell-cell adhesion and gaining invasive and migratory property to transform to mesenchymal cells. TGFβ is another inducer of EMT and Endoglin is a TGFβ co-repressor that downregulates TGFβ. Endoglin expression can be increased by PRH to inhibit TGFβ signaling and inhibit normal breast cell EMT in order to inhibit migration of immortalized prostate cells (Siddiqui et al.,

2017). Furthermore, in prostate cancer, PRH depletion inhibits cell migration, invasion and colony (Siddiqui et al., 2017).

It was described earlier that PRH regulates vascular development and VEGF signaling in leukemia. It was shown that PRH regulates the VEGF signaling pathway in hematopoietic cells. PRH represses *VEGF*, *VEGF1* and *VEGF2* expression in K562 leukemia cell lines by direct binding to the promoter regions of these genes (Noy et al., 2010). PRH overexpression in K562 cell lines shows increased apoptosis and it was concluded that decreased PRH expression leads to up-regulation of VEGF signaling to promote tumour survival. In breast cancer, PRH depletion also leads to increased VEGF signaling. Moreover, depletion of PRH drives proliferation and an increase in cancer stem cell-like properties (Kershaw et al., 2017). Furthermore, in breast cancer, overexpressing PRH can downregulate MMP-1 expression that inhibits cell migration (Nakagawa et al., 2003).

Another mechanism through which PRH increases tumour survival in K562 leukemic cells is by CK2 phosphorylating PRH. It was mentioned earlier that CK2 regulates the transcriptional activity and the stability of PRH by phosphorylating PRH and CK2 is a kinase that promote tumour growth in many cancers (Chua et al., 2017). CK2 promotes tumour growth by phosphorylating various proteins in different cancers that lead to increased expression of oncogenes or decreased activity of tumour suppressor genes (Chua et al., 2017). Treatment in K562 leukemic cells with the CK2 inhibitor Dasatinib results in decreased phosphorylation of PRH and reduced cell numbers.

In liver cancer, PRH expression is downregulated in poorly differentiated hepatocellular carcinomas (HCC) and well-differentiated HCC (Su et al., 2012a). Tumour formation was

inhibited by overexpressing PRH in a HCC cell line (HepG2) in nude mice. Besides liver cancer, there is also lower PRH mRNA expression in B-cell lymphoma, bladder carcinoma and pancreatic carcinoma shown in ONCOMINE database consistent with a tumour suppressor role in these cancers (Gaston et al., 2016).

The PRH protein localization was shown to relate to cancer. In breast cancer, PRH protein localization is dysregulated. PRH is found located predominantly in the cytoplasm in breast carcinomas rather than in both nuclear and cytoplasmic compartments in normal breast epithelial cells (Puppin et al., 2006). Similarly in thyroid carcinomas, PRH protein expression is only present in the cytoplasm, whereas in normal thyroid cells, it is present in both the nucleus and cytoplasm (Pellizzari et al., 2000).

1.2.8 PRH as an oncogene

In contrast, the oncogenic property of PRH is implicated in several subtypes of leukemia. In acute T cell lymphoblastic lymphoma, PRH is overexpressed by *LMO2* (LIM domain only 2) oncogene (Smith et al., 2014). Forced overexpression of PRH is oncogenic in T cell lineages. Mice injected with bone marrow cells overexpressing PRH form tumours from a precursor T cell population (George et al., 2003). In this model, transcriptionally active exogenous PRH lead to upregulation of proliferation and p53 expression suggesting that PRH is oncogenic in this tumour type.

High PRH mRNA expression in acute myeloid leukemia (AML) is correlated to poor survival (Shields et al., 2016). One of the mechanisms through which PRH promotes leukemogenesis is that PRH recruits Polycomb co-repressor complexes and represses cell cycle inhibitors such as p16 and p14 encoded by *CDKN2A* allowing increased cell cycle activity (Shields et al., 2016). Collectively, PRH can be a tumour suppressor gene as

well as an oncogene depending on context.

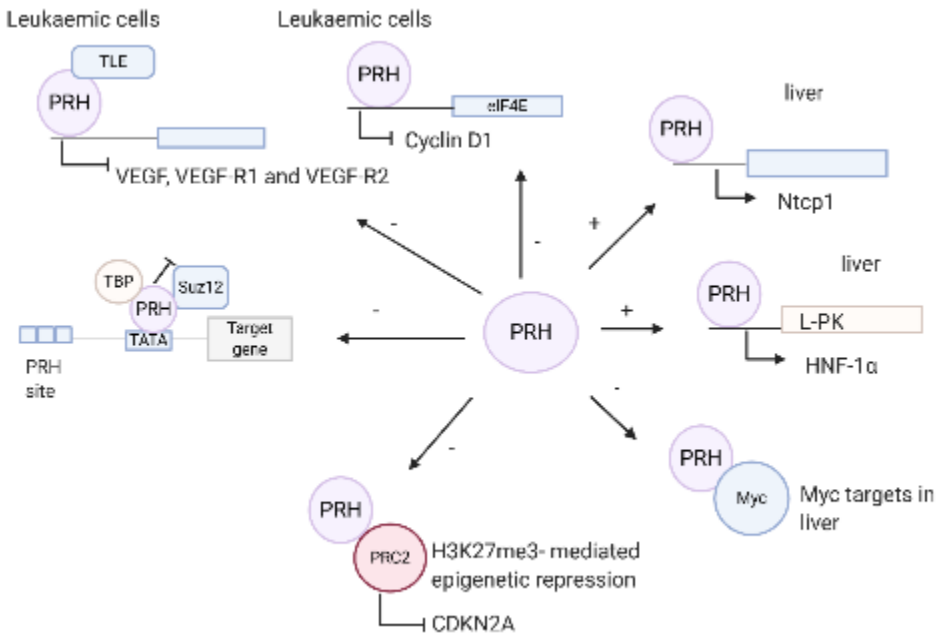

Figure 1.3 Summary of PRH regulation of gene expression. This diagram shows PRH interacting partners and the impact on gene regulation. PRH can repress VEGF by interacting with TLE in Leukemic cells (M. Guiral et al., 2001; Swingler et al., 2004a). PRH binds to eIF4E in PML and reduce Cyclin D1 protein expression (Topisirovic et al., 2003b). The C-terminus of PRH is able to activate Ntcp1(Denson et al., 2000) and interacts with HNF1α to activate L-PK in the liver (Tanaka et al., 2005). PRH interacts with oncoprotein c-Myc and disrupting c-Myc dimers to reduce cell proliferation in liver cancer (Marfil et al., 2015). PRH recruits polycomb complex PRC2 and represses cell cycle inhibitors (Shields et al., 2016a). PRH binds to TATA box to compete with TBP and interact with other activators (Minami et al., 2004).

1.3 Cell Signaling pathways

Cells receive signals and respond to the microenvironment by capturing signaling molecules produced by the tumour microenvironment through the expression of cell surface receptors or by secreting signaling molecules themselves. Additionally, cell surface proteins expressed on the cellular membrane are used to directly contact adjacent cell types through binding to receptors on adjacent cells. Binding of ligands to receptors allows the transduction of signaling pathways and thereby coordinates the function of cells. Cells are programmed to respond to specific extracellular signals. Cell signaling can be divided into different types based on the signal travelling distance

between the signaling and responder cells. Cells communication includes cell-cell contact, short distance (paracrine signaling) and long distant (endocrine signaling).

As mentioned, there are at least 19 well-established signaling pathways. Here, the most common cell signaling pathways utilized by cancer cells are briefly described.

1.3.1 Growth factor signaling

Growth factors refer to a subset of cytokines that are capable of stimulating cell growth, differentiation and survival. They can be classified into different families based on their functions, the cells they target, or their structure, such as the Epidermal growth factor (EGF) family, Vascular endothelial growth factor (VEGF) family and Wnt family (Di Domenico and Giordano, 2017). The growth factor receptors expressed on the cell surface bind to the growth factors and this leads to signal transduction and activation of signaling cascades. For example, EGF binds to its receptors known as EGF receptors including ErbB1 (Her1), ErbB2 (Her2), ErbB3 (Her3) and ErbB4 (Her4) and triggers a series of downstream signaling cascades including the PI3K/Akt pathway leading to cell cycle progression (Oda et al., 2005).

Receptor tyrosine kinases (RTK) are another important group of receptors that are important in regulating a range of cellular process. For example, c-MET (an RTK) and its ligand Hepatic Growth Factor (HGF) are involved in a wide range of malignancies (Peruzzi and Bottaro, 2006).

1.3.2 PI3K/Akt/mTOR pathway

The phosphatidylinositol-3-kinase (PI3K)/Akt and the mammalian target of rapamycin (mTOR) signaling are essential in maintaining normal homeostasis such as cell growth

and survival (Porta et al., 2014). This is mediated through phosphorylation of various downstream substrates at serine and threonine residues. PI3K/Akt pathway is activated by binding of hormone, growth factors or cytokines to RTK such as c-MET. Activated RTK monomers form dimers upon receptor binding and this results in the activation of the intracellular tyrosine kinase domain and phosphorylation of monomers. Activation of PI3K is stimulated directly through the binding of a regulatory subunit to the activated receptor or indirectly activated via adapter molecules such as the insulin receptor substrate (IRS) proteins (Shaw and Cantley, 2006). PI3K can also be activated by the GTP binding RAS protein. Activated PI3K phophorylates Phosphatidylinositol-4,5-bisphosphate (PIP2) to phosphatidylinositol-3,4,5-trisphosphate (PIP3). PIP3 recruits specific proteins to the plasma membrane to promote activation of the subsequent signaling cascade by acting as a docking phospholipid that binds specific domains (Fruman et al., 1998). The third position of the phosphate group of PIP3 can bind to both phosphoinositide-dependent kinase-1 (PDK1) and the AKT protein and recruit AKT to the plasma membrane, enabling PDK1 to access and phosphorylate Akt, leading to partial Akt activation. Then the phosphorylation of Akt at S473, either by the protein complex mTOR Complex 2 or by DNA dependent protein kinase, stimulates full Akt activity. Once Akt is activated, it regulates biological processes through phosphorylation of effector kinases or suppression of a broad array of proteins involved in cell growth, proliferation, adhesion and cell death (Testa and Bellacosa, 2001).

1.3.3 Wnt signaling

Canonical Wnt/β-catenin signaling pathway is another important developmental pathway that regulates cell proliferation (Kühl and Kühl, 2013). E-cadherin, a cell surface

protein forms a complex with catenins including α-catenin, β-catenin and γ-catenin at the cytoplasmic region (Reynolds and Carnahan, 2004). Alteration in cadherins can affect β-catenin nuclear localization. β-catenin is phosphorylated by a destruction complex involving the scaffold protein Axin, Adenomatous Polyplosis coli gene (APC), Glycogen synthase kinase 3 beta (GSK3β) and Casein kinase 1 (CK1α). β-catenin is targeted for proteasomal degradation in the absence of the Wnt ligand. The pathway is activated by soluble Wnt ligands from the tumour microenvironment binding to Frizzled receptors and low density lipoprotein receptor-related protein 1 (LRP) co-receptors. When β-catenin is absent in the nucleus, a complex containing TCF/LEF and an enhancer complex TLE/Groucho recruits histone deacetylase to repress gene expression. As with other signaling pathways, Wnt signaling crosstalks with other signaling pathways such as PI3K and c-MET/HGF pathways to control cellular events. Upon binding of c-MET to HGF, c-MET induces tyrosine phosphorylation of β-catenin and this leads to translocation of β-catenin to the cytoplasm (Thompson et al., 2011). Regarding the PI3k/mTOR pathway, Wnt signaling inhibits the GSK3β and activates the mTOR pathway (Inoki et al., 2006). Wnt signaling can also regulate the stability of Ras by inhibiting ubiquitination and degradation of Ras (Jeong et al., 2018).

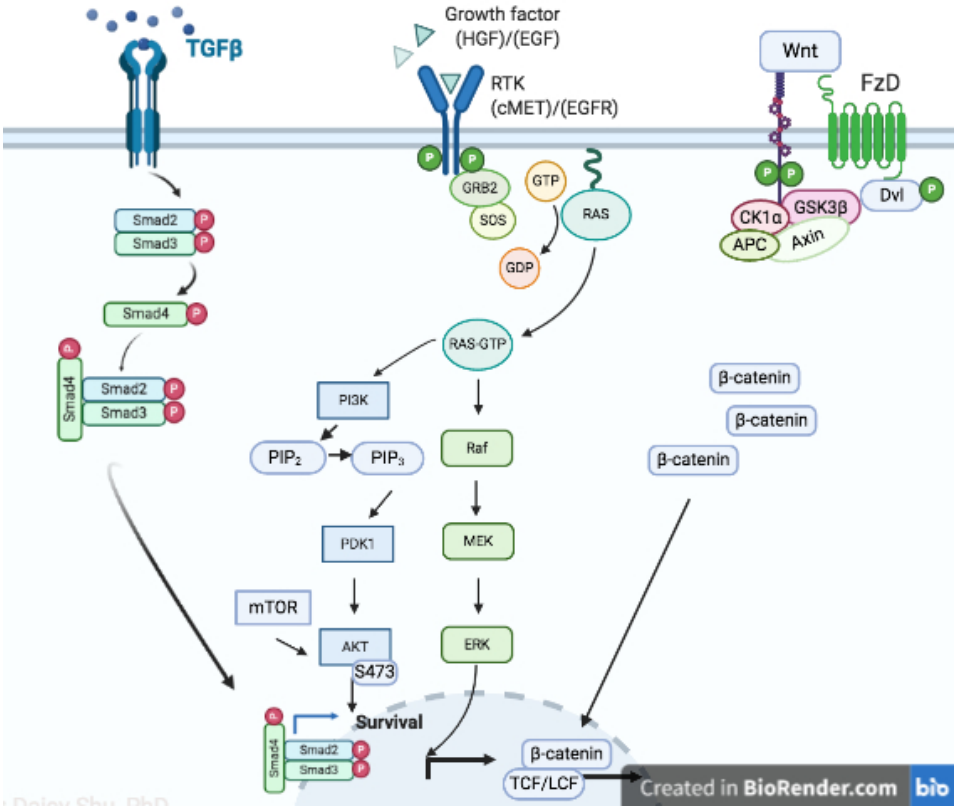

Figure 1.4 Cell signaling pathways including growth factor signaling, Wnt and TGFβ signaling. Growth factor /HGF/cMET signaling: EGF binds to its receptors known as EGF receptors. Activated EGF/EGFR recruits several adaptor proteins such as GRF2, which binds to the phosphotyrosine residue in EGFR and recruits Son of Sevenless (SOS) to the membrane. SOS then activates GDP/GTP exchange of Rat sarcoma viral oncogene homolog (Ras) and recruits Rapidly Accelerated Fibrosarcoma (RAF) to the membrane (Scaltriti and Baselga, 2006). Subsequently, RAF phosphorylates Mitogen-activated protein kinase kinases (MEKs) and activates the extracellular signal regulated kinases (ERKs). ERKs activate numbers of transcriptional regulators to induce cell growth and proliferation (Roberts and Der, 2007). The binding of HGF to c-MET leads to phosphorylation of its tyrosine kinase domain and subsequently signaling effector molecules are recruited. Activation of c-Met can stimulate Ras and Ras indirectly activates Raf and subsequently MEKs as described earlier. Wnt signaling: Upon ligand binding, LRP receptors are phosphorylated by GSK3β and CK1α and this leads to Dishevelled (Dvl) protein polymerization and LRP receptors are activated. Dvl polymers repress the activity of the destruction complex thereby stabilising β-catenin in the nucleus (Metcalfe et al., 2010). β-catenin then forms a complex with T-cell factor/lymphoid enhancer-binding factor (TCF/LEF) DNA binding proteins and co-activates with TCF to activate downstream Wnt target genes (MacDonald et al., 2009). TGFβ signaling: TGFβ binds to the type II TGFβ receptor and forms a heterodimer complex with type I TGFβ receptor to phosphorylate the type I TGFβ receptor at the glycine and serine rich motif (Derynck et al., 2001). This phosphorylation leads to activation of the SMAD pathway by phosphorylation of the kinase domain of receptor regulated Smad transcription factors (R-Smads); these phosphorylated-R-Smads translocate to the nucleus and regulate gene expression (Santibañez et al., 2011).

1.3.4 Notch signaling

Notch signaling is a highly conserved signaling cascade that is important in the process of development and homeostasis. For instance, Notch regulates cell proliferation (Go et al., 1998), differentiation (Honey, 2005) and apoptosis (Lundell et al., 2003) of

endothelial cells during embryo development. Unlike the majority of signaling pathways, Notch triggers a transcriptional response through cell-cell communication via a ligand-receptor interaction. In mammals, Notch has 4 transmembrane receptors and two types of ligands, Serrate/Jagged and Delta-like ligands (Baron, 2003). The Notch signaling cascade is activated by direct cell contacts that trigger the interaction between Notch receptors and its ligands. Notch target genes include the Hairy Enchancer of Split (Hes) family that represses differentiation, and c-Myc that drives proliferation (Borggrefe and Oswald, 2009). Besides these canonical targets, Notch signaling specifically activates genes in a tissue dependent manner. These genes include SRY-Box Transcription Factor 9 (Sox9), transforming growth factor (TGFβ) and hepatocyte nuclear factors 1β (HNF1β) which are important in hepatic lineage commitment (Hosokawa et al., 2015).

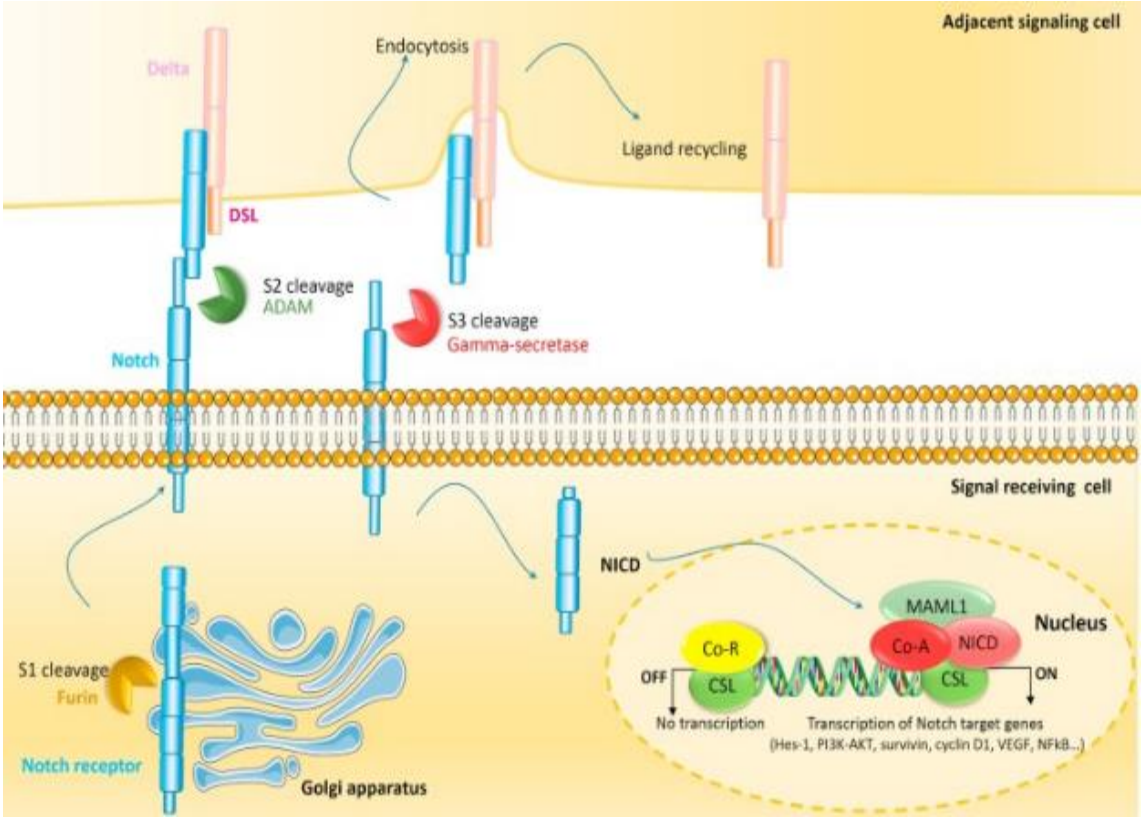

Figure 1.5 The Notch signaling pathway. Ligand binding promotes two proteolytic cleavage events in the Notch receptor. The first cleavage, S2, is catalyzed by a Disintegrin and metalloproteinase domain-containing protein 10 (ADAM10). This results in membrane-anchored Notch extracellular truncation (NEXT) which is then targeted by gamma-secretase at the second cleavage site S3. Gamma-secretase is an enzyme complex that contains presenilin, nicastrin, presenilin enhancer 2 (PEN2) and anterior pharynx-defective 1 (APH1) (Baron, 2003). The second cleavage releases the Notch intracellular domain (NICD) which translocates to the nucleus and cooperates with the DNA-binding protein CSL (RBPJ) and its co-activators Mastermind-like protein (Mam) and p300 to promote transcription (Kopan and Ilagan, 2009), adapted from (Majidinia et al., 2018).

1.3.5 TGFβ signaling

TGFβ signaling is important in embryogenesis and controls cell proliferation, migration and differentiation that are involved in normal adult homeostasis. Dysregulation of TGFβ signaling has been reported in several cancer types. TGFβ signaling is activated through the TGFβ receptors and activates a family of signal transducers SMAD. Apart from the Smad pathway, TGFβ also activates non-Smad pathways such as the PI3K/Akt pathway through interaction with the p85 subunit of PI3K (Zhang, 2017). Moreover, TGF-β activates mTORC2 and thereby leads to Akt activation and activates PI3K-Akt signaling

(Zhang et al., 2013).

1.4 Cancer hallmarks

About one in four deaths are caused by cancer in the UK ("Cancer Statistics for the UK," 2015). Previously, cancer was considered to be fundamental dysregulation of cell growth (Deshpande et al., 2005). However, there are additional aspects of cell dysregulation leading to cancer which have now been categorised as "hallmarks of cancer". Human tumours were classified to have 6 hallmarks including (i) sustained proliferative signaling, (ii) evasion of growth suppressors, (iii) resistance to cell death, (iv) potential to replicate limitlessly, (v) induction of angiogenesis and (vi) activation of tissue invasion and metastasis. Genome instability provides the foundation for genetic diversity during cell division and for cells to progressively acquire the capabilities mentioned above (Hanahan and Weinberg, 2011). In recent years, two additional hallmarks have been identified, including (vii) reprogrammed energy metabolism and (viii) evasion of immune destruction (Vinay et al., 2015). Furthermore, the concept of the tumour microenvironment playing a role in the development of cancer is now established. Within a tumour, there are a collection of apparently phenotypically normal stromal cells which create a tumour microenvironment allowing epithelial cells to acquire the "hallmarks" mentioned above (Mao et al., 2013). Here, we will discuss some of the key hallmarks that PRH participates in to promote tumour growth and metastasis in a range of cell types.

1.4.1 Cell cycle and proliferation

Uncontrolled cell proliferation is a hallmark of carcinogenesis and a range of factors contribute to proliferation including cell cycle related proteins and various signal transduction pathways that promote cell growth (Feitelson et al., 2015). We will describe the cell cycle and signaling pathways that are commonly dysregulated in cancer.

Dysregulation of cell cycle leads to uncontrolled cell proliferation. The cell cycle consists of M phase, G_1 phase, S phase, G_2 phase and G_0 phase. DNA replication occurs at the S phase whereas cytokinesis occurs at the end of the M phase. The G_1 phase is the gap between M phase and S phase during which the cells grow in size and prepare for DNA synthesis, whereas the G_2 phase is a gap between S phase and M phase in which the cells continue to grow and prepare for mitosis (Vermeulen et al., 2003). In the G_0 phase, the cells are in a quiescent state when the cells are not preparing for division. The cell cycle is regulated by cyclins, cyclin dependent kinases (Cdk) and Cdk inhibitors (CKI). Cdk forms complexes with specific cyclins to allow transition from one phase to another in the cell cycle. It is well established that there are five Cdks identified and they are active during cell cycle: G_1 (CDK4, CDK6 and CDK2), S (CDK2) and G_2/M (CDK1). Cyclins periodically activate Cdks and different cyclins are required at different phases of the cell cycle. For example, for entry to the G_1 phase, CDK4/6-Cyclin D complexes are crucial. There are three types of Cyclin D that bind to CDK4/6: Cyclin D1, Cyclin D2 and Cyclin D3. The functional differences between the cyclins are not well defined as more intense studies have been carried out on Cyclin D1 compared to the other cyclins. The complexes of cyclins and Cdk in various stages of the cell cycle are described in **figure 1.6.**

The activity of Cdks can be inhibited by CKI which either bind to Cdk directly or to the Cdk-cyclin complexes. The two main families of CKI are the INK4 family and Cip/Kip family (Sherr and Roberts, 1995). The INK family including p15 (INK4b), p16 (INK4a), p18 (INK4c), p19 (INK4d) are responsible for inhibiting G_1 Cdk complexes. INK4 proteins form complexes with Cdk4/6-cyclin D together with retinoblastoma (Rb). Phosphorylated Rb loss or hyperactivation of Cdk4/6 are commonly found in cancer (Du and Searle, 2009). In cancer, the Rb pathway is inactivated by either mutation or functional inactivation of Rb (Paternot et al., 2010). Moreover, the gene encoding Cyclin D is the second most upregulated locus in cancer. PRH was shown to be associated with regulating the cell cycle in PML by inhibiting Cyclin D1 protein expression through eIF4E interaction with PRH (Topisirovic et al., 2003). Cyclin D protein can be pharmalogically inhibited for example, inhibition of Cyclin D2 impairs the leukemic expansion of patient-derived AML cells (Martinez-Soria et al., 2018).

Another major CKI family is the Cip/Kip family including p21 (Waf1, Cip1), p27 (Cip2) and p57 (Kip2). p21 is known to be activated by the tumour suppressor p53 at the p21 promoter (Deiry et al, 1993). At the G_1/S checkpoint, the cell cycle arrest caused by DNA damage is p53 dependent. Loss of *TP53* function could lead to the survival of DNA-damaged cells and result in the inheritance of the genetic changes in daughter cells. In the normal state, the cell cycle inhibitors act as tumour suppressors to regulate cell growth and induce the death of damaged cells. For example, in a mouse model of Mixed-lineage leukemia-eleven nineteen leukemia (MLL-ENL), *CDKN2A* encoding p16 is a tumour suppressor required for cell cycle arrest and this gene is repressed by PRH thereby increasing leukemic cell proliferation (Shields et al., 2016).

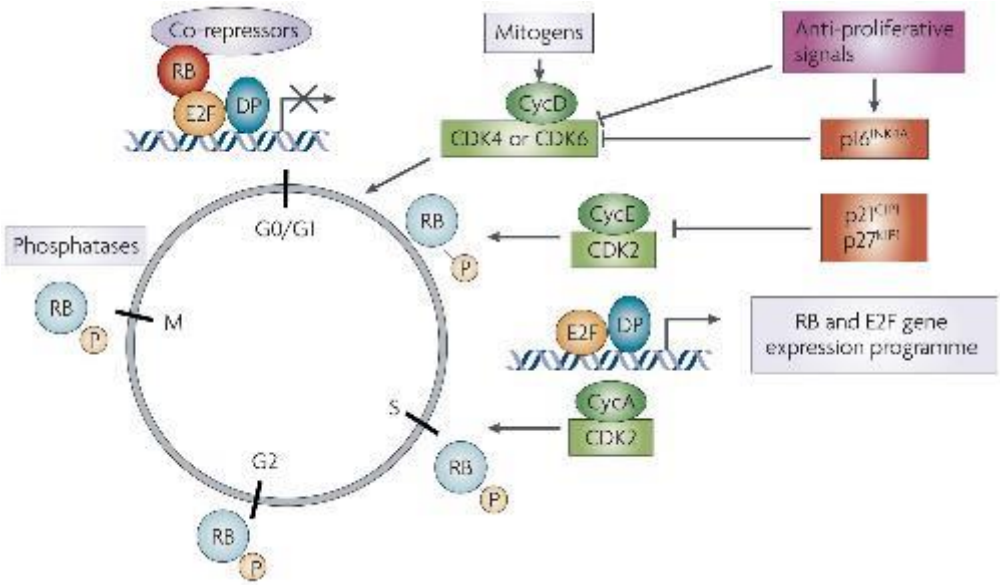

Figure 1.6 The cell cycle, adapted from (Knudsen and Knudsen, 2008) Cyclin D forms a complex with CDK4/6 for G1 entry. The CDK2-cyclin E complex is responsible for the regulation of cell entry to S phase from G1 phase (Ohtsubo et al., 1995). During S phase, binding of Cyclin A with CDK2 is required for the onset of DNA replication (Girard et al., 1991). Cyclin A binds with CDK1 to drive cells entry to M phase and a Cyclin B-CDK1 complex is required at a later stage of M phase (Arellano and Moreno, 1997). Cdk4/6-cyclin D inactivates Rb by phosphorylation that relieves transcription repression by the Rb-E2F complex and thus leads to G1 phase progression. E2F is released by phosphorylating Rb leading to the transcription of genes required for S phase entry (Hinds et al., 1992).

1.4.2 Signaling pathways regulating cell proliferation

There are well-known molecular pathways that contribute to cell proliferation. The first evidence of Notch involved in cancer was identified in human T-cell neoplasia. Notch acts as an oncogene in T-ALL by increasing expression of Myc, a global regulator of growth (Roderick et al., 2014). In terms of cell survival, the Notch gene *Hes1* suppresses the expression of an inhibitor of NF-κB (Cyld), activating NF-kB and enhancing T-ALL cell survival (Espinosa et al., 2010). After the discovery of Notch involvement in leukemia, Notch signaling was also implicated in a variety of solid cancers. Activation of Notch1 signaling was demonstrated to promote hepatocellular carcinoma (HCC) in a mouse model (Villanueva et al., 2012). It was shown that Notch has a key role in promoting HCC cell proliferation, invasion and migration (Huang et al., 2019).

The Notch signaling pathway is not exclusively oncogenic but is also tumour suppressive in skin, pancreatic epithelium and hepatocytes (Nowell and Radtke, 2017). In a mouse model, deletion of retinoblastoma protein (RB) and its two related family members p107 and p130 in mouse liver resulted in Notch upregulation whereas inhibition of the Notch signaling pathway led to accelerated HCC development (Lobry et al., 2011).

Aberrant Wnt signaling is also implied in various cancer types including melanoma, breast cancer, leukaemia and gastrointestinal cancer (Zhan et al., 2017). It is well established that Wnt signaling is involved in colorectal carcinogenesis (Polakis, 2012). Loss of APC expression is a key driver of colorectal cancer. Aberrant activation of Wnt signaling is also reported in liver cancer, mutation of *CTNNB1* encoding β-catenin is found in 15-25% of patients with HCC (Khalaf et al., 2018). The mutated β-catenin bypasses phosphorylation and subsequent degradation. Other studies show that β-catenin also promotes tumour cell survival by activating the growth factor receptor EGFR (Kim et al., 2019).

1.4.3 Apoptosis

One of the hallmarks of cancer is the cancer cell being able to evade apoptosis. Apoptosis is a type of programmed cell death and it is important in normal cell turnover, development and in the immune system. The mechanism of apoptosis involves a range of molecular cascades. The apoptosis pathway can be distinguished into intrinsic and extrinsic pathways. The intrinsic pathway of apoptosis is triggered by internal stimuli in the cells including DNA damage, hypoxia and oxidative stress (Karp, 2009). Activation of the intrinsic pathway leads to the release of pro-apoptotic protein including cytochrome-c into the cytoplasm (Danial and Korsmeyer, 2004). The intrinsic pathway is

regulated by the Bcl-2 family which are the pro-apoptotic proteins including Bax, Bak, Bad, Bcl-Xs, Bid, Bik, Bim and Hrk and anti-apoptotic proteins such as Bcl-2, Bcl-w and Mcl-1 (Reed, 1997). The anti-apoptotic proteins inhibit apoptosis by blocking the release of cytochrome c to the cytoplasm. Release of cytochrome c in the cytoplasm then activates Caspase-3 by forming a complex with Apaf-1 and Caspase-9 (Kroemer et al., 2007). The apoptosis pathway utilizes a caspase cascade which is a proteolytic cascade that can activate other caspases to amplify the signal for apoptosis and leads to rapid cell death (Hengartner, 2000). The extrinsic pathway is triggered by death ligands binding to the death receptors. The main death receptors are the tumour necrosis factor (TNF) family and the well established death ligands Fas ligand (FasL), TNFR1, DR3 and DR4 (Ashkenazi and Dixit, 1998). Following ligand binding, adaptor proteins including FADD and TRADD are recruited. The ligands and receptors form complexes with the adaptor protein to form a complex called death-inducing signaling complex (DISC) (O'Brien and Kirby, 2008). DICS then activates pro-caspase 8 and thereby initiates apoptosis by cleaving downstream caspases (Karp, 2009). The intrinsic and extrinsic pathways converge at Caspase-3 and Caspase-3 cleaves inhibitor of caspase-activated deoxyribonuclease (ICAD) to release CAD. CAD then degrades chromosomal DNA in the nucleus and causes chromatin condensation (Sakahira et al., 1998).

In the cancer state, tumour cells are often resistant to apoptosis. The best-known tumour suppressor gene, p53 is known to be involved in the induction of apoptosis. Activation of p53 is known to be a central event in HCC development as p53 dependent mitochondrial mediated apoptosis is often inhibited in HCC (Meng et al., 2014). The reduced expression of apoptotic proteins such as Bad and Bcl-2 are also associated with

poor prognosis of HCC (Hu et al., 2015). In breast cancer, PRH overexpression leads to increased apoptosis in the MCF7 cell line indicating that PRH has a role in apoptosis but the mechanism associated with this change is not known (Kershaw et al., 2017).

1.4.4 Metastasis and epithelial-mesenthymal transition (EMT)

Metastasis is a multi-step process used to describe the spread of a tumour from a primary organ to distant sites in the body. The metastasis process is facilitated by changes in cell morphology and behaviour known as epithelial- mesenchymal transition (EMT) (Nguyen et al., 2009). EMT promotes tumour cell invasion through the basement membrane and into the bloodstream, thus the tumour gains the ability to metastasize (Chaffer and Weinberg, 2011). EMT is a process in which epithelial cells obtain a mesenchymal phenotype and occurs during development and is critical for the generation of tissues and organs. It involves the loss of cell adhesion and communication through the destruction of tight, gap and adherens junctions, cytoskeletal re-organization and loss of apical polarity (Thiery and Sleeman, 2006). EMT can be characterized by the loss of adhesion molecules, such as E-Cadherin and Claudin, and increased expression of mesenchymal markers such as N-Cadherin, Vimentin, and the transcription factors Slug, Twist and Snail (Kalluri and Weinberg, 2009; (Peinado et al., 2004). A hallmark of EMT is the downregulation of E-Cadherin. Cadherins are cell surface glycoproteins responsible for Ca+ dependent cell-cell adhesion, growth, differentiation and maintaining the integrity of multicellular structure. As mentioned earlier, β-catenin, a co-activatory TF in the Wnt signaling pathway, is linked to the p120 cadherin-associated complex. β-catenin is bound to α-catenin, which allows the complex to make contact with the actin filaments and strengthening adhesion. As E-cadherin is produced

in the endoplasmic reticulum, it associates with β-catenin, and they translocate to the cell surface together. Binding of β-catenin is regulated by phosphorylation, and a decrease in the binding of β-catenin leads to proteasomal breakdown of E-cadherin (Saitoh et al., 2009).

Vimentin is a mesenchymal marker that is often found to be highly expressed in metastatic tumour types such as prostate cancer, gastrointestinal cancer and breast cancer (Satelli and Li, 2011). Claudin is an important component of tight junctions that maintain cell-cell contact. The tight junction is usually lost in the cancer state when cells become metastatic and invasive. Loss of Claudin expression is reported to be associated with poor prognosis in cancer patients (Morin, 2005).

In cancer cells, EMT TFs such as Twist, Zeb1, Snail and Slug are often aberrantly overexpressed and this leads to the loss of E-cadherin expression because the EMT TFs are known to bind to the E-cadherin promoter and directly repress expression of *CDH1* gene (Qin et al., 2019). The TFs involved in regulating expression of E-cadherin and Vimentin contribute to carcinogenesis. Zeb1 upregulates expression of Vimentin in HCC and thereby promotes tumour growth (Qin et al., 2019). Key TFs in EMT including Snail, Twist and Slug are reported highly expressed in HCC and are responsible for the metastatic change in HCC (Kasamatsu et al., 2004; Yang et al., 2009).

Many growth factors including TNFα and TGF-ß as well as inflammatory TFs such as NF-κB induce expression of the EMT TFs as well as elevating the activity of the Notch and Wnt signaling pathways. It is known that TGF-ß can induce EMT by altering expression of Snail which then forms a complex with the TGF-ß target protein SMAD3/4 that represses E-cadherin (Padmanaban et al., 2019). In prostate cancer, TGF-ß mediated

downregulation of PRH was demonstrated and was associated with EMT plasticity (De Assis Jr et al., 2020). The TGF-ß/SMAD pathway also interacts with Notch and Wnt signaling pathway. SMAD3 mediates the activation of Notch by TGF- ß and triggers increased expression of Notch downstream targets including *JAG1* and *HEY1* in myogenic cells (Blokzijl et al., 2003). The Notch downstream targets then induce *SNAI2* (Slug) expression and thereby reduce E-cadherin expression causing EMT (Leong et al., 2007).

Wnt signaling can regulate EMT through stabilizing Snail and ß-catenin in the presence of Wnt (Yook et al., 2006). It is also reported that the Wnt signaling pathway can regulate E-cadherin expression by repressing *CDH1* gene expression by binding with the TCF/β-catenin complex at *CDH1* promoter (Conacci-Sorrell et al., 2003).

It is noteworthy that EMT promotes invasion but does not always promote metastasis. Recent studies in a mouse model show that complete EMT is not always required for metastasis, it was reported that although decreased E-cadherin results in increased local invasion, its loss also reduces cell proliferation and survival and thereby decreases metastatic spread (Padmanaban et al., 2019). Thus, the role of E-cadherin in tumour growth and in metastasis is different.

1.4.5 Metastasis and anoikis resistance

Cells often undergo apoptosis after losing contact with neighbouring cells and this is termed anoikis. In order for the cells to survive after detachment, cancer cells develop anoikis resistance (Frisch and Francis, 1994). The intrinsic pathway is activated during anoikis. Anoikis is regulated by the Bcl-2 family, rapid translocation of Bax (a Bcl2 family protein) to the mitochondria causes release of cytochrome-c and activates apoptosis

upon caspase activation (Valentijn et al., 2003). There are at least three mechanisms of anoikis resistance. First is the inhibition of Caspase-8 by an endogenous inhibitor FLICE-inhibitory protein (FLIP) (Scaffidi et al., 1999). The second mechanism of anoikis resistance is the activation of PI3K/Akt pathway. This pathway is inhibited in normal cells by several factors including phosphatase and tensin homolog (PTEN) and GSK3β (Wyatt et al., 2014). Malignant cells gain anoikis resistance either through reduced PTEN expression or PTEN mutation (de Sousa Mesquita et al., 2017). The third mechanism of anoikis resistance is increased EMT. In a mouse model, depletion of E-cadherin expression was shown to increase cell survival after the cells lose adhesion to the ECM (Derksen et al., 2006). The crosstalk between EMT and the apoptosis signaling pathway is the reason why EMT has a role in anoikis resistance as some of the EMT regulators such as Snail and Twist also regulate genes involved in apoptosis. Snail represses E-cadherin expression to induce EMT and it is also reported to block Caspase-3 by downregulating PTEN to activate the pro-survival signal PI3K-Akt pathway which then leads to reduced apoptosis (Barrallo-Gimeno and Nieto, 2005).

1.4.6 Immune evasion

In order for the tumours to survive in the body, it must be able to evade the immune system. Immune editing is key to how tumours evade surveillance causing the tumours to lie latent in patients for years before re-emerging. Significant progress has been made to understand the molecular mechanisms underlying tumour evasion and the failure of immune surveillance, which ultimately contribute to tumour growth and metastasis. These mechanisms include immunosuppression driven by defects in anti-tumour immune response mediated by classical CD8+ cytotoxic T lymphocytes (CTL) and natural

killer (NK) cells. T regulatory (T_{reg}) cells are crucial immune cells that generate antigenic tolerance and promote cancer progression by suppressing anti-tumour immunity. It is reported that PRH has a role in inhibiting T_{reg} cell differentiation but it is not known if this contributes to reduced cancer progression (Jang et al., 2019). Tumours are also known to attack the immune system by switching the balance from Th1 to Th2 (immune deviation) in a TGF-β- and IL-10-dependent manner.

1.5 Liver and bile duct development

It was previously mentioned that cell signaling is required for normal embryonic development and proliferation. The activation of developmental signaling is often involved in cancer development. Here we describe the main events of liver and bile duct development in the embryo and the major signaling pathways that are involved.

1.5.1 Initiation of liver development

The liver develops from the endoderm and is one of the 3 germ layers formed during gastrulation (Zaret and Grompe, 2008). The endoderm gives rise to many organs including thyroid, pancreas and the liver. Hepatic specification occurs at E8.25 (Day 22 in human) and albumin is the first molecular evidence of liver development (Zaret and Grompe, 2008). The TF HNF1β stimulates expression of the TF FoxA in the prehepatic endoderm. Lack of HNF1β leads to impairment of hepatic specification (Xu et al., 2011). The expression of HNF1β is under the control of Notch signaling. Collectively, FoxA, GATA4 and HNF1β are important initiators of liver development.

Hepatic specification is induced by endoderm cells responding to extracellular signals. Fibroblast growth factor (FGF) is secreted by the cardiogenic mesoderm induced by

hepatic genes (Xu et al., 2011). However, FGF signaling from the cardiogenic mesoderm is not sufficient for hepatic specification. FGF as well as bone morphogenetic protein (BMP) produced by the septum transversum induces hepatic gene expression (Rossi et al., 2001). Wnt signaling was also shown to be important in liver induction. When the primitive gut becomes patterned along its anteroposterior axis, Wnt signaling must be repressed anteriorly to maintain foregut identity and to allow subsequent liver development. This repression depends on the appropriate secretion of Wnt inhibitors by the endoderm (McLin et al., 2007; Nejak-Bowen and Monga, 2008). At this stage, PRH is expressed restrictedly at the foregut definitive endoderm (Bort et al., 2004). PRH controls the proliferation rate and the positioning of the ventral foregut endoderm before the liver bud formation. In *PRH*$^{-/-}$ mice, there is no liver formation yet foregut development is normal and there is initial hepatic specification, but the liver bud fails to form by the liver precursor cells (Bort et al., 2004). This indicates that PRH targets genes in the ventral foregut endoderm, but little is known about the downstream signaling targets of PRH in this stage.

1.5.2 Formation of liver bud

The liver diverticulum forms from the primitive gut when the endoderm cells have been specified at day 22 in human (Severn, 1971). Endoderm cells called hepatoblasts line the diverticulum and become columnar and proliferate to develop the liver bud. Transcription factors have important roles in the formation of the liver bud. PRH promotes interkinetic nuclear migration of the hepatoblast so that they become columnar and also promotes hepatoblast proliferation (Hunter et al., 2007; Zhao et al., 2005). Studies showed PRH expression in anterior foregut endoderm adjacent to the

developing heart at E8.5 in mice (Martinez Barbera et al., 2000). This endodermal tissue forms the hepatic diverticulum, which interacts with the pre-cardiac mesoderm to begin formation of the liver and biliary tract in mice (Hallaq et al., 2004). Null mutation of PRH leads to failure to form the liver bud and results in a small and cystic liver due to loss of HNF4α and HNF6 expression in early hepatoblasts (Hallaq et al., 2004; Hunter et al., 2007). In the adult liver, PRH is found only expressed in differentiated hepatocytes suggesting that PRH plays a role in maintaining liver differentiation (Manfioletti et al., 1995). Hepatocyte nuclear factor (HNF) 1α is a liver-enriched transcription factor involved in liver differentiation and is also a HD protein of the POU domain subclass. This protein interacts with PRH homeodomain through its POU-homeodomain (Tanaka et al., 2005). As HNF1α plays a role in liver differentiation and the expression of PRH promotes differentiation, it is thought that PRH contributes to liver differentiation through interaction with HNF1α (Tanaka et al., 2005). In addition, PRH regulates the expression of HNF4α and HNF6 in early hepatogenesis and dysreguation of PRH leads to loss of HNF4α and HNF6 and thereby impairs normal hepatic structures in the late liver development process (Hunter et al., 2007). Further *in vitro* studies showed that PRH is necessary for a model of hepatic cell differentiation by repressing vascular endothelial growth factor (VEGF) signaling (Arterbery and Bogue, 2016). PRH was found to negatively regulate hepatocyte proliferation in liver development in this model.

1.5.3 Liver expansion

Once the hepatoblasts extend to the septum transversum, hepatoblasts continue to proliferate and the liver further expands. This process is regulated by several TFs, furthermore, Wnt signaling mediated by β-catenin is also responsible for cell

proliferation. Wnt binds to its receptor, Frizzled, inactivating the β-catenin degradation complex and this allows β-catenin to dissociate from the complex, to translocate to the nucleus, and bind to TCF/LEF transcription factors to control the transcription of Wnt target genes. Moreover, β-catenin seems to act as a central node at the intersection of multiple signaling cascades. It binds to HGF receptor, c-MET in hepatocytes and translocates to the nucleus upon HGF simulation (Apte et al., 2006).

1.5.4 Segregation of hepatobiliary lineage and bile duct formation

Hepatoblasts are the precursor of hepatocytes and cholangiocytes, and start to differentiate into hepatocytes and cholangiocytes at 56-58 days of gestation in humans. Hepatoblasts differentiate into a monolayer of cholangiocytes that forms the ductal plate (Ruebner et al., 1990).

Ductal plate formation around the portal vein branches is the first sign of bile duct development. Sox9 is the earliest biliary marker but it is not clear when the peripheral hepatoblasts commit to the biliary lineage (Antoniou et al., 2009). Sox9 is detected in endodermal cells in the diverticulum and its expression disappears once the hepatoblasts invade the septum transversum. Sox9 is re-expressed in the subset of cells near the portal vein and is restricted to the biliary lineage throughout liver development. *SOX9* is a direct target of Notch signaling as Notch1 expression upregulates *SOX9* expression *in vivo* by directly binding to the *SOX9* promoter region (Zong et al., 2009). *HES1*, one of the target genes of Notch signaling lies downstream of *SOX9* (Antoniou et al., 2009). Therefore, it is possible that Notch and Sox9 form a positive feedback loop. CK19 is another specific marker of biliary cells. The cholangiocytes precursors express higher CK19 than hepatoblasts as they differentiate and become columnar and form a

bilayer of CK19+ cells. The cholangiocytes then bud off from the ductal plate and form tubules.

A number of growth factors are involved in regulating the hepatoblast differentiation process including TGFβ, Notch ligands, Wnt ligands. PRH is another important transcription factor that is required in the differentiation of hepatoblasts as well as the morphogenesis of the extrahepatic bile duct. PRH knockout mice showed that the extrahepatic bile duct was absent (Hunter et al., 2007).

The TGFβ signaling pathway was the first pathway shown to regulate liver cell differentiation. A gradient of TGFβ/Activin with high levels in the periportal region and low levels in the parenchymal and this gradient is crucial for biliary differentiation because blocking the TGFβ pathway *in vivo* represses biliary differentiation (Clotman and Lemaigre, 2006). TGFβ induces expression of the biliary marker, Sox9 and represses the expression of hepatocyte marker, HNF4α(Margagliotti et al., 2007).

Notch signaling is required for ductal plate and tubule formation (Lozier et al., 2008). Upon ligand binding, the Notch intracellular domain translocates to the nucleus and mediates gene transcription when it associates with the DNA binding protein RBPJ (CSL). The formation of this complex increases the expression of biliary markers including HNF1β and Sox9, and downregulates hepatic markers such as HNF1α and HNF4 (Tchorz et al., 2009). Notch2 is essential for ductal plate formation as Notch2 knockout leads to complete absence of ductal plate in mice (Falix et al., 2014). This Notch2 knockout study showed that reduction of Notch2 expression affects the differentiation of hepatoblasts into cholangiocytes (Falix et al., 2014).

Another important effect of Notch signaling in bile duct development is the formation of the tubule that builds the architecture of the bile duct tree. Impaired Notch signaling in bi-potential hepatoblast progenitor cells (BHPCs) dose-dependently decreases the density of peripheral intrahepatic bile ducts, whereas activation of Notch1 results in an increased density (Sparks et al., 2010).

It was shown in a murine study that a specific Wnt ligand, Wnt3A induces bile duct differentiation which is characterized by the production of tubule-like structures found in the mice liver and the expression of CK19. Wnt/β-catenin signaling is crucial in the biliary lineage by repressing hepatocyte differentiation and promoting ductal plate remodeling. β-catenin knockout in developing hepatoblast leads to defects in hepatoblast survival and differentiation (Tan et al., 2008).

For the hepatocyte lineage, hepatoblasts express HNF4α, which is one of the genes that is expressed in mature hepatocytes, and is critical for their fate determination. PRH was shown to promote the hepatic lineage as well in the human embryonic stem cells by repressing eomesodermin (Watanabe et al., 2014).

1.5.5 Bile acid synthesis and regulation

Bile acids promote emulsification of lipids and are made up of cholesterol. Bile acids are made in the liver by hepatocytes through enzymatic reactions (Lefebvre et al., 2009). The majority of bile acids are reabsorbed in the intestine and return to the liver through the hepatic portal vein. The primary bile acids consist of cholic acid and chenodeoxycholic acid. Secondary bile acids are derived from the primary bile acids including deoxycholic and lithocholic acids through the action of the intestinal bacterial flora (Lefebvre et al., 2009). The bile acid is synthesized in the liver by cholesterol

conjugating to glycine or taurine and secreted into bile with increased solubility in response to fat. Bile acids not only promote absorption of fat but are also important in regulating epithelial cell proliferation, gene expression and lipid glucose metabolism. Dysregulation of bile acid synthesis can itself leads to oncogenesis or other disease. As bile acids are cholesterol with detergent properties, a high concentration of bile acids can lead to damage of the cell membrane and leads to the destruction of the intestinal epithelium.

The farnesoid X receptor (FXR) plays a central role in regulating bile acid synthesis and lipid metabolism (Lefebvre et al., 2009). The FXR can bind to both free and conjugated bile acids and also binds to an inverted repeat of an AGGTCA-like sequence at the FXR promoter leading to activation of gene transcription (Parks et al., 1999). Mouse experiments showed that FXR deletion leads to increased bile acids pool size and increased incidence of hepatocellular carcinoma (HCC) (Jansen, 2007). PRH is one of the target genes of FXR in mouse hepatocytes and the HepG2 cell line and FXR mediates transcription activation of PRH by binding to PRH at intron 1 (Xing et al., 2009). However, little is known about the molecular function of PRH in bile acid regulation.

1.6 Liver cancers

1.6.1 Hepatocellular carcinoma (HCC)

HCC is the most common primary liver cancer derived from hepatocytes. HCC is often associated with chronic liver diseases such as chronic hepatitis, HBV and autoimmune hepatitis and these lead to liver cirrhosis. There are many treatment options for HCC including surgical resection, liver transplantation, various chemotherapies and

radiotherapies (Goossens et al., 2015). The survival rate of HCC is low, with less than 50% 2 year survival due to late diagnosis (Golabi et al., 2017). Genome-wide analysis shows that *CTNNB1* mutation is the main driver of HCC causing immune suppression in patients with HCC. Commonly mutated genes such as *TP53*, mediator of Wnt and PI3K pathways are also reported to be frequently mutated in HCC. PRH acts as a tumour suppressor in HCC as PRH inhibits the activity of c-Myc through direct protein-protein interaction resulting, in inhibition of tumour growth (Marfil et al., 2015; Su et al., 2012b).

1.6.2 Cholangiocarcinoma

Cholangiocarcinoma (CCA) is the second most common primary liver cancer after HCC and accounts for 10% to 20% of primary liver cancer with poor prognosis. The incidence is increasing worldwide although CCA is a rare cancer in most countries (Blechacz, 2017). CCA refers to a heterogeneous group of malignancies of bile ducts that carry bile produced from the liver to the gall bladder and the small intestine. CCA arises from the epithelial cells of the biliary tract. There is currently no specific biomarker for CCA and only 30% of patients with CCA are eligible for surgery as patients usually present with metastatic CCA and therefore are not eligible for surgical resection (Cillo et al., 2019). CCA can arise from any part of the bile duct and this cancer is classified according to the anatomic location it arises from. Intrahepatic bile duct cancer arises from the bile duct tree within the liver and extrahepatic bile duct cancer affects bile ducts that are outside the liver. Hilar bile duct cancer arises from the junction of left and right hepatic ducts and distal bile duct cancer affects the bile duct area that is connected to the small intestine and pancreas (Razumilava and Gores, 2013).

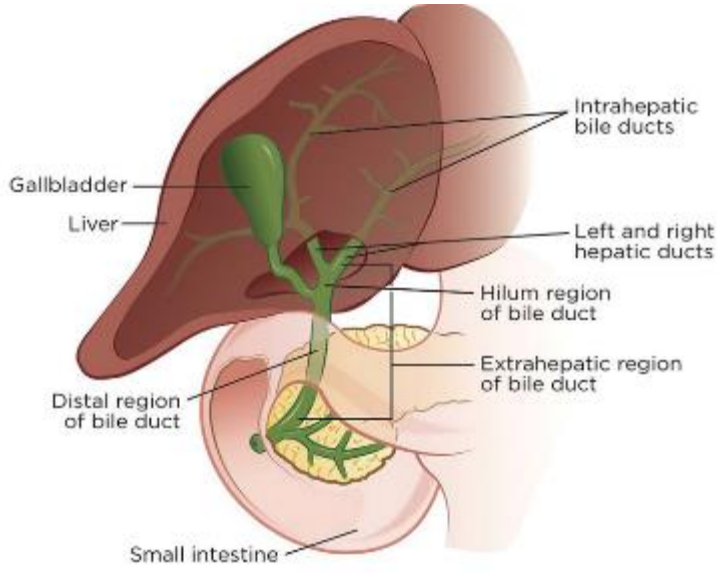

Figure 1.7 The anatomy of the liver and bile duct. Adapted from (Memorial Sloan Kettering Cancer Center).

1.6.3 Risk factors for CCA

The epidemiology profile of CCA exhibits geographical variation due to the exposure to different risk factors. Its incidence is relatively much higher in Asian countries especially in North Thailand, whereas in Europe, it is a rare cancer. The cause of CCA is not well defined but its risk factors are well established. Patients who suffer from chronic inflammation in the biliary tract have a higher risk for CCA (Blechacz, 2017).

Parasitic infection, primary sclerosing cholangitis (PSC), biliary-duct cysts, hepatolithiasis, and toxins are some of the causes of inflammation in the bile duct and they are well-established risk factors for CCA. In Asian countries, especially in Thailand, liver fluke (Opisthorchis viverrini) is a major risk factor for CCA and is claimed by the World Heath Organization (WHO) to be a causative agent. Liver fluke can be found in fresh water in Asian countries. In Thailand, people consume raw fish infected with liver flukes in their diet and are at risk of infection by the parasites. After infection, liver flukes can exist within the liver and the bile ducts and this eventually causes liver fluke

dependent physical damage to the bile duct as their growth injures the wall of the bile duct leading to ulcers (Pinlaor et al, 2013). Bile duct obstruction can also result from the parasitic infection and this increases bile duct pressure (Pinlaor et al, 2013). The physical damage to the bile duct leads to inflammation and is accompanied by a wound healing process that promotes the development of CCA. In addition to the physical damage of the bile duct by the parasites, the immune response causes more damage to the epithelial cells of the bile duct. Infiltration of inflammatory cells and cytokines are associated with the presence of the parasitic antigens in the biliary epithelium (Sripa and Kaewkes, 2000). One of the major inflammatory cytokines is interleukin 6 (IL-6). A high level of circulating IL-6 causes severe fibrosis around the parasitic infection area in the bile duct (Sripa et al., 2012). *In vitro* studies have shown that IL-6 promotes the proliferation of CCA by activating the expression of progranulin through the Akt-pathway in Mz-ChA-1 cells (Frampton et al., 2012). The release of oxygen radicals including nitrogen oxide (NO) and immune effector cells, such as macrophages, also play a major role in biliary epithelium injury (Pinlaor et al., 2004). These oxygen radicals can induce oxidative DNA damage to the biliary epithelium and the excessive NO produced by the immune cells has both cytotoxic and mutagenic effects and causes uncontrolled cell proliferation that leads to CCA (Miwa et al., 1987; Nguyen et al., 1992).

For European countries, primary sclerosing cholangitis (PSC) is the best-known risk factor for CCA but PSC is a rare disease. PSC is a chronic liver disease characterized by decreased bile flow (cholestasis) with inflammation and fibrosis of the intrahepatic and extrahepatic bile ducts (Sripa and Kaewkes, 2000). About 5% to 10% PSC patients develop CCA (Burak et al., 2004). Local production of inflammatory cytokines including

IL-6, NO and reactive oxygen species were detected in PSC lesions and the accumulation of DNA damage leads to transformation and CCA in PSC patients (Bonato et al., 2015). After malignant transformation, the neoplastic cholangiocytes release cytokines, chemokines and growth factors that induce stromal reaction and promote the invasive property of CCA. For example, platelet-derived growth factor (PDGF)-D plays a major role in mediating tumour-stromal interactions in CCA and stimulates the recruitment of oncogenic fibroblasts to promote invasion (Cadamuro et al., 2013). In both European and Thai cancers that are initiated by PSC or liver fluke infection, a common finding is that chronic uncontrolled inflammation is associated with the development of CCA.

1.6.4 Treatment for CCA

Surgical resection is the main curative treatment for CCA with the median survival duration of 12 to 36 months (Rizvi et al., 2018). However, patients often present with late stage metastasized malignancy and are not eligible for surgical resection. The standard treatment in the UK for patients who are not operable is chemotherapy with Gemcitabine and Cisplatin and the median survival is 11 months (Valle et al., 2010). The molecular heterogeneity of CCA leads to a lack of effective target therapy. Molecular aberration in CCA was investigated using integrated genomic analysis and a clinical trial is ongoing with the potential targets identified in the analysis. For example, receptor tyrosine kinase *FGFR2* fusions were identified in the study and an inhibitor of the kinase is currently in phase II clinical trial with manageable safety profile (Rizvi et al., 2018). The integrated genomic analysis showed that the proto-oncogene *KRAS* is mutated in 11-25% of CCA (Farshidfar et al., 2017). The activation of *KRAS* leads to upregulation of the MAPK pathway. An inhibitor of MEK, selumetinib, has shown median survival of 9

months in phase II clinical trial (Bekaii-Saab et al., 2011). The cell cycle gene *CDKN2A* encoding $p16^{INK4A}$ and $p14^{ARF}$ are negative regulators of the cell cycle and the loss of this gene is seen in 47% of CCA highlighting the potential of CDK4/6 inhibitor in treating CCA (Farshidfar et al., 2017a). CDK4/6 inhibitors is currently approved for breast cancer and is being evaluated in patients with CCA. Identification of genetic aberrations in CCA is important in establishing targeted therapy for CCA.

1.6.5 CCA cells origin

The cell of origin refers to the normal cell that receives the first cancer-causing mutation (Rycaj and Tang, 2015). In contrast, cancer stem cells are cells that sustain tumour growth and propagation (Visvader, 2011). The cell of origin in CCA exhibits enormous heterogeneity. Recent studies suggest that CCA has multiple cells of origin including differentiated cholangiocytes in ductules, the cholangiocytes within the peribiliary gland around the bile duct, and hepatic progenitor cells (Rizvi and Gores, 2013). It was shown that transformed hepatocytes, hepatoblasts and hepatic progenitor cells all facilitate development of liver malignancies ranging from CCA to HCC in mouse models (Holczbauer et al., 2013). It was suggested that cholangiocytes alone are not solely responsible for the development of CCA as CCA can involve the transformation of multiple cell types. For example, hepatocytes transform to biliary cells through activation of the Notch pathway and this leads to ICC development (Lu et al., 2016; Sekiya and Suzuki, 2012).

1.6.6 Genomic heterogeneity and molecular pathogenesis in CCA

The genomic heterogeneity of CCA is not only related to its anatomical location but also

associated with diverse risk factors. Gene mutations are often involved in cancer development. In CCA, the most common genetic mutations include *TP53* and *KRAS*. *TP53*, is a master regulator of genomic stability and has a mutation rate of 20% in CCA (Farazi et al., 2006). However, it is not known whether the mutation rate of *TP53* varies in the different subtypes of CCA. The alteration of p53 is associated with changes in the composition and the metabolism of cytotoxic biliary constituents (Furubo et al., 1999). Gene sequencing experiments revealed that there are more than 90 different types of *TP53* mutation in CCA (Khan et al., 2005). *TP53* mutation can be caused by liver fluke infection as products of the liver fluke metabolism can induce GC-AT transition in the *TP53* gene (Kamikawa et al., 1999).

KRAS mutations are found in both ECC and ICC and occur in early malignant progression from biliary intraepithelial neoplasia to ICC (Hsu et al., 2013). Patients presenting with mutations in *TP53* or *KRAS* have significantly lower survival rates (Churi et al., 2014). Smad4 is a transcription factor that mediates TGFβ activation and the SMAD4/TGFβ pathway negatively regulates epithelial cell growth (Miyaki and Kuroki, 2003). Loss of *SMAD4* expression is a hallmark for gastrointestinal cancer and it has frequently been observed in CCA (Kang et al., 2002).

Large scale genomic sequencing experiments have been performed by several research groups, in which one of the studies identified common mutations in liver fluke-related CCA and non-liver fluke related CCA (Jusakul et al., 2017). *ERBB2* amplifications and *TP53* mutations occur in liver fluke positive CCA whereas in liver fluke negative CCA, high copy-number alterations or epigenetic mutations such as Isocitrate Dehydrogenase (*IDH1/2*) were identified in whole-genome analysis (Jusakul et al., 2017). *RASA1*

encoding RAS P21 Protein Activator 1 (RASA1) was also found to be mutated and silencing of *RASA1* in CCA cell lines inhibits cell migration and invasion (Jusakul et al., 2017). Another large scale genomic study also identified *IDH* mutation leads to altered mitochondrial activity and chromatin modification in CCA (Farshidfar et al., 2017a). *IDH* mutation causes production of a metabolite D-2-hydroxyglutarate which is usually found in low levels in normal cells. High levels of D-2-hydroxyglutarate modulates the activity of metabolic and epigenetic tumour suppressor enzymes and thereby promotes cancer development (Reitman and Yan, 2010). Genome-wide approach also revealed genetic alteration differences between patients with intrahepatic CCA and extrahepatic CCA. It was found that *KRAS* mutations are common in both intrahepatic and extrahepatic CCA (Banales et al., 2020). The research group also found that *FGF2* fusions and *IDH* mutations are more common in intrahepatic CCA than in extrahepatic CCA (Banales et al., 2020). However, little is known about the common gene mutation in extrahepatic CCA. CCA Although genomic approaches yielding gene mutations and alterations are important in driving CCA, the genomic background of CCA remains heterogeneous. Most of the mutations or genetic alterations discovered in these studies are found in less than 10% of the study cohort.

1.6.7 Notch and CCA development

Several studies have shown that Notch signaling needs to be activated in CCA development and that Notch3 is a driver for CCA (Guest et al., 2016; Kodama et al., 2004). Knocking out the *NOTCH3* gene in mice causes attenuation of tumour growth and it was found that Notch3 works to encourage cancer cell survival via activation of the PI3k-Akt pathway (Guest et al., 2016). In CCA, integrated microarray analysis showed

that Notch signalling is one of the pathways most often involved in CCA (Jiao et al., 2018). Patients with overexpression of at least one of the Notch receptors are associated with poor prognosis. A recent study reported that most ICC tissue samples overexpress the Notch ligand, Jagged 1 (Hofmann et al., 2010). Animal models demonstrated that activated Notch signaling can transform both hepatic progenitor cells and differentiated hepatocytes into cholangiocytes leading to formation of CCA (Lu et al., 2016).

Among the four Notch receptors, the Notch1 receptor is the most studied and is strongly associated with the development of CCA. It was found that in four human CCA cell lines including TFK1, MzChA1, EgI1 and SZ1, Notch1 receptor and its ligand Jagged1 are overexpressed and promotes cell migration (Zender et al., 2013). Upregulated Notch1 expression also leads to EMT in that there is a loss of E-cadherin expression accompanied by increased Vimentin (Timmerman et al., 2004). In the mouse liver, stable overexpression of the Notch1 intracellular domain (NICD1) induces cystic cholangiocellular tumours after a long latent period. Another study using an anti-Notch1 antibody showed high occurrence of CCA-like tumours with reducing development of HCC-like tumours (Huntzicker et al., 2015). These findings suggested that overexpression of Notch1 contributes to the growth of CCA instead of promoting hepatocyte differentiation towards biliary cells. Notch2 is associated with normal bile development (Kodama et al., 2004). Notch2 expression is often upregulated in well-differentiated CCA. PTEN is a negative regulator of the Akt pathway and it often acts as a tumour suppressor (Oliva-González et al., 2017). A study using a PTEN-deleted mouse model showed that the Notch2 receptor is also highly expressed in PTEN deleted liver progenitor cells and inhibition of Notch2 receptor markedly suppresses CCA growth

(Wang et al., 2018). Moreover, Notch2 signaling is activated in AKT/Ras mice. Notch2 inhibition in these mice inhibits tumour formation and significantly reduces the existing tumour burden (Huntzicker et al., 2015).

Notch3 overexpression promotes CCA development by promoting CCA cell survival through PI3K-AKT pathways. It was demonstrated using mice with constitutive deletion of the Notch 3 gene that loss of a single copy of the *Notch3* gene is sufficient to inhibit growth of CCA (Guest et al., 2016). The role of Notch 4 in CCA is not well-established. CA125 is one of the biomarkers for diagnosing CCA. Current studies showed that Notch4 overexpression is associated with high serum levels of CA125 and poor prognosis (Wu et al., 2014).

1.6.8 Wnt signaling and CCA development

Dysregulation of the Wnt signaling pathway also contributes to the development of CCA. The canonical Wnt signaling pathway is upregulated in CCA (Loilome et al., 2014), and this in turn activates expression of cell cycle genes including *CCND2* and *CDKN2A* and promotes cell proliferation (Boulter et al., 2015). Xenograft experiments demonstrated that Wnt7B in tumour stroma is derived from recruited bone marrow-derived macrophages, and that these cells play a key role in CCA progression (Boulter et al., 2015). *In vivo* experiments also demonstrated that macrophage ablation inactivates the canonical Wnt cascade due to loss of Wnt7B expression and this results in a reduced number and volume of tumours (Boulter et al., 2015). *In vitro* experiments demonstrated that β-catenin knockdown can inhibit the growth of CCA by reducing the expression of the cell cycle protein, Cyclin D1 and can also inhibit cell proliferation (Loilome et al., 2014).

1.6.9 EMT and CCA

As with other cancer types, the EMT pathway plays a major role in CCA. The prognostic values of EMT associated proteins were evaluated in patients with CCA. The research showed that low expression of E-cadherin, and high expression of N-cadherin, Vimentin and Snail are associated with a lower survival rate (Tian et al., 2019). In normal conditions, E-cadherin is localized at the plasma membrane in the biliary epithelium, whereas in the cancerous state, E-cadherin is downregulated and localizes in the cytoplasm (Németh et al., 2009). Loss of E-cadherin expression is found in about 80% of CCA patients by IHC staining (Settakorn et al., 2005). Claudins are important components of the tight junction that maintain junction integrity and their expression are found to be mostly down-regulated in CCA tissues (Németh et al., 2009b). Claudins-4 and Claudins-7 are suggested to be potential markers used for distinguishing CCA from HCC (Ono et al., 2016).

Apart from loss of E-cadherin, patients with CCA present with increased Vimentin expression. Vimentin knockdown in the cells results in no change in other EMT markers such as Claudin-1 and Zonula occludens-1 (ZO-1) and no activation of MMPs suggesting Vimentin is required for the cells to acquire metastatic property rather than altering EMT (Saentaweesuk et al., 2018). The inflammatory mediators present in the microenvironment of CCA disrupt the integrity of tight junctions in the biliary epithelium.

As mentioned earlier, TFs associated with inducing EMT in CCA include the Snail family of TFs. There are three proteins within the Snail family including Snail1 (Snail), Snail2 (Slug) and Snail3 (Smuc) (Nieto, 2002). Immunofluorescence staining showed that Snail

is highly expressed in the nucleus in tumour samples from patients with CCA (Cardinale et al., 2015). Snail expression stimulated by TNF-α is correlated with the presence of metastasis as Snail is negatively associated with E-cadherin expression (Techasen et al., 2012). Another member of Snail family, Slug, is a also a repressor of E-cadherin and has also been shown to be upregulated in CCA and is associated with lymph node and distant metastasis (Zhang et al., 2010). Slug is associated with poor prognosis and it is suggested to be a marker to predict the outcome of surgical resection in patients with CCA (Zhang et al., 2010). The Twist family consists of Twist1 and Twist2 and Twist3 has been found to be overexpressed in CCA (Duangkumpha et al., 2014). Upregulated Twist1 expression is associated with increased expression of N-cadherin suggesting that Twist is closely related to the mesenchymal phenotype of CCA (Duangkumpha et al., 2014). The Zeb family of EMT related TFs include Zeb1 and Zeb2. Both *ZEB* family members are highly expressed in CCA but have low expression in normal tissue (Techasen et al., 2014). Thus, EMT is an important process in CCA development and associated with the clinical prognosis of CCA.

1.7 Cell lines used in this research

Since PRH plays a role in hepatic and bile duct development, PRH is investigated in a range of CCA cell lines in this thesis. Cell lines from Europe and Thailand are used in this study because they are derived from patients with very different etiology of the cancer. Cell lines from Thailand are derived from patients with chronic liver fluke infections whereas cell lines from Europe are from a variety of etiologies. CCA cell lines from Europe include CCLP and CCSW and both were isolated from patients presenting with

poorly differentiated CCA. Both CCLP and CCSW cells present with tight junction complex and are capable of forming tumours in nude mice.

AKN-1 is an immortalized bile duct cell line which retains a differentiated cholangiocyte phenotype with expression of CK8, CK18 and CK19, but does not express albumin, a hepatocyte marker. Although AKN-1 cells were isolated from a normal healthy liver, the AKN-1 bile duct cells can also develop into tumours at low frequency when injected to nude mice (Nussler et al., 1999).

The Thai CCA cell lines used in this research are HuCCA, RmCCA, KKU-100 and KKU-213. HuCCA was isolated from a Thai patient diagnosed with intrahepatic CCA and stained positive with CK19 antibody (Sirisinha et al., 1991). RmCCA is derived from a patient diagnosed with peripheral CCA and is also positively stained by CK19 to verify its biliary epithelial origin (Rattanasinganchan et al., 2006). RmCCA showed *in vitro* a low degree of invasiveness but exhibits high motility. KKU-100 and KKU-213 are two CCA cell lines from Thailand that are derived from patients with CCA who were infected with liver fluke (Sripa et al., 2005). The cell lines were positively stained with antibody for CA125 but not CK19, p53 or c-met. Both KKU-100 and KKU-213 are capable of forming tumours in nude mice (Sripa et al., 2005).

In addition to the CCA cell lines, primary biliary epithelial cells (BECs) were extracted from human primary non-cancerous livers with Alcoholic Liver Disease (ALD).

The human livers used for isolation of BECs were obtained from Dr. Simon Afford in the University of Birmingham Liver Unit and were unsuitable for transplantation.

	Cells	Origin	Tumour formation in nude mice	References
European cell lines	AKN1	Cholangiocytes from normal human liver	Yes	(Nussler et al., 1999)
	CCLP	Human primary cholangiocarcinoma tissue	Yes	(Shimizu et al., 1992)
	CCSW	Human primary cholangiocarcinoma tissue	Yes	(Shimizu et al., 1992)
	HuCCA1	Human primary cholangiocarcinoma tissue	Unknown	(Sirisinha et al., 1991)
Thai cell lines	RmCCA	Human primary cholangiocarcinoma tissue	Unknown	(Rattanasinganchan et al., 2006)
	KKU-100	Human primary hilar cholangiocarcinoma tissue related to liver fluke	Yes	(Sripa et al., 2005)
	KKU-213	Human primary intrahepatic cholangiocarcinoma tissue related to liver fluke	Yes	(Sripa et al., 2005)
Primary cells	Biliary epithelial cells	Cholangiocytes isolated from patients with either fatty liver disease or alcoholic liver disease	No	NA

Table 1 The cell lines used in this study.

1.8 Aim of the research

PRH can act as a tumour suppressor or an oncogene in different cancer types. However, the role of PRH in CCA is not known. Therefore, this research will focus on investigating the role of PRH in CCA. As the treatment options for CCA are limited, new targets for drug treatments will be investigated and repurposing drug screening for new treatment appoaches will be discussed.

The main aims of my research project are as follows:

- To characterise PRH expression in a range of CCA cell lines and primary cells.
- To investigate the role of PRH in CCA in terms of its effect on cell proliferation, migration, invasion and colony formation by knockdown and overexpression experiments.
- To identify PRH target genes in CCA and the mechanism underlying this regulation.
- To develop novel drug treatments for CCA.

CHAPTER 2

Materials and Methods

2. Materials and Methods

2.1 Cell Culture Protocols

2.1.1 Adherent Cell Culture

CCLP, CCSW, AKN-1, KKU-100 and KKU-213 cells were cultured in Dulbecco's Modified Eagle Medium (DMEM)(D5796, Sigma), supplemented with 10 % foetal bovine serum (FBS)(F7524, Sigma), 1 % penicillin and streptomycin (5000 U/ml Penicillin and 5 mg/ml streptomycin (P4458, Sigma) and 1% non-essential amino acids (100x (M7145, Sigma)). Cells were grown in tissue culture flasks (T75) incubated in a humidified incubator at 37 °C with 5 % CO_2. HuCCA and RmCCA cells were cultured in the same conditions but used Fn12 media with 1 % penicillin and streptomycin without the supplementation of 1 % non-essential amino acids.

Passaging cells

For routine maintenance, cells were diluted one in fifteen when they were 90 % confluent, usually every 3 to 4 days. To detach the adherent cells, the medium was first removed from the flask and the cells were washed with 1x phosphate-buffered saline (PBS)(18912014, ThermoFisher). Cells were then trypsinized by 1x Trypsin-EDTA (T3924, Sigma) for 3 mins or until the cells detached at 37 °C. Once the cells were suspended, the trypsin was neutralized by resuspension in an equal volume of fresh complete media (DMEM with supplements) and transferred to a new T75 flask. Cells were checked on a daily basis using a light microscope for confluency and absence of infection.

2.1.2 Cryopreservation of cells

At 90% confluency, cells in a T75 flask (4 million cells) were frozen to maintain cell line stocks. The cells were detached from the flask by adding trypsin as described in section 2.2.1. The cells were pelleted by centrifugation at 500 g for 5 min. The supernatant was then discarded and the cell pellet was re-suspended in 1 ml of freezing medium consisting of 10% (v/v) of DMSO in their respective growth medium. The cell suspension was then transferred to a cryovial and placed inside a Mr Frosty (BDH) at room temperature that was then transferred to a -80 °C freezer. The cells were then stored in liquid nitrogen within a week for long term storage.

2.1.3 Thawing cells

Cells that were taken from liquid nitrogen were immediately thawed in a water bath at 37 °C. These cells were then transferred to 14 ml of pre-warmed complete medium in a T75 cell culture flask. The T75 flask containing the cells were placed inside the cell culture incubator. The medium was replaced by fresh complete medium the next day.

2.1.4 Mycoplasma Test

Mycoplasma tests using the EZ-PCR Mycoplasma Testing Kit (Biological Industries) was performed to ensure that there was no mycoplasma contamination according to the manufacturer's instructions. In brief, 1 ml of cell culture supernatant was centrifuged at 16,000 g for 10 min to sediment mycoplasma. The supernatant was then discarded and the pellet resuspended in 50 µl of buffer and heated at 95 °C for 3 mins. PCR for mycoplasma DNA was then carried out. The denaturing step was performed at 94 °C for 30 secs, amplification step at 94 °C for 30 secs, annealing step at 60 °C for 2 mins with

35 cycles. The PCR product was loaded on a 2 % agarose gel and visualized following gel electrophoresis.

2.1.5 Primary biliary epithelial cells (BECs) isolation

Primary BECs cell culture and media

Primary biliary cells (BECs) were cultured in 50 % DMEM (D5796, Sigma) and 50 % Fn12 media (F7524, Sigma), with 5 % heat inactivated FBS (F9665, Sigma), 0.01 % insulin (1 mg/ml)(RP10935, Gibco), 1 % of 1 µg/ml cholera toxin (C34779, ThermoFisher), 1 % of 200 nM Tri-iodo-thyronine (T3)(T6397, Sigma), 1 % of 2 µg/ml hydrocortisone (H0888, Sigma), 0.001 % of 100 µg/ml of hepatocytes growth factor (HGF)(H5791, Sigma) and 0.001 % of 100 µg/ml of epidermal cell growth factor (EGF)(E4127, Sigma). BECs were grown on a collagen coated T25 flask.

Collagen coated flask

10 µg /cm^2 of Collagen, Type I solution from rat tail (Sigma, C3867) was used to coat cell culture flask for primary cells. The 100 mg stock collagen was diluted 1:200 in 2 ml of sterile water and placed in a T25 flask using a pipette. The flask was left in the incubator at 37 °C for 3 hours or overnight at 4 °C. Excess liquid was then removed from the flask by washing with sterile PBS and the flask was left to dry overnight.

Preparation of collagenase

5 ml of a stock solution of 6.4 mg/ml Collagenase Type I (2x) (Worthington Biochemical Corporation) was filtered using a syringe with 0.2 µm filter. The filtered solution 5 ml was added to 45 ml of sterile PBS in a 200 ml beaker.

Preparation of the Percoll solution and gradient

Percoll (MFCD00131830, Sigma) was first diluted into a working stock: 100 % percoll. This was created by by adding 90 ml of the manufacture's stock percoll to 10 ml of 10x PBS. Two further working stocks of percoll were prepared. The first solution is 33% percoll diluted in PBS (33 ml 100 % stock plus 77ml 1x PBS) and the second solution is 77 % percoll diluted in PBS (77ml 100 % stock plus 33ml 1x PBS). To make the percoll gradient, 3 ml of 33 % percoll was first aliquoted into eight 15 ml falcon tubes. Then, 3 ml of 77% percoll was carefully dispensed underneath the 33% percoll without disturbing the 33% percoll layer.

Preparation of antibody and beads

10 µl of 0.5 mg/ml anti-CD326 (EpCAM) antibody (Thermofisher) was added to 10 µl of dynabeads (16203, Thermofisher).

Isolation of BECs

The liver slice was placed on a sterile petri dish and finely chopped using two sterile scalpels. The diced tissue was added to sufficient amount of collagenase in PBS (see above) up to a total volume of 100 ml and incubated in the humidified incubator at 37 °C and 5 % CO_2 for 30 mins. The digest was then filtered through a fine mesh with 2.36 mm pore size and the filtrate was collected in a fresh sterile beaker. The remaining digest on the mesh was washed with PBS several times until the total volume of filtrate reached 200 ml. The filtrate was aliquoted into eight 50 ml falcon tubes and centrifuged at 800 g for 5 mins. The supernatant was removed and discarded. The 8 pellets were each resuspended into 6 ml of PBS and the suspension was pooled into four 50 ml falcon tubes by adding PBS and then centrifuged. The 4 pellets were then resuspended each

into 6 ml of PBS and pooled into one 50 ml falcon tube. The pellet was then resuspended with PBS and made up to 24 ml. 3 ml of the cell suspension was added on top of each of the eight percoll gradients and centrifuged at 800 g for 20 mins with brake speed set at 0. The top fat layer was removed after centrifugation. The cells are found within the percoll and form a discrete band of tissue lysate. The cells from each gradient were removed carefully with a pipette and pooled in a 50 ml falcon. 14 ml of PBS was added to the pooled cells and mixed gently by hand. The isolated cells were then centrifuged for 5 mins at 800 g. The PBS was discarded without disturbing the pellet. The pellet was resuspended with 0.5 ml PBS and transferred into one 15 ml falcon tube. 20 µl of 0.5 mg/ml anti-CD326 (EpCAM) antibody (14-9326-82, Thermofisher) conjugated to Magnetic dynabeads (16203, Thermofisher) was added into the cells and incubated for at least 30 mins in the incubator. After incubation, PBS was added to the cells attached with beads and antibody to 10 ml in a 15 ml falcon tube. Isolation of the biliary cells from the tissues was achieved by positive selection of the beads bound to the biliary cells using a magnetic rack. The remaining PBS (containing other cell types) was removed and the beads/bile duct cells were resuspended in BECs media and placed in the collagen coated T25 flask described above.

2.1.6 Transient transfection of plasmid DNA

shRNA transfection

1 x 10^6 cells were plated to each well of a 6 well plate 24 hours before the transfections. Transient transfections were carried out using Polyethylenimine (PEI, 1 mg/ml) (408727, Sigma) diluted in H_2O (pH 7.5) when the cells reached 50 to 80 % confluency (approximately 2 million cells). For each confluent well of a 6-well plate, 2 µg DNA was

added to 100 µl of serum-free DMEM followed by 1 mg/ml PEI in dH_2O, pH 7.5. The mixture was vortexed for 10 seconds and incubated for 10 mins at room temperature. Media was removed from each well and 600 µl of DMEM with 10% FBS was added to the cells in each well. Then the PEI-DNA transfection mix was added to the cells. Cells were then incubated at 37 °C for 2 hours. After 2 hours, 2 ml of fresh DMEM with 10 % FBS was added on top of the transfection mix in each well and cells were incubated for 24 hours. The transfection media was then discarded and replaced with 2 ml of DMEM for 24 hours. Experiments were carried out on the cells 48 hours total after transfection.

siRNA transfection

Transient siRNA transfections were carried out using Lipofectamine 3000 (L3000001, Invitrogen) according to manufacturer instructions. For transfection of 0.5 x 10^6 cells, cells were trypsinzed in the T75 flask, cells were then washed, centrifuged and 0.5 x 10^6 cells were counted and plate plated in a single well of a 6 well plate, 3.75 µl of Lipofectamine was added to 250 µl of reduced serum media, Opti-Mem (pre-warmed), followed by 2.5 µl of 10 µM siRNA in an eppendorf (**Table 2**). The lipofectamine mixture was incubated at room temperature for 30 mins. This complex was then added to cell pellet containing 0.5 x 10^6 cells and incubated at 37 °C in 5 % CO_2 for 3 hours. After 3 hours each well was topped up with 2 ml of culture media.

Target	Source
VIM (5nmol)	Qiagen (SI00302190)
RB1 (5nmol)	Qiagen (SI00301651)

Table 2 SiRNA used in this study.

2.1.7 Generation of stable cell line

Determination of concentration of antibiotics for stable cell lines generation

Puromycin (Gibco, Life Technologies) at 10 mg/ml was used for CCLP cells selection after transfection with Origene shRNA plasmids and G418 (10131035, ThermoFisher) at 300 mg/ml was used for AKN-1 cells selection after transfection with pEGFP-PRH-Myc plasmids. Cells were plated in a 6-well tissue culture plate at a cell density of 1x 10^6 cells per well. Puromycin and G148 were added to 80 % confluent cells at a range of 0 to 1 µg/ml and the cells were incubated for 5 days. 5 days later, the lowest concentration of Puromycin and G148 that cause 100 % cell death was chosen to select transfected cells. For CCLP control and CCLP PRH KD cells, 0.025 µg/ml Puromycin was used for selection. For AKN-1 control and PRH overexpressing AKN-1 cells, 300 µg/ml G418 was used for selection.

Generation of stable cell line with antibiotics using negative selection

2 x 10^6 CCLP cells were transiently transfected with shRNA plasmids (pHushEVC (TR30012, Origene) and pHuSh-PRH-49 (TR312464, Origene) (see section 2.1.12 for map). PEI was used for transfection as described above in section 2.1.6. AKN1 cells were transiently transfected with pEGFP-PRH-Myc or pEGFP (see section 2.1.12 for the map). To produce a stable cell line, antibiotics were added to the medium 24 hours after the

PEI transfection with the shRNA plasmids and every 3 days thereafter to select the knockdown (KD) cells. After approximately 2 weeks, cell colonies were formed and the cells that were not transfected were killed by the antibiotics. Remaining clones on the 6-well plate were then expanded by transferring to a T25 flask to form a polyclonal knockdown population. After the cells were 90 % confluent, cells were then transferred to a T75 flask.

2.1.8 Adenoviral infection of cells

Stock adenovirus were obtained from Dr. G. Newby, University of Bristol who amplified the viruses in HEK293 cells and then purified them over a Caesium Chloride gradient. The number of plaque forming units (pfu) per ml was calculated by end point dilution in HEK293 cells (from Dr. G. Newby). For infection of cells, 1 x 10^6 of cells (CCLP and CCSW) were counted and re-suspended in DMEM with reduced serum (2 % FBS), 1% penicillin and streptomycin (P4458, Sigma) and 1% non-essential amino acids (100x (M7145, Sigma) and plated into each well of a 6 well plate. The cells were then infected with adenovirus containing either Myc-PRH (AdPRH), Myc-PRH-N187A (AdN187A) or Empty vector (AdEmpty). Viruses were added to the wells containing 2 ml of media with 1 x 10^6 cells to give the multiplicity of infection (MOI) of 50. The following equation was used to calculate the volume of viruses needed to infect 1 x 10^6 of CCLP cells.

MOI = (Volume of virus (L) x virus titre (pfu/ml))/number of cells to be infected

The virus titre for AdPRH is 1.515 x 10^{14}, therefore by using the equation above, it is 50 = (Volume of virus x 1.515 x 10^{14})/1 x 10^6

The volume of AdPRH required to infect 1 x 10^6 CCLP cells is 3.3 µl. The virus titre for AdN187A and AdEmpty is 2.18 x 10^{14} pfu/ml and 3.4 x 10^{14} pfu/ml respectively.

The cells were then incubated at 37°C overnight. The media in the wells was then replaced by normal culture media after 24 hours and the cells were incubated for another 24 hours and were then harvested for experiments 48 hours after initial infection.

2.1.9 Agarose Gel Electrophoresis

Agarose gels were cast by dissolving molecular grade agarose (Bio41026, Bioline) into 100 ml of 1x TBE electrophoresis buffer and was heated carefully by microwave until the agarose was dissolved. The 10x TBE buffer was made up of 1M Tris base, 1M Boric acid and 0.02 M EDTA. The 10x TBE was then diluted 1 in 10 using distilled water. 5 µl of 10 mg/ml Gel red (G725, GoldBio) was then added to the gel when it is cooled down to about 40 °C. The gel was then immediately poured into a gel casting tank and left to set for 30 min. The gel was placed in an electrophoresis tank and filled with TBE buffer. 6x DNA Hyperladder IV (Bio33056, Bioline) in loading blue buffer and DNA samples diluted into loading blue buffer were loaded into the gel. The gel was run at 100V with constant current for 30 min. Gel images were captured using SyngeneII gel doc system.

2.1.10 Plasmid transformation into *E.Coli*

Bacteria strain

Alpha-select gold efficiency, Bioline*: Escherichia coli* (*E. coli*) T1 Res: Genotype- F-deoR endA1 recA1 relA1 gyrA96 hsdR17(rk-,mk+) supE44 thi-1 phoA Δ(lacZYA-argF)U169 Φ80lacZΔM15 l.

Transformation

Competent cells (Alpha-select gold efficiency, Bioline) were thawed on ice and 50 ng of plasmids was added gently to the competent cells and incubated for 15 min. The cells were then heat shocked for 30 secs at 42 °C and placed on ice for 2 min. The competent cells with plasmid were then transferred to 500 µl Luria Broth (LB)(Sigma) in a flask and incubated for 1 hr at 37 °C in a shaker. 200 µl of bacterial culture was then spread onto LB agar plates containing 100 µg/ml ampicillin and incubated overnight at 37 °C.

2.1.11 Plasmid Maxi Preparation

A single colony was inoculated into a 5 ml culture grown overnight with shaking at 37 °C. 500 µl of bacterial culture from the overnight incubation was added to 200 ml of LB with antibiotics and grown overnight in a shaker at 500 rpm at 37 °C. The plasmids were extracted using an Endotoxin-free Maxi DNA kit (10023, Qiagen). The principle of this kit is that after lysis of the bacteria the DNA is passed over an anion exchange tip. The lysed sample is loaded into the tip and DNA binds selectively under low salt and pH conditions. Impurities are removed by medium salt washes. The DNA is then eluted with high salt solution and desalted using isopropanol. Briefly, the large bacterial culture from overnight incubation was centrifuged at 6000 g for 15 min at 4 °C and the pellet was re-suspended in 5 ml of Buffer P1 and then 5 ml of Buffer P2. Buffer P1 is a resuspension buffer that denatures protein and contains EDTA for destabilizing the bacterial membrane and inhibit DNases. Buffer P2 contains 1 % SDS and 200 mM NaOH that used conjucated with buffer P1 to destabilizing membrane and release DNA from cells. The lysate was then mixed until viscous and incubated at room temperature for 3 mins. 10 ml of ice-cold Buffer P3 was then added and transferred to Qiafilter cartridge. Buffer P3

is the neutralizing buffer used to stop the reaction from buffer P1 and P2. The lysate was incubated for 10 min at room temperature and filtered to a 50 ml falcon tube. 5 ml Buffer ER was then added and incubated on ice for 30 min. Qiagen-tip 500 was equilibrated with 25 ml of Buffer QBT during the 30 min incubation. The lysate was then allowed to flow through the Qiagen-tip 500 under gravity. The Qiagen-tip was then washed twice with 30 ml of Buffer QC and the DNA was eluted with 10 ml of Buffer QN. Isopropanol was then added to precipitate the DNA and centrifuged at 15,000 g for 30 min at 4 °C. The DNA pellet was then washed with 70% ethanol and centrifuged at 15,000 g for 10 min. The DNA pellet was then air dried and resuspended in 100 µl of Tris-EDTA (TE). The DNA concentration was then measured using a Nanodrop.

2.1.12 Plasmid Maps

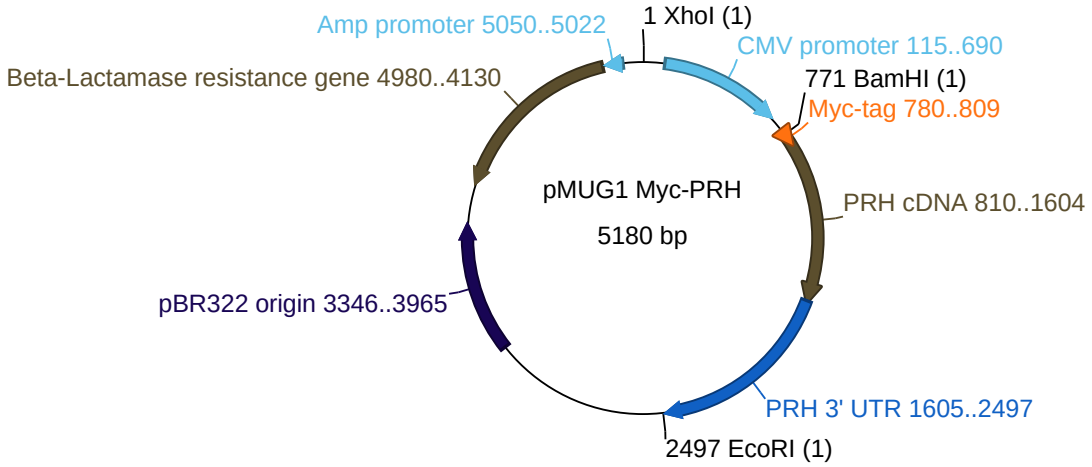

Figure 2.1 Diagram of PMUG1 Myc-PRH plasmid

pMUG1 Myc-PRH and deletion plasmids

This plasmid encodes a fusion protein of 7-270 amino acid of PRH tagged with Myc 9B11 epitope fused in frame at the N-terminus of PRH (Bess et al., 2003a). pMUG1-Myc-PRH N187A was created previously and encodes a mutated PRH protein at the N187 position within the PRH homeodomain resulting in Alanine at the 187 position instead of Asparagine (Desjobert et al., 2009).

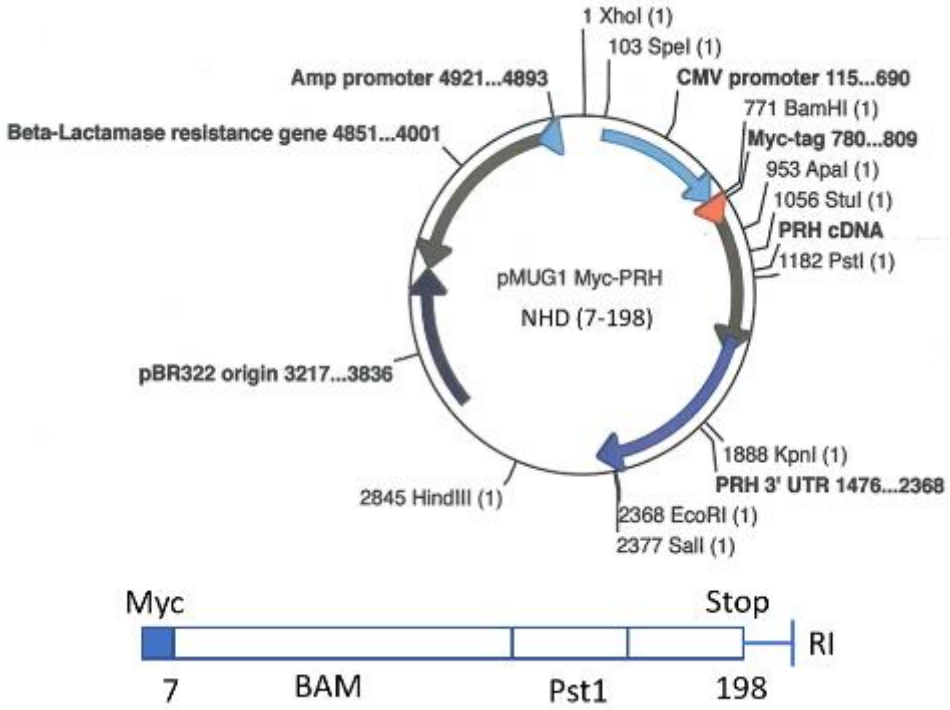

Figure 2.2 Diagram of pMUG1 Myc-PRH 7-198 (NHD, with C-terminus deletion)

The PRH N-terminal plasmids pMUG1-PRHN7-132 and pMUG1PRHN50-132 and the PRH HD-C terminal plasmid pMUG1136-270 were subcloned previously by Dr. P-S Jayaraman.

pMUG1 Myc-PRH 7-198 (NHD, with C-terminus deletion)

The plasmid pMUG1 Myc-PRH 7-198 is derived from pMUG1 Myc-PRH 7-270 and contains a stop codon immediately after amino acid 198 and deletes PRH 3'UTR sequence present in pMUG1 Myc-PRH 7-270 so that the EcoRI site present in pMUG1 Myc-PRH 7-270 is immediately adjacent to the stop codon. Construction of this plasmid

was through ligation of a BamHI to PstI fragment from pMUG1Myc-PRH 7-270 and a PstI-EcoRI PRH PCR fragment terminating at amino acid 198 within PRH. Cloning and sequencing performed previously by Dr PS. Jayaraman.

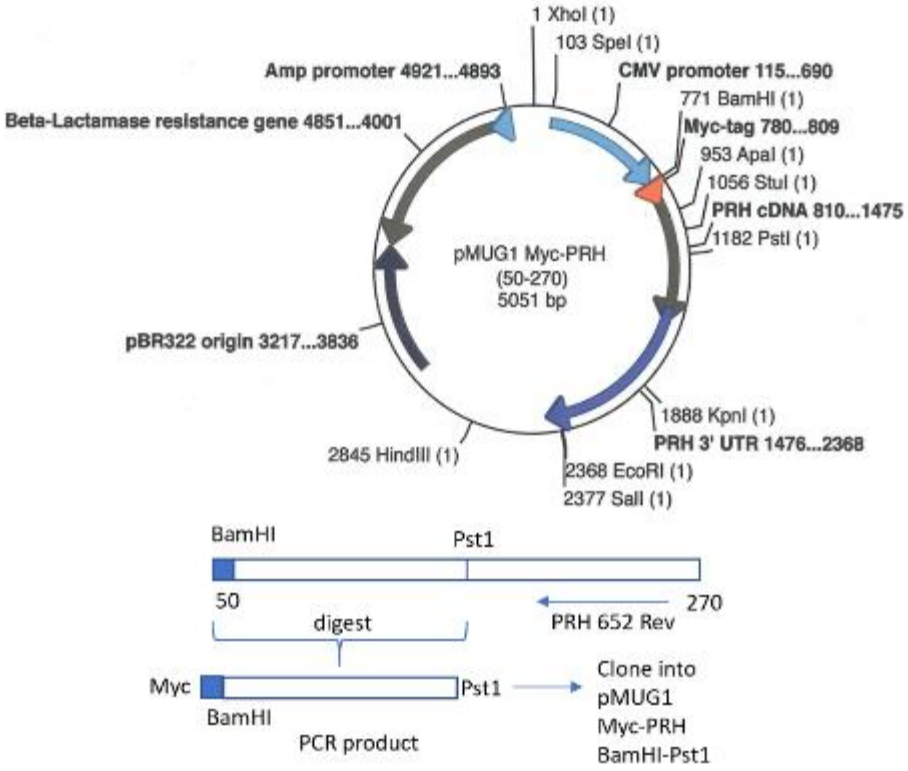

Figure 2.3 Diagram of pMUG1 Myc-PRH 136-270 (HDC, N-terminus deletion)

pMUG1 Myc-PRH 136-270 (HDC, N-terminus deletion)

The plasmid pMUG1 Myc-PRH 136-270 was constructed by using PCR to generate a fragment corresponding to the PRH cDNA but with a BamHI site at the 5' end and the Myc 9B11 epitope in frame with amino acid 136 of PRH. Cloning was performed by generating a BamHI-PstI fragment using a 5' oligonucleotide PCR primer containing the Myc epitope as mentioned above and a 3' oligonucleotide corresponding to PRH cDNA

and including the PstI restriction site present within the PRH cDNA. The resulting BamHI-PstI PCR fragment was cloned into pMUG1-PRH7-270 so that the N-terminus was truncated removing amino acids 7-136. Cloning and sequencing performed previously by Dr P. Noy.

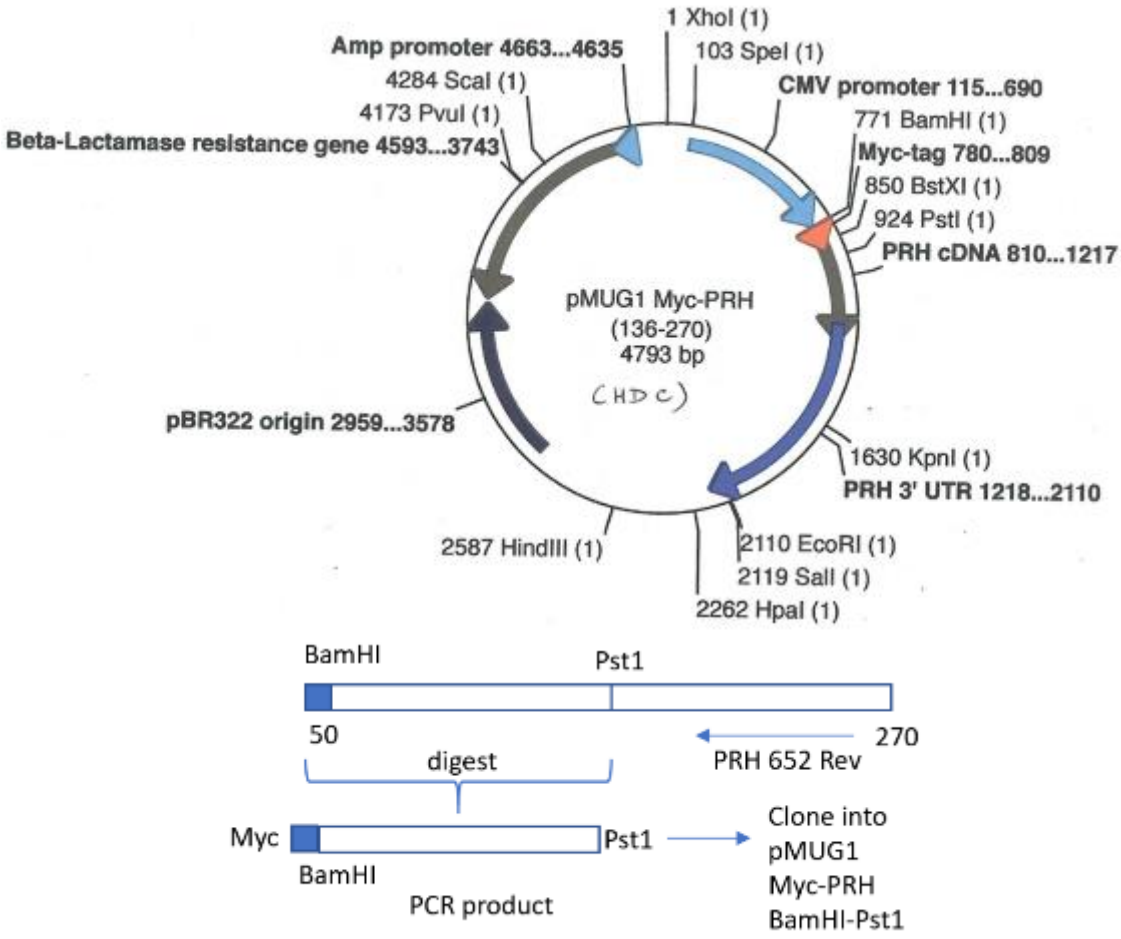

Figure 2.4 Diagram of pMUG1 Myc-PRH 50-270

pMUG1 Myc-PRH 50-270

The plasmid pMUG1 Myc-PRH 50-270 was constructed the same as the pMUG1 Myc-PRH 136-270. Instead, the resulting BamHI-PstI PCR fragment was cloned into pMUG1-PRH 7-270 so that the N-terminus was truncated removing amino acids 7-50. Cloning and sequencing performed previously by Dr P. Noy.

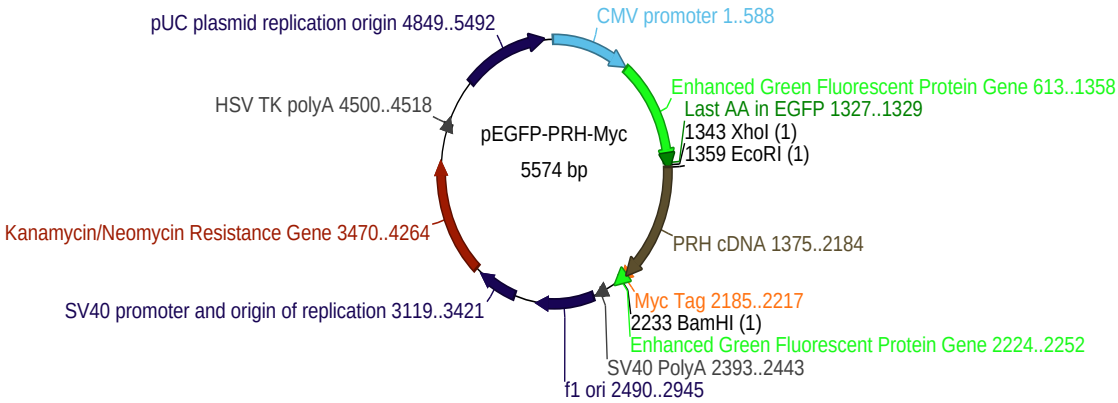

Figure 2.5 Diagram of pEGFP-PRHMyc and pEGFP-PRH

pEGFP-PRH$_{Myc}$ and pEGFP-PRH

pEGFP-PRH was generated by inserting the human PRH cDNA from the cloning vector pBluescript-PRH in frame with GFP, between EcoRI and KpnI sites in pEGFP-C1 (Addgene plasmid #45769). pEGFP-PRH contains an in-frame translation stop at the end of the PRH coding sequence and also contains the 3' UTR from the *PRH/HHEX* gene. A PstI-KpnI fragment was generated which retained the PRH coding sequence to amino acid 270 but instead of the PRH in-frame translation stop codon an in-frame Myc tag was inserted followed immediately by a translation stop codon. This creates a double-tagged protein with GFP at the N- terminus and the Myc-tag epitope at the C-terminus of PRH. The

cloning removes the 3' UTR sequence. All clonings were performed previously by Dr. PS Jayaraman.

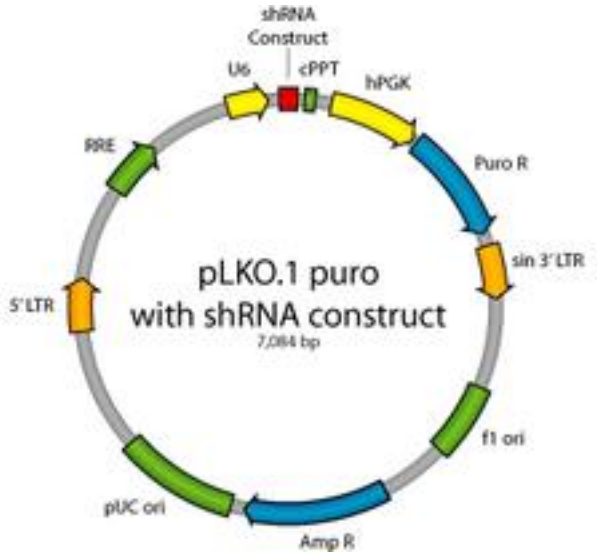

Figure 2.6 Diagram of Hhex shRNA and scrambled control

Hhex shRNA and scrambled control

The Hhex shRNA and the control shRNA were obtained from Origene (TR312464) and Origene (TR30012) respectively. The DNA sequence for PRH shRNA knockdown is CTGTGATCAGAGGCAAGATT and the scrambled control sequence does not target known mammalian genes.

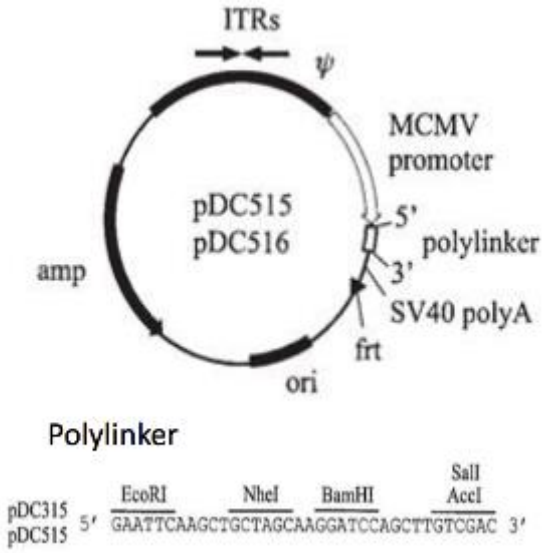

Figure 2.7 Diagram of Adenoviral vector pDC515

Adenoviral vector pDC515

pDC515 (Microbix Biosystems) is the viral shuttling vector used to produce adenovirus (Palmer and Ng, 2008) and this is made replication-deficient by site-specific FLP-mediated recombination. The empty vector that did not code for any transgene is known as AdEmpty. For AdPRH and AdPRHN187A, the EcoRI-BamHi fragment encoding the Myc-PRH fusion from pMUG1-PRH and pMUG1-N187A plasmids were excised using restriction enzymes EcoRI and BamHI and the fragments were blunted with micrococcal nuclease and ligated into pDC515 in the polylinker site (R M Kershaw et al., 2017). Cloning and adenoviral preparation by Dr G. Newby (University of Bristol).

2.2 Western blotting

2.2.1 Extraction of whole cell protein

Approximately 1 million cells (about 70 % confluency) were plated in one well of a 6-well plate 24 hours before protein extraction. At 24 hours, the cells with 90 % confluency were washed twice with 1 ml 1x PBS (4°C). To produce a whole cell lysate 250 µl of RIPA buffer was added drop by drop to the adherent cells. The cells were then resuspended in RIPA buffer by pipetting up and down (at least 10 times) and transferred to Eppendorf tubes. The lysate was incubated at 4 °C for 45 mins. Cell debris was removed by centrifugation at 4 °C for 10 mins at maximum of 6000 g. The supernatant was collected and transferred to a sterile 1.5 ml Eppendorf and stored at -20 °C.

2.2.2 Determining protein concentration

Bradford assays were carried out to determine the protein concentration of cell lysates. For the assay, Bradford reagent (5000006, Biorad) was diluted 1:5 with dH_2O and 5 µl protein lysate was added to the diluted Bradford reagent to make up a total of 1 ml solution. For the blank, 5 µl protein lysate was replaced by RIPA buffer. The 1 ml mixture was then mixed carefully and then transferred to a cuvette and protein concentration was measured by spectrophotometer at 545 nm. A standard curve was generated by diluting BSA to 0 µg, 2 µg, 4 µg, 6 µg and 10 µg with Bradford reagent (1:5 in dH_2O, Bio-rad). The following equation was generated from the standard curve and was used for calculating the protein concentration:

$y=1.0834x + 0.0629$, y= absorbance and x = the protein concentration in mg/ml.

2.2.3 Protein separation

Protein was separated by SDS-Polyacrylamide Gel Electrophoresis (SDS-PAGE) by molecular weight. Front and back glass plates from BIoRad casting apparatus were clamped into a casting frame and the frame was clamped into a stand. A 10 % (w/v) resolving gel was prepared using 2.5 ml of 1.5 M Tris pH 8.8, 3.3 ml of 30 % Acrylamide, 4 ml of ddH_2O, 100 µl of 10 % SDS, 90 µl of 10 % ammonium persulphate (APS, Sigma) diluted in water and 10 µl Tetramethylethylenediamine (TEMED, Sigma). The resolving gel solution was pipetted between the glass plates up to three quarters of the height of the plates so that at least 2 cm of stacking gel was able to be pipetted on top. 0.5 ml of Isopropanol was immediately added before the gel was set to remove any air bubbles and to obtain a clean surface. The gel was polymerized after approximately 15 mins and the isopropanol was discarded. A 5 % stacking gel was prepared by mixing 3 ml ddH_2O, 1.25 ml of 0.5 M Tris (pH 6.8), 700 µl of 30 % Acrylamide, 50 µl of 10 % SDS, 50 µl of 10 % APS and 10 µl TEMED. The stacking buffer was then pipetted on top of the polymerized resolving gel and a 1 mm width gel comb was inserted in between the plates. After 15 mins, the polymerized resolving and stacking gel was then placed into the electrophoresis tank and filled with 1x running buffer **(Table 3)**. Protein lysates were then prepared with 1x Laemmli and RIPA buffer to ensure equal amount of protein (approximately 10 µg) was loaded and 20 µl of protein lysate mixture and 5 µl protein ladder was loaded in each well of the gel after boiling at 95°C for 5 mins. The gel was then electrophoresed for 45 mins at 200 V with constant current.

2.2.4 Transfer of protein

The proteins on the gel were then transferred to a polyvinylidene fluoride (PVDF) membrane. The membrane was activated in methanol for 1 min and was washed with dH_2O for 3 mins and placed into 1X transfer buffer. Sponge pads and 2 pieces of filter papers were soaked in 1X transfer buffer. The gel and the membrane were sandwiched between the sponge pads and filter papers and were placed in the cassette. A tube was used to roll over the sandwich to prevent any air bubbles in the cassette. The cassette was then placed into a Bio-Rad Mini Trans-Blot Cell, filled with 1x transfer buffer and an ice pack was used to keep it cool. The proteins were then transferred at 100 V with constant current for 1 hour.

2.2.5 Protein detection by antibodies

After transfer, the membrane was incubated with 20 % w/v milk (Marvel) in PBS with 0.1% Tween (PBS-T) for 1 hour to allow the membrane to be coated with proteins and prevent non-specific binding of antibodies. After 1 hour, the membrane was washed with PBS-T three times, each for 5 mins with agitation. After that, the membrane was incubated with primary antibody for 1 hour. The primary antibody was diluted either in 5% w/v milk (Marvel) in 5 ml PBS-T or in 5% w/v Bovine Serum Albumin (BSA) in PBS-T with 15 µl Sodium Azide. The membrane was then washed 3 times as before and incubated with secondary antibody for 1 hour. The secondary antibody, a horseradish peroxidase (HRP) conjugated antibody raised against the animal that the primary antibody was raised in, was diluted 1 in 5000 in 5 % w/v milk in PBS-T. Generally, either HRP anti-rabbit secondary (AP156P, Sigma) or HRP- anti mouse secondary (AP127P, Sigma) was used. The membrane was then washed as described above. During the last

wash, the enhanced chemiluminescence (ECL) solution (RPN2232, GE Healthcare) was prepared by mixing the two detection solutions in a ratio of 1:1, made up to a total volume of 1 ml per membrane. The membrane was stained with ECL solution and incubated for 1 min. The membrane was then placed into a cassette and exposed to Hyperfilm (Amersham), and developed using a PROTEC Ecomax X-Ray Film Processor. The exposure time was adjusted depending on the bands seen on the film. If the membrane was reprobed for detection of a second protein using another antibody, the membrane was stripped using stripping buffer (see Table 3 for stripping buffer) for 15 mins with agitation. The membrane was then given a quick rinse in PBS-T and was reblocked overnight and re-probed with antibody of interest as described above.

2.2.6 Densitometry analysis

Densitometry analysis was carried out using ImageJ software to compare the density of the bands. The western blot film with appropriate exposure was scanned. The bands on the autoradiographic film were selected by using the ImageJ software. A lane plot analysis was performed to analyze the selected areas and a graph was generated. A line was drawn at the background level, the area under the peak was quantified which is equal to the density of the bands. The same process was carried out for the loading control protein, Lamin A/C. The densitometry of the protein of interest was divided by the densitometry of Lamin A/C in order to obtain the relative band intensity.

Buffer	Recipe
RIPA Buffer	150mM NaCL 1% NP-40 0.5% sodium deoxycholate 0.1% SDS 50mM Tris pH 8.0
1.5 M Tris, pH 8.8 (Resolving gel)	90.8 g Tris Base 500 ml H_2O 2 g SDS
0.5 M Tris, pH 6.8 (Stacking gel)	6.06 g Tris Base 100 ml H_2O 0.4 g SDS
4x Sample Loading Buffer, pH 6.8	20% v/v Glycerol 10% v/v 2-Mercaptoethanol 4% SDS 0.004% Bromophenol blue 125mM Tris base
1X Running Buffer	100 ml SDS-PAGE Tank buffer Tris-glycine (Geneflow) 900 ml H_2O
10X Transfer Buffer	30.3 g Tris Base 144 g Glycine 1L H_2O
1X Transfer Buffer	100 ml 10X Transfer Buffer 200 ml Methanol 700 ml H_2O
10X Stripping Buffer, pH 2.2	15 g Glycine 1 g SDS 10 ml Tween-20 1 L H_2O

Table 3 Buffers for Western Blotting

2.3 Biochemical fractionation

2.3.1 Nuclear and Cytoplasmic fractionation and protein extraction

1x 10^7 cells were plated on 100 mm Corning petri dish 24 hours before protein extraction. Cells were harvested by scraping with PBS. The cells were then centrifuged at 500 g for 5 mins to obtain cell pellet. After centrifugation, the PBS was removed. The biochemical fractionation protocol from Klenova et al. was followed (Klenova et al., 2002). To obtain the cytoplasmic fraction, the cell pellet was resuspended in 100 µl of

Tween-20 lysis buffer: 25 mM Tris, pH 8, 25 mM NaCl, 2 mM EDTA, 1X protease inhibitor cocktail (50X stock diluted in 1 ml water, Promega), 0.5% Tween and incubated for 15 mins. Cells were pelleted at 6000 g by centrifugation after incubation at 4°C. The supernatant was collected and was made up to 200 µl with Tween-20 lysis buffer containing 500 mM NaCl. To obtain the nuclear fraction, the nuclear pellet was resuspended in 100 µl Tween-20 lysis buffer containing 500 mM NaCl and 50X protease inhibitor cocktail was added and incubated on ice for 15 mins. After incubation, the lysate was then centrifuged at 10,000 g for 15 mins and the supernatant was recovered. 20 µl of both the cytoplasmic fraction and nuclear fraction was stored as input in -20 °C after diluting to 50 µl with 4X sample loading buffer.

2.3.2 Immunoprecipitation

Immunoprecipitation of proteins from cytoplasmic and nuclear fractions was carried out. Protein A/G magnetic beads (0.1 mg/ml) (88802, ThermoFisher) were washed with Tween 20 lysis buffer twice and added to each of the cytoplasmic and nuclear protein samples in low binding Eppendorf tubes (MCT-150-L-C, Axygen). 2 % BSA and 1 mg/ml primary antibody was added to the samples and incubated on the roller at 4°C for 3 hours. After incubation, the beads were separated by magnetic separation by placing the Eppendorfs on a magnetic rack. The supernatant (unbound protein) was discarded and the beads were washed for 5 min with 1 ml of Tween-20 lysis buffer containing 200 mM NaCl 5 times each. The proteins were then eluted from the washed beads using 50 µl of 1X loading buffer after incubation of beads at 95 °C for 10 mins. The eluted protein was separated from the beads by magnetic separation on a magnetic rack allowing 50 µl of supernatant to be recovered.

PRH (M3)	Mouse	1:10,000 in BSA	In house
Notch3	Rabbit	1:1000 in milk	D118B, CST
Cyclin D2	Rabbit	1:250 in BSA	D52F9, CST
p27 Kip1	Rabbit	1:1000 in BSA	#2552, CST
E-cadherin	Rabbit	1:1000 in BSA	#3195, CST
Vimentin	Rabbit	1:5000 in BSA	#5741, CST
Claudin1	Rabbit	1:1000 in BSA	#9782, CST
Snail	Rabbit	1:1000 in BSA	#9782, CST
Slug	Rabbit	1:1000 in BSA	#9782, CST
Rb	Mouse	1:1000 in BSA	#9969, CST
Phospho-Rb (Ser807/811)	Rabbit	1:1000 in BSA	#9969, CST
Myc-tag	Mouse	1:1000 in BSA	#2276, CST
Keratin-7	Rabbit	1:1000 in BSA	D1E4, CST
GFP	Mouse	1:1000 in BSA	#4B10, CST
Tubulin	Rabbit	1:1000 in BSA	#2125, CST
β-actin	Rabbit	1:1000 in BSA	#4970, CST
Lamin A/C	Rabbit	1:5000 in BSA	#376248, Santa Cruz
Anti-rabbit IgG, HRP-linked Antibody	Rabbit	1:5000 in milk	AP156P, Sigma
Anti-mouse IgG, HRP-linked Antibody	Mouse	1:5000 in milk	AP127P, Sigma

Table 4 Antibodies used in this study

2.4 Quantitative PCR

2.4.1 RNA extraction

RNA was extracted from the cells using an ISOLATE II mini kit (BIO-52072, Bioline). The kit uses silica membrane as nucleic acid binds well to silica membrane in the presence of chaotopic salt but protein does not bind. 1 million cells were plated into a 6-well plate. After 24 hours, the cells were washed twice with PBS at 4°C. 2-mercaptoethanol (2-Me) was added to the RNA lysis buffer at 1:10 ratio from the kit. For each sample, 350 µl of RNA lysis buffer and 2-Me mixture was added to each well and incubated for

approximately 2 mins. The lysate was transferred to a purple filter placed in a 1.5 ml column tube provided in the kit and were centrifuged for 1 min. The purple filter was discarded and 350 µl of 70 % ethanol was added to the filtrate in the column tube. The ethanol and filtrate mixture were then transferred to a blue filter tube placed in a 1.5 ml column tube and was centrifuged for 30 seconds. The RNA was bound on to the silica membrane in the filter tube. The blue filter tube with the RNA was then placed to a new 1.5 column tube and 250 µl of membrane buffer was added onto the membrane and was centrifuged for 30 seconds to facilitate the binding of the RNA to the silica membrane. The RNA was treated with DNase I for 30 mins to remove genomic DNA. The isolated RNA on the membrane was then washed with 250 µl wash buffer 1 by centrifuging for 1 min. The RNA on the membrane was then washed twice by 600 µl wash buffer 2 for 30 seconds each. Finally, the RNA was eluted with 60 µl of RNase-free water. The concentration of RNA was then quantified using NanoDrop. The DNA concentration is calculated using the absorbance at 260 nm (A260) considering A260 of 1.0 = 50 µg/ml pure DNA plasmid; the A260 / A280 ratio is also calculated to determine the purity of the purified DNA plasmid, ratio between 1.9 and 2.1 were considered high-quality plasmid DNA.

2.4.2 Complementary DNA production

QuantiTech Reverse Transcription Kit (205311, Qiagen) was used to convert RNA to complementary DNA (cDNA). The reagents in the kits were all thawed on ice. For each sample, 1 mg of RNA was diluted in RNase-free water to make a total volume of 12 µl. 2 µl of gDNA wipeout buffer 7x was then added to the RNA mixture. The samples were then incubated at 42 °C for 2 mins and allowed to cool down at 4 °C for 1 min and were

placed on ice afterwards. A master mix was prepared composed of 1 µl of Quantiscript Reverse Transcriptase Enzyme, 1 µl of Quantiscript RT Buffer 5x, and 1 µl of RT Primer Mix for each sample. 6 µl of the master mix was added to each sample to make up a total volume of 20 µl reaction mixture. The samples were incubated at 42 °C for 15 mins, followed by 3 mins incubation at 95 °C. The cDNA samples were then kept in -20 °C and ready to be used.

2.4.3 Quantitative PCR

Selection of primers:

Most primers sequences were obtained from the literature. For primers that were not previously published, Primer3 software was used to design the primers. Primer pairs were chosen so that the melting temperature of all the primers were the same in order that the primers were all able to be used at the same annealing temperature. The designed primers contain at least 40 % of GC content and the length of primers are between 18 to 22 bp long. The primers were all ordered from Sigma. Primer stocks: Primers were prepared from the stock by adding corresponding amount of H_2O (Sigma) to the oligomer pellet to give a 100 mM stock solution. The primers were then diluted 1 in 10 in water and stored as working stocks (10 mM). 1 in 100 dilution of working concentration of primers was used in the PCR Master mix (see below) results in a final concentration of 100 µM.

Primer specificity:

Primer specificity was checked by melting temperature analysis of the primer products on the Rotor Gene Q using Rotor Gene software and by electrophoresis of the PCR product on an agarose gel.

Primer efficiency:

Primers used in this study are listed in **Table 5**. The efficiency of the primers was obtained from a standard curve plotted for each primer pairs. The standard curve was plotted using 2-fold serial dilution of cDNA (neat, ½, ¼ etc. using at least 5 dilution points) including undiluted cDNA. qPCR reactions were assembled in a master mix (see below) containing no DNA (water only 1 µl), undiluted cDNA (1 µl) or each cDNA dilution (1 µl). The master mix was then aliquoted into tubes in quadruplicate for each dilution and PCR reactions performed in the Rotor-Gene Q PCR Cycler using thermal parameters described below. R^2 values > 0.9 and efficiencies >1.8 were accepted.

Master Mix: qPCR was performed using Rotor-Gene SYBR Green PCR Kit (204143, Qiagen). A total volume of 35 µl master mix was prepared for each primer pair composed of 17.5 µl of 2x SYBR Green (containing dNTPs with dUTP), 3.5 µl of 100 µM forward primer, 3.5 µl of 100 µM reverse primer and remainder with PCR H_2O (RNase and DNase-free water). 35 µl of the master mix solution was aliquoted into a 200 µl PCR tube with either sterile RNA and DNA free water (1 µl) or with cDNA (1 µl). The master mix was mixed carefully by pipetting up and down 10 times. After mixing, 7.5 µl of the reaction mixture was aliquoted into each of four PCR quadruplicate tubes (9018905, Qiagen).

The reaction tubes were placed into a Qiagen Rotor-Gene Q PCR cycler. The thermal parameters were: 95 °C for 15 seconds, 62 °C for 10 seconds and 72 °C for 10 seconds, repeated for 40 cycles.

For experiments, each biological replicate was carried out as a technical quadruplicate. The data was analyzed by RotorGene software, Ct was obtained by setting a threshold value of 0.1 (10 % above background) for each sample. β-actin was used as the

housekeeping gene unless otherwise stated.

Relative gene expression was then calculated using the Efficiency Calibrated Mathematical Model (Pfaffl, 2001) which included primer efficiency. The equation used for each biological repeat was:

$$\text{Expt} = E^{Ct\ (\text{house-keeping gene})} / E^{Ct\ (\text{Gene of Interest})}$$

E is the primer efficiency for the housekeeper gene primer (from the standard curve) and gene of interest for each primer pair. Fold change was obtained by dividing the product of the equation for the experiment above by the corresponding values from the experimental control. For statistical analysis the values obtained from the experiment were transformed into $\log_2$ values in Excel and the same repeated for the control values. A two-tailed Student T-test was carried out between control and the experimental sample.

Primers	Forward/Reverse Sequences
PRH/HHEX	5'-AAACCTCTACTCTGGAGCCC-3' 5'-GGTCTGGTCGTTGGAGAATC-3'
NOTCH3	5'-CCTAGACCTGGTGGACAAG-3' 5'-ACACAGTCGTAGCGGTTG-3'
CCND2	5'-GGACATCCAACCCTACATGC-3' 5'-CGCACTTCTGTTCCTCACAG-3'
CDKN1B	5'-CCGGCTAACTCTGAGGACAC-3' 5'-AGAAGAATCGTCGGTTGCAG-3'
CDKN2B	5'-AAGAGTGTCGTTAAGTTTACG-3' 5'-ACATCGGCGATCTAGGTTCCA-3'
***CDH1* (E-cadherin)**	5'-GTAACGACGTTGCACCAACC-3' 5'-AGCCAGCTTCTTGAAGCGAT-3'
VIM	5'-GCACCCTGCAGTCATTCAGA-3' 5'-GCAAGGATTCCACTTTACGTTCA-3'
KRT-7	5'-TGTGGATGCTGCCTACATGAGC-3' 5'-AGCACCACAGATGTGTCGGAGA-3'
***ALB* (Albumin)**	5'-GATGAGATGCCTGCTGACTTGC-3' 5'-CACGACAGAGTAATCAGGATGCC-3'
SNAI1	5'-GAGGCGGTGGCAGACTAG-3' 5'-GACACATCGGTCAGACCA-3'
***SNAI2* (Slug)**	5'-GGCTGCTTCAAGGACACATT-3' 5'-TTGGAGCAGTTTTTGCACTG -3'
ZEB1	5'- GCACCTGAAGAGGACCAGAG-3' 5'- TGCATCTGGTGTTCCATTTT-3'
***ZEB2* (TWIST)**	5'-TCTCGCCCGAGTGAAGCCTT-3' 5'-GGGAGAATTGCTTGATGGAGC-3'
β-actin	5'-AAAGACCTGTACGCCAACAC-3' 5'-GTCATACTCCTGCTTGCTGAT-3'

Table 5 Primers used for PCR amplification for gene expression

2.4.4 RNA sequencing and bioinformatics

RNA was isolated using the Isolate II kit was described in the previous section. 5 µl of at least 100 ng/µl DNase treated RNA was sent to Genomics Birmingham (University of Birmingham) for a quality check. An RNA integrity number (RIN) was calculated by the facility and RNA with RIN higher than 9 (having little or no degradation) was then

processed for library preparation and RNA sequencing (RNA-seq) by the facility. The Illumina TruSeq RNA Library Prep kit was used to prepare the sequencing library. The total RNA was purified and adaptors were ligated to cDNA during library preparation. Illumina sequencing of 75 bp paired end reads was then performed by the facility. A minimum of 2 x 35 million reads per sample were generated. The sequencing raw data was then received in FastQ file format.

Bioinformatics

Bioinformatics analysis on the raw RNA-seq data was performed using Galaxy software. The FastQ files were first uploaded to the software and were concatenated by selecting the Text Manipulation option. The concatenated files were then quality checked and a FastQC Read Quality report was generated for each sample to make sure that all the reads are long enough (70s) and there was no over-represented sequence. The adaptors were then trimmed using Trim Galore. The genome was then aligned to the Hg 19 homo sapiens reference genome using the TopHat Gapped-read mapper on the trimmed reads. Differential expression analysis was performed using DEseq2. A normalised count table and a DEseq2 file were exported to Excel. Gene Ontology analysis was performed using the PANTHER webserver (http://www.pantherdb.org) and Gene Set Enrichment Analysis for Hallmark gene sets was performed using the Broad Institute GSEA webserver. (http://software.broadinstitute.org/gsea/msigdb). Ranked GSEA analysis was performed using the Gene Set Enrichment Analysis software downloaded from the Broad Institute GSEA (https://www.gsea-msigdb.org/gsea/login.jsp;jsessionid=4528C25EEA9A48F54E3254147E61860E). The DEGs from DEseq file was uploaded to the software as a rnk file. MSigDB Gene Sets was

then selected and the GSEA analysis was carried out. The gene set enrichment plots according to the pathway queried were then generated. Volcano plots were also generated using Graphpad.

2.6 Chromatin Immunoprecipitation (ChIP)

2.6.1 Cross-linking

1x 10^7 cells were infected with Myc-PRH Adenovirus and Empty adenovirus for 48 hours as described above. For each ChIP, 5 million cells were infected in T75 flask and were trypsinized, washed with PBS and then pelleted in 5 ml of media. 400 µl of Methanol-free formaldehyde (Pierce™ (28906), Thermo Scientific) was then added to the cell pellet with DMEM and re-suspended to a final concentration of 1% in the fume hood. After 10 mins incubation of cells with formaldehyde with agitation, the formaldehyde was quenched by adding 2 M glycine (W328707**,** Sigma) to a final concentration of 0.4 M and made up to 12 ml final volume of the cell mixture with formaldehyde and glycine. The cells were then pelleted by centrifugation at 500 g for 5 mins followed by two ice-cold PBS washes. Ice-cold buffer A (see table 6) was then added to re-suspend the cell pellet and incubated for 10 mins on the rotary stirrer at 4 °C. The nuclei were then pelleted by centrifugation and then re-suspended in ice-cold buffer B. After 10 mins incubation at 4 °C with agitation, the nuclei were pelleted and snap frozen with dry ice at -80 °C.

2.6.2 Optimization of sonication

The nuclei were re-suspended in ice-cold ChIP buffer I (300 µl buffer / 1 x 10^7 cells). The nuclei and buffer mixture were then transferred to a low-binding tube (Axygen). The

chromatin was sonicated using the Biorupter (Diagenode, USA) at high power 240W, 30 sec ON; 30 sec OFF.

The length of sonication of the chromatin was optimized before the ChIP experiment using a selected number of cycles (0, 15, 20, 25, 30, 35 and 40 cycle) to ensure that the majority of the fragments range between 200-500 bp. The fragments sonicated from different cycles were then electrophoresed on an agarose gel to check the fragmentation. Figure shows that cycle 25 is optimal for CCLP cells as a smear can be seen where the longest fragments are on average 200-500 bp **(Figure 2.8)**. Over-fragmentation should be avoided.

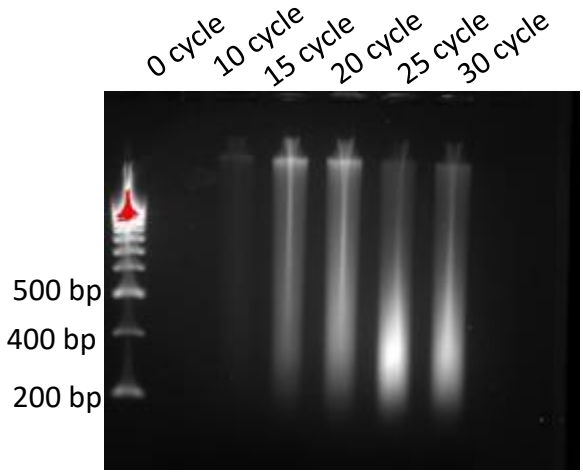

Figure 2.8 Image of gel for optimization of sonication

Immunoprecipitation of chromatin

After sonication, the fragmented DNA was centrifuged for 10 mins at 16,000 g at 4 °C in an eppendorf. The supernatants were then transferred to a clean low binding tube. The chromatin from 25 cycles was then diluted with 3X ChIP Buffer at a ratio of 1:3 total volume 250 µl. 25 µl/250 µl of this diluted chromatin (not immunoprecipitated) was taken as the input for normalization at the end of the experiment (see below).

Protein A/G Magnetic Beads (88802 Pierce™, Thermo Scientific) (10 µl per IP) were washed twice with phosphate buffer pH 8 by rotating the tube so that the beads travel across the liquid by magnetic force and then the beads were re-suspended in 100 mM phosphate buffer (10 µl per IP). 3 µg of antibody (Myc-tag #2276, CST; or Vimentin #5741, CST or IgG, sc-2027 Santa Cruz Biotenchology) and BSA (0.5% w/v final concentration) diluted in water were mixed with the Protein A/G Dynabeads. The dynabeads and antibody mixture was incubated for 2 hours at 4 °C with rotation. The diluted chromatin (425 µl) was added to the dynabeads-antibody mixture and incubated for 3 hours at 4 °C with rotation. The beads were then washed with 1ml of Wash buffer 1, twice with Wash buffer 2 (1 ml), once with LiCl buffer (1 ml) and twice with TE/NaCl buffer by rotating the tube on the magnetic rack so that the beads are travelling from one side of the tube to the other. For each wash, the beads were resuspended in the washing buffer and incubated for 10 mins at 4 °C with rotation. Finally, the beads were transferred to a clean low binding tube and incubated with 50 µl of elution buffer for 15 mins at room temperature with shaking on the shaker. This was repeated to produce two elutions that were pooled in a low binding eppendorf tube. Reverse cross-linking was then performed by adding 1 µl of RNase A (10 mg/ml) and incubating the eluted antibody-DNA complexes for 30 mins at room temperature. 4 µl of 5 M NaCl, 2 µl of 0.5 M EDTA and 1 µl of proteinase K (50 mg/ml) were then added to the chromatin and the chromatin was incubated overnight in a water bath at 55 °C.

After overnight incubation, the DNA was isolated and purified by adding AxyPrep Mag™ PCR clean up beads (Axygen, Biosciences) at a ratio of 1:1.8. The DNA and bead mixture was incubated at room temperature on the bench for 10 mins. The beads were then

washed twice with 80 % ethanol and left to air-dry for 10 mins. Before the beads were completely dried off, the DNA was eluted with 50 µl of TE buffer.

The DNA product can either be used for qPCR or genomic sequencing. For qPCR, 4 µl of ChIP DNA product from 50 µl was used in the qPCR master mix per primer pair and for the input DNA 4 µl/ total volume input DNA was used in the mastermix per primer pair.

Calculation of ChIP enrichment:

In general, all regions of the genome should be amplified strongly and equally by PCR in the absence of IP. In the absence of an antibody or with a non-specific antibody there should be no DNA amplified resulting in a very low Ct value (approx.> Ct 40). The ChIP qPCR signal is represented as a percentage of input; this is the chromatin (specific gene or region of interest) detected by qPCR that has been immunoprecipitated by the protein-antibody complex as a percentage of the qPCR signal for the same gene or region of interest in the genome without immunoprecipitation.

ChIP enrichment for a gene as a Percentage of input can be calculated as follows:

Percentage input =100x (dilution factor for IP) x 2^(Adjusted Ctinput - CtChIP)

(i) Calculation of adjusted Ct input:

The input Ct is adjusted to reflect the volume of input used in the qPCR reaction.

Thus, the adjusted $Ct_{input} = Ct_{input} - Log_2$(dilution factor)

E.g Thus if from 500 µl chromatin take 50ml for "Input" and add 10ml to PCR reaction

10 µl of input ie, 10/500 x 100/1 = 2% of "Input"

Dilution factor = 100/2 = 50. Log2(50) = 5.64

Therefore, adjusted Ct input = Ct input – 5.64

(ii) Calculation of Dilution factor for IP:

Eg. From 500 µl chromatin use 450ml for “ChIP” and finally resuspend DNA in 100 µl. Then use 4 µl in the PCR reaction

450 = 450/500 x 100/1 = 90% of “Chromatin” used for ChIP and then

4/100 used in PCR= 3.6% of “Chromatin” finally used for ChIP in PCR (ie 4/100 x 90% = 0.04 x 90% = 3.6%)

Dilution factor for ChIP = 100/3.6 = 27.8

% input = 100 x 27.8 x 2^(Adjusted Ctinput - CtChIP)

ChIP enrichment can also be calculated as a Fold change enrichment. This is calculated by normalizing the percentage input from the ChIP for a specific region performed withthe specific antibody to the negative control ie a non-specific antibody such as IgG or the Myc antibody in cells where there is no expressed Myc-PRH protein. In the experiments in this thesis where the Myc antibody is used for IP against Myc-PRH, the control is the Myc antibody used to IP proteins in cells infected with empty vector.

A second method for fold change enrichment is to normalize the percentage input for a specific region relative to the percentage input for negative control regions in the chromatin. The established negative control regions are chromosomes 18 and 22 which are regions of closed chromatin (Thibodeau et al., 2017) where there are no expressed genes and where therefore no ChIP signal should be detected. The second method requires that additional PCR reactions for the negative control regions are performed.

The data shown in the results are displayed as percentage input either in the presence or absence of specific antibody or relative to the negative control regions.

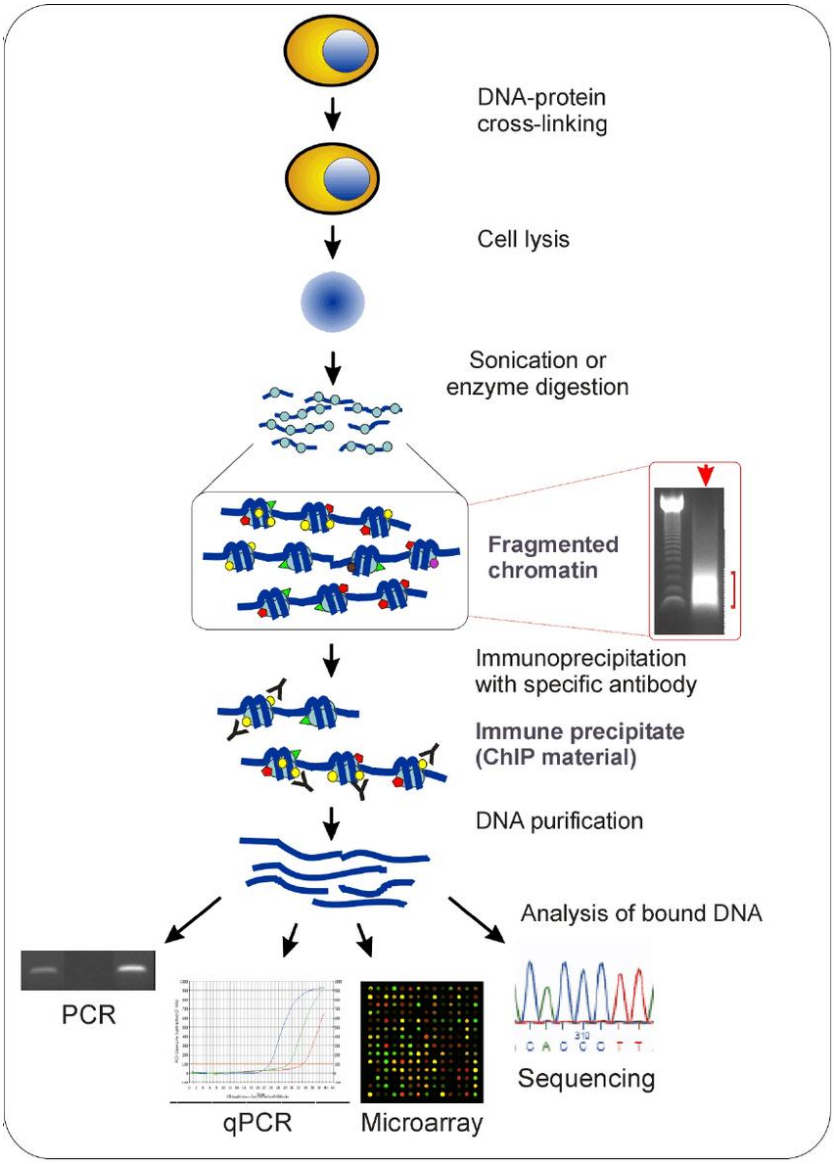

Figure 2.9 Work-flow of ChIP (Collas and Dahl, 2008).

2.6.3 ChIP-sequencing

The DNA product from ChIP was sent for ChIP-sequencing to Ishanvi Lifesciences (India). The sequencing library was prepared using NEBNext Ultra II DNA Library preparation kit (E7645S) and the sequencing was performed by using Illumina Hiseq 2500 generating 100bp reads (40 million reads/sample). The raw data from the sequencing was received in FastQ file format. Galaxy software was used to analyze the sequencing data. The data underwent quality control in the Galaxy software tool. The QC report showed no

overrepresented sequences or higher A/T base pair content than G/C base pair content. The data was then trimmed to remove adaptors using TrimGalore tool and the sequenced fragments were aligned to the hg19 genome by using the genome tool Bowtie2. Bam files were produced from the alignment. The blacklisted regions were removed using the Bedtools Intersect intervals. Peaks were called using the MACS2 program. The program produced BED files that contain a list of locations of the 'called peaks'. The files were then saved to UCSC genome browser for visualizing the ChIP peaks.

Buffer	**Recipe**
Buffer A	10 mM HEPES, pH 8 10 mM EDTA 0.5 mM EGTA 0.25% Triton X-100 1x Protease inhibitor cocktail (PIC)
Buffer B	10 mM HEPES, pH 8.0 200 mM NaCl 1mM EDTA 0.5 mM EGTA 0.01 % Triton X-100 1x PIC
ChIP Buffer	25 mM Tris-HCl, pH 8.0 150 mM NaCl 2 mM EDTA 1 % Triton X-100 0.25 % SDS 1x PIC
3x ChIP Dilution Buffer	25 mM Tris-HCl, pH 8.0 150 mM NaCl 2 mM EDTA 1 % Triton X-100 7.5 % Glycerol 1x PIC
Wash Buffer 1	20 mM Tris-HCl, pH 8.0 150 mM NaCl 2 mM EDTA

	1 % Triton X-100 0.1 % SDS
Wash Buffer 2	20 mM Tris-HCl, pH 8.0 500 mM NaCl 2 mM EDTA 1 % Triton X-100 0.1 % SDS
LiCl Buffer	10 mM Tris-HCl, pH 8.0 250 mM LiCl 1 mM EDTA 0.5 % NP-40 0.5 % Na-deoxycholate
TE/NaCl Buffer	10 mM Tris-HCl, pH 8.0 50 mM NaCl
Elution Buffer	100 mM NaHCO3 1 % SDS

Table 6 Buffers for ChIP.

ChIP Primers	**Sequences**
CDKN1B	5'-GGTTGCATACTGAGCCAAGT-3' GACTAGAATGCCAGGTCAAATAC-3'
CDKN2B	5'-ACAGGCTGTCATTGTAACACT-3' 5'-GGGATGGAGAGAAAAGACGC-3'
Ch18	5'-TTCAGTCTGGTGGTGGTGAACTA-3' 5'-GCCTTGGGAAATCCATCTTTT-3'
Ch22	5'-CCTGGAGGGCTTGGAGATG-3' 5'-GATCCTACGGCTGGCTGTGA-3'

Table 7 Primers used for manual ChIP-qPCR.

2.7 Proliferation and apoptosis assay

2.7.1 Proliferation assay

Proliferation activity was measured using the Click-iT Edu Microplate Assay (Molecular Probes, Invitrogen). Briefly, 10,000 cells were plated in a 96 well plate in triplicate and 24 hours later. 100 µl of 10 µM Edu was added to the cells and incubated for 2 or 4 hours depending on cell types in the 37°C incubator. Optimization of Edu incorporation time was performed for each cell type. All cell types apart from primary BECs were incubated with Edu for 2 hours. The incubation time for primary BECs with EdU was 4 hours. Cells

without Edu incubation were used as a control. After incubation with Edu, media was removed and 50 µl/ well of Click iT Edu Fixative (provided) was added to all wells (including no EdU control) and incubated for 5 mins at room temperature. From this point +/- EdU wells are treated identically. 30 µl/plate of Oregon green 488 azide and 1.2 ml/plate of Click-iT buffer additive (provided) was added on top of the Click iT Edu Fixative and incubated for 25 mins in the dark. The 96 well plate was wrapped in aluminium foil to prevent exposure to light. After incubation, the reaction buffer was removed and the wells were washed with 200 µl/ well 1x blocking buffer (provided) twice by pipetting. 50 µl/well of 1:400 HRP conjugate (provided) was added and incubated for 30 mins. After incubation, the HRP conjugate was removed and 200 µl/well of PBS was pipetted to wash the wells twice. 100 µl/well of OPD Peroxidase substrate (P9187, Sigma) was added to each well and incubated for approximately 15 mins. The plate was read at 450nm with a plate reader spectrophotometer. The cells were then fixed with methanol and then stained with 0.02% w/v crystal violet blue in water. Absorbance 450 nm was measured using a spectrophotometer plate reader. The amount of crystal violet blue staining is proportional to cell number. The Edu signal obtained was divided by the signal obtained from crystal violet blue to obtain the cell number normalized EdU reading.

2.7.2 Apoptosis assay

Caspase-3 activity was measured using the EnzChek Caspase-3 Assay Kit II (Molecular Probes, Invitrogen) which measures Caspase 3 enzyme activity by FITC excitation/emission measurement. The rhodamine 110-derived substrate (Z-DEVD-R110) used in the kit is a non-fluorescent bisamide compound that is converted to the

fluorescent monoamide and then to the even more fluorescent R110 product upon enzyme cleavage. Thus, high levels of cellular Caspase 3 activity should result in high fluorescence emission at wavelength 500 nm. In brief, cell lysates from at least 1 million cells were resuspended in 50 µl of the 1X lysis buffer (provided). The lysed cells were centrifuged at 5000 rpm for 5 min to pellet the cellular debris. The cell lysates can be stored in -80 °C until assays were performed. After thawing, 50 µl of the supernatant was then transferred to each well of a 90 well plate. 50 µl of the 1X lysis buffer was used as a no-enzyme control. To each well, 50 µl of the 2X working substrate (5 µm Z-DEVD-R110) (provided) was added and incubated for 30 mins. Fluorescence was measured at 485 nm excitation and 520 nm emissions with a spectrophotometer plate reader. For quantitation the R110 reference standard curve for fluorescence emission by R110 substrate was prepared by diluting the 5 mM stock solution of R110 reference standard ranging from 0-25 µM **(Figure 2.10)**. The Caspase-3 activity in the lysate sample is calculated using the formula displayed on the standard curve by substituting the fluorescence reading as y and x refers to the Caspase-3 activity.

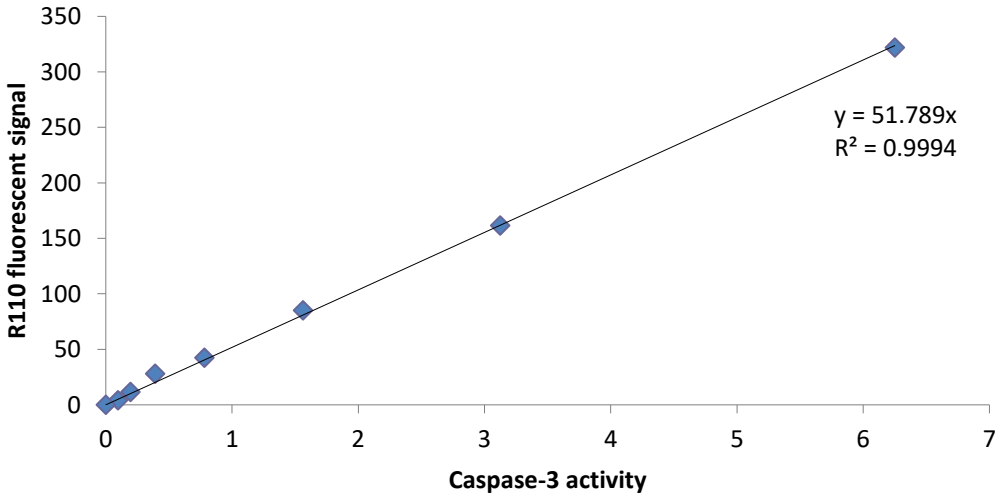

Figure 2.10 Standard curve for Caspase-3 assay.

2.7.3 Flow cytometry

Apoptosis kit (Annexin V Alexa Fluor™ 488 & Propidium Iodide (PI))(V13241, ThermoFisher) was used. Cells (1 x 10^6 cells/ml) were scraped out in ice cold PBS and pelleted by centrifugation at 500 g. 100 µl 1x Annexin-binding Buffer, 5 µl Annexin V staining and 5 µl PI were added to the cell pellet and resuspended. The cells were incubated for 15 min at room temperature in the dark. 400 µl 1x Annexin-binding Buffer was added to the cell suspensions. The stained cells were transferred to 5 ml sterile non-pyrogenic FACs tubes. A CyAn ADP flow cytometer was used for performing flow cytometry and gating was set to filter out dead cells or cell debris by generating a SSC vs. FSC plot. Summit software was used to analyze the data. The Annexin V APC channel was selected for the Annexin staining experiment. Cells without staining were used as a negative control and cells stained with PI were used as a positive control.

2.8 Colony formation assay

Two layers of 2-Hydroxyethyl agarose (Agarose VII)(A0701, Sigma) were prepared, 0.6 % 2-Hydroxyethyl agarose bottom layer and 0.3 % agarose for the cell-containing layer.

Preparation of working stock of agarose gel

3 % agarose was prepared by adding 0.9 of 2-Hydroxyethyl agarose followed by 30 ml of distilled water in a 100 ml glass bottle. It was then microwaved 3 times on low power and each for 15 seconds and gently swirled. The 3 % stock agarose-containing bottle was autoclaved and then stored at room temperature.

Preparation of bottom layer of agarose gel

The bottom layer of the agarose gel was made using 0.6% of agarose gel. This was prepared by mixing the stock 3 % agarose solution (above) to pre-warmed DMEM containing 10 % FBS in a ratio of 1:4. 2 ml of this mixture was then gently added to each well of a 6 well plate. The 6 well plate was then placed into 37 °C incubator for 3 hours in order to set the mixture. After the mixture was set, the cell-containing layer made up of 0.3 % agarose gel was prepared.

Preparation of upper layer

Cells were trypsinized and diluted to a cell concentration of 2 x 10^4/ml in DMEM. The stock agarose 3 % gel was pre-warmed to 37 °C and then gently mixed with media in a ratio of 1:4 to make 0.6 % agarose. 1 ml of the cells was mixed with 1 ml of 0.6 % agarose resulting in a 0.3 % agarose/cell mixture. 1 ml of the cell-agarose mixture was gently pipetted on top of the bottom layer of 0.6 % agarose in each well of the 6-well culture plate (2 x 10^4/ml) to create the upper layer. The 6-well plate was then placed in 37 °C incubator for 10 days. After 10 days, 5 images were taken for each well. The images were then analyzed using Image J.

2.9 Migration and invasion assay

2.9.1 Migration assay

For comparison of two conditions, migration assays for each condition was performed in technical triplicates. Therefore, for each condition approximately 4 x 10^6 cells were grown in one well of a 6 well plate (50 % confluency) for each assay. Cells were then starved for 24 hours in serum-free medium with 0.2 % BSA and treated with 1 mM hydroxyurea for 24 hours to prevent cell proliferation. Cells were trypsinized as

described in section 2.1.1 and an equal volume of media was used to inhibit further trypsin activity. Cells were then washed with PBS, counted and then diluted in serum-free media with 0.2% BSA to a concentration of 10^6/ml.

24 well ThinCert™ inserts (662610, Greiner bio-one) were placed in the wells of a 24-well plate. 600 µl DMEM with 10 % FBS was added to each well of the cell culture plate and then 200 µl of cells at concentration of 1 x 10^6/ml were added to each insert together with 1 mM hydroxyurea. After 72 hours, incubation in the 37 °C cell culture incubator, the medium was removed from the inserts and replaced by 450 µl of 8 µM calcein-AM1 (17783, Sigma). After 45 min incubation, the inserts were transferred to a fresh 24 well plate containing 500 µl pre-warmed Trypsin-EDTA in each well. The cell culture inserts were then discarded after the migrated cells were trypsinized and 200 µl of the Trypsin with cells mixture from each well was transferred to a black flat bottomed 96 well plate (CLS3925-100EA, Sigma). The fluorescence signal was read in a fluorescence plate reader at an excitation wavelength of 485 nm and an emission wavelength of 520 nm.

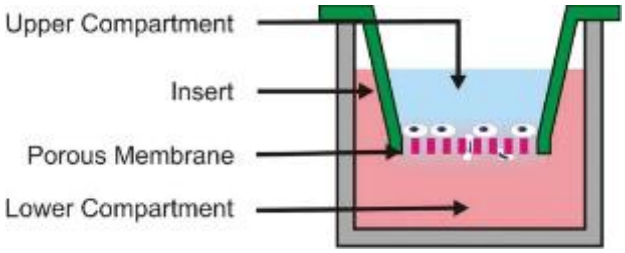

Figure 2.11 Diagram of migration assay

2.9.2 Invasion assay

Cells were grown and pre-treated exactly as described for migration assays above, except that for invasion assays cells were diluted to 5 x 10^4 cells/ml. For each experimental condition the assay was performed in triplicate.

For invasion assays, 8.0 µm polycarbonate membrane (CLS 3464 Corning costar) inserts were placed in each well of a 24 well plate. 50 µl of Matrigel™ (1:10) (BD Biosciences) in serum-free medium was pre-warmed to room temperature and pipetted on top of the inserts. The matrigel was left to set at 37 °C for 30 mins. 200 µl of cells in a density of 5 x 10^4 in serum free medium with 1 mM hydroxyurea was added on top of the matrigel and 500 µl of complete media was added at the bottom wells. The plate was incubated in the cell culture incubator for 24 hours. After incubation, the matrigel and cells mixture were removed from the top of the inserts by a cotton bud. Cells invaded to the other side of the membrane were fixed with 100% methanol for 5 mins and were stained with 0.4 % crystal violet blue diluted in methanol for 5 mins. Cells were then counted under the light microscope manually after washing with H_2O.

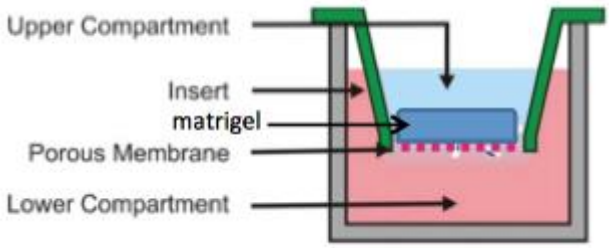

Figure 2.4: Diagram of invasion assay

2.10 Cumulative growth curves

To set up a cumulative growth curve, 2 x 10^5 cells were plated in triplicate in a 12-well plate. The cells were counted and re-plated every 48 hours. After washing with PBS and trypsinization, cells were transferred to an Eppendorf tube and counted by mixing 10 µl of Trypan blue (T6146, Sigma) with 10 µl of cells in the medium. 10 µl of Trypan blue-cells mixture was then transferred to a haemocytometer and cell counting was performed using microscope and clicker. The formula to calculate the cell number is as follows:

Number of cells/ml = Average cell count per square x 1/2 x 10^4

At every time-point, 2 x 10^5 cells were re-plated. This cell counting process was repeated every 48 hours until Day 9. Number of cells/ml was plotted with time.

2.11 MTT cell viability assay

For MTT assays, approximately 5 x 10^4 tumour cells were seeded into each well of a 96 well plate. A standard curve was plotted with MTT signal against cell number. The graph shows that the signal is proportional to the cell number within the cell number range for CCLP cells **(Figure 2.12)**.

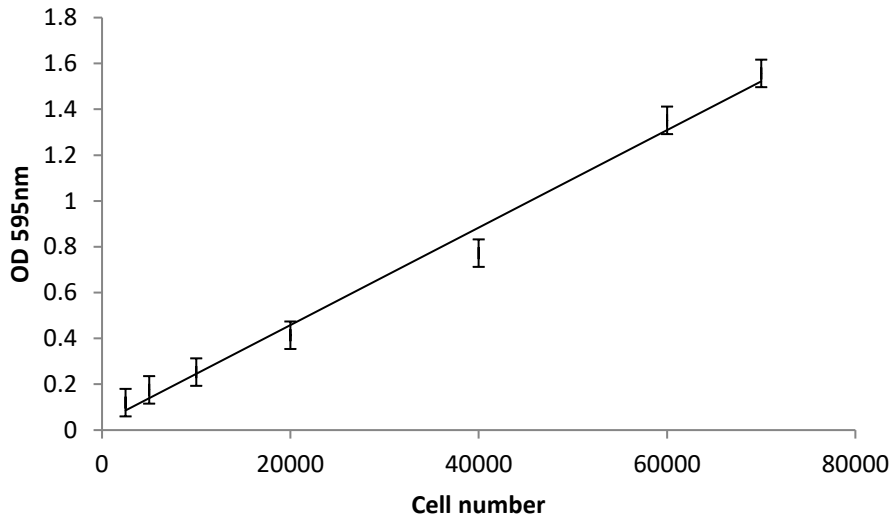

Figure 2.12 Standard curve of MTT signal against cell numbers.

Cell drug dose response curves were performed as follows: Cells were plated (5 x 10^4) in 96 well plates in triplicate. Drugs or Vehicle only were added to cells 24 hours after plating. After incubation for different drug treatments (24 or 96 hours), the cells were then incubated with 0.5 mg/ml MTT (3-(4,5-dimethylthiazol-2-yl)-2,5-diphenyltetrazolium bromide)(M5655, Sigma) dissolved in 100 µl DMEM for 3 hours. The formazan dye was solubilized with 100 µl Dimethyl sulfoxide (DMSO)(67-68-5, Fisher Scientific). The optical density was then taken at 595nm.

Drug dose response curves were generated using Prism. The log(inhibitor) versus response were chosen for the LD50 calculation in prism and the equation for the calculation is Y = Bottom value + (Top value-Bottom value)/(1+(X/LD50)). The top value refers to the maximum response (top of the curve) and the bottom value refers to the maximally inhibited response (bottom of the curve).

2.12 Statistical Analysis

The statistical significance of the data expressed in fold change or numerical variation with normal distribution such as proliferative rate, migration and invasion rate were determined using the two-tailed Student unpaired T-test. For data sets involving multiple group comparison such as comparing effect of various drug treatments, standard two-way ANOVA was used followed by the Bonferroni correction to compare all variables against the background (vehicle control). All data are presented as standard deviation (+/- SD) or standard error means (SEM). A p-value < 0.05 was considered to be statistically significant.

CHAPTER 3

Investigating the role of PRH in cholangiocarcinoma cells

3. Investigating the role of PRH in cholangiocarcinoma cells

3.1 PRH expression is upregulated in CCA

To examine the role of PRH in CCA, we first examined PRH expression in the public RNA sequencing data from The Cancer Genome Atlas (TCGA) cohort of CCA (45 samples)(https://www.cancer.gov/about-nci/organization/ccg/research/structural-genomics/tcga) **(Figure 3.1A)**. The data shows that PRH mRNA expression (mean $\log_2$ FC 5.5) is highly upregulated in almost all the intrahepatic and extrahepatic CCA samples when normalized to PRH expression in all other TCGA cancer cohorts. The mRNA expression levels are independent of changes in copy number for the *HHEX* (*PRH*) gene (**Figure 3.1A right panel**). Meanwhile in HCC, PRH mRNA expression is downregulated which is the opposite of the PRH mRNA data for CCA. As a comparison for expression, the $\log_2$ fold change gene expression of oncogenes (*MYC, NOTCH3*) and tumour suppressor genes (*SMAD4* and *TP53*) known to be altered in CCA were queried in the same database (**Figure 3.1Bi)**. The copy number and mutation profile are also queried in the same database shown in **Figure 3.1Bii and 3.1C**. Comparing PRH expression with *MYC* and *NOTCH3* in the TCGA database we find that MYC expression is also upregulated but its expression ($\log_2$ FC 1.9) is lower than of *PRH* and is more variable between the 45 CCA samples with some samples showing decreased MYC expression. *NOTCH3* expression is also generally upregulated (log2 FC 1.8) but the upregulation again is not as high as that of *PRH/HHEX*. *SMAD4* gene expression is most often downregulated among the 45 patient samples when normalizing to the average *SMAD4* expression in

other cancers. This expression pattern is in agreement with its role as a tumour suppressor in CCA.

Since the known oncogenes and tumour suppressor proteins show changes in expression in keeping with their known functions in the cell, we infer that PRH shows high expression because it has an oncogenic role in the bile duct cells. However, it remains possible that high PRH expression could be an artefact of normalization. Artefacts of normalization could include, for example, underestimation of *MYC* expression levels because it is an oncogene that is often upregulated in many cancer types and therefore its expression in CCA might not appear high relative to *MYC* expression across all other cancers in the TCGA database, whereas high *PRH/HHEX* expression is limited to a smaller number of cancer types. Moreover, *PRH/HHEX* expression can also be downregulated in a large number of cancers. The copy number variation of the genes is mostly independent of the expression level in the TCGA database except for *SMAD4* where there are deletions in the copy number and this is reflected in the low expression of *SMAD4* in the database.

TP53, a well-established tumour suppressor gene is also shown to have frequent high expression in the TCGA CCA dataset despite that many of the patients in the database show deletions in the copy number profile. One reason for this could be that the expressed *TP53* gene is a mutant as the mutated gene has oncogenic properties. However, according to the data, only a minority of samples (14 %) in the cohort show mutations. Therefore, it is equally possible that *TP53* expression levels are also an artefact of normalization that occurs because *TP53* is downregulated or mutated in other cancer types.

(A)

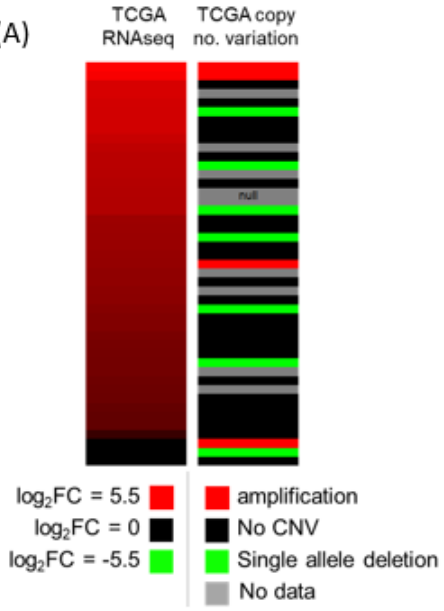
TCGA RNAseq
TCGA copy no. variation
null
log2FC = 5.5
log2FC = 0
log2FC = -5.5
amplification
No CNV
Single allele deletion
No data

(Bi)

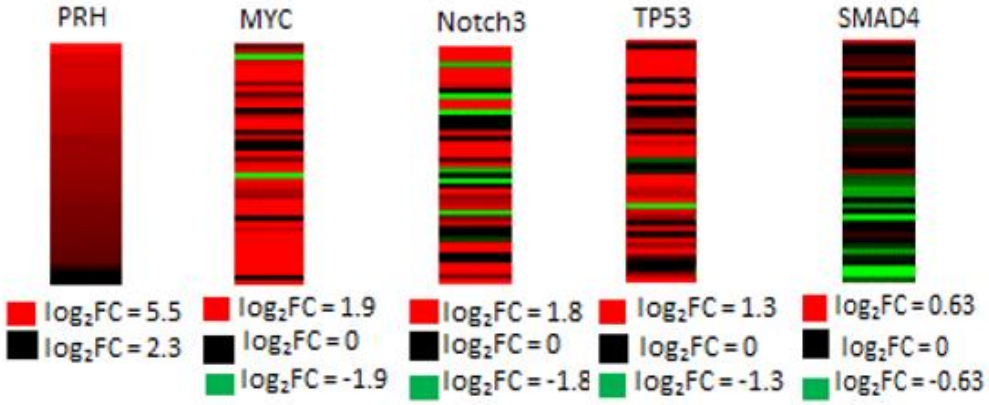
PRH
MYC
Notch3
TP53
SMAD4
log2FC = 5.5
log2FC = 2.3
log2FC = 1.9
log2FC = 0
log2FC = -1.9
log2FC = 1.8
log2FC = 0
log2FC = -1.8
log2FC = 1.3
log2FC = 0
log2FC = -1.3
log2FC = 0.63
log2FC = 0
log2FC = -0.63

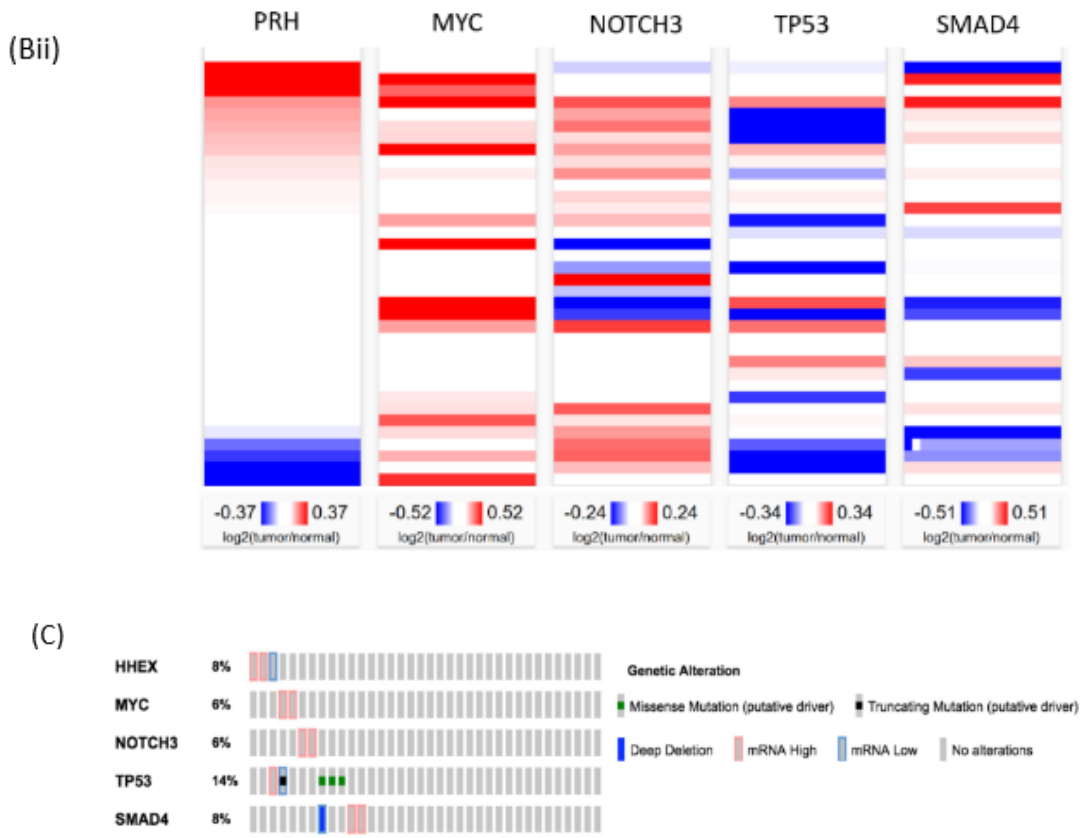

Figure 3.1 Public TCGA data on *PRH/HHEX* mRNA expression and *PRH/HHEX* mutation profile. (A)(Left panel) The log2 fold change of PRH expression normalized across all the cohorts in TCGA database per gene of 45 patients with CCA. The log2 FC shows the mean-centered value (Right panel). PRH copy number variation profile mapping of the patient of the left panel. (Bi)TCGA dataset of *TP53*, *SMAD4*, *PRH/HHEX*, *MYC* and *NOTCH3* expression by RNA-seq from UCSC Xena using 45 CCA patient samples, normalized across their expressions in all TCGA cohorts. (Bii) TCGA data showing the copy number variation profile for PRH, MYC, NOTCH3, TP53 and SMAD4. (C) TCGA data showing the mutation profile of HHEX (PRH), MYC, NOTCH3, TP53 and SMAD4 from the same dataset in Bi.

To understand the importance of high PRH expression, we further queried *PRH* expression in CCA samples in public databases; we used the Gene Expression Profiling Interactive Analysis (GEPIA) database (http://gepia.cancer-pku.cn/). This database uses TCGA data (n=34) but includes RNA-seq data for normal samples from all tissue types from the Genotype Tissue Expression (GTex) database (https://www.gtexportal.org/home/) as a comparison. Interestingly, GEPIA showed that across various tumour types, CCA is the only cancer type in which *PRH* is highly upregulated compared to normal control samples (n=9)**(Figure 3.2)**.

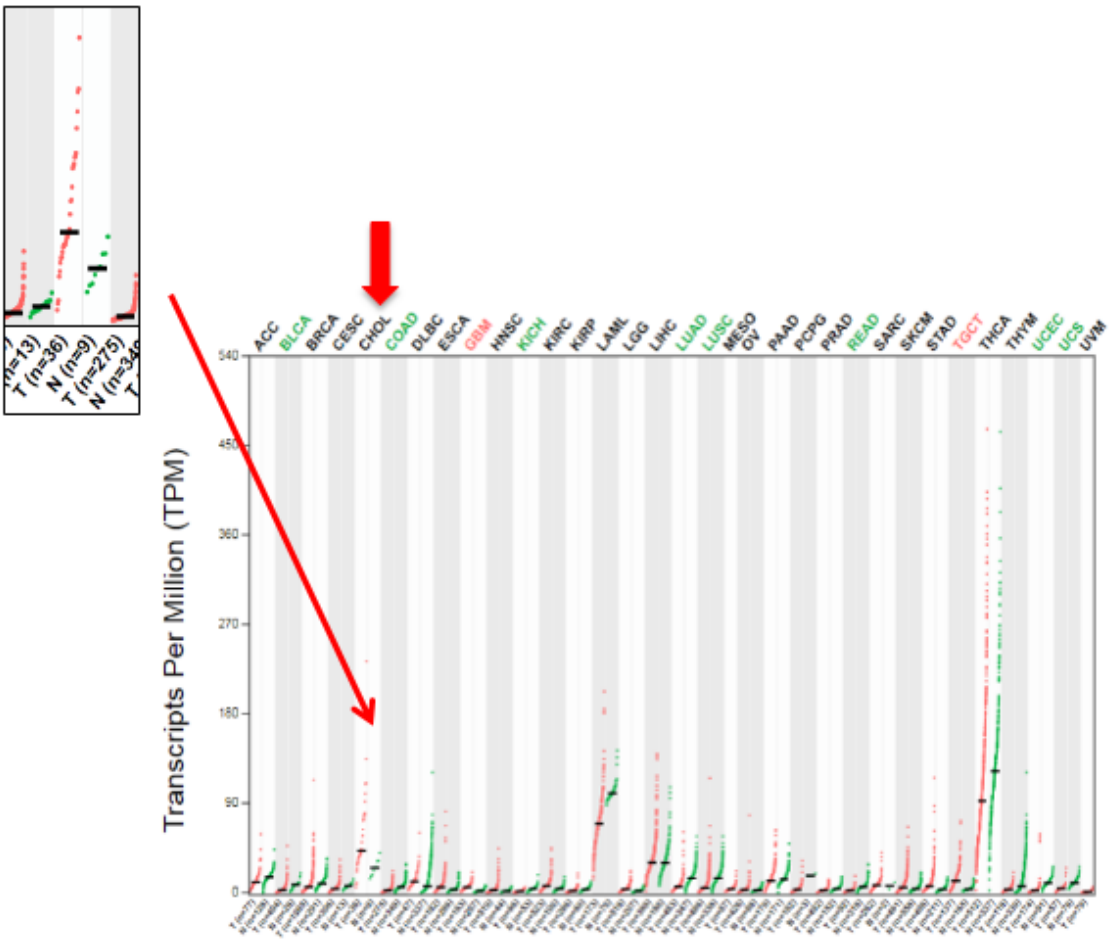

TCGA	Detail
ACC	Adrenocortical carcinoma
BLCA	Bladder Urothelial Carcinoma
BRCA	Breast invasive carcinoma
CESC	Cervical squamous cell carcinoma and endocervical adenocarcinoma
CHOL	Cholangio carcinoma
COAD	Colon adenocarcinoma
DLBC	Lymphoid Neoplasm Diffuse Large B-cell Lymphoma
ESCA	Esophageal carcinoma
GBM	Glioblastoma multiforme
HNSC	Head and Neck squamous cell carcinoma
KICH	Kidney Chromophobe
KIRC	Kidney renal clear cell carcinoma
KIRP	Kidney renal papillary cell carcinoma
LAML	Acute Myeloid Leukemia

LGG	Brain Lower Grade Glioma
LIHC	Liver hepatocellular carcinoma
LUAD	Lung adenocarcinoma
LUSC	Lung squamous cell carcinoma
MESO	Mesothelioma
OV	Ovarian serous cystadenocarcinoma
PAAD	Pancreatic adenocarcinoma
PCPG	Pheochromocytoma and Paraganglioma
PRAD	Prostate adenocarcinoma
READ	Rectum adenocarcinoma
SARC	Sarcoma
SKCM	Skin Cutaneous Melanoma
STAD	Stomach adenocarcinoma
TGCT	Testicular Germ Cell Tumors
THCA	Thyroid carcinoma
THYM	Thymoma
UCEC	Uterine Corpus Endometrial Carcinoma
UCS	Uterine Carcinosarcoma
UVM	Uveal Melanoma

Figure 3.2 GEPIA data of PRH expression. GEPIA data of *PRH/HHEX* mRNA expression across 33 tumour types including CCA. For each TCGA tumour (red), its matched normal and GTEx data (green) are given; T: tumour; N: normal; n: number. Y axis: transcript per million (log2(TPM + 1)). X axis: number of tumour and normal samples. The data for CCA is labelled as CHOL (see the arrow).

We next investigated the expression of *PRH* mRNA and protein in Thai (liver fluke associated) and UK (non-liver fluke associated) CCA cell lines using qPCR. As seen in **Figure 3.3A**, HuCCA and RmCCA (Thai) show high levels of *PRH/HHEX* mRNA expression, whereas CCLP (European), CCSW (European) and KKU-213 (Thai) show an intermediate amount of *PRH* mRNA expression. KKU-100 (Thai) shows a very low level of *PRH/HHEX* mRNA expression but AKN-1 and primary BECs show almost undetectable levels of *PRH/HHEX* mRNA expression (C^t value >40). These findings demonstrate that *PRH/HHEX* mRNA is elevated in tumour cell lines relative to primary cholangiocytes.

An in-house mouse monoclonal antibody (M3) has been generated in the Jayaraman Lab to detect endogenous PRH protein and has been previously characterized (Bess et al., 2003b; Swingler et al., 2004). Although the molecular weight of PRH protein is 30 kDa, it is known to be an SDS resistant protein that can migrate as a dimer (approximately 60kDa) but predominantly migrates with an apparent molecular weight of 37 kDa on SDS-PAGE (Soufi et al., 2006). **Figure 3.3B** shows that high levels of PRH protein expression were detected using Western blotting with the M3 antibody in HuCCA and RmCCA cells, intermediate levels in CCLP, CCSW, KKU-213 and KKU-100 and very low levels in BECs and AKN1 cells (Top panel). Lamin A/C protein was used as a loading control (Bottom panel). The Western blot was carried out with three independent passages of cells and densitometry was carried out to quantitate the result **(Figure 3.3C)**. The mRNA level of *PRH/HHEX* detected by qPCR correlates with the PRH protein levels detected by Western blot. In conclusion, PRH is expressed in all CCA cell lines with significantly lower expression in the immortalized cholangiocyte cell line AKN-1 and the non-cancerous primary BECs. The cell lines and primary BECs data are in accordance with

the public sequencing data seen in the TCGA and GEPIA databases that PRH is expressed at high levels in CCA cells compared to cholangiocytes.

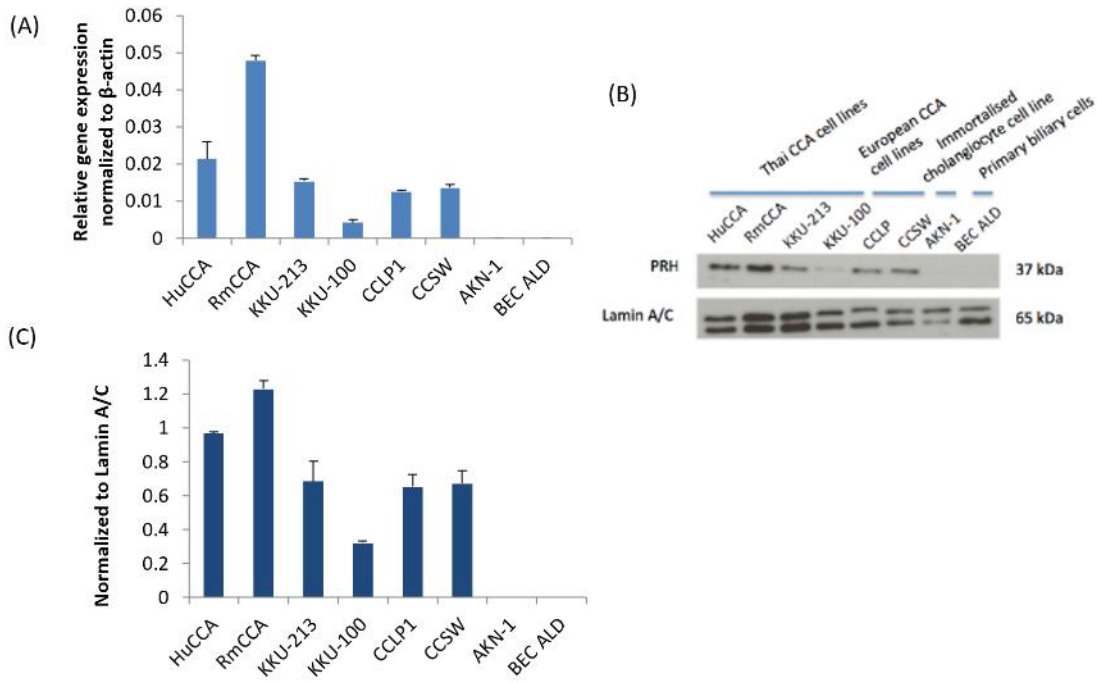

Figure 3.3 Characterizing PRH expression in a range of CCA cell lines, immortalised cholangiocytes and primary BECs. qPCR measuring the mRNA expression of *PRH/HHEX* in CCA cell lines and also primary biliary epithelial cells (BECs) from a patient with alcoholic liver disease (ALD). *PRH* expression in each case was normalized against β-actin (n=3). (B) Representative Western blotting showing PRH protein expression in a panel of CCA cell lines, the immortalized cholangiocyte cell line AKN-1 and primary BECs from a patient with ALD. Whole cell protein extracts were taken from each cell line plated in one well of a 6 well plate and grown to confluence. In each case, 10 µg of protein was loaded into each lane and endogenous PRH detected using a mouse M3 polyclonal antibody. Lamin A/C antibody was used to detect Lamins to determine protein loading (n=3). (C) Quantification of the PRH protein intensity from the Western blot using Image J where the PRH band intensity is normalized against the loading control Lamin A/C (n=3). The error bars represent the Standard Deviation (SD) of three biological repeats of experiments.

Immunohistochemistry (IHC) was performed by Dr P. Kitchen with the in-house PRH M3 antibody on a CCA tissue microarray obtained commercially (Abcam)**(Figure S1A)**. The data shows that PRH protein is also upregulated in primary CCA tissues compared to border non-involved bile duct tissues.

Collectively, mRNA and protein expression of PRH in CCA cell lines are highly upregulated. This is in accordance with staining observed in these primary CCA tissue

microarray samples.

3.2 PRH knockdown in CCA inhibit cumulative cell growth

As PRH is highly upregulated in CCA cells lines and CCA primary tissues relative to primary bile ducts and primary BECs, we investigated the effect of PRH KD on tumour cell growth. We chose the CCLP cell line for knockdown experiments because they express PRH at high levels and are relatively easy to transfect. To generate the PRH KD cell line, 1 x 10^6 CCLP cells were seeded in a 6 well plate and transfected with a pRs-Hush-shRNA PRH/HHEX construct (Origene, TR312464). This construct encodes shRNA targeting the *PRH/HHEX* gene and puromycin resistance or transfected with scrambled shRNA as a control (Origene, TR30012). The PRH knockdown and scramble control cells were selected with puromycin (0.25 µl/ml) for three weeks to produce polyclonal cell lines and three PRH knockdown (KD) clones were generated. Details of this protocol are described at **section 2.1.7**. To confirm the PRH knockdown, qPCR and Western blot analysis were carried out with control shRNA and PRH shRNA KD cell lines. **Figure 3.4A** shows the PRH transcript levels in all three knockdown clones are decreased compared to the control. Clone 1 has the most significant knockdown (p=0.0078). Western blotting was carried out to confirm the knockdown using the M3 anti-PRH antibody. **Figure 3.4B** shows that the PRH protein in clone 1 is strongly downregulated compared to the control. Surprisingly, clone 3 has even higher PRH expression than the control which is not expected. It is possible that the shRNA did not integrate into the genome but having other unknown effects on the cells that increases PRH expression.

To determine the effect of PRH KD on the growth of the cell population, 2 x 10^5 knockdown (clone 1 (49-1)) cells or paired control cells were plated in triplicate in a 12 well plate. Cells were counted every 48 hours until day 10 **(See section 2.10)**. This experiment was performed three times independently. **Figure 3.4C** shows the cumulative growth curves for PRH KD clone 1 and control calculated using the three biological repeats. The CCLP PRH KD cell cumulative cell number is much lower than that of control cells. **Figure 3.4D** shows the doubling time of PRH KD and its control cells **(doubling time calculation at section 2.10)**. The doubling time of PRH KD CCLP is 1.4 times longer than that of control CCLP cells. Additional clones were also investigated for cumulative growth and their growth curves and showed similar results (performed by Dr P. Kitchen, data not shown).

It can be concluded that knockdown of PRH in CCLP cells inhibits the rate of increase in the growth rate of the KD cell population compared to control CCLP cells.

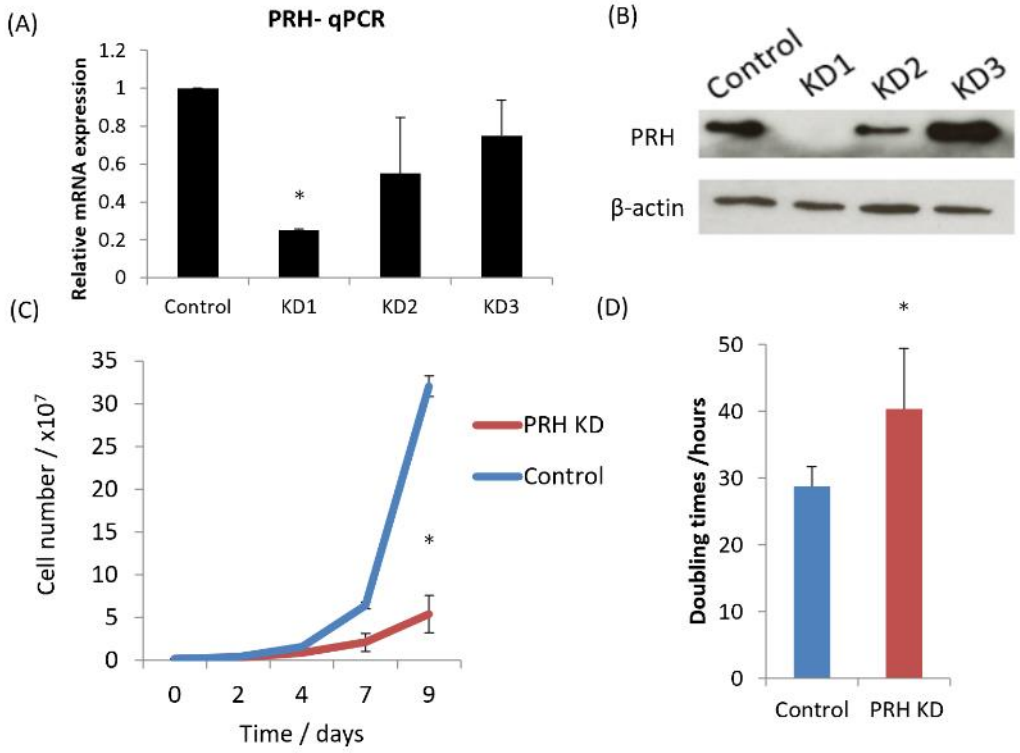

Figure 3.4 PRH KD inhibits cumulative cell number in CCLP. (A) *PRH* mRNA expression in three independent clones was measured by qPCR. β-actin was used as the housekeeping gene and *PRH/HHEX* and housekeeper were normalized against their expression in the scrambled shRNA control cells. Statistical test: Two-tailed unpaired T-test (n=3; *p=0.0078). (B) Western blots showing PRH protein expression in three independent PRH KD clones was detected using M3 polyclonal mouse antibody. b-actin antibody is used to detect b-actin protein loading control in the same samples. Whole cell protein extracts were generated from one well of a 90% confluent 6 well plate, 10 µg of protein was loaded into each well (C) Cumulative growth curve of PRH KD CCLP cells (clone 49-1) and its paired scrambled control grown for 9 days with three different passages. Statistical test: Two-tailed unpaired T-test (n=3; *p=0.02) (D) Doubling time of PRH KD (clone 49-1) and shRNA scrambled control CCLP cells calculated from the growth curves produced after three different passages. Statistical test: Two-tailed unpaired T-test (n=3; *p=0.04). Error bars show the SD among the three experimental repeats.

3.3 PRH knockdown inhibits cell proliferation

To investigate whether the decrease in cell numbers in PRH KD CCLP cells is due to a decrease in proliferation or to an increase in apoptotic activity, Edu proliferation and Caspase-3 apoptosis assays were carried out. The Edu assay is based on incorporation

of a nucleotide analogue into DNA and a click reaction—a copper-catalyzed covalent reaction between an azide and an alkyne that allows labeling of the newly synthesized DNA containing Edu. After two hours of Edu incubation, Edu is incorporated into newly synthesized DNA and is labeled with the click reaction. Horseradish peroxidase (HRP)-antibody is then used to detect the product of the click reaction. To determine if the proliferation rate is altered, the Edu incorporation is normalized to cell number by staining cells with crystal violet blue and the signal was read by a fluorescence microplate reader. The signal detected reflects the rate of DNA synthesis and this is used as a measure of the rate of cell division. **Figure 3.5A** shows that PRH KD CCLP cells are significantly less proliferative compared to the control CCLP cells in Edu assays.

In order to further examine whether PRH has an effect on altering the cell cycle profile of CCLP cells, flow cytometry following membrane permeabilization of cells with Igepal detergent and propidium iodide (PI) staining of DNA was performed on PRH KD CCLP cells and controls. PI is a DNA binding dye that allows the accurate quantification of DNA content in the cells by flow cytometry. Cells in S phase have more DNA content compared to those in G_1 phase so cells in S phase take up more PI and fluoresce brighter and give a higher signal. Cells in G_2 phase have their DNA content doubled after mitosis so cells in G_2 phase have double the signal compared to G_1 phase. PE Texas red channel (wavelength: 615 nm) was selected when conducting flow cytometry in order to detect the signal from PI. **Figure 3.5B** shows the histogram of the cell cycle profile (PI staining) of PRH KD (top panel) and the control (bottom panel) for a representative experiment and **Figure 3.5C** shows pooled data from three repeats of PI staining followed by flow cytometry. For PRH KD cells, it can be seen that a lower percentage in the population

(9%) are in S phase compared to control (26%)($p<0.05$). Moreover, there are more PRH KD cells in G_1 (81%) phase compared to the controls (G_1: 67%). These data are in agreement with the Edu incorporation data. As a higher percentage of the cell population of PRH KD cells are in G_1 phase compared to controls, this suggests that PRH KD cells take a longer time to go through G_1 phase.

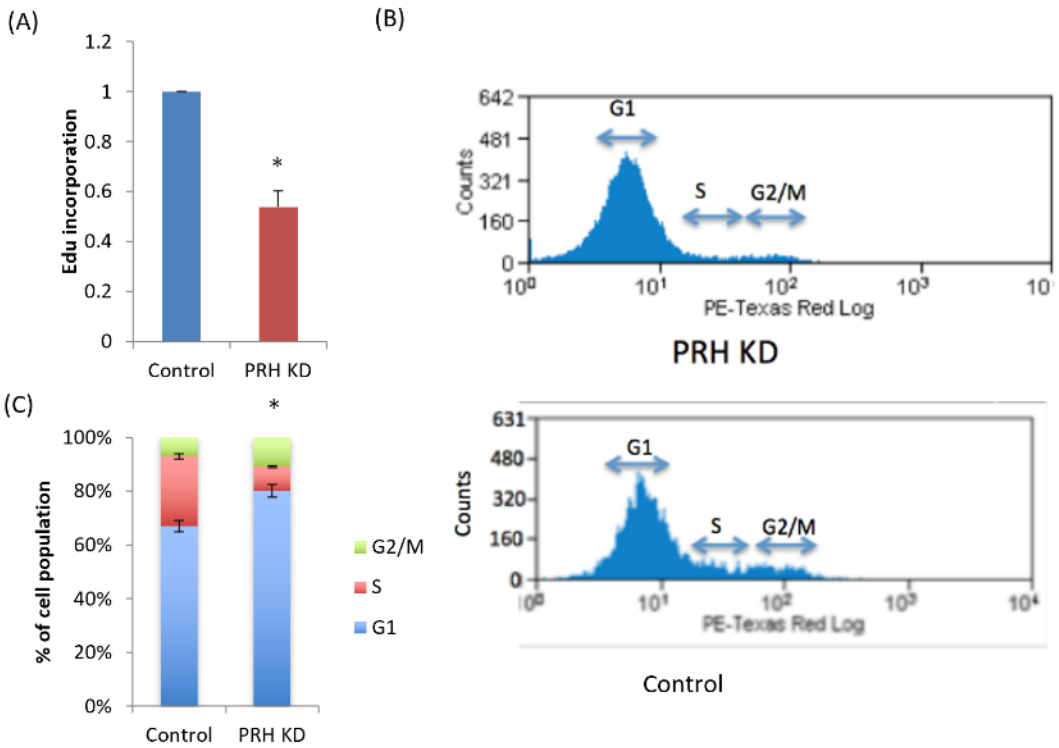

Figure 3.5 PRH depletion decreases cell proliferation in CCLP. (A) Proliferative activity of PRH KD cells normalized to scrambled control CCLP cells. Cells were incubated in Edu for 2 hours and click reaction was detected using HRP-conjugated antibody and OPD substrate. Absorbance was measured at 450 nm. Edu incorporation was normalized to cell number by staining cells with crystal violet blue and the signal was read by a fluorescence microplate reader. Error bars show the SD for the three experimental repeats. Statistical test: Two-tailed unpaired T-test (n=3; *p=0.03) (B) Representative plots for PI staining of PRH KD and control cells showing cell cycle profile using the PE-Texas Red Log channel at 565 nm. (C) Quantification of the cell cycle profile by Flow cytometry. Error bars show the SD of three biological repeats of the experiment. Statistical test: Two-tailed unpaired T-test (n=3; *p<0.04), there is significant difference in G1 and S phases.

A Caspase-3 dependent apoptosis assay was performed to determine whether PRH KD has any pro-apoptotic effect on CCLP cells. The Caspase-3 assay (Thermo fisher) is a

fluorescent assay using FITC excitation/emission measurement to measure Caspase-3 activity. The rhodamine 110-derived substrate (Z-DEVD-R110) used in the kit is a non-fluorescent bisamide compound that is converted to the fluorescent monoamide and then to the even more fluorescent R110 product upon enzyme cleavage. Thus, high levels of cellular Caspase-3 activity should result in high fluorescence emission at wavelength 500 nm. A standard curve using increasing concentrations of R110 was plotted to show a linear relationship between the amount of R110 released in the reaction to allow quantification of Caspase activity **(See M&M section 2.7.2)**. CCLP cells treated with Staurosporin for 24 hours were used as a positive control for Caspase 3 activity as it is a well-characterized apoptosis inducer (Belmokhtar et al., 2001). Both the PRH KD and control CCLP cells have low Caspase-3 activity compared to the positive control. However, PRH KD CCLP cells have (1.7 times) less Caspase-3 activity than the control CCLP cells ($p<0.05$) shown in **Figure 3.6A**.

To determine whether this small change in Caspase-3 activity results in biologically significant change in apoptosis, we carried out Annexin V-FITC staining followed by flow cytometry. Annexin is a cellular protein that allows detection of apoptosis as it can bind to phosphatidylserine molecules that translocate to the extracellular membrane of the cell when the cells undergo apoptosis. Flow cytometry was used to detect the signal using the Annexin V-FITC channel at 525 nm. By staining the cells with both PI and Annexin V-FITC, apoptosis and necrosis can be differentiated (**Figure 3.6B)**. Early apoptosis (R6) results in Annexin V staining alone, late apoptosis (R4) results in Annexin V staining together with PI staining of DNA. Necrosis (R3) is distinguished by PI staining in the absence of Annexin staining and viable cells identified by no staining with either

PI or Annexin (R5). **Figure 3.6B** shows the quantification of the flow cytometry results of three independent passages of control and PRH KD cells. There is no statistically significant difference in the early or late apoptotic activity of PRH KD cells compared to control CCLP cells in this experiment, although there is a small but reproducible difference in Caspase-3 activity of PRH KD cells.

Figure 3.6C shows a representative dot plot that reveals the early and late apoptotic activities of CCLP KD and control CCLP cells.

We conclude that PRH KD cells are less proliferative than control cells and this accounts for the slower growth observed in the PRH KD cell population.

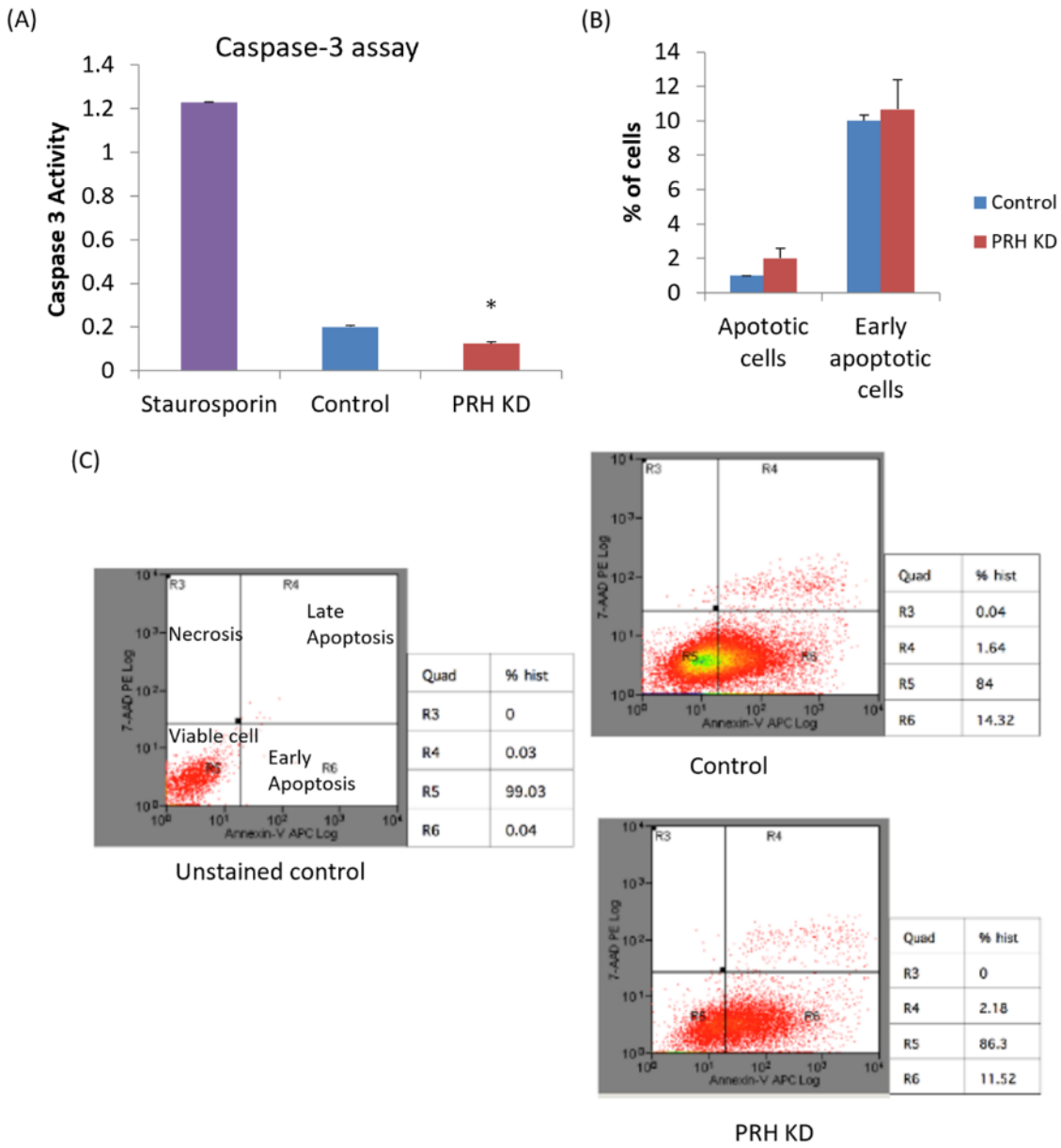

Figure 3.6 PRH depletion does not change apoptotic activity in CCLP. (A) Caspase-3 activity was measured by using EnzChek Caspase-3 Assay Kit. 1 µm Staurosporin was used as a positive control. Error bars show the standard error mean among the three experimental repeats. Statistical test: Two-tailed unpaired T-test (n=3; *p<0.05) (B) Flow cytometry with Annexin V staining measuring apoptosis events in CCLP KD and control cells at 525 nm. Annexin-V APC-Log channel was selected. Area of dot-plot R6 represents early apoptotic cells and area R4 represent apoptotic cells at late apoptosis stage. The error bars represent the Standard Deviation (SD) of three biological repeats of experiments. (C) Quantification of flow cytometry data with Annexin staining. Statistical test: Two-tailed unpaired T-test. Independent experiments n=3.

3.4 PRH knockdown changes cell morphology and inhibits cell migration and invasion

Close examination of the morphology of the PRH KD and paired control cells show a difference in morphology (**Figure 3.7A)**. The PRH KD cells are more adherent and rounder in shape and grow adjacent to one another compared to control cells suggesting an epithelial phenotype compared to the elongated mesenchymal control cells. Western blotting experiments with E-cadherin antibody show that CCLP cells have no expression of E-cadherin whereas PRH KD cells have high E-cadherin expression **(Figure 3.7B)**. Vimentin, a mesenchymal marker is also decreased in the PRH KD cells when detected using an anti-Vimentin antibody by Western blotting. These observations suggest that PRH KD CCLP leads CCLP cells to undergo mesenchymal to epithelial transition (MET).

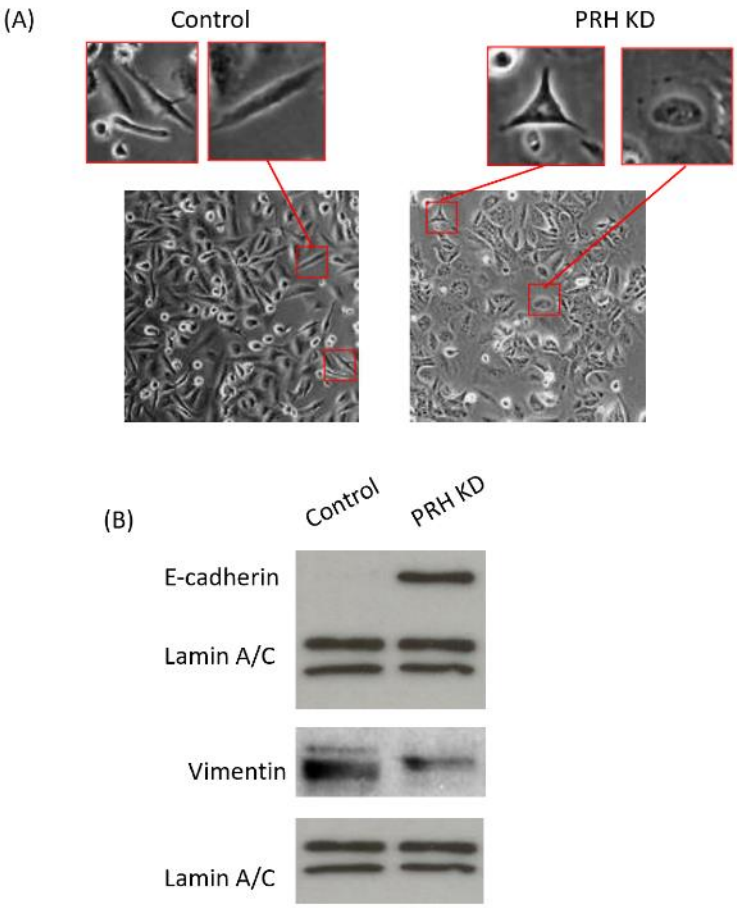

Figure 3.7 PRH KD leads to MET. (A) Morphology of stably transfected PRH KD and control CCLP cells grown at similar cell density. Image taken at 10x by light microscope. (B) Representative Western blots showing E-cadherin and Vimentin expression in PRH KD and control CCLP cells using monoclonal rabbit anti-E-cadherin and monoclonal rabbit anti-Vimentin antibodies. Whole cell protein extracts were produced for each cell line (1×10^6 cells) plated in a single well of a 6 well plate, 10 µg of protein was loaded into each lane. Lamin A/C was used as a loading control.

As PRH KD leads to MET, the migration and invasion of PRH depleted CCLP cells were investigated. Migration assays were performed by plating 2×10^5 cells on a transwell filter insert in a 24 well plate in a serum gradient (2-10 %). Proliferation was inhibited by hydroxyurea treatment (1 mM) for 24 hours and at the same time the cells were also starved with reduced serum (2 %) in media 24 hours before the experiment. Cells that migrated to the other side of the filter towards high serum were stained with Calcein after 72 hours. Calcein is a cell dye that allows measurement of cell viability and hence cell number. The migrated cells stained with Calcein will give a fluorescence signal that

can be detected with a plate reader at emission wavelength of 520 nm. **Figure 3.8A** shows that PRH KD CCLPs are less migratory compared to control CCLP cells.

To investigate if PRH KD has an effect on cell invasion, 1 x 10^4 cells starved with reduced serum (2 %) for 24 hours and also incubated with 1mM hydroxyurea were plated on a layer of Matrigel (10 %) placed on a transwell filter insert in a 24 well plate. Proliferation was inhibited by 1 mM hydroxyurea treatment for 24 hours before the start of the invasion assay and throughout the assay. Cells that invaded to the other side of the transwell filter in response to a serum gradient (2-10 %) for 24 hours were counted under the light microscope after staining of the invaded cells with crystal violet blue which allows visualization of viable cells. **Figure 3.8B** shows that PRH KD cells are also less invasive compared to controls.

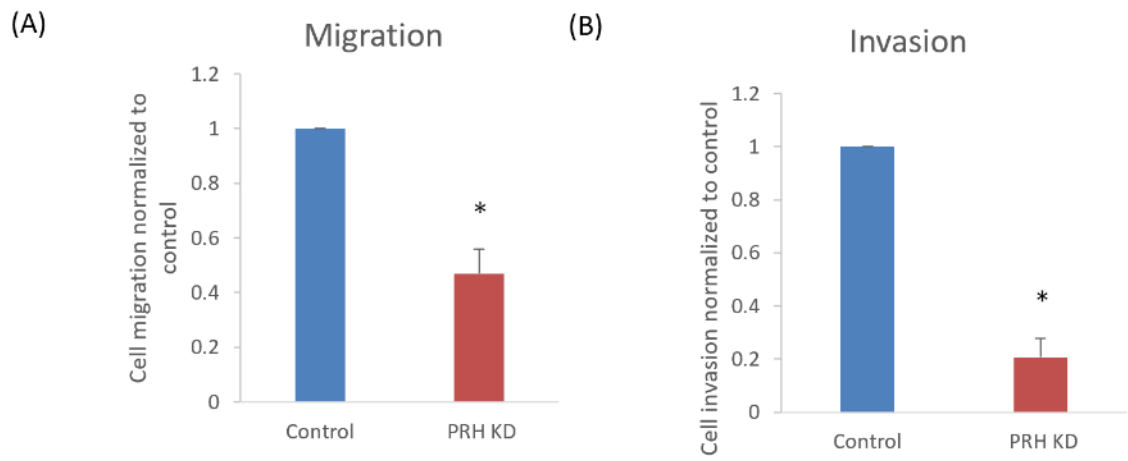

Figure 3.8 PRH KD inhibits cell migration and invasion. (A) Fluorescence signal of migrated PRH KD cells normalized to control CCLP cells. Migrated cells traverse through transwell filter in a 2-10% serum gradient for 72 hours. 1 mM hydroxyurea was added for 24 hours before the migration assay and throughout the assay to inhibit proliferation. Statistical test: Two-tailed unpaired T-test (n=3; *p=0.03) (B) Invasion of PRH KD normalized to control CCLP cells. PRH KD or control cells are plated on transwell filter coated with 10% Matriel Gel. Invaded cells traverse through transwell filter in a 2-10% serum gradient for 24 hours. 1 mM hydroxyurea was added for 24 hours before the invasion assay to inhibit proliferation. The cells were counted following crystal violet staining. Statistical test: Two-tailed unpaired T-test (n=4; *p=0.03). Error bars show the SD among the three experimental repeats.

3.5 PRH knockdown cells decreases colony formation and reduces tumour size and numbers in vivo

Since morphology and invasion are altered in the PRH KD cells and the cells appear to undergo MET, we next examined whether PRH knockdown affects the ability of CCLP cells to withstand anoikis using the colony formation assay. The colony formation assay serves as a marker for tumour forming properties of cells as anoikis resistance is only found in cells that are no longer dependent on cell-cell contacts for survival. Anoikis refers to anchorage-dependent cells undergoing apoptosis in the absence of support from the surrounding extracellular matrix (Paoli et al., 2013). Anoikis resistance is a property of both Cancer Stem Cells and their progeny - the larger set of Cancer Stem Cell-like cells as it does not directly measure cancer stem cell self-renewal.

The colony formation assay was performed by plating 10^3 cells per well in a 6-well plate on soft agar (**See M&M section 2.8**). Images of control and PRH KD colonies were taken with light microscope after 10 days and the images were analyzed by ImageJ software. **Figure 3.9A** shows that PRH knockdown cells form fewer colonies in soft agar than the CCLP control cells. A histogram was plotted to show the distribution of number of colonies of different sizes using Image J software for both PRH KD and control CCLP cells **(Figure 3.9B)**. In general, the average size of the colonies formed by the PRH knockdown cells is smaller than the control cells **(Figure 3.9C)**. It can be seen that PRH KD cells form almost no colonies larger than 1.2 µm in diameter **(Figure 3.9B)**. We conclude that PRH KD decreases anoikis resistance and also decreases the proliferation of surviving cells in this assay.

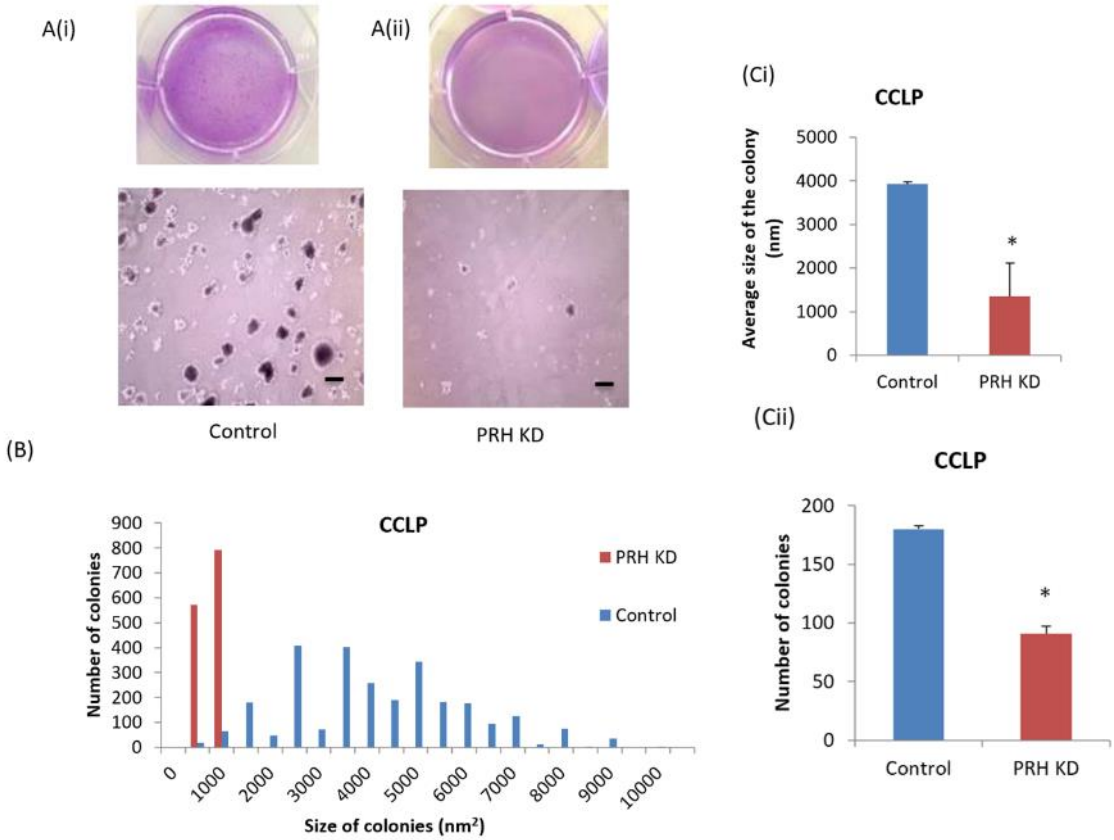

Figure 3.9 PRH depletion inhibits colony formation in soft agar. (A) Image of plates showing colonies formed by (i) CCLP shRNA scrambled control cells and (ii) PRH KD CCLP cells and insets show images of individual colonies taken under light microscope at magnification 10x. The scale bar represents 20 µm in length. (B) Image J was used to analyze the images to determine the number of colonies and size of each colony in each image. A histogram was plotted to show the number of colonies of each size formed by PRH KD and control CCLP cells. The histogram shows pooled data from 3 biological repeats of the colony formation assay with 5 images taken for each cell line. (Ci) Average size of the colonies formed by PRH KD and control CCLP cells. Error bar shows the SD among the three experimental repeats. (Dii) Average number of the colonies formed by PRH KD and control CCLP cells. Error bar shows the SD for the three experimental repeats. Statistical test: Two-tailed unpaired T-test (n=3; *p<0.001).

Colleagues in the wider Jayaraman collaboration further tested the ability of PRH KD cells to form tumours by growing the PRH KD CCLP cells in xenograft experiments. The *in vivo* xenograft experiment was carried out by Dr. Danielle Clark and supervised by Professor Kevin Gaston and Dr Sebastian Olten (University of Bristol). Experiments were performed by growing 1 x 10^7 PRH KD or control CCLP cells and injecting them subcutaneously into 9 nude mice and the tumour size was measured over 25 days. Tumours were only generated in 3/9 mice injected with PRH KD cells compared to 9/9

controls **(see appendice S1B)**. The size of tumours in the mice injected with PRH KD cells were significantly smaller compared to the controls.

In summary, PRH KD decreases population growth, increases cell doubling-time and decreases the cell proliferation rate. Moreover, PRH KD decreases the cell migratory and invasive properties of CCLP cells and these changes are consistent with an increased MET. In addition, PRH KD inhibits anchorage-independent growth of CCLP cells *in vitro* and the reduction of PRH levels inhibits CCLP tumour growth in a xenograft model. Collectively these results suggest that endogenous PRH can function as an oncoprotein in CCLP and that it regulates both cell proliferation and cell invasion.

3.6 RNA sequencing and Gene Set Enrichment Analysis to identify differential gene expression and altered pathways in PRH KD cells

To characterize the mechanisms that lead to the phenotypic changes observed we carried out transcriptomics. In order to identify the PRH target genes involved in the KD phenotype, RNA-sequencing (RNA-seq) was carried out with total adenylated RNA from two independent PRH KD clones of CCLP cells and paired control cells at their early passage (p3). Total RNA was extracted and RNA integrity was assessed on a bioanalyzer and 100 ng/ml of RNA with at least RIN 9 was sent for library preparation to C. Whalley (Genomics unit of UoB) using NextSeq HIGHv2.5 150 cycle sequencing kits. Approximately 2 x 35 million reads/sample were produced from the Illumina sequencing with 75 bp paired end reads for this experiment. The reads refer to the number of cDNA fragment sequences produced by the sequencing and paired end refers to each cDNA fragment being sequenced from each end. Initial bioinformatics analysis of the RNA-seqdata was performed using Galaxy software by Dr. Phil Kitchen (See details of

bioinformatics in **section 2.4.4**). The reads were mapped to the genome and then counted; the count data was normalized to the length and GC content of the gene. A scatter plot showing the $\log_2$ expression (normalized count) for control against KD is shown in **Figure 3.10**. The scatter plot shows genes that are not differentially regulated in black and genes that are differentially regulated in red. 189 genes are downregulated and 430 gene are upregulated in PRH knockdown cells.

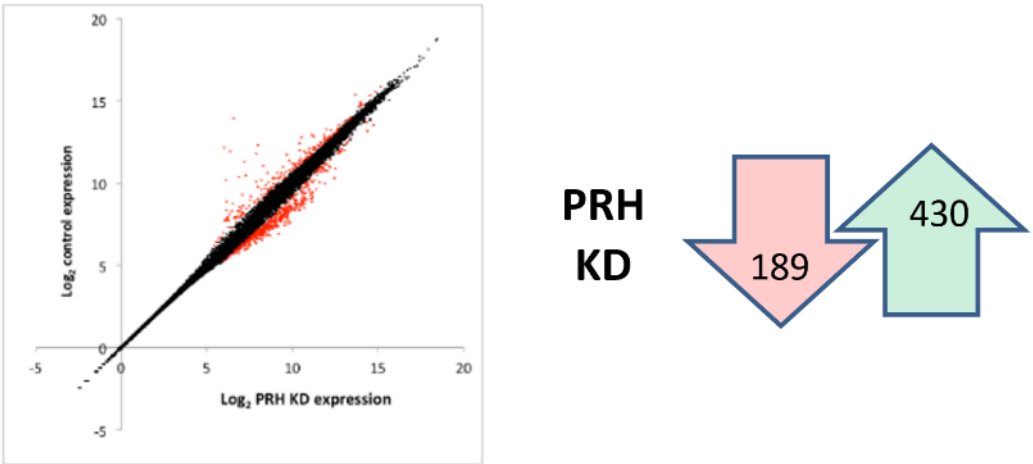

Figure 3.10 RNA-seq on PRH depleted and control CCLP cells. Scatter plot (left) showing the log2 expression of differentially expressed genes (DEG) in PRH KD CCLP cells compared to scrambled vector control cells. Red dots above the diagonal are genes that are differentially upregulated and red dots that are underneath the black dots are the genes that are downregulated. The number of genes that are differentially expressed in positive or negative direction (right).

Galaxy software also allows differential gene expression (fold change) and statistical analysis to be carried out on the normalized count file and a Deseq2 file was generated to show changes in gene expression (fold change), p-value and q-value. P-value lower than 0.05 indicates genes that are significantly altered in two replicates. The q-value refers to an adjusted p-value with an optimized FDR (false discovery rate). A q-value of 0.05 means that it is accepted that 95% of samples that are found to be statistically significant will not be false positive. In all our RNA-seq analysis, $q<0.05$ was accepted

and all genes irrespective of magnitude of fold change that had q-value of <0.05 were used for subsequent analysis.

To validate the RNA-seq data, the expression of selected genes such as *NOTCH3* and *CDH1* were examined using qPCR and corresponding protein levels for Notch3 and E - cadherin were examined using Western blotting. These genes were chosen because they have a fold change >1.5 and are also known to be important in the development of CCA. In agreement with the RNA-seq data, there is a reduction in *NOTCH3* and *CCND2* gene expression **(Figure 3.11A and Figure 3.11B)**. Anti-Notch3 antibody detects both the full-length Notch receptor at 120 kDa and the two truncated intracellular domains of Notch3 resulting from the first and second cleavages in the Notch signaling pathway at 90 and 100 kDa. Both the full length and truncated Notch3 proteins are downregulated in the PRH KD cells in agreement with the decrease in *NOTCH3* expression at transcript level **(Figure 3.11C)**. Surprisingly, the Cyclin D2 antibody was not able to detect any Cyclin D2 protein in these experiments in either the PRH KD cells or control cells even at concentration of 30 µl/loading of protein in several repeats of this experiment (data not shown). The Cyclin D2 antibody was confirmed to be a specific antibody because it is able to detect Cyclin D2 in other cell types and can detect very low levels of Cyclin D2 protein in CCLP at long exposures in Western blotting experiments **(Figure 3.13)**. The reason for the lack of staining is not known but is likely to be because Cyclin D2 protein levels is likely very low even in CCLP cells.

Apart from Notch3 and Cyclin D2, RNA-seq showed upregulation of *CDKN1B* and *CDKN2B* in PRH KD CCLP cells **(Figure 3.11A)**. qPCR and Western blot were carried out to verify the result. **Figure 3.11B** shows that the transcript level of *CDKN1B* (p27) and

CDKN2B (p15) of PRH KD CCLP cells are significantly upregulated compared to control CCLP cells. Western blot was performed for p27 and **Figure 3.11D** shows that PRH KD also increases the protein levels of p27 (*CDKN1B*) in CCLP cells**.** Alterations in the cell cycle genes *CCND2* (decreased), *CDKN1B* and *CDKN2B* (increased) likely underlie the decrease in proliferation observed in the PRH KD CCLP cells.

As mentioned in section 3.4, PRH KD cells also changes cell morphology and restores E-cadherin expression. The RNA-seq data together with qPCR data are in agreement with Western blotting data showing that PRH KD restores E-cadherin expression **(Figure 3.7B)** and the change in this gene is likely to play a major role in MET observed for these cells **(Figure 3.7A)**. Interestingly, RNA-seq and qPCR show that Vimentin gene expression is unchanged whereas in PRH KD cells decreased Vimentin protein expression is observed. Further investigation of the gene expression of Vimentin with cell number and PRH expression will be discussed in the next chapter.

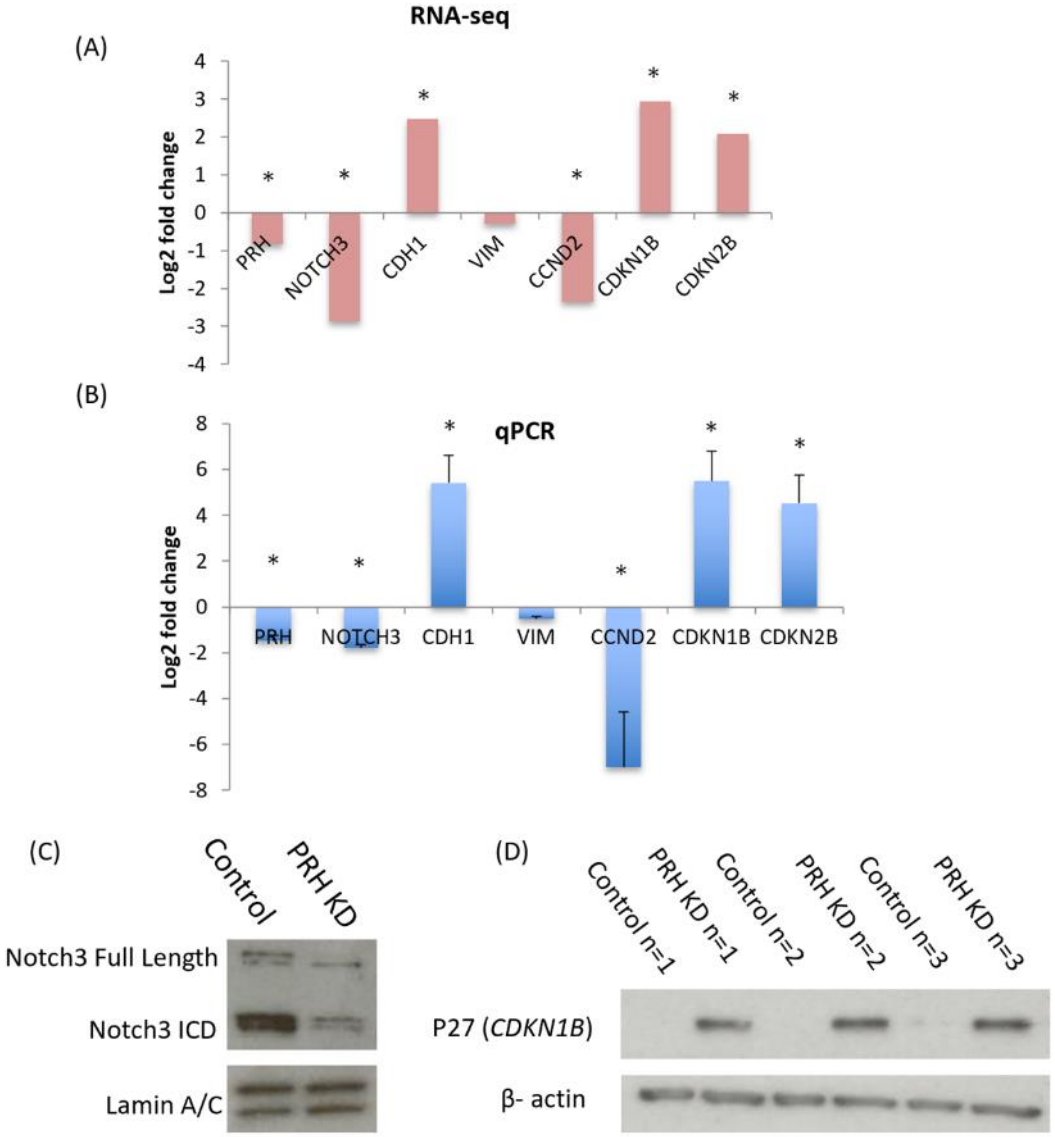

Figure 3.11 The effect of PRH KD on cell cycle and EMT genes. (A) The bar chart shows the $\log_2$ fold change of *NOTCH3*, *CDH1*, *CCND2*, *CDKN1B* and *CDKN2B* mRNA expression of PRH KD CCLP and control cells in the RNA-seq data. The experiment was repeated twice (*q<0.05). (B) qPCR showing the $\log_2$ fold change of the mRNA expression of *PRH*, *NOTCH3, CDH1, CCND2, CDKN1B and CDKN2B* in PRH KD normalized against control CCLP cells. The mRNA expression of each gene is normalized to β-actin in both control and KD cells. Statistical test: Two-tailed unpaired T-test (n=3; *p<0.05). The error bars represent SD of three biological repeats of experiments. (C) Representative Western blots showing expression of the full length Notch3 protein and the intracellular domain of the Notch3 protein in PRH KD and control CCLP cells. Western blotting was repeated in three different passages and same results were obtained. 10 µg of protein was loaded into each well. (D) Western blots showing p27 (*CDKN1B*) protein expression in three different passages of PRH KD and control CCLP cells. 10 µg of protein was loaded into each lane and detected with p27 and β-actin antibodies.

After validation of several DEGs in RNA-seq data, two types of bioinformatic analysis were initially performed by Dr P. Kitchen on the PRH KD RNA-seq differentially expressed gene (DEG) hits ($q<0.05$). These analyses included Gene ontology (GO) and Gene Set Enrichment analysis (GSEA). These analyses were extended using Ranked GSEA distribution analysis and visualized using Volcano plots.

GO analysis was performed using the PANTHER software (Protein analysis through evolutionary relationships). An ontology is a representation of information within a given biological domain base on the biological process, molecular function or cellular component. PANTHER is part of the Gene Ontology Reference Genome Project designed to classify genes in terms of their functions for analysis. The p-value for GO terms represents the probability of encountering at least a certain number of genes out of the total genes in the list annotated to a particular GO term, given the proportion of genes in the whole genome that are annotated to that GO Term. This means that the GO terms shared by the genes in the input list are compared to the background distribution of annotation in the genome and the fold enrichment then calculated. Fold enrichment is calculated by comparing the background frequency of the total genes annotated to that term to the sample frequency representing the number of genes inputted that are under the same term. Fold enrichment of a term refers to 'overrepresented compared to the background' and is represented as a positive fold enrichment value (Dalmer and Clugston, 2019). Results are presented from highest to lowest fold enrichment, using results with a p-value smaller than 0.05. GO analysis was performed on all the differentially expressed genes from the PRH KD and control CCLP RNA-seq ($q<0.05$) using

the biological process annotation. The overrepresented GO terms were selected using a 0.05 false discovery rate (FDR) cut-off (Benjamini and Hochberg, 1995).

It was identified by GO analysis that enrichment of genes associated with cell proliferation, cell adhesion, cell differentiation and cell migration from the major ontology branch "Biological process" are ranked as the top 10 overrepresented terms in differentially expressed genes of PRH KD and control CCLP cells **(Figure 3.12)**. These terms indicate that there are sets of genes associated with for example, proliferation and migration that are altered in the KD cells as would be expected from the phenotype of the KD cells discussed earlier.

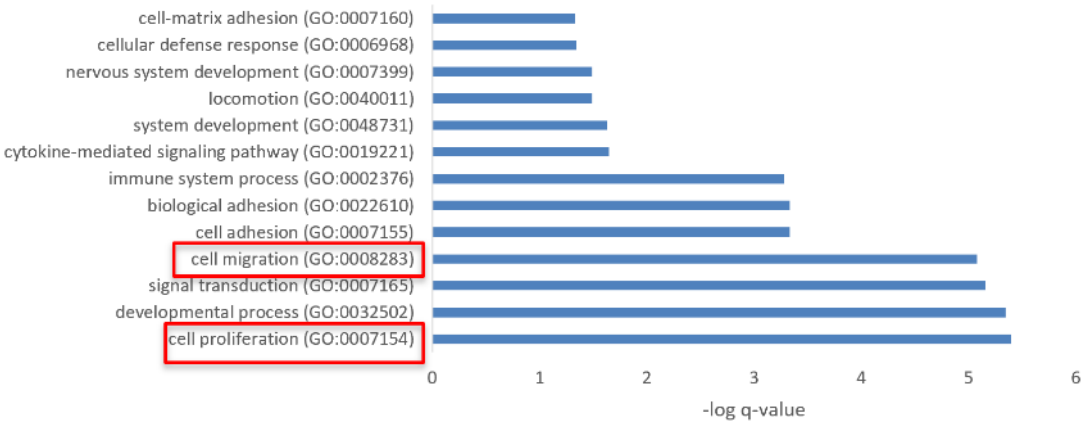

Figure 3.12 Gene ontology analysis on RNA seq data. Gene ontology analysis (Panther) of the PRH KD DEG. The list represents the pathway that are enriched and are ranked according to the log10 q-value. The red boxs indicate the phenotypes that were changed when PRH levels was depleted.

Gene Set Enrichment Analysis (GSEA) analysis was also carried out on the RNA-seq data to assess whether a specific set of genes is more associated with a trait in the hallmark dataset than the remaining genes. GSEA appears more informative than GO as particular pathways defined by "Hallmark gene sets" can be identified rather than just broader processes. In this analysis, sets of genes are carefully defined based on their biological function in multiple experiments and are termed "Hallmark gene sets" (Liberzon et al.,

2015). GSEA allows the identification of the pathways that are altered by determining if the genes within the hallmark gene-set are randomly distributed in the list of differentially regulated genes or enriched. The analysis involves the calculation of an enrichment score. Normalized enrichment scores (NES) and multiple adjusted p-values (q-values) are calculated by the software. The enrichment score refers to the extent to which a "hallmark gene set" is overrepresented. The score is calculated by scanning through the differentially regulated genes by the algorithm and the score increases when the algorithm spots a gene that is present in the Hallmark gene set and the score decreases when the genes in the hallmark gene set is not present in the differentially regulated gene set. Thus, although GO and GSEA are similar, the enrichment scores are calculated differently.

GSEA using the Molecular Signatures Database (MSigDB) Hallmark gene sets (Liberzon et al., 2015) ($q<0.05$) shows that PRH KD leads to significant enrichment of genes in many pathways. Notably the pathways with the lowest adjusted P value (q-value) are associated with estrogen response and EMT **(Figure 3.13)**. Changes in multiple genes in the EMT pathway are consistent with the altered PRH KD morphology and phenotype. Pathways that are known to associate to cell proliferation in CCA such as mTOR and Wnt pathways are also enriched (Boulter et al., 2015; Wu et al., 2019). Enrichment of genes in these pathways might account for the decreased proliferation in PRH KD CCLP cells. Interestingly although *NOTCH3* is downregulated in the CCLP PRH KD cells the Notch pathway is not enriched in the RNA-seq analysis.

To further analyze the EMT pathway, a ranked enrichment plot was generated using the GSEA software by inputting the DEG list and corresponding $\log_2$ fold change **(Figure**

3.13B). These plots indicate the genes that are enriched in the pathway and also rank them by log_2 gene expression; the green curves indicate the enrichment score curves. The plots show that the differentially expressed genes in the EMT pathway in CCLP KD cells are mostly upregulated. The plots also show the distribution and location of the EMT related DEG in the ranking underneath the green curves. At the bottom of the plots the value of the ranking metric of the DEGs along the gene list is shown. The ranking metric is a measurement for the correlation between the gene and the phenotype, in this case, it refers to EMT.

The log_2 fold change for the genes that are enriched in the EMT pathway can also be used to generate Volcano plots which illustrate the relationship between enrichment and fold change in gene expression. Volcano plots were plotted for the EMT pathway for the GSEA datasets of CCLP KD cells using the DEGs and the log_2 fold change obtained from the GSEA software and the corresponding q-values for GSEA enrichment. The Volcano plot shows some of the key genes that are differentially regulated by PRH related to EMT pathway **(Figure 3.13C)**. These genes include *POSTN*, *IGFBP3* and *COLA3A* strongly upregulated genes and *LAMA3*, *CDH1* and *THBS1* strongly downregulated genes. A full list of the DEGs in the EMT pathway in PRH KD cells are shown as a heatmap **(Figure S3)**. In conclusion, RNA-seq experiments indicate that PRH KD results in the alteration of many genes associated with the cell cycle, Wnt and EMT pathways and with estrogen regulation.

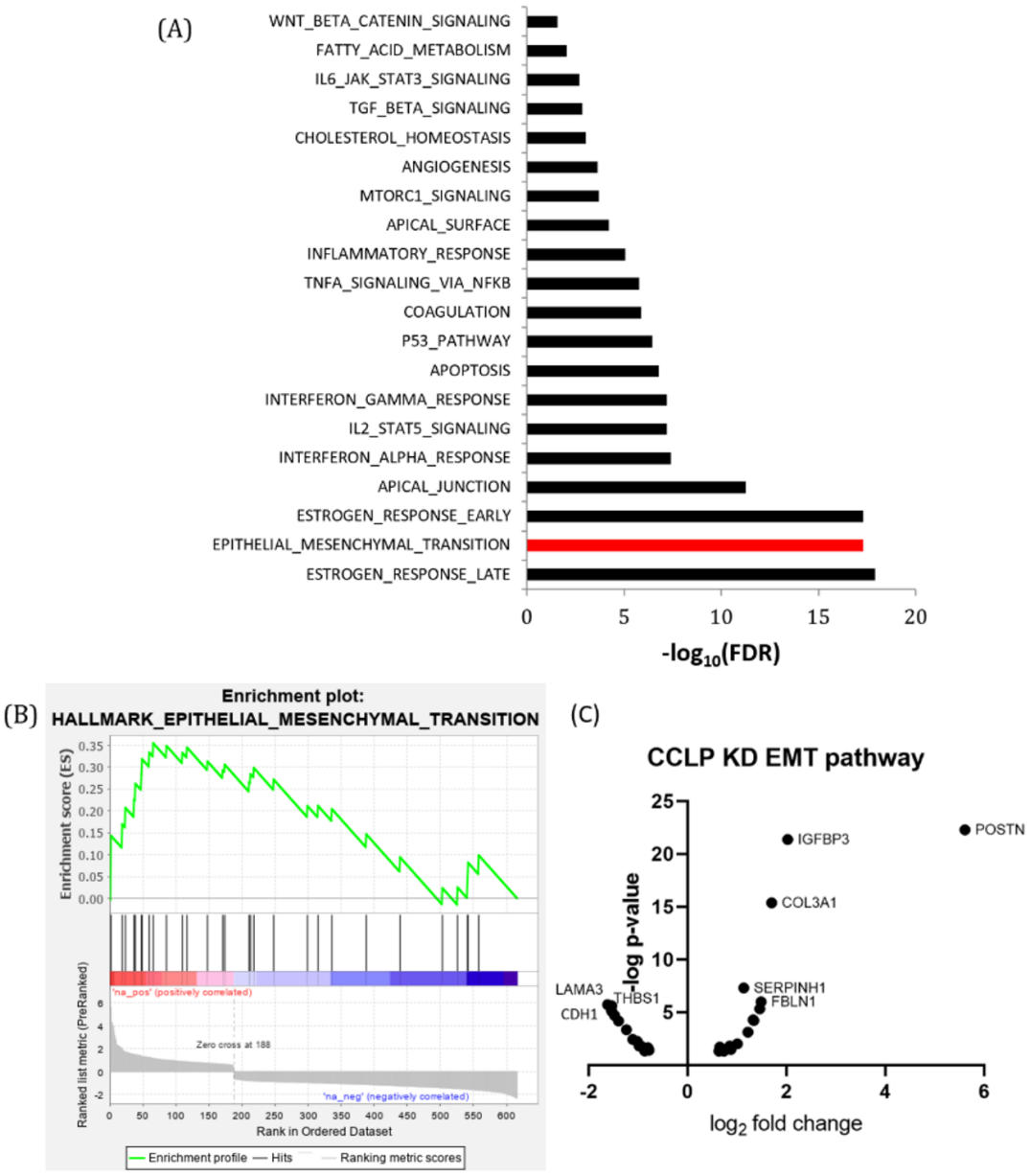

Figure 3.13 GSEA of PRH KD CCLP cells with the hallmark gene sets. (A)The list represents the hallmark gene sets that are enriched in PRH KD DEG. FDR is the false recovery rate (q). (B) Enrichment plot for EMT pathway for RNA-seq data of CCLP KD cells. (C) Volcano plot showing differentially regulated genes in the EMT pathway when PRH is depleted.

This RNA-seq data provides a useful starting point to identify genes that are altered that might explain the phenotypic changes observed upon PRH KD and in addition gene ontology and GSEA provide a systems-wide view of the pathways that are altered.

3.7 PRH overexpression increases cumulative cell number

Depletion of PRH leads to decreased malignancy and alteration of genes in many pathways, therefore, we next examined the effect of PRH overexpression on CCLP and CCSW cell lines by adenoviral infection. Adenoviruses have a high efficiency of transduction making them useful expression vectors and they can infect many mammalian cell types that express the adenoviral CAR receptor. To overexpress PRH, an adenovirus expressing a Myc epitope-tagged PRH cDNA encoding PRH amino acids from 7-270 (AdPRH) or adenoviral empty vector (AdEmpty) were used to infect CCLP and CCSW cell lines at multiplicity of infection (MOI) 50. For detail protocol see **section 2.1.8**. Cells infected with empty vector were used as a control. RNA and protein lysates were collected from cell pellets 48 hours after virus infection. qPCR and Western blot were carried out to detect the level of PRH expression. All infections showed high protein expression relative to cells infected with empty adenovirus so only clones that were confirmed to express very high PRH mRNA expression were chosen to investigate the effect of PRH on cell number. We used the three adenoviral-PRH infections resulting in the highest PRH mRNA levels detected by qPCR for analysis of cumulative cell growth and proliferation.

Figure 3.14A(i) shows the qPCR result of six individual infections with AdPRH and AdEmpty infected CCLP cells and four of them show high PRH overexpression. The mean PRH expression over three virus infections are 259-fold higher in AdPRH CCLP than AdEmpty cells. **Figure 3.14A(ii)** confirms PRH protein overexpression using Myc-tag antibody.

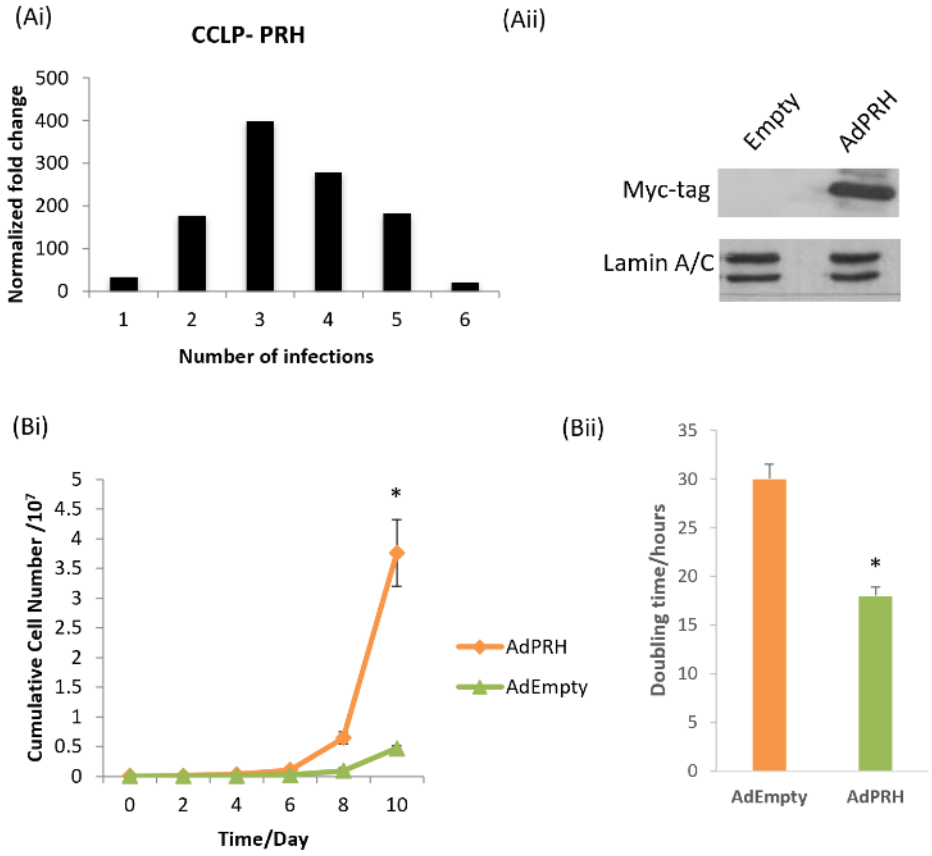

Figure 3.14 PRH expression in AdPRH and AdEmpty infected CCLP cells. (A)(i) qPCR for *PRH/HHEX* expression normalized to β-actin following AdPRH or AdEmpty infection in CCLP. (ii) Western blot detecting Myc-tagged PRH using an anti-mouse Myc-tag antibody and detecting Lamin A/C as loading control in the same experiment. (B)(i) CCLP cells were independently infected three times with AdPRH and AdEmpty. Cells were counted 48 hours after infection. Cells were trypsinized and counted in triplicate for each experimental repeat every 48 hours until Day 9. Statistical test: Two-tailed unpaired T-test (n=3; *p<0.05) (B)(ii) Doubling time of CCLP infected with AdPRH and empty vector. Statistical test: Two-tailed unpaired T-test (n=3; *p<0.05). Error bars show the SD among the three experimental repeats.

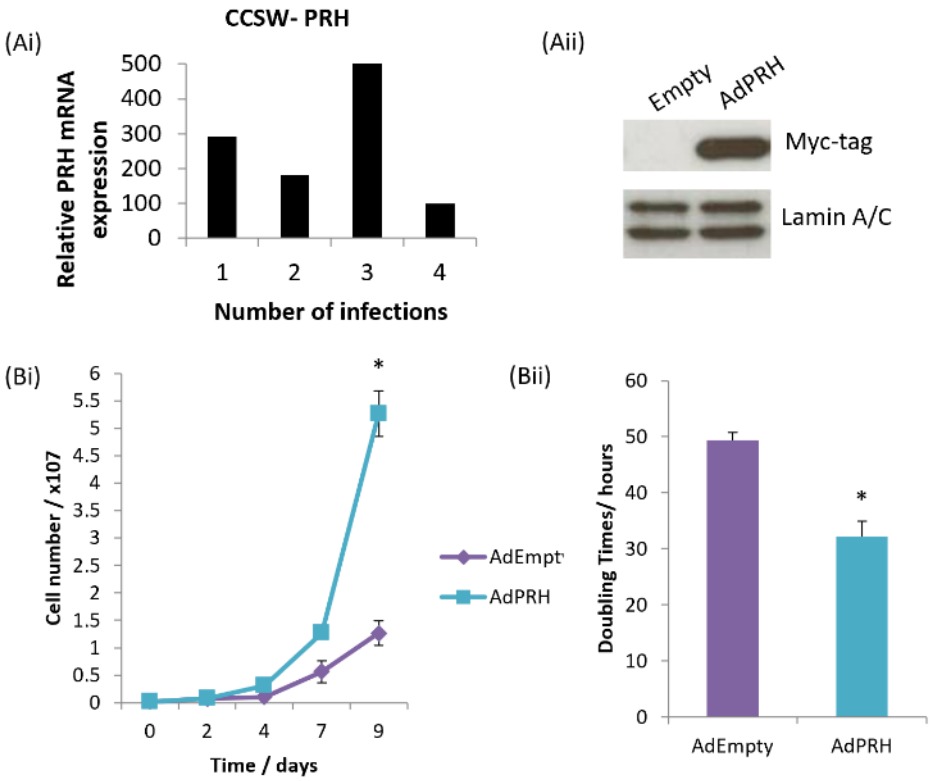

Figure 3.15 PRH overexpression increases cumulative cell number in CCSW. (A)(i) qPCR result of *PRH/HHEX* expression in four adenovirus infections in CCSW normalized to β-actin. (ii) Western blots using an anti-mouse Myc-tag antibody detecting the exogenous PRH expression and Lamin was used as loading control. (B)(i) CCSW cells were independently infected three times with AdPRH and AdEmpty. Cells were counted 48 hours after infection. Cells were trypsinized and counted in triplicate for each experimental repeat every 48 hours until Day 9. Two-tailed unpaired T-test (n=3; *p<0.05) (B)(ii) Doubling time of CCSW infected with AdPRH and AdEmpty. Statistical test: Two-tailed unpaired T-test (n=3; *p<0.05). Error bars show the SD among the three experimental repeats.

Cumulative growth curves were plotted for AdEmpty and AdPRH infected CCLP cells, **Figure 3.14Bi** shows that AdPRH CCLP cells grow faster compared to AdEmpty CCLP. The doubling time of CCLP cells decreased from 30 hours to 20 hours when PRH is overexpressed as shown in **Figure 3.14Bii**. The experiment was repeated in the CCSW CCA cell line. In agreement with the CCLP data, PRH overexpressing CCSW cells grow faster and have 1.5 times shorter doubling time compared to control as shown in **Figure 3.15**.

3.8 PRH overexpression increases cell proliferation

To investigate whether the increase in cell numbers brought about by PRH overexpression is due to increased in proliferation or decreased apoptotic activity, Edu proliferation and Caspase-3 assays were carried out using three independent biological repeats. The PRH overexpression in the cells was checked by Western blotting with a Myc-tag antibody for each experiment. **Figure 3.16A** shows that AdPRH CCLP cells are significantly more proliferative compared to the AdEmpty CCLP cells in Edu incorporation assays. Similar results were obtained when the experiments were repeated in CCSW cells. AdPRH infected CCSW cells resulted in increased proliferation compared to controls **(Figure 3.16B).** PI staining followed by flow cytometry was next carried out to examine the cell cycle in AdPRH infected CCLP cells and controls. CCLP cells expressing exogenous PRH have a much higher percentage of cells in G_2/M phase (19 %) compared to controls (2 %) and also a small but significant increase in S phase (27 %) compared to controls (21 %) **(Figure 3.16C)**. The quantification of the flow cytometry is shown in **Figure 3.16D**. The cell cycle profile is in agreement with Edu incorporation experiments showing that AdPRH promotes DNA synthesis. The cell cycle experiments further show that AdPRH can increase the percentage of cells that have completed DNA synthesis but the cells are delayed in G_2M suggesting that there may be additional effects of PRH on the G_2/M transition.

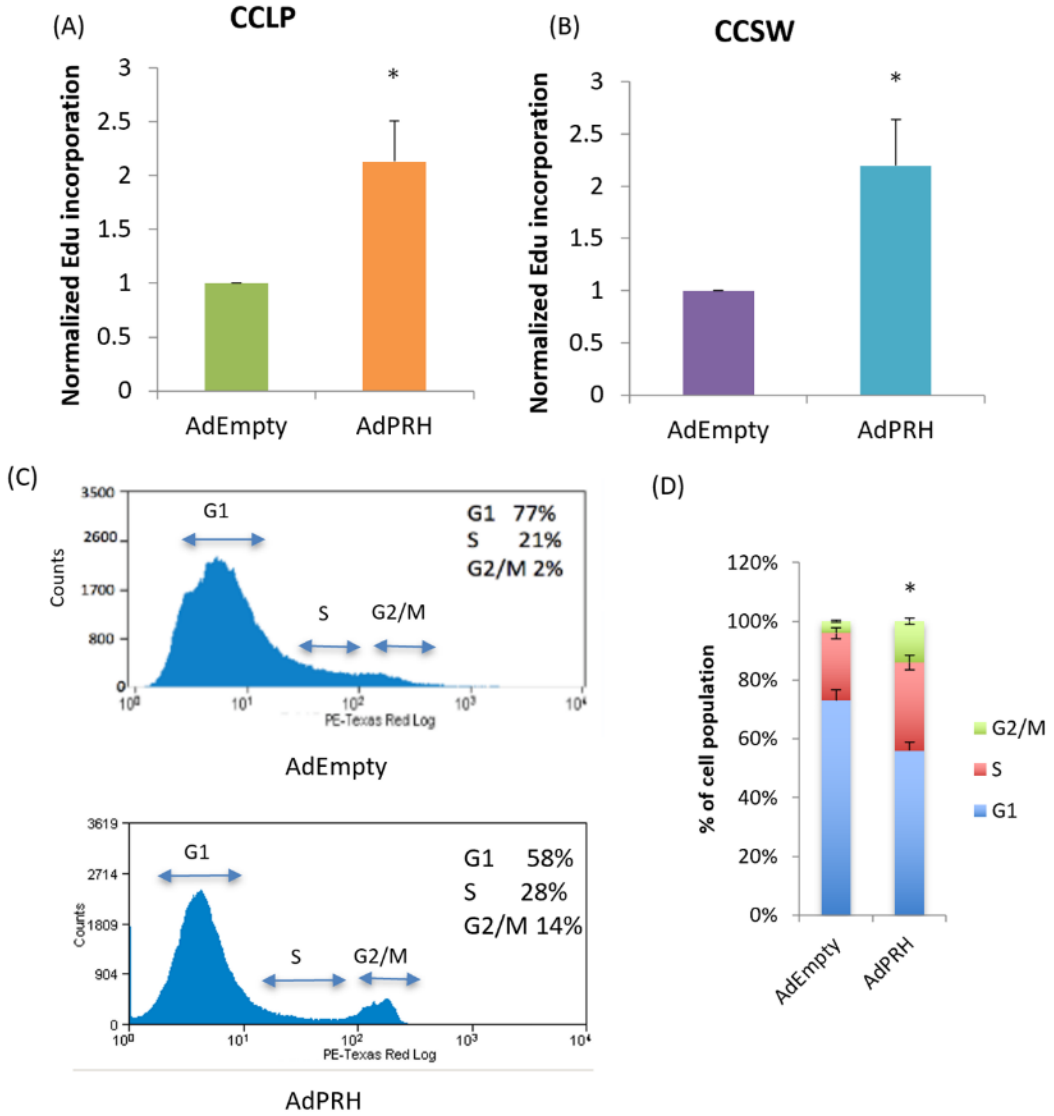

Figure 3.16 PRH overexpression increases cell proliferation in CCLP and CCSW. (A) Proliferative activity of AdPRH and AdEmpty infected CCLP cells. Cells were incubated in Edu for 2 hours and click reaction was detected by an HRP-conjugated antibody and OPD was added and absorbance was measured at 450 nm. Error bars show the SD among the three experimental repeats. Statistical test: Two-tailed unpaired T-test (n=3; $p<0.05$) (B) Proliferative activity of AdPRH and AdEmpty infected CCSW cells. Error bars show the standard error mean among the three experimental repeats. (n=3; $p<0.05$). (C) Representative FACs plots for PI staining of AdPRH and AdEmpty infected CCLP cells showing cell cycle profile using the PE-Texas Red Log channel. (D) Quantification of the cell cycle profile by flow cytometry. Error bars show the SD among the three experimental repeats. Statistical test: Two-tailed unpaired T-test (n=3; *$p<0.05$).

A Caspase-3 assay was performed to determine whether PRH OE has any pro-apoptotic effect on CCLP cells. The experiment setup for PRH overexpression was described in section 2.1.8. 1 µM Staurosporin treatment for 24 hours was used as a positive control. Both the AdPRH and AdEmpty control CCLP cells have low Caspase-3 activity compared

to cells treated with Staurosporin. However, CCLP cells infected with AdPRH have less Caspase-3 activity compared to the control CCLP cells (**Figure 3.17A)**. Similar results were observed when CCSW cells were infected with AdPRH, the AdPRH infected CCSW cells had significantly less Caspase-3 activity **(Figure 3.17A)**.

As data from the Caspase-3 assay shows a difference between AdPRH and AdEmpty CCLP cells, Annexin-V and PI staining was performed to further examine the effect of PRH on apoptosis. **Figure 3.17B** shows a representative dot plot following flow cytometry of Annexin V and PI stained cells of the percentage of the early and late apoptotic AdPRH CCLP and AdEmpty CCLP cells population and **Figure 3.17C** shows the quantification over three repeats. Interestingly, AdPRH and AdEmpty cells show no significant difference in apoptosis in these experiments.

In conclusion, Caspase-3 activity is altered but there is no significant change in basal apoptosis. This is probably because the decrease in Caspase-3 activity is not sufficient to decrease basal apoptosis. Exogenous PRH therefore results in an increase in cell number through increased DNA synthesis/proliferation rather than through decreased apoptosis.

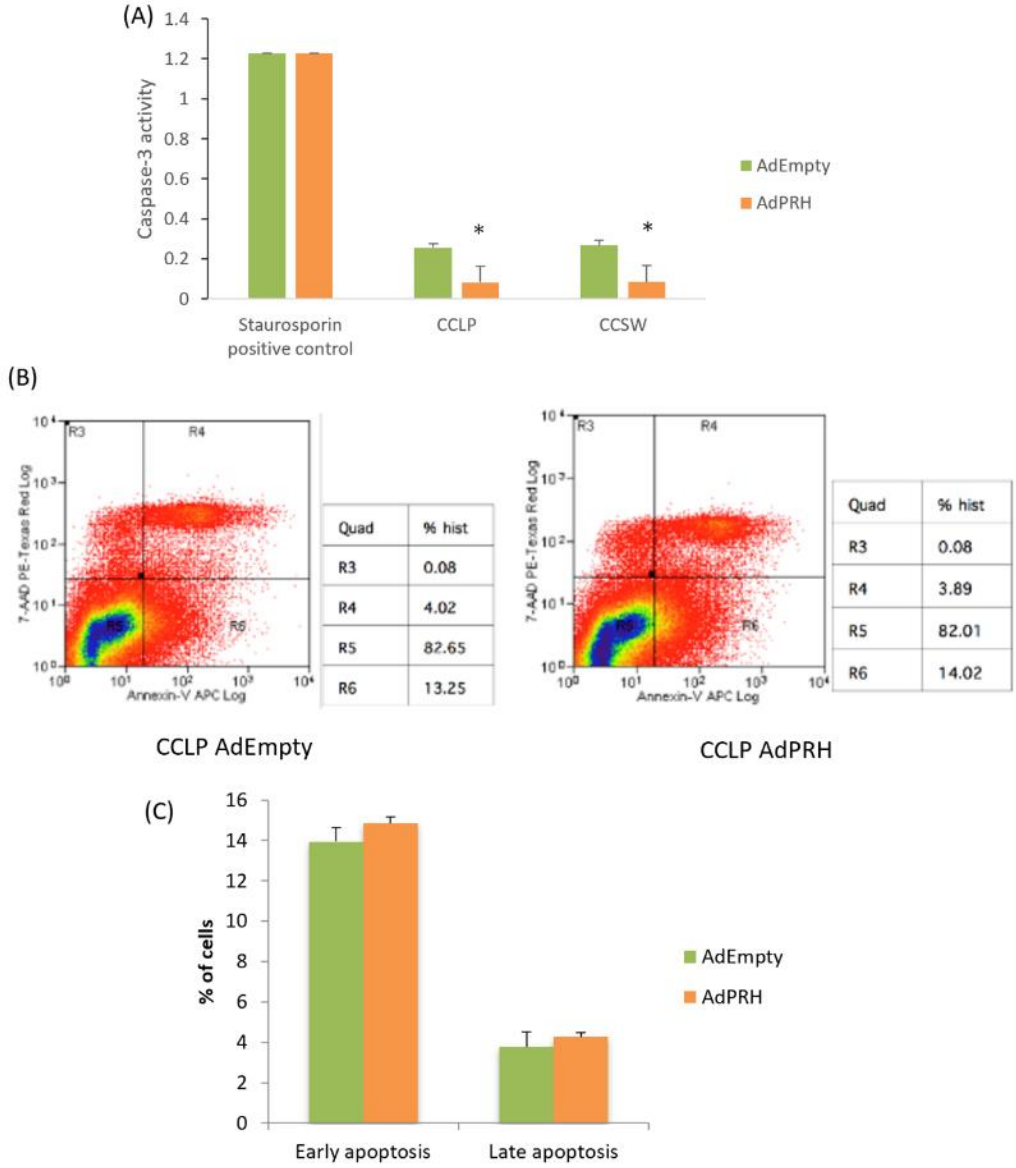

Figure 3.17 Exogenous PRH has no effect on apoptosis in CCLP cells. (A) Caspase-3 assay were carried out on 1 x 10^6 of AdPRH or AdEmpty infected (MOI 50) CCLP and CCSW cells at 48 hours post infection using the Caspase-3 kit Statistical test: Two-tailed unpaired T-test (n=3; *p<0.05). (Bi) FACs followed by Annexin V staining on AdPRH and AdEmpty CCLP cells. (Bii) Quantification of the FACs data showing the early apoptotic cells and apoptotic cells in AdPRH or AdEmpty CCLP. Statistical test: Two-tailed unpaired T-test (n=3). Error bars show the SD among the three experimental repeats.

3.9 PRH overexpression increases cell migration, invasion

CCLP cells are mesenchymal and would not be expected to show altered morphology with PRH overexpression. However, to determine whether elevated PRH expression can increase the migratory and invasive capacity of the tumour cell line, transwell migration and invasion assays were conducted as described for PRH KD cells (**see section 2.9**). The cells were infected with virus in serum reduced media (2% FBS) and after 24 hours the adenovirus infected cells were then plated for migration or invasion assays in the presence of 1 mM hydroxyurea and 0.1 % BSA in serum free media for another 24 hours before the invasion or migration assay was performed. Thus, the assays are initiated 48 hours post infection and in the presence of hydroxyurea. The migration assay occurs over 72 hours and the invasion assay over 24 hours. As predicted PRH overexpression increases both their migratory and invasive capacity **(Figure 3.18A&B).** Similar results were obtained when CCSW cells were examined for the effects of PRH OE on migration and invasion in the same experimental procedures (**Figure 3.18A&B).** In summary, PRH KD in CCLP mesenchymal cells decreases cell proliferation, migration and invasion and induces MET, whereas, PRH OE in mesenchymal cells increases cell proliferation, migration and invasion.

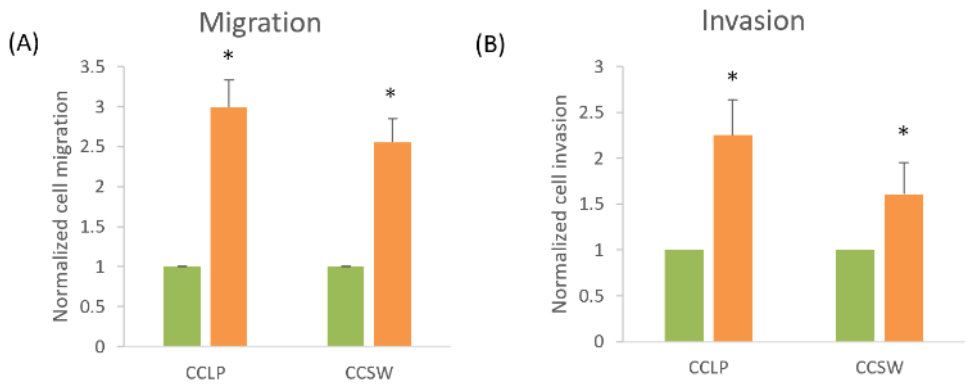

Figure 3.18 PRH overexpression increases cell migration and invasion in CCLP and CCSW cells. (A) Cell migration of AdPRH and AdEmpty infected CCLP and CCSW cells through a transwell filter in a 2-10% serum gradient. 1 mM hydroxyurea was added 24 hours before the migration assay to inhibit proliferation. Statistical test: Two-tailed unpaired T-test (n=3; *p<0.05) (B) Invasion of AdPRH and AdEmpty infected CCLP and CCSW cells through transwell filter with 10% matriel gel, 1 mM hydroxyurea was added 24 hours before the invasion assay to inhibit proliferation. Statistical test: Two-tailed unpaired T-test (n=3; *p<0.05). Error bars show the SD among the three experimental repeats.

3.10 Identify differential gene expression by PRH overexpression by RNA-sequencing

Given the changes in phenotype observed upon PRH overexpression, we next examined the gene expression changes associated with increased proliferation and invasive behavior. To achieve this, RNA was isolated from CCLP cells infected with AdPRH or empty adenovirus from two independent infections. RNA integrity analysis, library preparation and RNA sequencing were performed by Dr. C Whalley (Genomic unit in UoB) as previously described. Initial bioinformatic analysis of RNA-seq data was carried out by Dr. P Kitchen. A scatter plot showing $\log_2$ fold change of the gene expression for AdPRH infected cells against control AdEmpty infected cells is shown using the mean $\log_2$ data (normalized counts) **(Figure 3.19)**. The scatter plot shows differentially regulated genes in red. The right panel indicates the number of genes that are altered; 889 genes are downregulated and 1410 gene are upregulated in PRH OE cells.

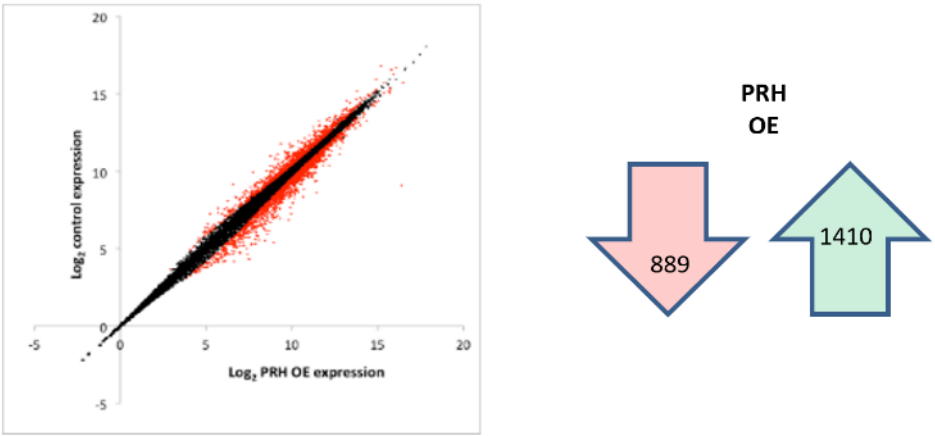

Figure 3.19 RNA-seq of PRH OE and control CCLP cells. Scatter plot showing the mean log2 expression of expressed genes in AdPRH infected CCLP cells compared to AdEmpty infected cells (left). Red dots above the black dots are genes that are differentially upregulated and red dots that are below the black dots are the genes that are downregulated. The number of genes that are differentially expressed in AdPRH infected CCLP cells compared to AdEmpty cells (right) (Data from Dr. P Kitchen).

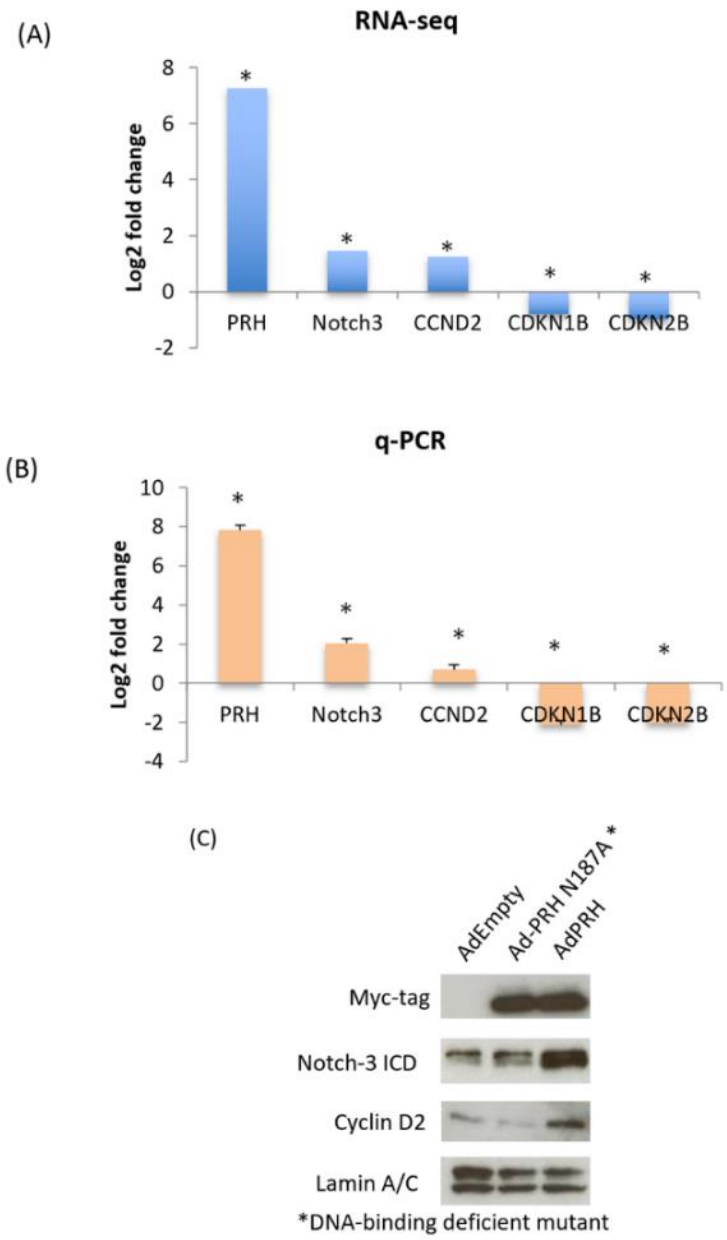

Figure 3.20 PRH overexpression effects on genes associated with proliferation in CCLP cells. (A) The bar chart shows the $\log_2$ fold change of *PRH, NOTCH3, CCND2, CDKN1B and CDKN2B* mRNA expression of AdPRH CCLP and AdEmpty cells in the RNA-seq data. (n=2; *q<0.05) (B) qPCR showing the mRNA expression of *NOTCH3*, *CCND2*, *CDKN1B* and *CDKN2B* in AdPRH and AdEmpty infected control CCLP cells. The mRNA expression is normalized to β-actin. Statistical test: Two-tailed unpaired T-test (n=3; * p<0.05). The error bars show the SD of three experimental repeats. (C) Representative Western blots showing Notch3 and Cyclin D2 protein expression in AdPRH, AdPRH-N187A infected cells and AdEmpty control CCLP cells. Lamin was used as a loading control. 10 µg of protein was loaded into each lane. The experiment was repeated in three different passages of CCLP cells and all show a similar result.

To validate the RNA-seq data, the expression of selected genes was examined using qPCR and protein expression examined using Western blotting. In agreement with the

RNA-seq data, there is an upregulation of the cell cycle gene *CCND2* and notably there is also an increase in expression of *NOTCH3* **(Figure 3.20A&B).** In addition, repression of cell cycle inhibitor genes including *CDKN1B* and *CDKN2B* was confirmed **(Figure 3.20A&B)**. **Figure 3.20C** shows that increased Notch3 and Cyclin D2 protein levels were also detected in Western blotting experiments when AdPRH was expressed in the cells. The exogenous Ad(Myc-tagged)PRH was detected using monoclonal antibody against the Myc epitope and Lamin A/C (monoclonal) was used as a loading control. Interestingly, an N187A point mutation (M. Guiral et al., 2001; Noy et al., 2010) in the PRH homeodomain which disrupts PRH binding was unable to increase the expression of Cyclin D2 or Notch3, demonstrating that the wild type PRH homeodomain is required for expression of these genes.

GO analysis of the RNA-seq data shows that genes in the Wnt and EMT pathways are enriched in RNA-seq from AdPRH expressing cells **(Figure 3.21)**. Both canonical and non-canonical Wnt pathways are enriched as well as pathways associated with proliferation, migration and VEGFR signaling. This pathway analysis is consistent with the phenotypical change observed in PRH overexpressing CCLP cells giving rise to increased proliferation, migration and invasion.

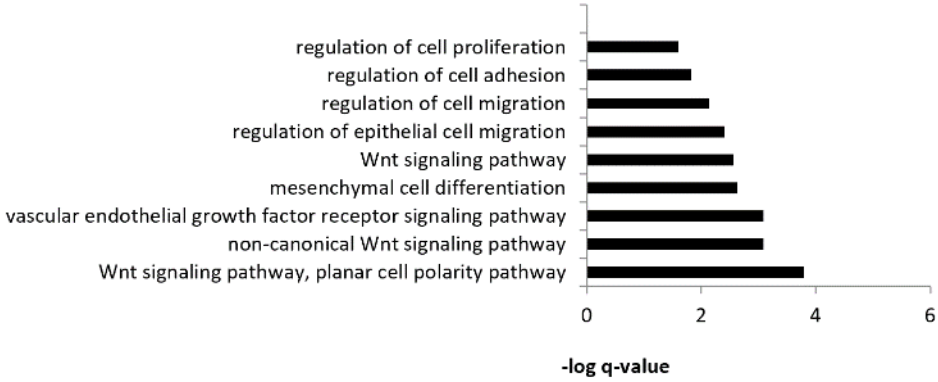

Figure 3.21 Gene ontology analysis of the PRH OE DEGs. The list represents the pathways that are enriched and ranked by q-values.

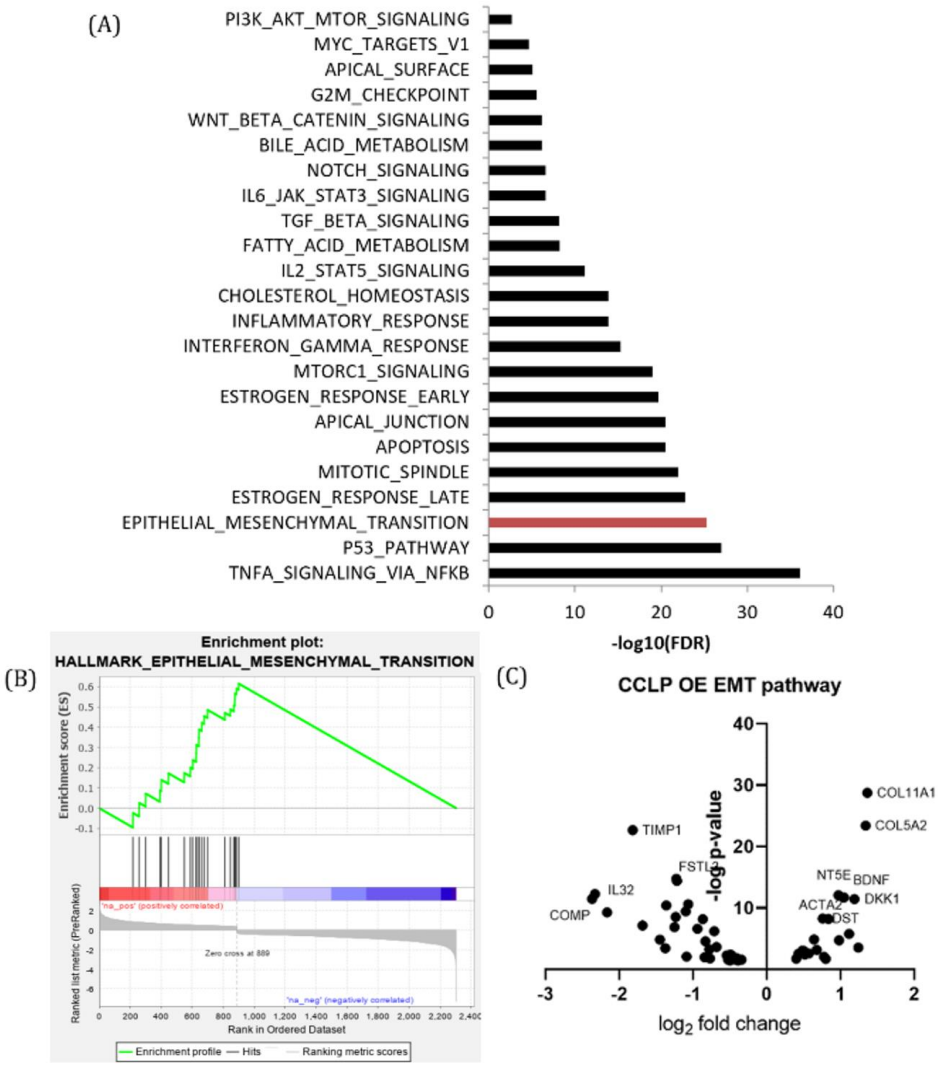

Figure 3.22 GSEA of PRH OE CCLP cells with the hallmark gene sets. (A) The list represents the hallmark gene sets that are enriched in PRH OE DEG. FDR is the false recovery rate. EMT pathway is ranked the top 3 in the list of the hallmark gene sets. (B) Enrichment plot for EMT pathway for RNA-seq data of AdPRH CCLP cells. (C) Volcano plot of the DEGs in EMT pathway of RNA-seq data of AdPRH CCLP cells.

GSEA of differentially regulated genes was also carried out on the RNA-seq data to identify the pathways that are enriched in AdPRH infected CCLP cells. Upon PRH overexpression the three most enriched pathways are the TNFα and NFkB signaling pathway, the p53 pathway and the EMT pathway. The set of genes associated with G_2M and the mitotic spindle are also enriched with PRH overexpression which could explain the increased number of cells in G_2M in cell cycle experiments.

Of additional interest in the GSEA data was the finding that Notch pathway and PI3K/Akt pathway genes are also enriched in the PRH overexpression gene set **(Figure 3.22A).** This is of consequence as *NOTCH3* oncogenic activity in CCA models is at least partly due to non-canonical Notch signaling via PI3K/Akt (Guest et al., 2016).

PRH overexpression also led to enrichment of multiple pathways that are altered in CCLP PRH KD cells such as pathways associated with the Wnt signaling pathway, the estrogen response pathway and the EMT pathway. To further analyze the gene set in the EMT pathway a ranked Gene Set Enrichment plot and a volcano plot were generated from the RNA-seq data for the EMT pathway showing some of the DEGs regulated by overexpressed PRH in CCLP cells. **Figure 3.22B** shows the EMT genes in the pathway are mostly upregulated. A heatmap showing the full list of EMT genes regulated by AdPRH is shown in **Figure S3A**. The volcano plot ($\log_2$ fold change against the log q value for each gene) shows genes that are strongly differentially regulated with good statistical significance. These include genes encoding collagens (COL) which are strongly upregulated by PRH **(Figure 3.22C)**.

Interestingly very few of the genes (10 %) that are regulated by PRH in the EMT pathway in overexpressing cells are also regulated by PRH in the PRH KD cells and vice versa **(See Figure S3B for Venn diagram)**. Thus, although the PRH protein can regulate EMT pathway in both situations the genes regulated by PRH differ. This is likely related to the fact that CCLP cells are mesenchymal and remain so with PRH overexpression but become epithelial upon PRH KD.

Although RNA-seq data indicates that the EMT pathway is enriched in cells overexpressing PRH only the EMT TF *SNAI1* is increased with PRH overexpression **(Figure 3.24A)**. Proteins associated with EMT or with cell-cell adhesion or cell migration were investigated using Western blotting. In agreement with RNA-seq data, the EMT TF Snail1 is upregulated by AdPRH relative to controls **(Figure 3.24B)**. The tight junction protein Claudin is repressed by PRH overexpression. RNA-seq and Western Blotting show that PRH OE does not change the protein expression of Slug (*SNAI2*) in CCLP cells. In conclusion, these data suggest that PRH overexpression further increases the mesenchymal phenotype even in the highly mesenchymal and motile CCLP cell line which do not express E-cadherin **(Figure 3.23)**. Thus, in summary, PRH overexpression and PRH KD have opposite effects on cell morphology, EMT and proliferation. Of note, in PRH KD CCLP cells, we previously demonstrated that *CDKN1B* and *CDKN2B* are upregulated. In contrast, the RNA- seq data for PRH OE shows that *CDKN1B* and *CDKN2B* are repressed **(Figure 3.22A)** and qPCR also shows repression of *CDKN1B* and *CDKN2B*, validating the RNA-seq data **(Figure 3.22B)**, demonstrating that PRH KD and OE have opposite effects on at least some critical cell cycle genes.

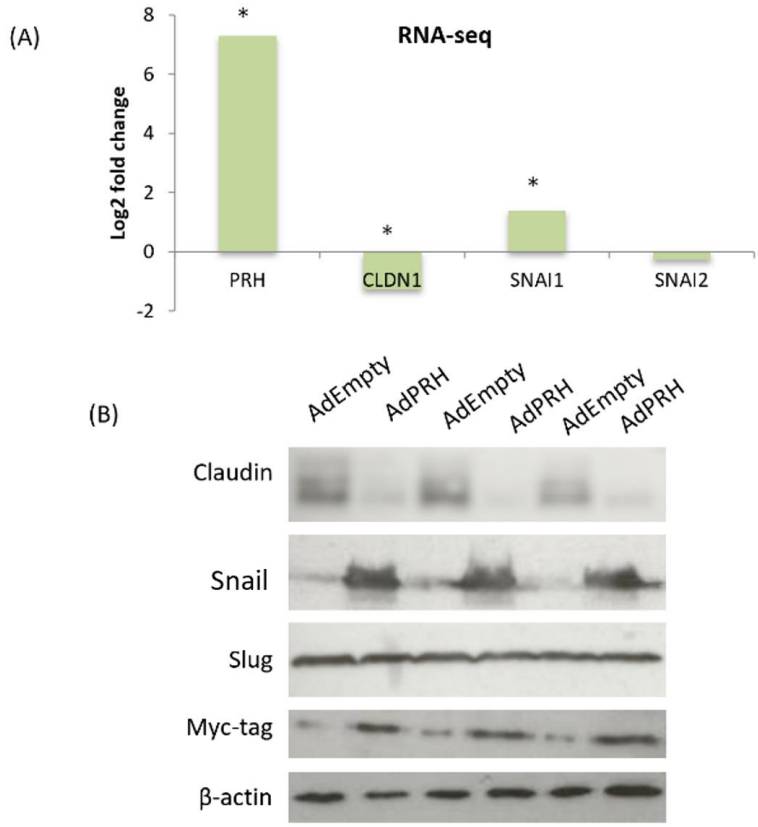

Figure 3.23 Expression of EMT related genes in PRH OE and control cells. (A) RNA-seq data showing the expression of EMT related genes. Statistical test: Two-tailed unpaired T-test (n=2; *q<0.05). Error bars show the SD among the three experimental repeats. (B) Western blots showing EMT protein expression including Claudin, Snail1 and Slug in three biological repeats of AdPRH and AdEmpty control CCLP cells. Myc-tag antibody was used to show PRH overexpression in the CCLP cells and an anti-β-actin antibody was used as a loading control. 10 µg of protein was loaded into each lane.

To better understand the regulation of gene expression by PRH, we compared the number of genes differentially regulated by PRH KD and PRH overexpression and identified genes regulated by both conditions. The Venn diagram shows genes that are downregulated or upregulated in PRH KD and PRH OE and summarizes the effect of PRH OE and KD on gene expression **(Figure 3.24A)**. There are a total of 53 genes differentially regulated in both PRH OE and KD condition. Surprisingly, only 18 genes are both downregulated when PRH is overexpressed and upregulated when PRH is knocked down. Additionally, 35 genes are upregulated when PRH is overexpressed and are downregulated when PRH is knocked down. Further GSEA analysis was carried out on

the 53 genes that are differentially regulated in both PRH OE and KD conditions. The GSEA analysis showed that the majority of these 53 genes are involved in the EMT pathway **(Figure 3.24B).**

The RNA-seq data for genes involved the Notch signaling, cell cycle and EMT pathway under condition of PRH OE and PRH KD are shown in **Figure 3.24C**. The *NOTCH3* gene is one of the 53 genes that are differentially regulated in both PRH OE and KD data sets and Notch3 protein is implicated in control of proliferation in CCA (Guest et al., 2016). Little is known about how Notch3 promotes EMT in CCA but it is implicated in promoting EMT in other cell types (Lin et al., 2018). Notch3 is not the only component in the Notch signaling pathway that is regulated by PRH when PRH is overexpressed. The RNA seq data GSEA shows that the Notch signaling pathway is enriched. In addition to *Notch3*, *Notch1* and *DLL3* (a Notch ligand) are also both downregulated in PRH KD and upregulated in PRH OE CCLP cells. The RNA-seq data also shows that many ligands in the Notch signaling pathway are regulated by both PRH KD or PRH OE including *JAG1*, *JAG2* and *DLL4* but surprisingly not always in opposite directions. Interestingly, *PSEN* is regulated by PRH and is part of the γ-secretase complex; PSEN is only altered in PRH OE conditions and this could explain the large increase in Notch3 intracellular domain protein upon PRH OE **(Figure 3.22)**.

For cell cycle genes, the RNA-seq data shows that *CCND2*, *CDKN1B* and *CDKN2B* are all regulated by PRH in both PRH KD and PRH OE conditions but *CCND1* is not strongly regulated in either condition. For the EMT pathway, only the EMT TF *SNAI1* is significantly upregulated by PRH OE.

In summary although PRH knockdown and PRH overexpression both regulate the same pathways only the minority of genes in any pathway are regulated in opposite directions. However, these genes may be critical regulators of the cell cycle or cell morphology.

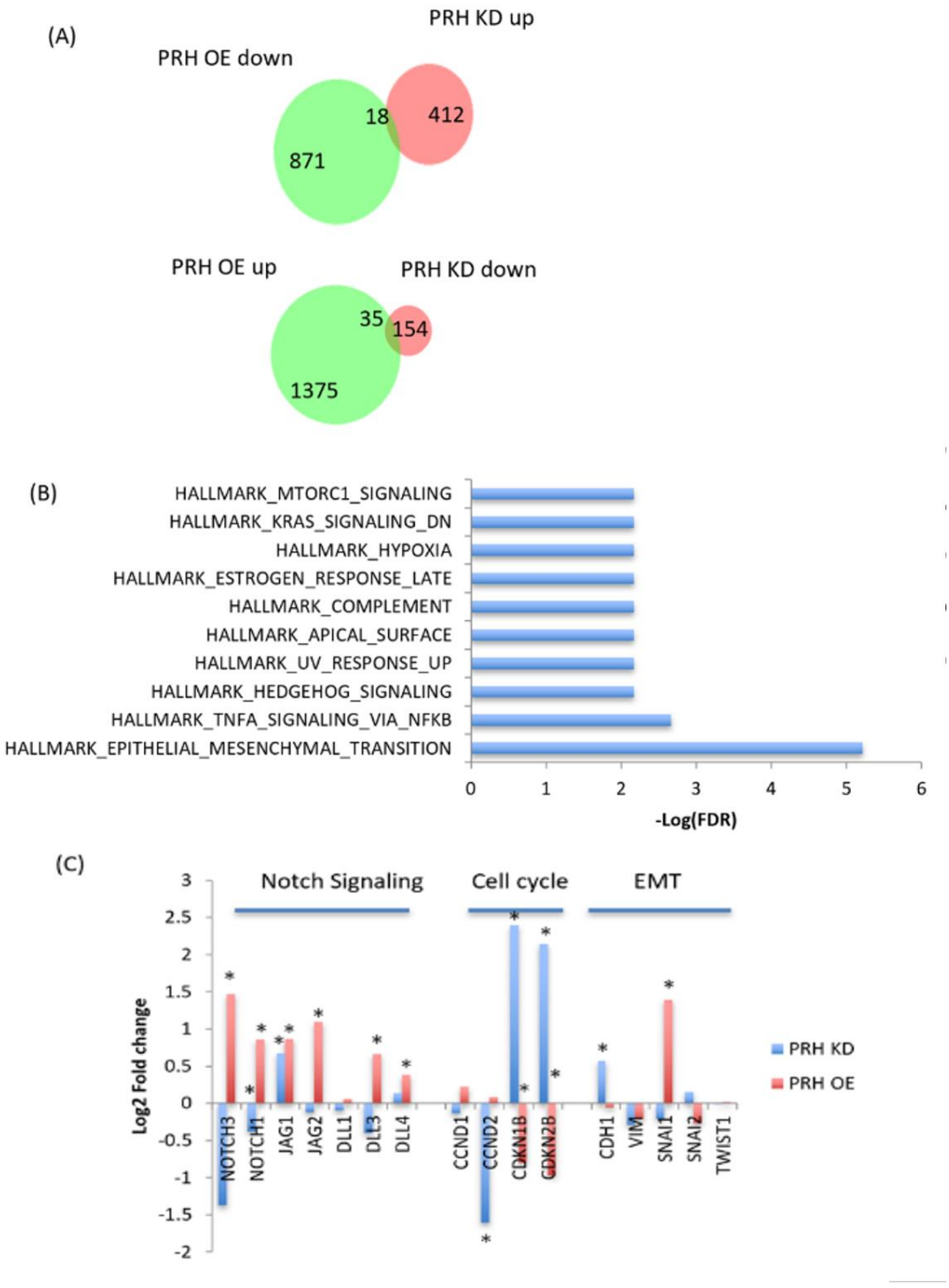

Figure 3.24 Identifying differential gene expression by PRH KD and OE by RNA-seq. (A) Number of differentially expressed genes (DEGs) detected in PRH KD and OE experiments. (B) Gene set enrichment analysis using Hallmark gene sets for PRH OE and KD DEGs. FDR – false discovery rate. (C) RNA-seq gene expression of notch signaling, cell cycle and EMT pathways. Red bars represent Hallmark sets that are enriched in both PRH KD and OE DEG lists (n=2; *q<0.05).

CHAPTER 4

The mechanism of PRH regulating cell cycle and EMT genes in tumour cells

4. The mechanism of PRH regulating cell cycle and EMT genes in CCA tumour cell lines

4.1 The expression of Notch3, Cyclin D2, and E-cadherin in multiple CCA cell lines

To determine whether the relationship between PRH expression and specific target genes or proteins identified in the RNA-seq experiments can be observed in other CCA cell lines, the protein expression of Notch3, Cyclin D2 and E-cadherin was investigated in a panel CCA cell lines, and in primary BECs using Western blotting **(Figure 4.1)**. It can be seen that only PRH and Notch3 are highly expressed in all tested CCA cell lines, whereas Cyclin D2 expression is high in all CCA cell lines other than CCLP. E-cadherin is not expressed in the CCA cell lines but is highly expressed in the AKN-1 and BECs. We hypothesize that elevated PRH is activating Notch3 and Cyclin D2 expression but repressing E-cadherin expression in the different CCA cell lines. One possible reason for low Cyclin D2 expression in CCLP cells could be that although *CCND2* expression is activated by PRH, the stability of the Cyclin D2 protein in CCLP cells is low and could be regulated by other pathways such as the mTOR pathway which is activated in CCLP (Balcazar et al., 2009).

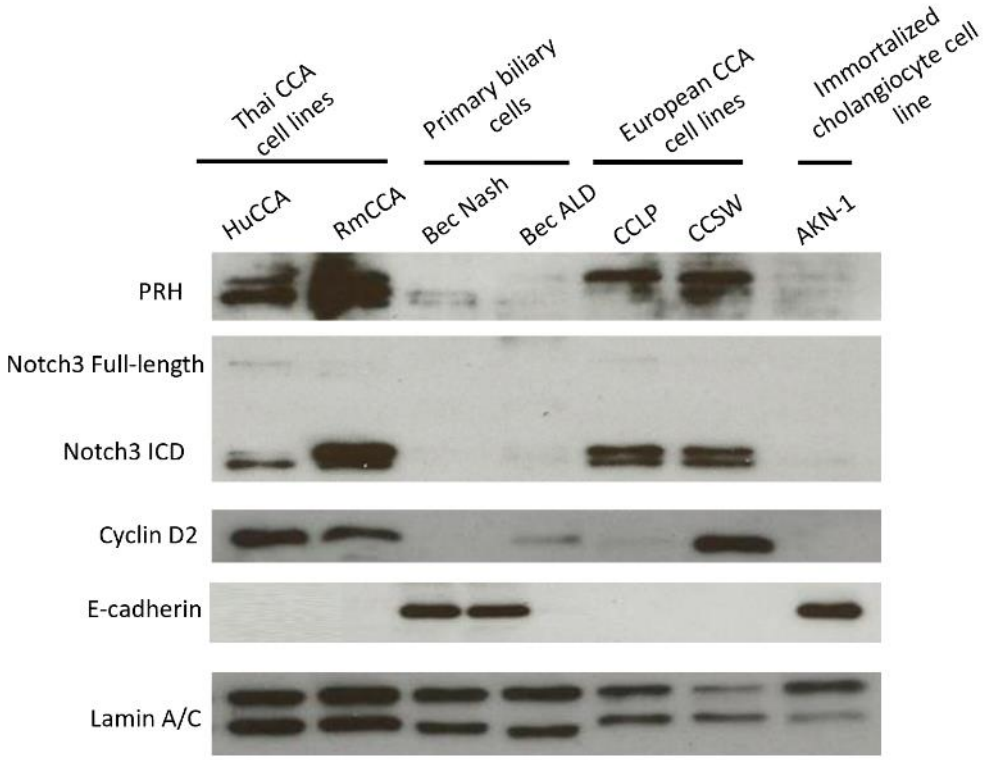

Figure 4.1 Endogenous PRH protein and potential PRH target proteins in CCA cell lines and primary cells. Representative Western blots (n=3) showing PRH, Notch3, Cyclin D2 and E-cadherin staining in a panel of CCA cell lines, primary BECs and an immortalised cholangiocyte cell line, AKN-1. Lamin A/C is used as loading control. 10 µg of protein was loaded into each lane. The experiments were repeated 3 times using 3 different passages of cells.

We showed previously in **section 3.8**, PRH overexpression in CCSW cells also increases their proliferation. In PRH overexpressing CCSW cells, *NOTCH3* and *CCND2* mRNA expression is increased **(Figure 4.2A)**. Western blot shows that PRH overexpression also increased Notch3 and Cyclin D2 protein expression in CCSW **(Figure 4.2B)**. CCSW cells transfected with a plasmid encoding the PRH N187A protein (pMUG1-N187A) do not show increased Notch3 expression and Cyclin D2 expression whilst cells transfected with wild type PRH do show increased Notch3 and CCND2. Western blot shows that PRH overexpression also increased Notch3 and Cyclin D2 protein expression in CCSW **(Figure 4.2B)**. CCSW cells transfected with a plasmid encoding the PRH N187A protein (pMUG1-N187A) do not show increased Notch3 expression and Cyclin D2 expression whilst cells

transfected with wild type PRH do show increased Notch3 and Cyclin D2. Since Notch3 is also elevated in all the tumour cells we investigated the role of Notch3 in the control of proliferation in CCLP cells.

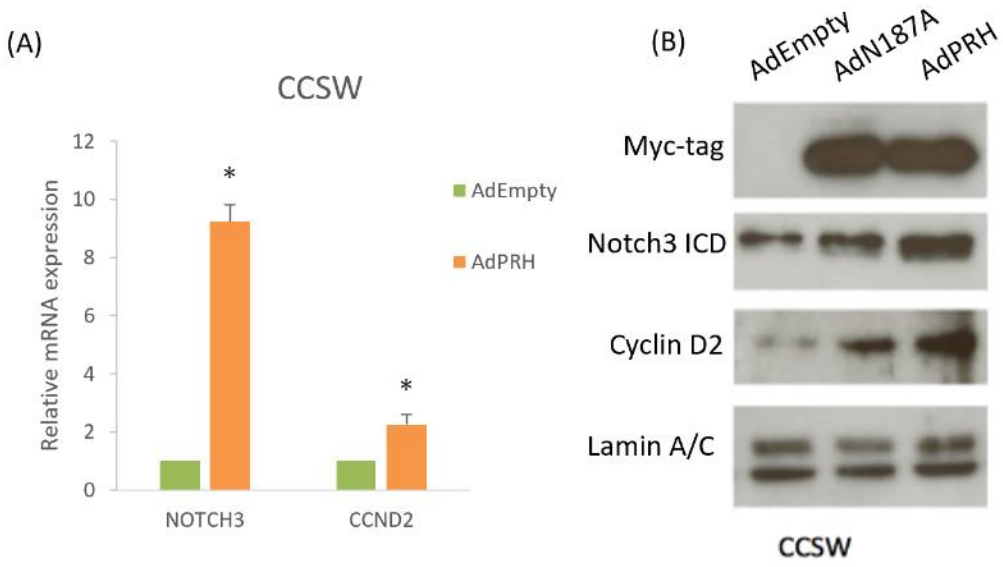

Figure 4.2 PRH OE upregulates Notch3 and Cyclin D2 expression in CCSW. (A) qPCR showing the mRNA expression of *NOTCH3* and *CCND2* in five independent adenoviral infections of AdPRH and AdEmpty CCSW cells normalized to β-actin. Statistical test: Two-tailed unpaired T-test (n=5; * $p<0.05$). Error bars show the SD among the three experimental repeats. (B) Representative Western blots showing Notch3 and Cyclin D2 protein expression in AdPRH, AdPRH-N187A infected cells and AdEmpty CCLP cells. 10 µg of protein was loaded into each lane. The experiment was repeated five times in five individual adenoviral infected AdPRH CCSW and control and show similar results.

4.2 PRH forms a positive feedback loop with Notch3

NOTCH3 is one of the genes that is altered in both the CCLP PRH OE and PRH KD RNA-seq datasets and it is also activated by PRH in CCSW cells; furthermore, Notch3 is highly expressed in all the tumour cell lines investigated. Notch3 is known to be important for CCLP proliferation (Guest et al., 2016) however it is not known whether Notch3 regulates the *PRH/HHEX* gene or any PRH targets. To better understand the role of Notch3, we depleted Notch3 expression in CCLP cells. Three different Notch3 shRNA encoding different targeting sequences or a non-targeting shRNA cloned into pLKO

(Sigma-Aldrich, TRCN0000363316) were transfected into the CCLP cells and selected with Puromycin for two weeks (performed by Dr P. Kitchen) (see **2.1.12** for plasmid map). Western blotting was then carried out on the resulting clones to assess the expression of Notch3 KD in each cell line. Clone 3 shows a strong knockdown of the full-length protein and the Notch 3 ICD **(Figure 4.3A)**. Therefore, the Notch3 KD clone 3 (N3KD3) was chosen for further experiments. In Edu incorporation experiments, the clone N3KD3 showed a decrease in proliferation and we also observed a change in morphological phenotype **(Figure 4.3B and 4.3C)**. The N3KD3 cells appeared more epithelial than controls and very similar in phenotype to PRH KD cells with morphological changes that suggest MET has occurred upon N3KD. E-cadherin and PRH protein expression were investigated in the N3KD CCLP cells by Western blotting and it can be seen that E-cadherin is increased in these cells whilst PRH expression is decreased in N3KD3 cells compared to controls **(Figure 4.3D)**. Cyclin D2 protein expression is also lost in these cells see **figure 4.3D**. Since we demonstrated that Notch3 is downregulated in PRH KD CCLP cells **(Figure 3.11)** and here we show that PRH protein and RNA are downregulated in N3KD3 CCLP cells **(Figure 4.3D)**, we infer that PRH and Notch3 form a positive feedback loop to regulate each other. Moreover, the Western blotting data and qPCR data for PRH and Notch3 shows that they both regulate *CDH1* (E-cadherin) expression which very likely contributes to the MET observed (see **Figure 3.7** compare to **Figure 4.2**). They also both regulate *CCND2* which likely contribute to the effects on proliferation observed in the N3KD3 CCLP cells.

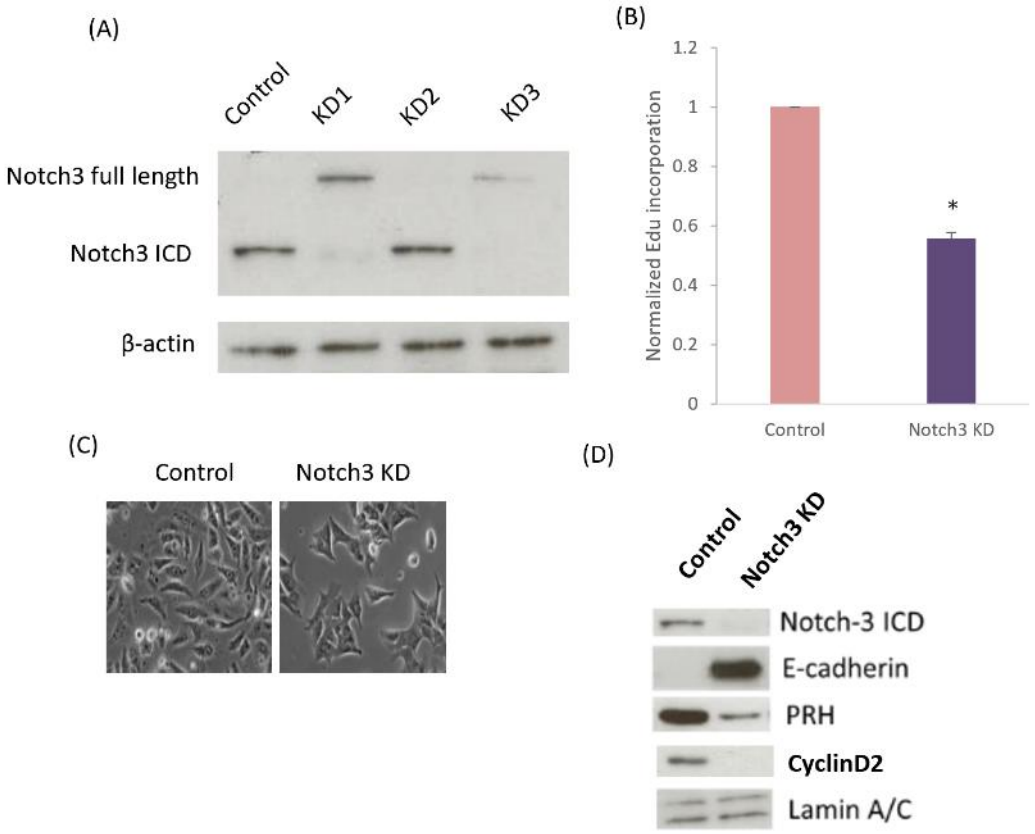

Figure 4.3 Notch3 KD decreases cell proliferation and leads to MET in CCLP cells. (A) Western blots showing Notch3 protein expression of three clones of CCLP cells following Notch3 shRNA or empty control shRNA and selection of transfected cells with puromycin after 2 weeks. 10 µg of protein was loaded into each lane. β-actin was used as a loading control. (B) Edu incorporation proliferation assay of Notch3 KD cells and controls normalized to cell numbers. The cells were incubated with Edu for 2 hours. Error bars show the SD among the three experimental repeats. Statistical test: Two-tailed unpaired T-test (n=3; * $p<0.05$). (C) Microscopic images showing the morphology of Notch3 KD and control CCLP cells; magnification: 10x. (D) Representative Western blots showing the protein expression of Notch3, E-cadherin and PRH in Notch3 KD and control CCLP cells. Lamin A/C was used as a loading control. 10 µg of protein was loaded into each lane.

4.3 PRH regulates proliferation, EMT and Cyclin D2 via Notch 3

To understand if Notch3 is essential for PRH to regulate proliferation, we infected CCLP N3KD3 cells and matched non-template control shRNA (NT) cells in parallel with AdPRH or AdEmpty. Western blotting was carried out using Notch3 antibody to show that Notch3 is depleted in the N3KD3 cells and Myc-tag antibody was used to show that Myc-tagged PRH is overexpressed in N3KD3 cells (**Figure 4.4A**).

Edu proliferation assays show that AdPRH overexpression in stable N3KD cells is not sufficient to promote cell proliferation **(Figure 4.4B)**. However, AdPRH infection in the

Empty shRNA control cells increases proliferation compared to Ad-EVC controls. Thus, Notch3 protein expression appears to be critical for PRH expression and for the effect of endogenous PRH on proliferation.

Since Notch3 activity is required for PRH on proliferation and Notch3 KD decreases *CCND2* expression, we wondered if overexpressing PRH with AdPRH in the N3KD3 cells would influence *CCND2* expression. Western blotting was performed using protein obtained from control shRNA or N3KD3 cells infected with AdEmpty or AdPRH. The Western blot shows that the expression of CyclinD2 is increased with AdPRH and Cyclin D2 is downregulated when Notch3 is depleted but the expression cannot be restored when the N3KD3 cells are infected with AdPRH **(Figure 4.4A)**. This demonstrates that high PRH is insufficient to increase *CCND2* at transcript level or Cyclin D2 at protein level when Notch3 is depleted and that Notch3 is critical for PRH dependent Cyclin D2 expression.

As MET was observed with morphological change when either PRH or Notch3 is depleted and we showed that Notch3 and PRH form positive feedback loop to regulate each other, we wondered if the regulation of EMT related genes by PRH also requires Notch3 expression. Western blotting was performed using protein obtained from control shRNA cells, N3KD3 cells, N3KD3 cells infected with AdEmpty or AdPRH as above. The Western blot shows that AdPRH represses E-cadherin expression and the expression of E-cadherin is restored in N3KD3 cells but E-cadherin expression remains in the N3KD3 cells even the cells are infected with AdPRH. Vimentin protein and mRNA expression are regulated by Notch3 and at the protein level, Vimentin is regulated by PRH. We wondered whether Vimentin is also co-regulated by Notch3 and PRH at the protein level.

The expression of Vimentin is decreased by Notch3 KD and AdPRH is unable to increase Vimentin expression in the N3KD3 cells **(Figure 4.4A)**.

To determine whether Notch is regulating the genes transcriptionally or post transcriptionally, quantitative PCR was carried out on the RNA extracted from control shRNA cells, and N3KD3 cells infected either with AdEmpty or AdPRH. The qPCR data agrees with the Western blotting that *CDH1* (E-cadherin) and *CCND2* (CyclinD2) are downregulated by Notch3 KD but not upregulated by AdPRH in the N3KD3 cells (**Figure 4.4C**). The expression of *VIM* is downregulated by depletion of Notch3 and it is not increased further with AdPRH in N3KD3 cells. Thus, the EMT genes tested were shown to be regulated by PRH in a Notch3 dependent manner rather than independently of Notch3. The *FLT4* gene encodes a tyrosine kinase receptor and is known to be regulated by PRH in other cell types where Notch3 is not highly expressed (Gauvrit et al., 2018). *FLT4* is expressed in CCLP cells and qPCR shows that *FLT4* is upregulated in AdPRH infected CCLP cells and downregulated upon Notch3 depletion, but *FLT4* expression becomes upregulated in N3KD3 cells infected with AdPRH. This demonstrates that the *FLT4* gene is an example of the set of genes that are regulated by PRH but not critically influenced by Notch3 levels. Collectively, it can be concluded that PRH activates E-cadherin, Vimentin and Cyclin D2 in a Notch3 dependent mechanism.

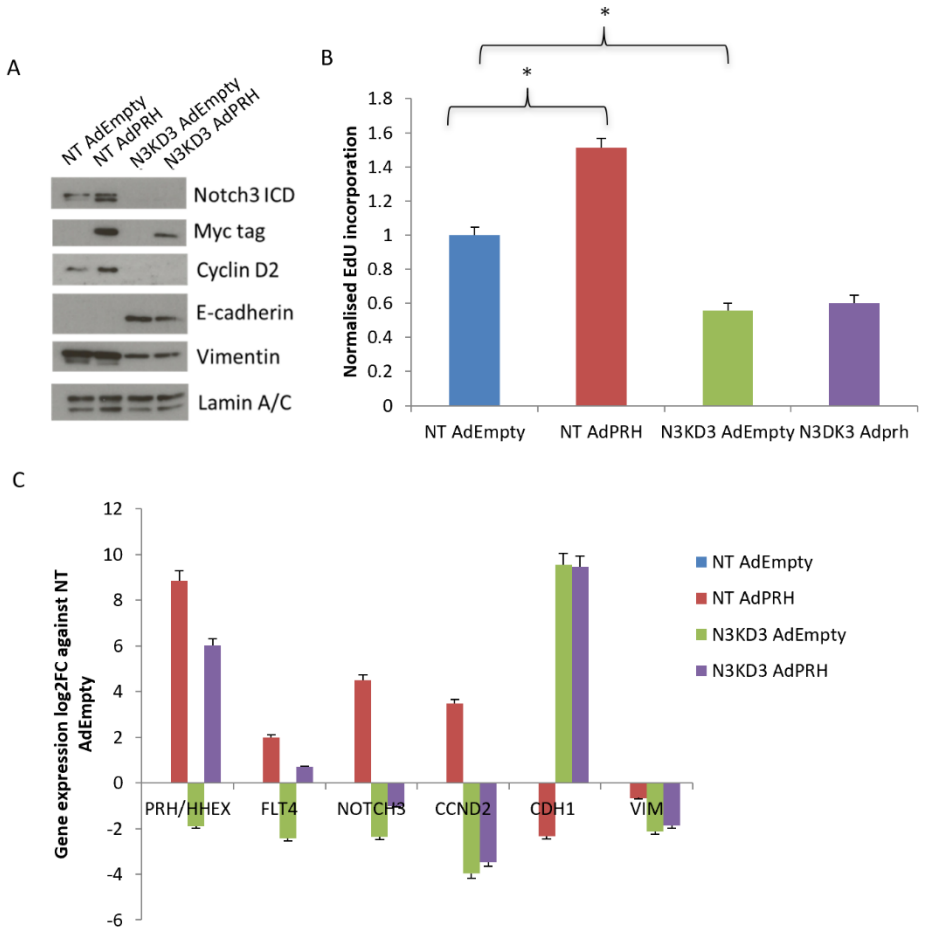

Figure 4.4 PRH regulates EMT and Cyclin D2 via Notch3. (A) Representative Western blots of EMT proteins E-cadherin, Vimentin and Cyclin D2 in CCLP cells infected with AdPRH in the presence of Notch3 shRNA or Empty shRNA (n=3). (B) Proliferation of CCLP cells overexpressing Myc-PRH in the presence or absence of Notch3 shRNA. Error bars show the SEM among the two experimental repeats. Statistical test: One-way ANOVA followed by Bonferroni correction (n=3, * $p<0.05$). (C) qPCR analysis of several genes from CCLP cells overexpressing AdPRH in the presence of absence of Notch3 shRNA identifying PRH and Notch3 correlated expression signatures. The expression was normalized against β-actin. Statistical Analysis: One-way ANOVA followed by Bonferroni correction (n=3). Error bars show the Standard error means among the two experimental repeats.

4.4 PRH regulation of endogenous Vimentin expression is influenced by cell confluency

We previously observed a decrease in Vimentin protein expression in CCLP cells when either PRH and Notch3 was depleted and we showed that PRH regulates Vimentin protein in a Notch3 dependent mechanism. However, in CCLP cells PRH overexpression and PRH depletion in the PRH KD cell line did not result in significant changes in expression of the *VIM* gene in RNA-seq or qPCR experiments. We wondered whether the lack of regulation of the Vimentin gene by PRH in the PRH KD and AdPRH

experiments could be a consequence of the effects of cell confluency/density. Vimentin expression has previously been reported to be influenced by cell confluency in a breast cancer cell line (Gasior et al., 2019).

To examine whether cell confluency is influencing the expression of Vimentin in CCLP cells and also the response to PRH, both shRNA control and PRH KD CCLP cells were grown at three confluency conditions in a 6 well dish: Sparse confluency (5 x 10^5 cells, 40 %), medium (8 x 10^5 cells, 60 %) and fully confluent (1 x 10^6 cells, 100 %). Cells were infected with AdPRH for 24 hours and cells were plated at the three cell densities. The cells were then grown in parallel for another 24 hours and then RNA was extracted and qPCR was performed for *VIM*, *PRH/HHEX* and *BACT* (β-actin) genes. The experiment was repeated twice independently using cells from different passages. **Figure 4.5A** shows that in CCLP shRNA control cells, *VIM* mRNA expression increases with increasing cell density. Similarly, *VIM* gene expression also increases with cell density even in the PRH KD cell line although the levels of *VIM* mRNA expression are considerably lower **(Figure 4.5A)**. To examine the effect of PRH overexpression CCLP cells were infected with AdPRH or AdEmpty for 24 hours before plating the infected cells at sparse, medium or high cell density for a further 24 hours. RNA was extracted and qPCR was performed for *VIM* mRNA expression. **Figure 4.5B** shows that exogenous PRH increases *VIM* expression strongly at sparse or medium cell density but has little effect at high cell density. The cells grown at high confluency show no significant change in Vimentin gene expression between AdPRH and AdEmpty control CCLP cells whereas the same cells grown at medium to low confluency do show increased Vimentin expression in the presence of exogenous PRH **(Figure 4.5B)**.

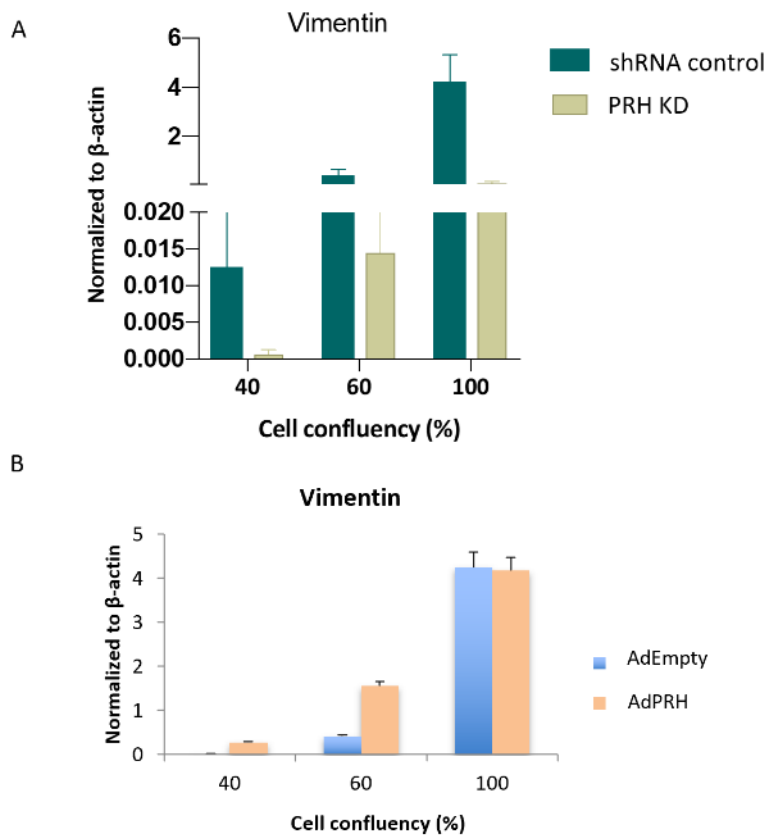

Figure 4.5 Vimentin expression is dependent on cell confluency. (A) qPCR showing the transcript level of *VIM* normalized to β-actin from PRH KD and control shRNA cells grown at different cell densities for 24 hours (n=2). Error bars show the SD among the three experimental repeats. (B) qPCR showing the transcript level of *VIM* normalized to β-actin for CCLP cells infected with AdPRH or AdEmpty 24 hours after plating at the different cell densities and AdEmpty cells (n=2). Error bars show the SEM among the two experimental repeats.

Since cell density affects the expression of Vimentin, we wondered if cell density also affects the expression of PRH. The RNA extracted from control shRNA cells grown in sparse, medium and high cell density from the experiment described above was used for qPCR. The qPCR data shows that PRH expression increases with increasing cell density **(Figure 4.6A)**. PRH expression in the PRH KD cells was also shown to increase with cell density while remaining depleted compared with control cells **(Figure 4.6B)**. In contrast in CCLP cells infected with AdPRH, exogenous PRH expression was extremely high and did not change with cell confluency **(Figure 4.6C)**. We conclude that PRH KD cells have lower levels of *VIM* mRNA expression than control cells but the difference in

VIM expression in control and PRH KD cells is not as apparent at higher cell densities. The RNA-seq experiments performed with PRH KD cells in the previous chapter were not performed with cells grown at the same cell density as the control and PRH KD cells grow at very different rates and this could explain why *VIM* was not identified as a PRH regulated gene in previous RNA seq experiments. In summary, we found that endogenous PRH is able to regulate endogenous Vimentin expression. In the AdPRH CCLP experiments, exogenous PRH regulates Vimentin in CCLP cells when cells are at low density but not when CCLP cells are at high cell density and Vimentin expression is already high.

Collectively the data indicates that the Vimentin gene is regulated by PRH and by Notch3 just as the *CDH1* and *CCND2* genes. However, Vimentin regulation by PRH is dependent on both Notch3 expression and also influenced by cell density.

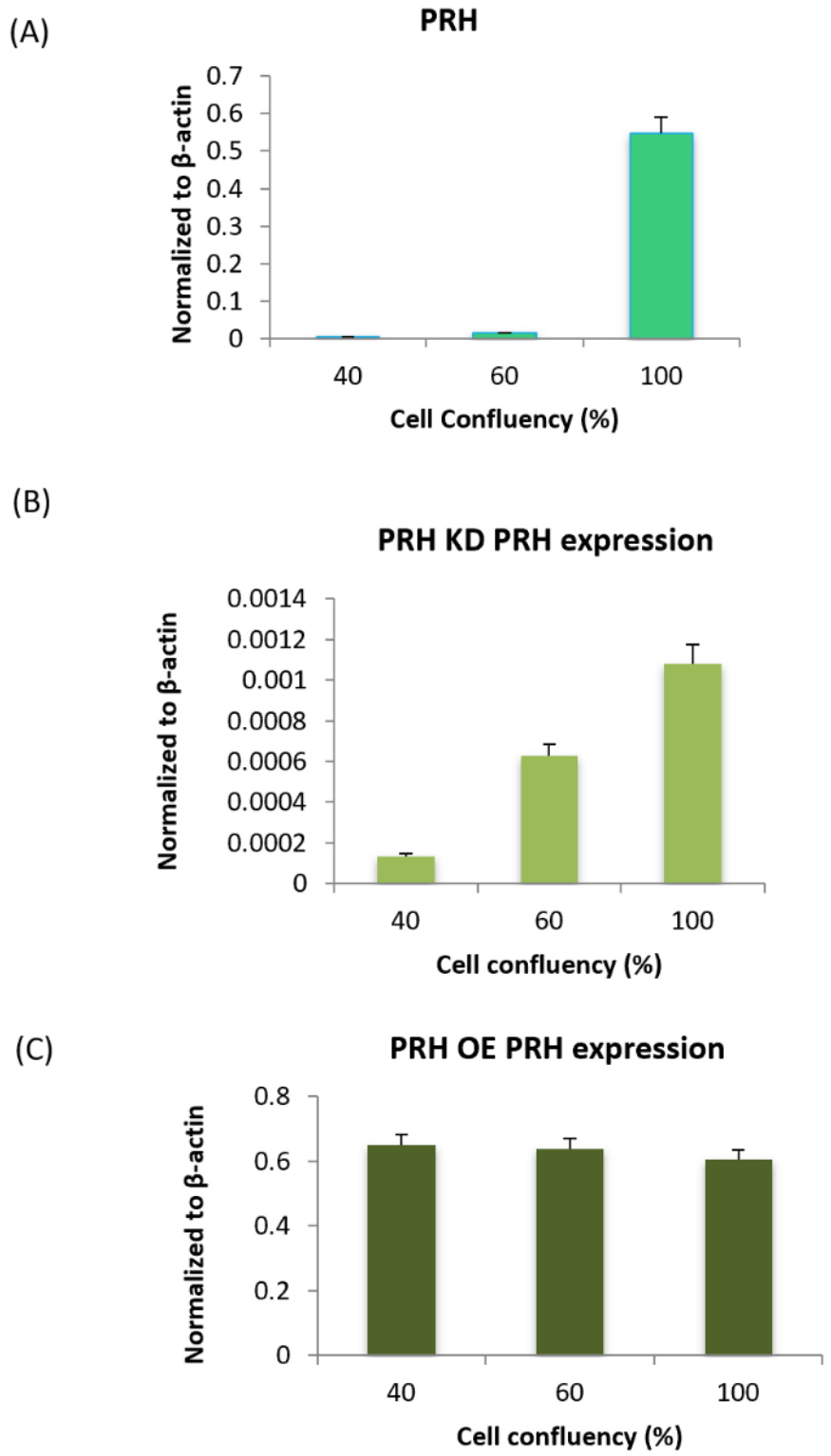

Figure 4.6 PRH expression is affected by cell confluency. (A) qPCR showing *PRH/HHEX* mRNA expression in different cell density in CCLP cells (n=2). (B) qPCR showing *PRH/HHEX* mRNA expression in different cell densities in PRH KD CCLP cells (n=2). (C) qPCR showing *PRH/HHEX* mRNA expression in different cell density in AdPRH infected CCLP cells (n=2). Error bars show the SEM among the two experimental repeats.

4.5 PRH directly regulate *CDKN1B*, *CDKN2B* and *VIM* through DNA binding

To better understand the mechanisms that PRH uses to regulate its target genes we identified direct targets of PRH using chromatin immunoprecipitation (ChIP) with the Myc-tagged PRH protein. Previously, the Myc antibody has been shown to be useful for quantitative ChIP of Myc-PRH in breast cancer cells (Kershaw et al., 2014). Endogenous PRH could not be used for these experiments as suitable antibodies for ChIP are not available. In ChIP, chromatin and protein are cross-linked using formaldehyde. The chromatin is then fragmented by cycles of sonication. Immunoprecipitation (IP) for the protein of interest bound to chromatin is then performed followed by reversal of crosslinks and removal of the proteins yielding the DNA fragments associated with the protein of interest. To determine if a specific region of chromatin associated with a gene is bound by the protein, PCR for a region from a specific gene is followed by PAGE to visualize the PCR product or alternatively the PCR fragment is assessed by quantitative PCR for enrichment of specific binding. The eluted DNA can also be used for ChIP-sequencing (ChIP-seq). ChIP-seq is a technique to allow detection of binding sites for the protein within chromatin throughout the genome. It should be noted that in this technique the protein can be directly crosslinked to DNA or indirectly crosslinked through another protein such as another transcription factor or a histone.

To identify the genes that are associated with PRH chromatin was prepared from adenoviral Myc-PRH or empty adenovirus infected CCLP cells and ChIP was carried out on the chromatin prepared from these cells using the Myc 9B11 antibody. Empty adenoviral infected CCLP chromatin was incubated with Myc antibody as a negative control to allow assessment of the non-specific background, for example, DNA non-

specifically associated with the antibody magnetic beads instead of Myc antibody. Sonicated chromatin input (that has not been through immunoprecipitation) is used as a reference for all regions of the genome as all regions should be equally represented. Quantitative ChIP analysis was performed by calculating enrichment of the gene of interest as a percentage of the input (**see M&M section 2.6**). The primer pairs for each gene were based on called peaks identified in parallel ChIP-seq experiments in CCLP cells (performed by Dr. P. Kitchen). Negative control primers within two regions of low gene density and condensed chromatin within chromosome 18 and chromosome 22 were used as a control in ChIP experiments. Transcription factor binding is not expected at the chromosome 18 and 22 regions because the chromatin is condensed (Thibodeau et al., 2017). Following ChIP with Myc-PRH expressing cells, qPCR showed that there is enrichment of sequences for PRH binding at *CDKN1B* and *CDKN2B* genes after normalizing against input DNA but no binding at the Chromosome 18 and 22 loci **(Figure 4.7A)**.

To examine the binding of Myc-PRH across the genome the ChIP-seq data obtained by Dr P Kitchen was utilized. ChIP was performed exactly as described and the eluted DNA was sent for ChIP-seq (Ishanvi Life Sciences, India) following quantification of the DNA on TapeStation and Qubit. The library pool was sequenced using IlluminaHiseq 2500 (100 x2 BP generating 40-50 millionreads). Bioinformatics was performed by to identify ChIP-peaks representing genome-wide binding sites of PRH that are within 100 kb of the nearest transcription start site (using HOMER). Cell cycle genes *CDKN1B* and *CDKN2B,* inhibitors of Cyclin-dependent kinases encoding p27 and p15 have PRH ChIP peaks.

CDKN1B has a large number of strong peaks near the 3' region of the gene whereas CDKN2B has multiple weaker peaks across the whole gene **(Figure 4.7B and 4.7C)**.

The ChIP-seq data (called peaks associated with genes) was then analyzed using GSEA and this allowed the identification of hallmark pathways that are enriched. The pathways identified as enriched included pathways related to proliferation (G_2M checkpoint), EMT, IL6, p53 and TNF-α signaling **(Figure 4.8A)**. The detailed bioinformatics analysis to obtain the ChIP-seq called peaks data is included in (**M&M section 2.6.3**). A Venn diagram was plotted using Biovenn using the Myc-PRH ChIP-seq dataset and the Myc-PRH RNA-seq dataset. The intersection of the data sets shows that 143 genes are both activated by PRH and also potential PRH direct targets in ChIP whereas 397 genes are both downregulated and potential PRH direct targets **(Figure 4.8B)**. GSEA on the genes that are direct targets of PRH and also differentially regulated was carried out. **Figure 4.8C** shows the GSEA on the overlap of these sets; there is enrichment of directly regulated genes in the apoptosis pathway.

A

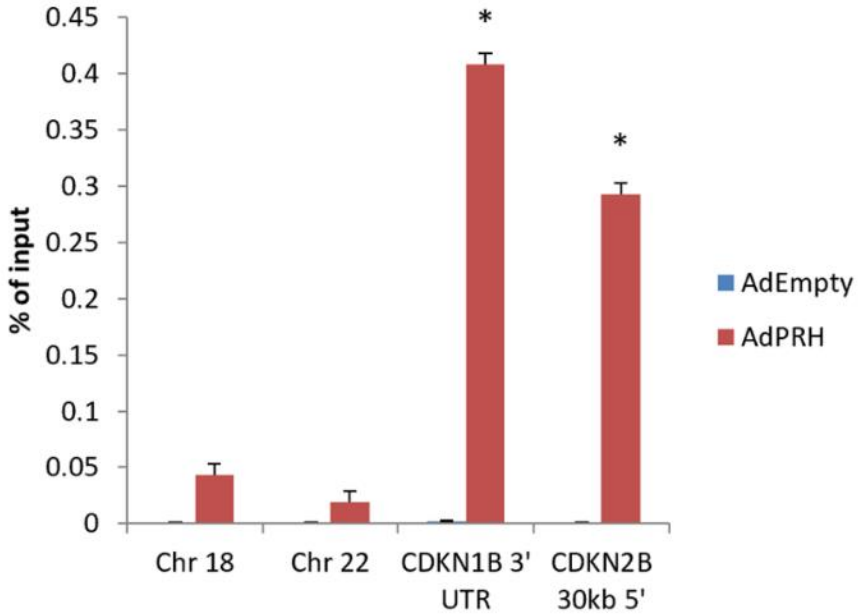
0.45
0.4
0.35
0.3
0.25
0.2
0.15
0.1
0.05
0
% of input
*
*
AdEmpty
AdPRH
Chr 18
Chr 22
CDKN1B 3' UTR
CDKN2B 30kb 5'

(B) *CDKN1B*

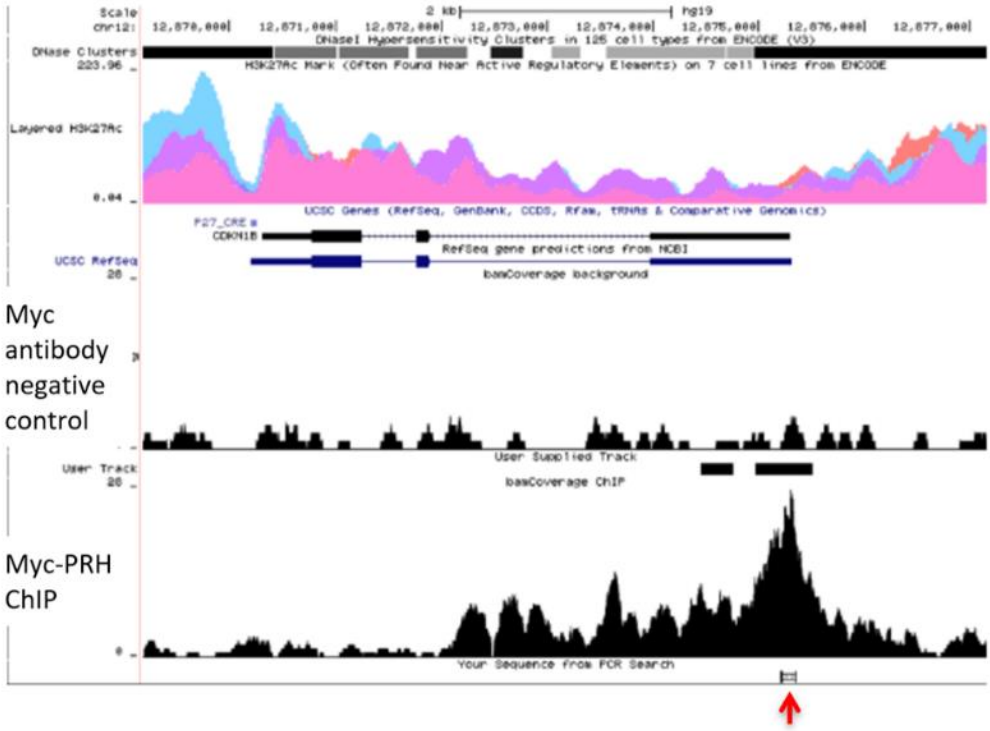
Myc antibody negative control
Myc-PRH ChIP

(C) *CDKN2B*

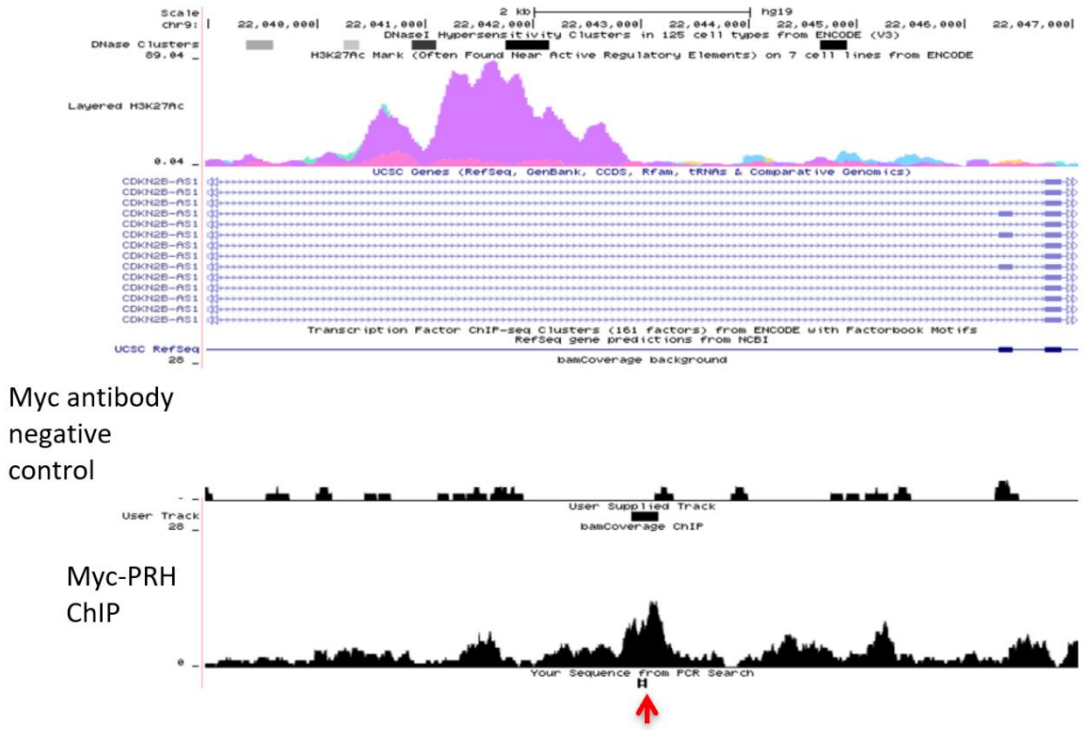

Figure 4.7 PRH regulates *CDKN1B* and *CDKN2B* through DNA binding. (A) 25 µl (5.8%) of input was taken from the chromatin sample (425 µl). Statistical test: Two-tailed unpaired T-test (n=2; *q<0.05). (n=3; *, p<0.05). Error bars show the SD means among the three experimental repeats. ChIP-seq track obtained from UCSC showing PRH target genes and the location of the ChIP peaks and the background. Red arrow indicates the location of the ChIP primer for the manual ChIP. The H3K27Ac track shows the enrichment of H3K27Ac histone modification across the genome. (B) *CDKKN1B* gene (C) *CDKN2B* gene.

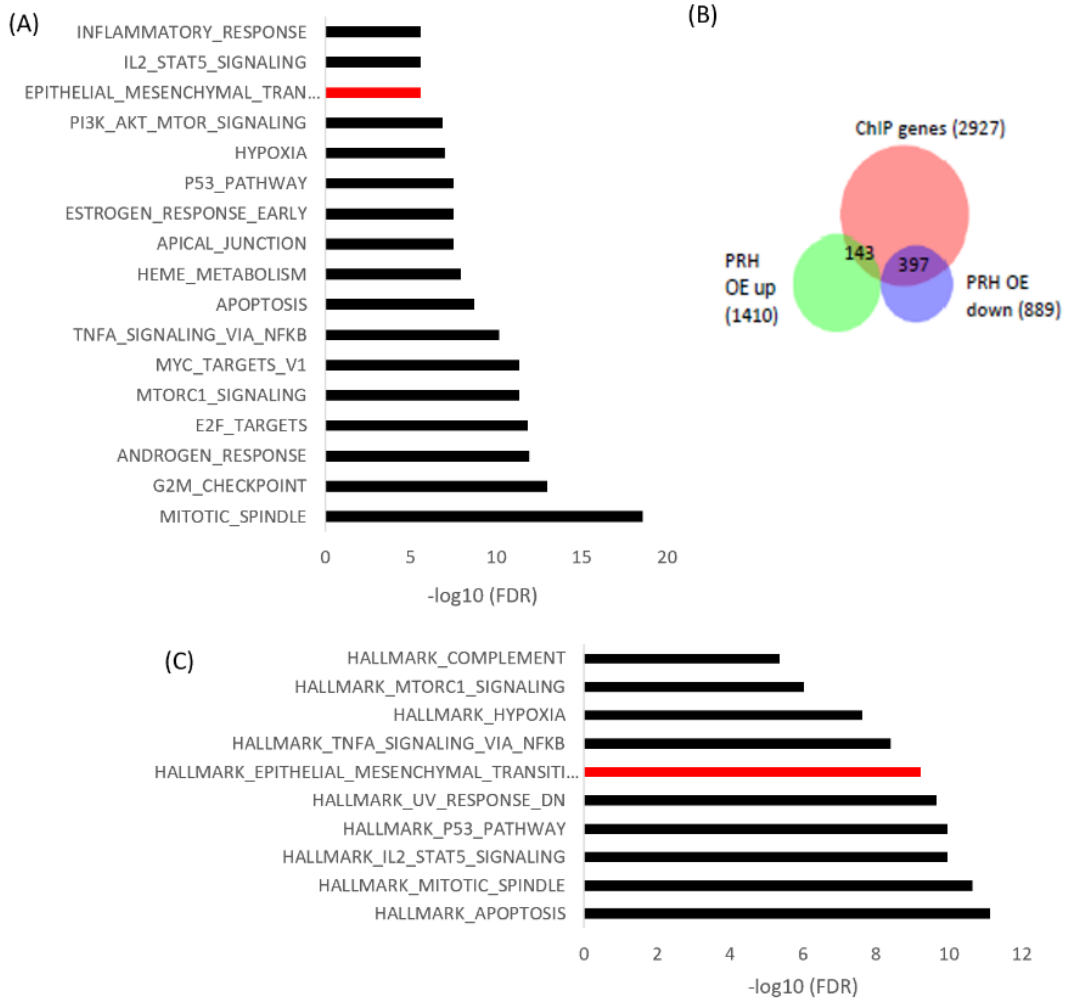

Figure 4.8 CCLP ChIP-Seq GSEA. (A) The list represents the hallmark gene sets that are enriched in the ChIP-seq data set from Myc-PRH overexpressing cells. The EMT pathway is in the list and is highlighted red. FDR is the false recovery rate for enrichment sets. (B) Venn diagram showing the number of DEGs in the PRH OE RNA-seq data and the ChIP-seq data. (C) The list represents the hallmark gene sets that are both enriched in PRH OE ChIP-seq and RNA-seq dataset and EMT is one the pathways in the list and is highlighted red.

Since GSEA of the ChIP-seq data showed enrichment of the EMT pathway we wondered whether the *CDH1* or *VIM* genes show a 'called peak' for PRH. ChIP-seq data in the genome browser shows multiple broad ChIP peaks within and near the *VIM* gene. This data suggests that Vimentin is a direct target of PRH **(Figure 4.9A)**. The data also shows that apart from *CDKN1B* and *CDKN2B*, *CDKN1A* is also a direct target of PRH **(Figure 4.9E)**. Surprisingly, *CDH1* did not show a called peak in the ChIP-seq experiment.

Moreover, the genes corresponding to the transcription factors that regulate *CDH1 SNAI*/*TWIST*/*ZEB* EMT also did not show binding of PRH. There was also no binding of PRH within 100 kb of the *NOTCH3* gene or the *CCND2* gene **(Figure 4.9B, C and D)**. Therefore, we conclude that these genes are not directly regulated by PRH.

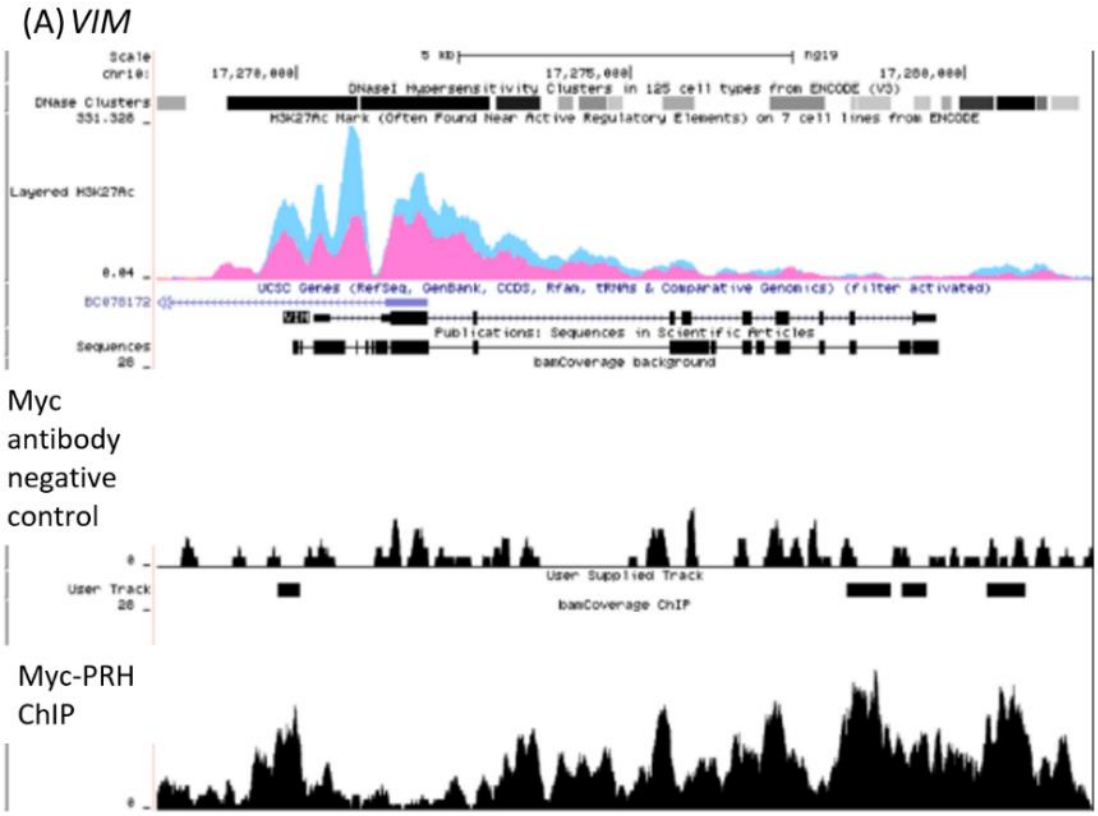

(B) *NOTCH3*

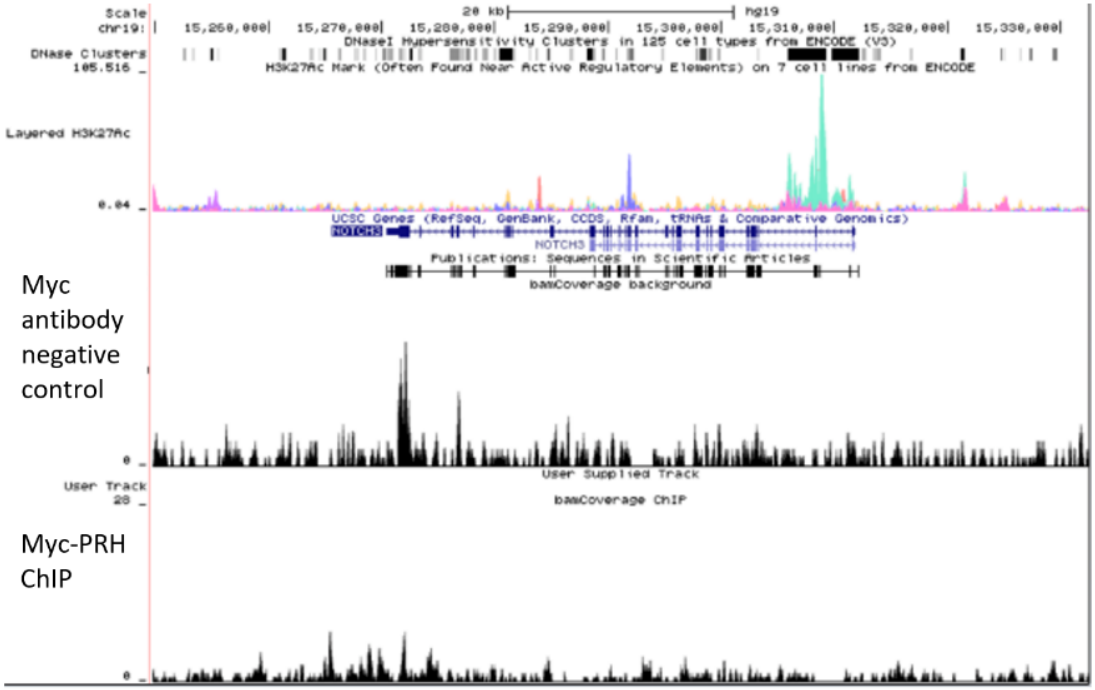

(C) *CCND2*

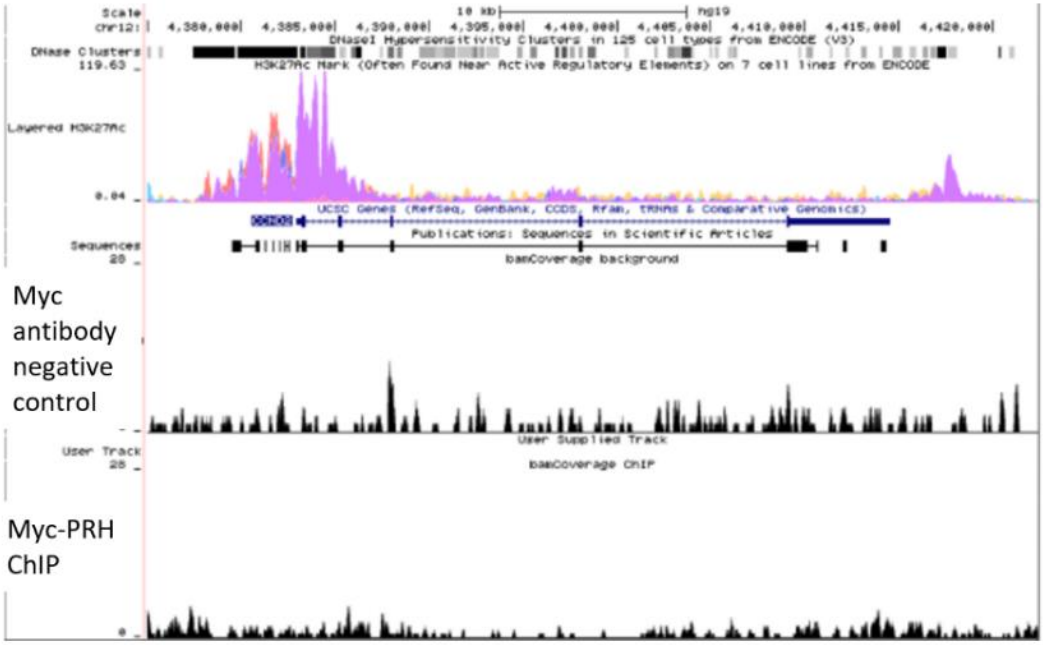

(D) *CDH1*

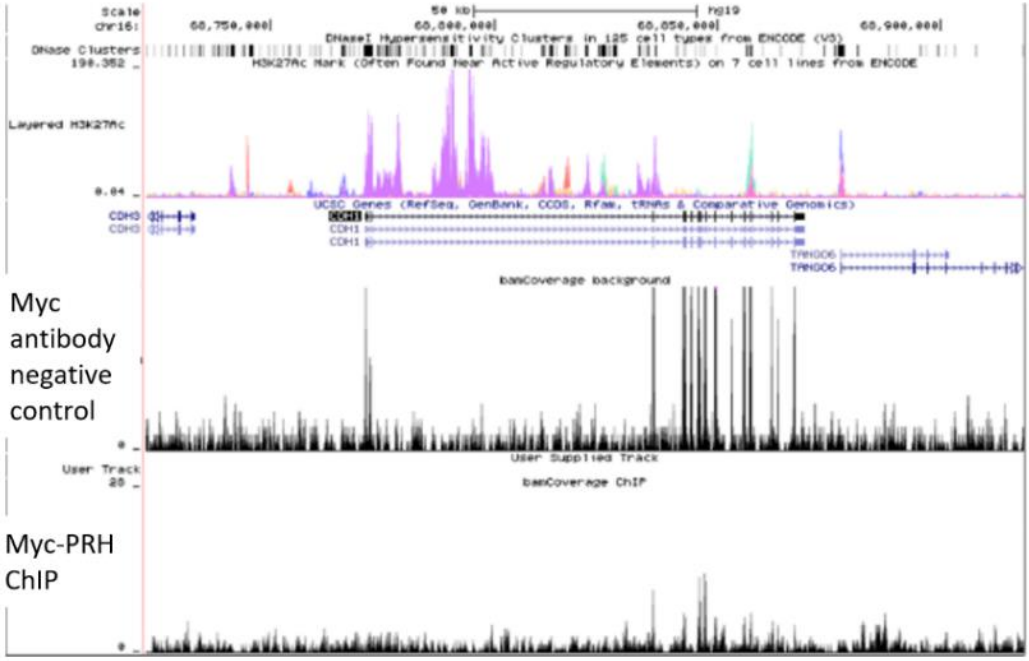
Scale
chr16:
50 kb
hg19
60,750,000
60,800,000
60,850,000
60,900,000
DNase Clusters
DNaseI Hypersensitivity Clusters in 125 cell types from ENCODE (V5)
H3K27Ac Mark (Often Found Near Active Regulatory Elements) on 7 cell lines from ENCODE
Layered H3K27Ac
UCSC Genes (RefSeq, GenBank, CCDS, Rfam, tRNAs & Comparative Genomics)
CDH3
CDH1
TMEM106
bamCoverage background
Myc antibody negative control
User Supplied Track
User Track
bamCoverage ChIP
Myc-PRH ChIP

(E) *CDKN1A*

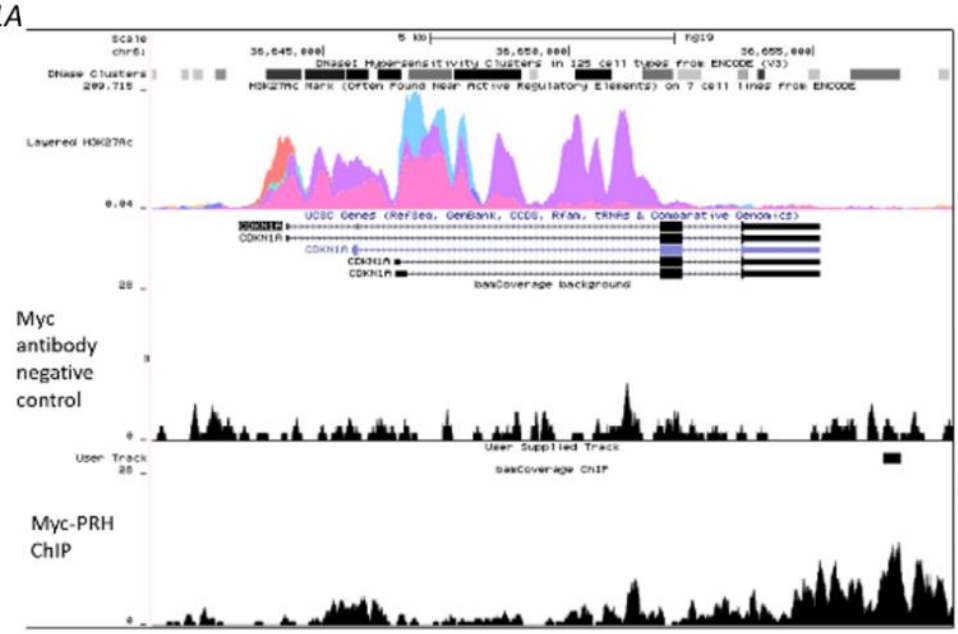

(F) *HES1*

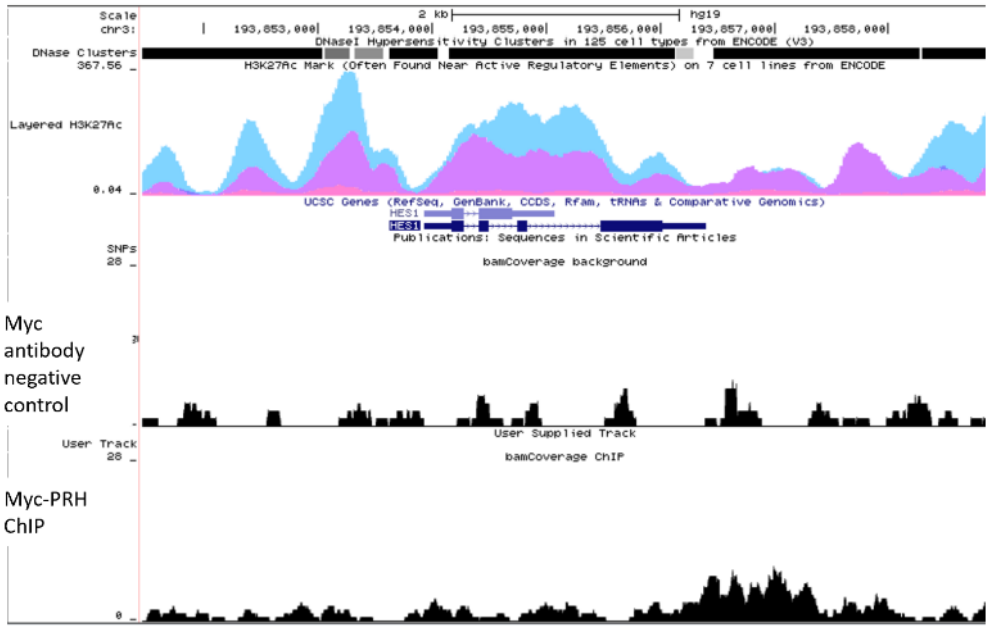

Figure 4.9 ChIP-seq track from UCSC software on other PRH target genes. ChIP-seq track obtained from UCSC showing PRH target genes and the location of the ChIP peaks and the background. Red arrow indicates the location of the ChIP primer for the manual ChIP. The H3K27Ac track shows the enrichment of H3K27Ac histone modification across the genome. (A) *VIM* gene (B) *NOTCH3* gene (C) *CCND2* gene (D) *CDH1* gene (E) *CDKN1A* gene and (F) *HES1* gene. ChIP-seq track obtained from UCSC showing no ChIP peaks for *NOTCH3*, *CCND2* and *CDH1*.

Although *NOTCH3, CCND2* and *CDH1* are not direct targets we wondered whether DNA binding by the PRH homeodomain was still required for the mechanism of regulation by PRH. The previous chapter showed that cells infected with the AdPRHN187A mutant did not cause upregulation of Notch3 and Cyclin D2 proteins or mRNA although AdPRH was able to increase expression **(Figure 3.20)**. This experiment suggests DNA binding is important for regulation of Notch3 expression by PRH in CCLP cells. As PRH does not bind near the *NOTCH3* gene we infer regulation involves binding of PRH at another gene or noncoding RNA that indirectly regulates *NOTCH3*. ChIP-seq data shows ChIP peaks near the *HES1* gene (**Figure 4.9F**). Therefore, it is possible that *HES1* mediates the PRH regulation of Notch3. However, we cannot rule out the possibility that the N187A mutation also disrupts protein-protein interactions made by the PRH protein and therefore the mutation also decreases the interaction of PRH with specific proteins that are required for the regulation of the *NOTCH3, VIM* and *CDH1* genes.

4.6 Vimentin and PRH both promote proliferation

We have established that Notch3 and PRH both regulate cell proliferation and also regulate each other. Moreover, we have shown that they both regulate Vimentin and that Vimentin is a direct target for PRH. Although Vimentin is best known through its ability to influence cell motility and the mesenchymal phenotype. It is also known to regulate cell proliferation in certain cell types including fibroblasts (Danielsson et al., 2018). To determine whether Vimentin can influence CCLP cell proliferation, Vimentin was depleted using siRNA in CCLP cells. Multiple Vimentin siRNA were tested to identify a siRNA that is able to knockdown Vimentin effectively (performed by Ms Gagan Kaur). **Figure 4.10A** shows that Vimentin siRNA #5 (SI00302190, Qiagen) reduces Vimentin

protein most effectively compared to the non-targeting siRNA (All stars) as a control. Therefore, Vimentin siRNA #5 was chosen for further experiments. Edu incorporation assays show that CCLP cells are less proliferative when Vimentin is knocked down **(Figure 4.10B)**. A change in morphology was also observed when Vimentin was depleted. The cells become round in shape and appear to have a more epithelial phenotype **(Figure 4.10C)**.

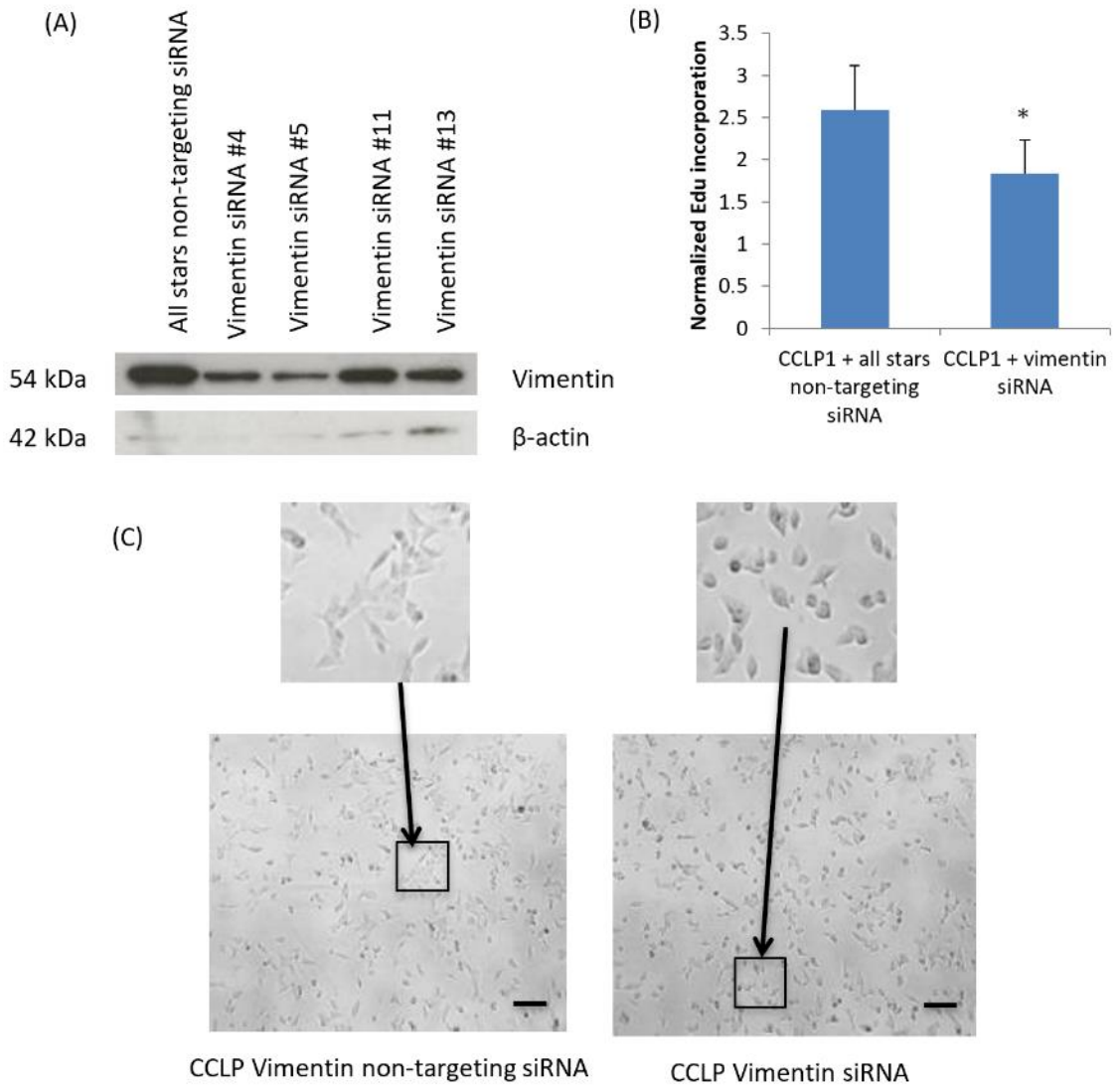

Figure 4.10 Vimentin KD decreases cell proliferation and changes cell morphology in CCLP cells. (A) Western blots showing Notch3 protein expression of four clones of siRNA transfected Vimentin knockdown CCLP cells. β-actin was used as a loading control. (B) Edu incorporation proliferation assay normalized to cell number of Vimentin KD cells and controls. Error bars show the SD among the six experimental repeats. (n=6; $p<0.05$). (C) Microscopic images showing the morphology of Vimentin KD and control CCLP cells using light microscope; magnification: 10x. Scale bar represent 10 µm.

Quantitative-PCR following siRNA transfection of CCLP cells was carried out to investigate if Vimentin has a role in regulating genes associated with proliferation. **Figure 4.11A** shows that Vimentin knockdown leads to an upregulation of *CDKN1B* gene expression and also a downregulation of *CCND2* gene expression, similar to the effect of PRH KD on the expression of these genes. However, there is no change in *CDKN2B* and

NOTCH3 gene expression unlike the changes seen in these genes upon PRH KD. Western blotting confirms p27 (*CDKN1B*) is upregulated by Vimentin knockdown and Cyclin D2 (*CCND2*) is downregulated by Vimentin knockdown **Figure 4.11B**. Thus, these genes are altered by Vimentin depletion in the same direction as by PRH depletion in CCLP cells. Of note although total Lamin expression is maintained the expression of the two isoforms Lamin A/C is altered toward increased Lamin C expression when Vimentin is depleted using the Lamin A/C antibody.

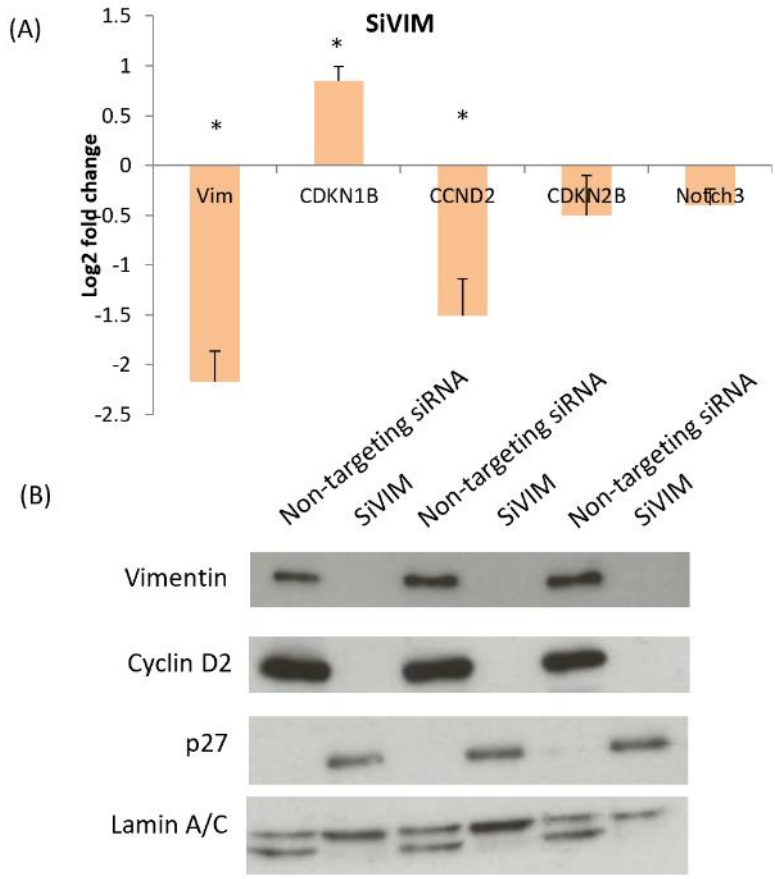

Figure 4.11 Vimentin KD regulates cell cycle genes in CCLP cells. (A) qPCR showing gene expression of cell cycle genes normalized to β-actin in siRNA Vimentin KD cells CCLP. (n=3; *, $p<0.05$). The error bars show the SD of three experimental repeats. (B) Western blots showing three repeats of the protein expression of Vimentin, Cyclin D2 and p27 in three individual SiRNA transfections of CCLP. Detection of LaminA/C was used as a loading control. 10 µg of protein was loaded into each lane.

In order to investigate whether there is an additive effect of PRH and Vimentin on proliferation, Vimentin was transiently depleted for 48 hours in the control shRNA and the paired shRNA PRH KD cell line using the Vimentin siRNA #5. In parallel both cell lines were treated with the all-star control siRNA using transient transfection. Western blot was performed to confirm Vimentin knockdown in control cells and in the PRH KD cells. As expected, the PRH protein level is lower in the PRH KD cells. Western blotting confirms Vimentin KD in control and PRH KD cells **(Figure 4.12A)**. Edu proliferation assays were conducted in these cells. As expected, PRH KD cells are less proliferative than the shRNA control. Interestingly, Vimentin depletion results in decreased proliferation compared to shRNA control cells and results in a further reduction of proliferation in the PRH KD cells **(Figure 4.12B)**. Quantitative-PCR shows that Vimentin depletion in PRH KD cells show a further reduction of *CCND2* expression compared to Vimentin KD in control cells. However, the cells show no further modulation of *CDKN1B* gene expression in Vimentin depleted PRH KD cells compared to the Vimentin siRNA transfected cells (p=0.7). **(Figure 4.12C)**. Therefore, the effect of PRH KD on proliferation is additive with Vimentin depletion, moreover there is an additive effect observed with reference to decreased gene expression for *CCND2.* Although there is a similar trend for *CDKN1B* gene expression levels with Vimentin and PRH depletion the result is not statistically significant.

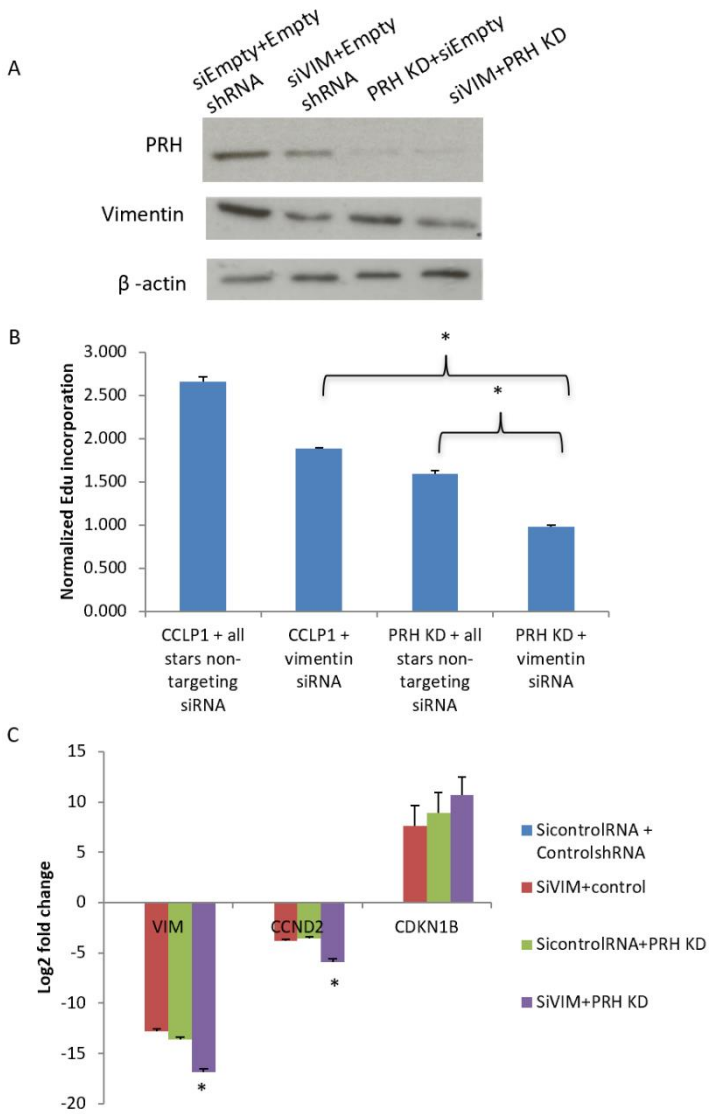

Figure 4.12 The effects of PRH and Vimentin double knockdown on proliferation in CCLP. (A) Representative Western blots for PRH and Vimentin protein expressions in CCLP shRNA control and PRH KD cells in the presence or absence of Vimentin siRNA to confirm the PRH and Vimentin KD. (B) Proliferation of CCLP control shRNA cells and PRH KD cells in the presence or absence of Vimentin siRNA. Statistical Analysis: One-way ANOVA followed by Bonferroni correction (n=3, * $p<0.03$). (C) q-PCR analysis of several genes in PRH KD CCLP in the presence or absence of Vimentin siRNA investigating the effect of Vimentin KD on cell cycle genes expressions in PRH KD cells. Statistical Analysis: One-way ANOVA followed by Bonferroni correction (n=3, * $p<0.05$). The error bars show the SD of three experimental repeats.

We wondered whether the decrease in proliferation and altered gene expression brought about by PRH depletion (and consequent Notch3 decrease) involves Vimentin. To address this, we examined whether the positive effect of exogenous PRH on *CCND2* expression and repression of *CDKN1B* is also influenced by Vimentin. We infected cells with AdPRH or AdEmpty for 24 hours and then the cells were transiently transfected

with all-star control siRNA or Vimentin siRNA for 48 hours followed by RNA extraction or protein extraction of cells. This experiment involves CCLP cells with four different conditions: CCLP cells transfected with empty siRNA and infected with empty virus control, CCLP cells transfected with Vimentin siRNA and infected with empty virus control, CCLP cells infected with AdPRH and transfected with empty siRNA and CCLP cells infected with AdPRH and transfected with Vimentin siRNA. Western blotting was carried out to confirm PRH overexpression and Vimentin knockdown **(Figure 4.13A)**. Cells were grown at high confluency to minimize any effects of AdPRH on endogenous Vimentin expression **(See Figure 4.13A)**. Quantitative-PCR shows that Vimentin depletion results in decreased *CCND2* and increased *CDKN1B* whereas cells infected with AdPRH and Vimentin depletion results in loss of the effect of AdPRH on *CCND2* and *CDKN1B* expression **(Figure 4.13B)**. Furthermore, Edu experiments also show that siVimentin reduces proliferation and AdPRH causes an increase in proliferation in control cells but when PRH is overexpressed in the siVimentin CCLP cells, the cells regain their proliferative capacity with the same amount of Vimentin expression **(Figure 4.13C)**. Therefore, we conclude that the effect of PRH on proliferation is not mediated by Vimentin.

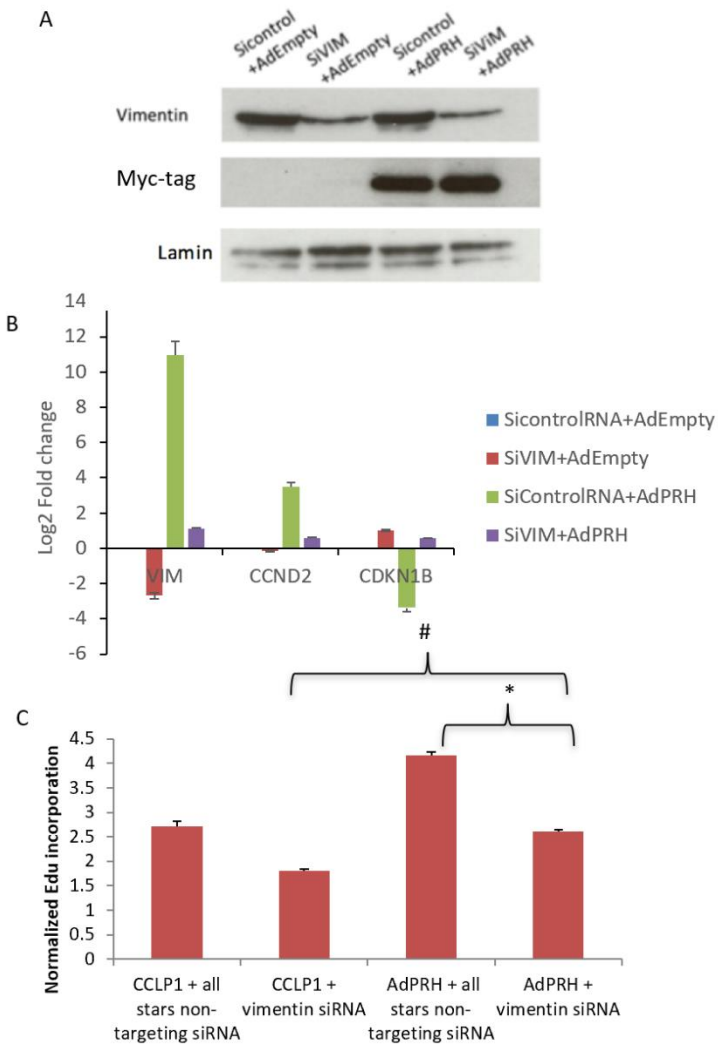

Figure 4.13 The effects of PRH and Vimentin double knockdown on proliferation in CCLP. (A) Representative Western blots for PRH and Vimentin protein expression in AdPRH infected CCLP in the presence or absence of Vimentin siRNA to confirm the adenoviral infection AdPRH and Vimentin KD. 10 µg of protein was loaded into each lane. (B) q-PCR analysis of gene expression of *VIM, CCND2* and *CDKN1B* in PRH KD CCLP in the presence or absence of Vimentin siRNA investigating the effect of Vimentin KD on cell cycle genes expressions in PRH OE cells. Statistical Analysis: One-way ANOVA followed by Bonferroni correction (n=3, * $p<0.05$). (C) Proliferation of CCLP overexpressing Myc-PRH in the presence or absence of Vimentin siRNA. Statistical Analysis: One-way ANOVA followed by Bonferroni correction (n=3, * $p<0.05$, # $p>0.05$). The error bars show the SD of three experimental repeats.

In order to understand the mechanism whereby Vimentin and PRH regulate cell cycle genes, we examined whether Vimentin can modulate DNA binding by PRH to regulate gene expression. ChIP using the Myc-tag antibody was performed with CCLP cells infected with AdPRH either in the presence of control siRNA or siRNA against Vimentin.

Previously we have shown that the binding of PRH to the *CDKN1B* and *CDKN2B* genes only occurs in cells that express AdPRH; that is the Myc antibody does not ChIP non-specifically (**See section 4.5**). Following ChIP of Myc-PRH performed as described previously **(section 4.5)**, primers for *CDKN1B* and *CDKN2B* were used for the qPCR and primers for chromosome 18 and chromosome 22 were used as a negative control. The quantification suggests that Vimentin depletion impairs the ability of Myc-PRH to bind to *CDKN1B* and *CDKN2B* **(Figure 4.14)**. As previous ChIP-seq data indicated *CCND2* is not directly bound by *PRH*, the regulation of this gene was not tested in the experiment. We conclude that there is an additive effect of PRH and Vimentin on proliferation but that the effect of PRH on proliferation is not entirely mediated by Vimentin. Rather there may be some Vimentin dependent regulation as well as Vimentin independent regulation of cell cycle and other genes. However, it appears that the regulation of *CDKN1B* and *CDKN2B* by *PRH* is dependent on Vimentin under the experimental conditions.

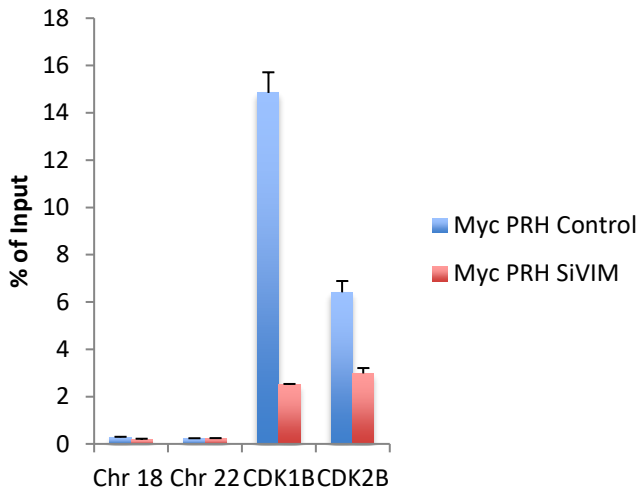

Figure 4.14 Vimentin KD impairs the DNA binding ability of PRH to CDKN1B and CDKN2B. Manual ChIP-qPCR in CCLP overexpressing Myc-PRH with or without Vimentin siRNA showing the enrichment of *CDKN1B* and *CDKN2B*. (n=2). The error bars show the SEM of two experimental repeats.

4.7 PRH regulates Vimentin through protein-protein interaction

Since Vimentin is able to regulate PRH binding in ChIP experiments, we next investigated whether Vimentin could directly associate with PRH through protein-protein interactions. CCLP cells were transfected with expression plasmids pMUG1 Myc-PRH or pMUG1 empty vector for 48 hours and co-Immunoprecipitation (co-IP) assays were performed using the Myc-tag antibody. Fractionation of cells into the nucleus and cytoplasmic fraction were performed prior to the co-IP **(See M&M Section 2.3)**. CCLP cells transfected with the pMUG-1 empty plasmid was used as a negative control. Western blotting was carried out with the Myc-tag and Vimentin antibody against endogenous Vimentin protein to show that Myc-PRH and Vimentin can be immunoprecipitated respectively. Tubulin and Lamin A/C antibodies were used to detect corresponding proteins that serve as loading controls and also confirm cytoplasmic and nuclear fractionation respectively. **Figure 4.15A** shows that Myc-PRH is immunoprecipitated by the Myc antibody and that Vimentin can be co-

immunoprecipitated strongly together with PRH protein in both the cytoplasmic and nuclear fractions. There is a very low level of Vimentin detected in the co-IP in the absence of Myc-PRH which is the result of non-specific binding to beads. Unexpectedly, Lamin and Tubulin can also be detected in the co-IP in nuclear and cytoplasmic fractions respectively. To prevent this, we increased the wash conditions from 5 washes to 10 washes but despite this, Tubulin and Lamin were still present in the IP samples. In order to confirm the interaction between PRH and Vimentin, the co-IP was performed again using a Vimentin antibody for the pull down and the Myc-tag antibody was used for Western blotting detection of Myc-PRH after SDS PAGE separation. **Figure 4.15B** shows that Vimentin is pulled down by the Vimentin antibody whether Myc-PRH is expressed or not. However, the IP for Vimentin is increased in the presence of Myc-PRH. Further the co-IP of Myc-PRH can be strongly detected by the Myc-tag antibody in the Vimentin IP in both cytoplasmic and nuclear fractions. Although Tubulin and Lamin are still present in the IP samples, stronger Vimentin and Myc-PRH bands are observed in the IP samples compared with the input suggesting that Vimentin interacts with Myc-PRH.

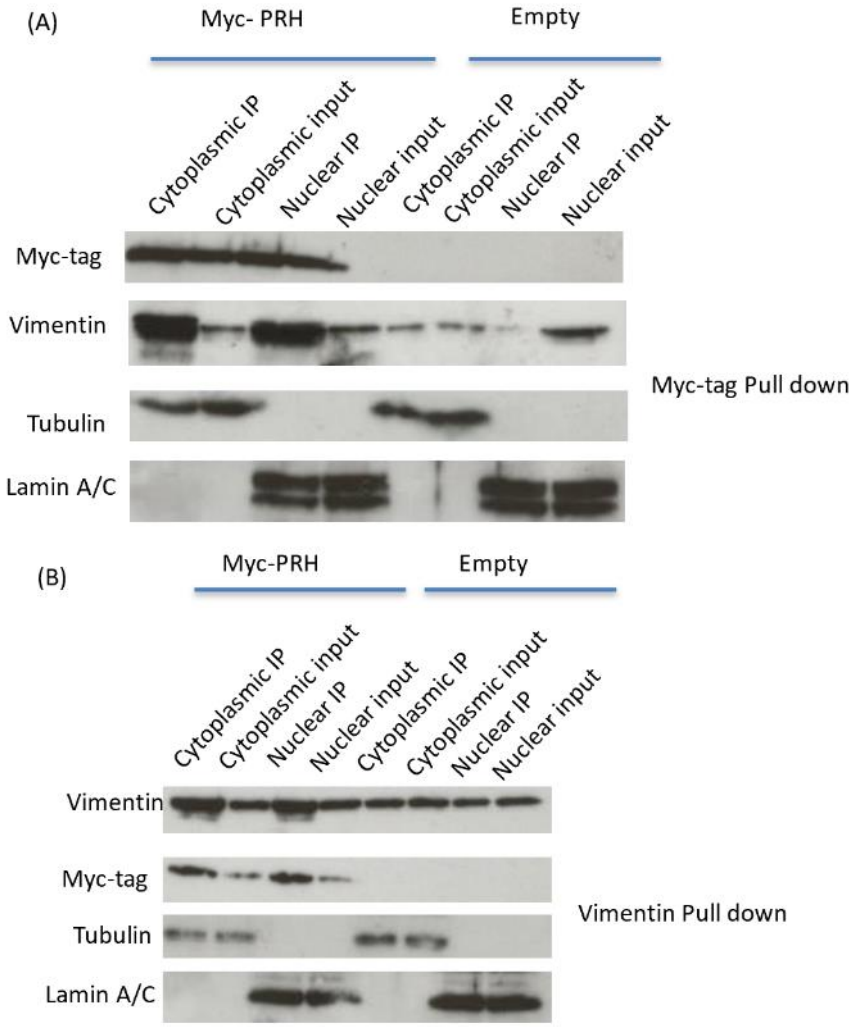

Figure 4.15 PRH interacts with Vimentin in both cytoplasm and nucleus in CCLP cells. (A) Representative Western blots showing IP using anti-Myc antibody in CCLP overexpressing either AdPRH or AdEmpty. Anti-Vimentin antibody was used for probing. Anti-Tubulin and Lamin was used to confirm cytoplasmic and nuclear fractions respectively. 20% input was loaded. The IP was performed twice independently in two different passages of CCLP cells and show similar outcome. (B) Representative Western blots showing IP using anti-Vimentin antibody in CCLP overexpressing either AdPRH or AdEmpty. Anti-Myc tag antibody was used for probing. Anti-Tubulin and Lamin was used to confirm cytoplasmic and nuclear fractions respectively. 20% input was loaded. The IP was performed twice independently in two different passages of CCLP cells and show similar outcome.

Further co-IP experiments were carried out to identify the region of the PRH protein that Vimentin interacts with. CCLP cells were transfected with PRH expression plasmids encoding PRH truncations: N-terminal PRH (pMUG1-PRH_{7-198}) and C-terminal PRH with N-terminus deleted (pMUG1-$PRH_{136-270}$). IPs were carried out using the Myc-tag antibody and detection of interacting proteins by Western blotting was carried out with Vimentin antibody as described previously. **Figure 4.16A** shows $PRH_{136-270}$ lacks the ability to interact with Vimentin, whereas the PRH N-terminus is still able to interact with Vimentin. Therefore, it can be concluded that PRH interacts with Vimentin through its N-terminal domain. As before all the co-IPs in the nuclear fraction contain Lamin A/C. The reason for this could be that there is a large complex containing Vimentin and Lamin A/C that includes PRH or that non-specifically bound Lamin A/C is pulled down with the beads. Further IP was carried out to determine the region in the N-terminus that interacts with Vimentin. CCLP cells were transfected with pMUG1-PRH_{50-270} or pMUG1-PRH_{7-198} using the Myc-tag antibody. **Figure 4.16B** shows that in cells transfected with pMUG1-PRH_{50-270} the truncated PRH protein still able to interact with Vimentin, demonstrating that the first 50 amino acids are not required for the PRH-Vimentin interaction. To determine if the homeodomain is involved in the interaction, the pMUG1-PRH-N187A plasmid encoding the DNA binding mutant alongside wild type control were transfected into CCLP cells and empty plasmid was transfected into CCLP cells as a negative control. **Figure 4.16C** shows that the PRH protein with a point mutation in the DNA binding domain cannot interact with Vimentin efficiently compared to wild-type PRH as there is only a faint Vimentin pull down in the Western blot at 55 kDa. These experiments indicate that the Vimentin-PRH interaction occurs through

amino acid 50-136 and also implicates the DNA binding recognition helix within the PRH homeodomain as of importance for the Vimentin-PRH interaction. Given that Vimentin and PRH interacts directly using regions of the N-terminus (50-270) and the interaction is influenced by the mutation with in the PRH homeodomain that is also known to influence DNA binding activity, we propose that DNA binding by PRH and Vimentin interaction is closely coupled. Since the N187A mutation and the PRH_{7-198} proteins that did not co-IP did not also decrease the amount of Lamin A/C in the blot we infer that the Lamin A/C proteins are non-specifically associated with the magnetic beads.

Importantly, we have shown that PRH and Vimentin both promote cell proliferation and that PRH activates the expression of Vimentin when cells are at low density and Vimentin levels are low in the cells. Further, we have shown that Vimentin and PRH both regulate specific cell cycle genes, *CCND2* and *CDKN1B* in the same direction. Vimentin depletion decreases PRH DNA binding to the *CDKN1B* promoter and decreases repression by PRH at this gene. Moreover, Vimentin depletion even increases *CDKN1B* expression and Vimentin depletion when PRH is highly expressed from a viral promoter results in decreased repression of *CDKN1B* by exogenous PRH. We conclude that Vimentin modulates PRH activity at specific genes through direct interaction with PRH and in the case of *CDKN1B*, Vimentin is functioning to co-repress this gene with PRH.

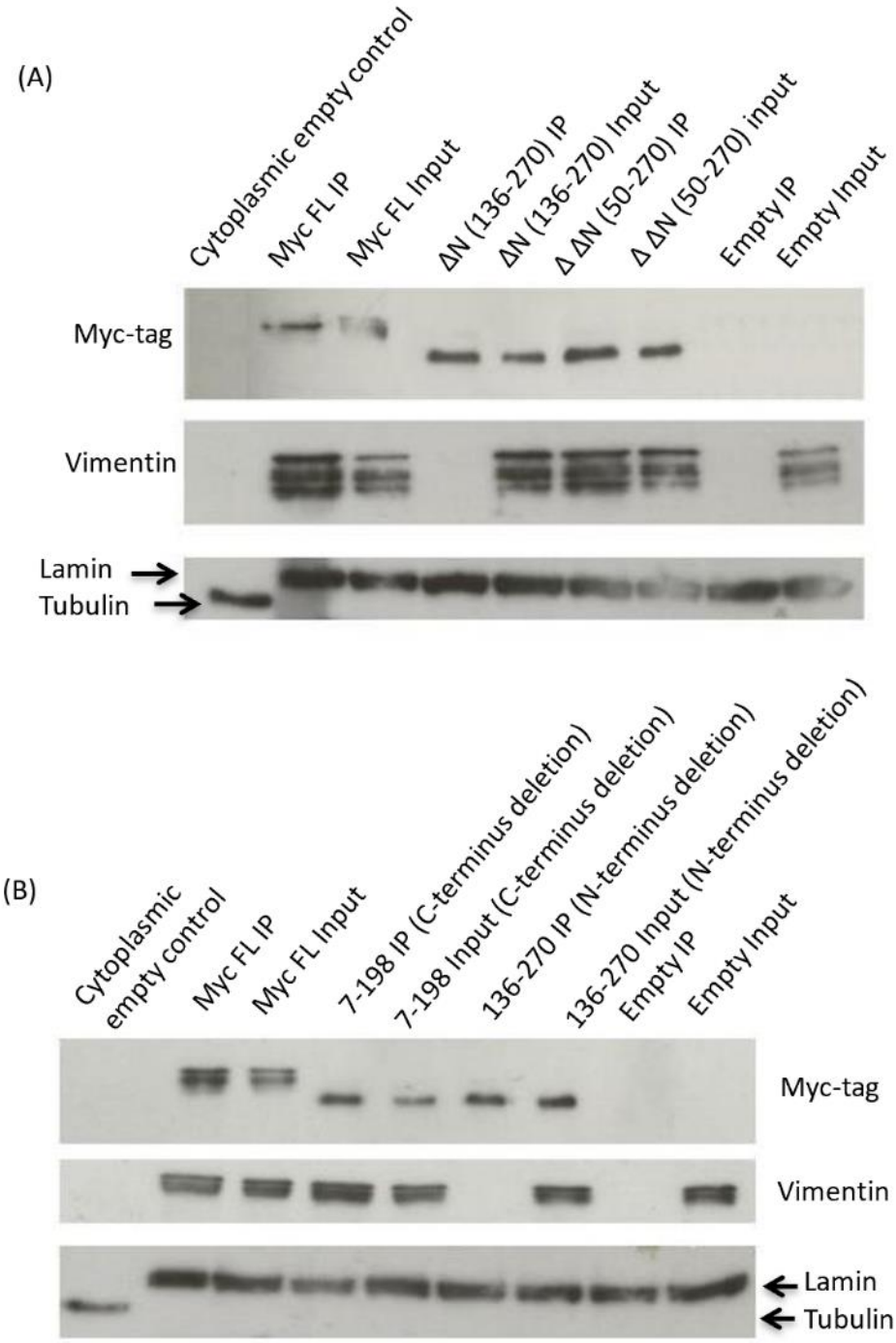
(A)
Cytoplasmic empty control
Myc FL IP
Myc FL Input
ΔN (136-270) IP
ΔN (136-270) Input
Δ ΔN (50-270) IP
Δ ΔN (50-270) input
Empty IP
Empty Input
Myc-tag
Vimentin
Lamin
Tubulin
(B)
Cytoplasmic empty control
Myc FL IP
Myc FL Input
7-198 IP (C-terminus deletion)
7-198 Input (C-terminus deletion)
136-270 IP (N-terminus deletion)
136-270 Input (N-terminus deletion)
Empty IP
Empty Input
Myc-tag
Vimentin
Lamin
Tubulin

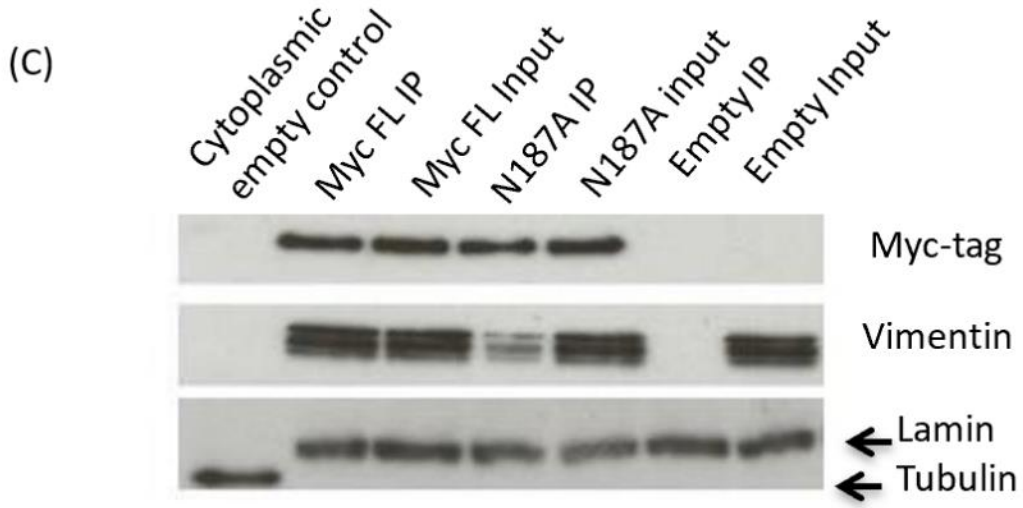

Figure 4.16 PRH interacts with Vimentin at N-terminal domain. (A) Representative Western blots showing co-IP using anti-Myc antibody pull down in CCLP transfected with plasmids encoding full length (FL) Myc-PRH, C-terminus deleted (7-136) or N-terminus deleted PRH mutant (136-270) or control. Anti-Vimentin antibody was used for probing interacting proteins. Anti-Tubulin and Lamin was used to confirm cytoplasmic and nuclear fractions respectively. The numbers in the brackets indicate the size of the PRH protein. The IP was performed twice independently in two different passages of CCLP cells and show similar outcome. (B) Representative Western blots showing co-IP using anti-Myc antibody in CCLP cells transfected with plasmids encoding full length (FL) Myc-PRH, Myc- PRHN187A or control. Anti-Vimentin antibody was used for probing. Anti-Tubulin and Lamin was used to confirm cytoplasmic and nuclear fractions respectively. The IP was performed twice independently in two different passages of CCLP cells and show similar outcome. (C) Representative Western blots showing IP using anti-Myc antibody in CCLP transfected with plasmids encoding full length (FL) Myc-PRH. Anti-Vimentin antibody was used for probing. Anti-Tubulin and Lamin was used to confirm cytoplasmic and nuclear fractions respectively. The IP was performed twice independently in two different passages of CCLP cells and show similar outcome.

To examine whether Vimentin also interacts with PRH protein in AKN-1 cells, co-IP experiments were performed in AKN-1 cells. AKN-1 GFP-PRH-Myc transiently transfected cells were fractionated into nuclear and cytoplasmic fractions 48 hours after transfection. A Myc-tag antibody was used to IP GFP-PRH-Myc exogenous protein and then the blot was probed with Myc to detect the fusion protein or with Vimentin antibody to detect the protein interaction. **Figure 4.17** showed that Myc antibody can only pull down the GFP-PRH-Myc protein in cells expressing the fusion protein. Vimentin can co-IP together with PRH protein in the cytoplasmic and nuclear fractions but Vimentin is not pulled down in the absence of GFP-PRH-Myc. Again, Tubulin and Lamin

are detected in the IP samples even after increasing the number of washes and in the absence of the fusion protein indicating that these proteins are pulled down non-specifically by the beads. Further experiments are needed to determine whether the interaction between PRH and Vimentin in AKN-1 cells is mediated to any degree by laminA/C or tubulin.

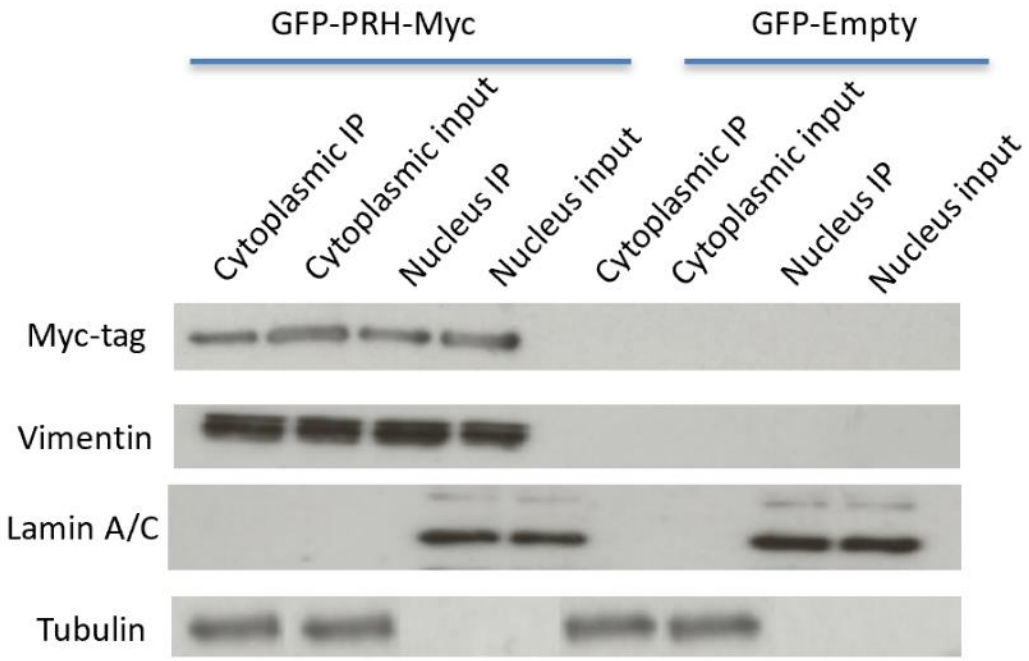

Figure 4.17 PRH interacts with Vimentin in both the cytoplasm and the nucleus in AKN-1 cells. Representative Western blots showing IP using anti-Myc antibody in AKN-1 overexpressing either GFP-PRH-Myc or GFP control. Anti-Vimentin antibody was used for probing. Anti-Tubulin and Lamin was used to confirm cytoplasmic and nuclear fractions respectively. The IP was performed twice independently in two different passages of AKN-1 cells and show a similar outcome.

To confirm Vimentin interacts with PRH and to identify additional nuclear protein partners for PRH in CCLP cells, immunoprecipitation (IP) was performed on CCLP cells transfected with either pMUG1-Myc-PRH or pMUG1 empty vector plasmid. The Myc-tag antibody was used for the IP following fractionation of CCLP cells into nuclear and cytoplasmic fractions as described above and the eluted proteins from the IPs were electrophoresed using SDS-PAGE. Silver-staining was carried out to visualize nuclear and

cytoplasmic proteins. In the nuclear fraction following IP the predominant silver stained band at 37kDa was sent for mass spectrometry (region 3). There were two additional silver stained bands on the SDS PAGE gel at 55 and 65 kDa (regions 1 and 2) in the nuclear fraction not present in the control which were also sent for mass spectrometry. In the cytoplasmic fraction of the Myc-PRH IP there were many silver stained protein bands that were not observed in the empty vector control IP **(Figure 4.18A)**. However, only the strongest silver stained band at 25kDa was excised and sent to the mass spectrometry facility in the University of Birmingham. The mass spectrometry was carried out using the QExactive HF Orbitrap mass spectrometer (ThermoFisher Scientific). The mass spectrometry scan was then searched against Uniprot database using Protein Discovery 2.2 software, Sequest HT algorithm (Thermo Fisher). Variable modifications were deamidation (N and Q), oxidation (M) and phosphorylation (S, T and Y). Data were filtered with a false discovery rate (FDR) of 0.01. Proteins with at least two high confidence peptides were accepted as a real hit. Proteins identified by mass spectrometry in the nuclear IP fraction with at least 2 peptides were as follows: band 1 (65-75kDa)- PRH/HHex and Band 2 (55k-65kDa) -PRH and Vimentin. Band 3 - Heat shock protein CH60 (60 kDa). Band 4 from the cytoplasmic compartment did not show any proteins other than Keratin and albumin which were identified in all bands in the gel due to unavoidable contamination from the environment (**Figure 4.18B and appendice S2)**. Strikingly PRH is present in band 1 and 2 rather than its calculated molecular weight (30kDa) because it is predominantly an SDS resistant dimer in SDS-PAGE. Importantly Vimentin is shown to be an interacting protein in these experiments.

(A)

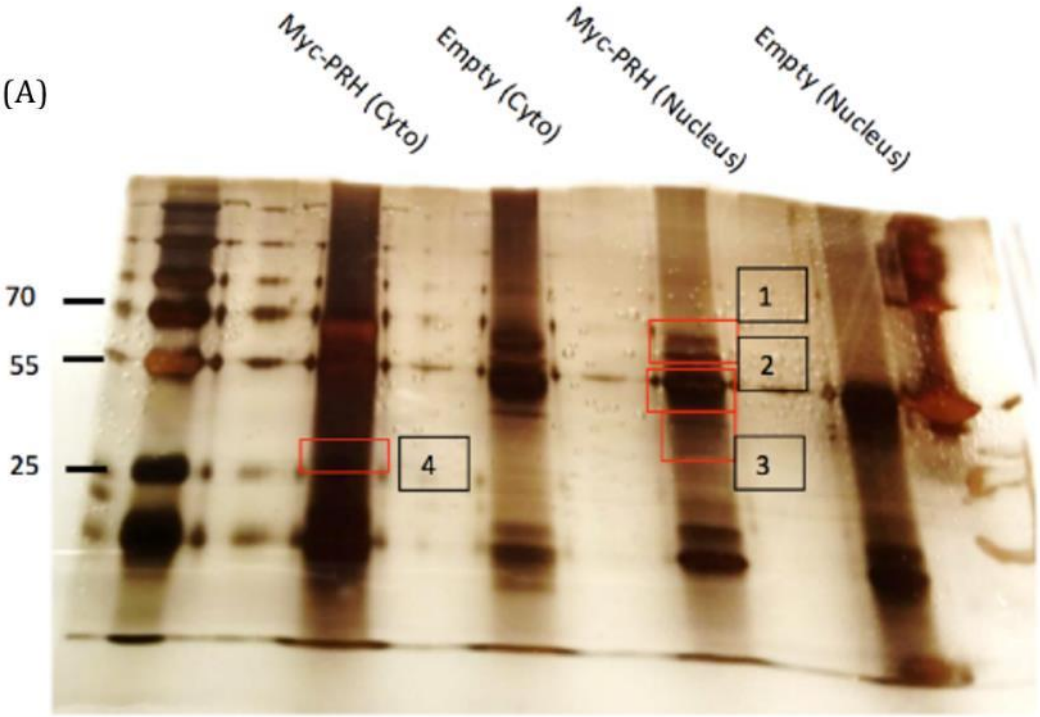
Myc-PRH (Cyto)
Empty (Cyto)
Myc-PRH (Nucleus)
Empty (Nucleus)
70
55
25
1
2
3
4

(B) Band 2

Accession	Description	Score	Coverage	# Proteins	# Unique Peptides	# Peptides	# PSMs	# AAs	MW [kDa]	calc. pI
P04264	Keratin, type II cytoskeletal 1 OS=Homo sapiens GN=KRT1 PE=1 SV=6 - [K2C1_HUMAN]	29.32	19.10	2	7	7	8	644	66.0	8.12
P35527	Keratin, type I cytoskeletal 9 OS=Homo sapiens GN=KRT9 PE=1 SV=3 - [K1C9_HUMAN]	7.83	6.26	1	2	2	2	623	62.0	5.24
P35908	Keratin, type II cytoskeletal 2 epidermal OS=Homo sapiens GN=KRT2 PE=1 SV=2 - [K22E_HUMAN]	6.53	3.76	3	2	2	2	639	65.4	8.00
P08670	Vimentin OS=Homo sapiens GN=VIM PE=1 SV=4 - [VIME_HUMAN]	6.51	6.87	2	2	2	2	466	53.6	5.12
P13645	Keratin, type I cytoskeletal 10 OS=Homo sapiens GN=KRT10 PE=1 SV=6 - [K1C10_HUMAN]	6.41	3.25	1	2	2	2	584	58.8	5.21
P02768	Serum albumin OS=Homo sapiens GN=ALB PE=1 SV=2 - [ALBU_HUMAN]	4.67	2.46	1	1	1	1	609	69.3	6.28
P08779	Keratin, type I cytoskeletal 16 OS=Homo sapiens GN=KRT16 PE=1 SV=4 - [K1C16_HUMAN]	3.13	4.02	1	1	1	1	473	51.2	5.05
B2RXH8	Heterogeneous nuclear ribonucleoprotein C-like 2 OS=Homo sapiens GN=HNRNPCL2 PE=1 SV=1 - [HNRC2_HUMAN]	3.04	3.41	4	1	1	1	293	32.1	5.44
Q03014	Hematopoietically-expressed homeobox protein HHEX OS=Homo sapiens GN=HHEX PE=1 SV=1 - [HHEX_HUMAN]	3.01	4.07	1	1	1	1	270	30.0	7.24

Figure 4.18 Mass spectrometry on Myc-PRH IP of CCLP. (A) Silver staining of cytoplasmic (Cyto) and nuclear fraction of IP using anti-Myc-tag antibody in CCLP overexpressing Myc-PRH. (B) Mass spectrometry result on the corresponding gel band #2.

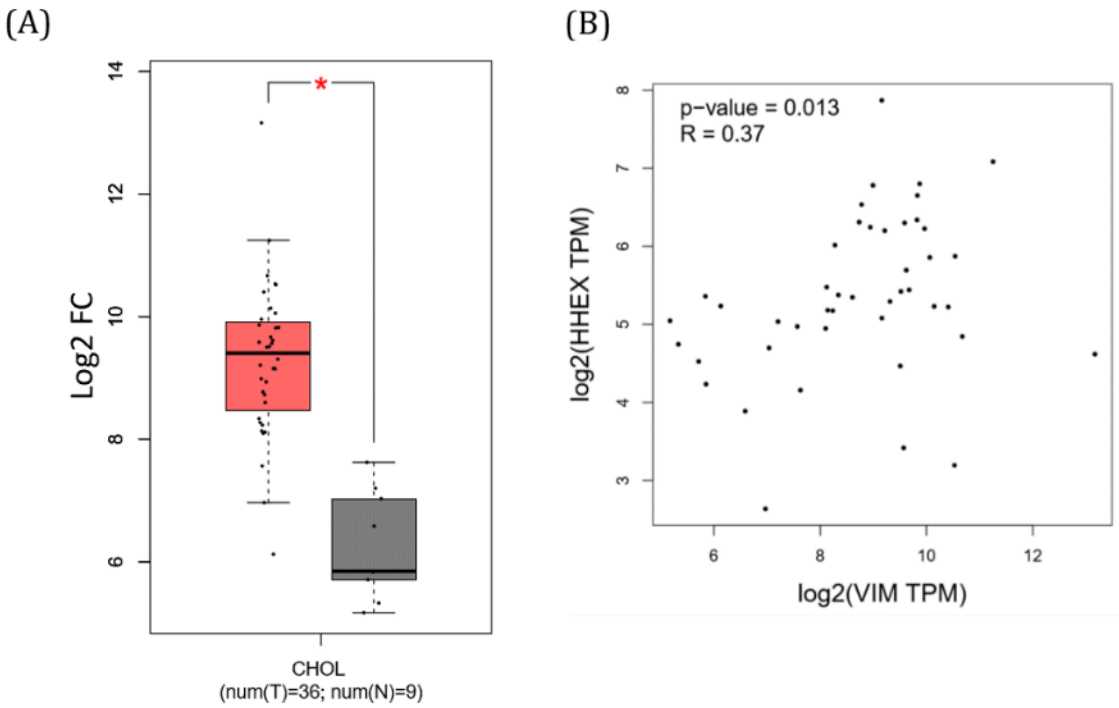

Figure 4.19 The *PRH/HHEX* RNA expression correlate with VIM in the GEPIA dataset. (A) *VIM* RNA expression is upregulated in the GEPIA CCA cohort. Statistic analysis: Unparied two tailed T-test. (B) The expression of *VIM* in the CCA cohort correlates with *PRH/HHEX* expression.

Given the interaction between PRH and Vimentin and also the regulation of Vimentin by PRH in CCLP cells we wondered if there is a correlation between *PRH/HHEX* and *VIM* gene expression in CCA samples. GEPIA data for *VIM* expression in CCA patients show that *VIM* is highly upregulated in CCA samples compared to *VIM* expression in normal tissue samples. Moreover, the expression of *VIM* correlates with PRH expression in the TCGA dataset **(Figure 4.19)**.

In conclusion PRH activates *VIM* gene expression when Vimentin levels are low and cell density is low. Moreover, Vimentin protein also interacts with PRH N-terminus in CCLP cells and the interaction is involved in the regulation of specific cell cycle genes which contribute to regulation of cell proliferation by PRH. Finally, the two proteins are highly co-expressed in CCA patients.

CHAPTER 5

Investigating the role of PRH in AKN-1 and primary BECs

5. Investigating the role of PRH in AKN-1 and primary BECs

5.1 PRH overexpression drives proliferation in AKN-1 and primary BECs

Data from CCLP and CCSW suggest that overexpression of PRH protein in CCA cells drives proliferation through altered expression of multiple genes associated with cell proliferation including increased *NOTCH3* and *CCND2* gene expression and repression of *CDKN1B* and *CDKN2B* genes. However, it is not known whether PRH will also increase the proliferation of immortalized AKN-1 cholangiocytes or primary untransformed BECs and whether any changes of proliferation will be mediated through modulation of the same pathways or genes.

AKN-1 cells retain expression of biliary markers and were spontaneously isolated (Nussler et al., 1999). Initial experiments with adenoviral PRH showed that AKN-1 cells are not infected even at high multiplicity of infection. AKN-1 cells were therefore transfected with plasmids expressing PRH cDNA and selectable resistance markers to achieve PRH expression.

In order to determine which plasmids express PRH at high levels in AKN-1 cells, several plasmids expressing PRH cDNA in frame with sequences encoding antibody epitopes such as Myc or GFP were transiently transfected into cells using PEI transfection **(See M&M section 2.1.6)**. RNA was then isolated from cells transiently transfected with pEGFP-PRH (GFP-PRH), pMUG1-PRH (Myc-PRH), pEGFP-PRH-Myc (GFP-PRH-Myc) or corresponding empty vector controls. pEGFP-PRH is a plasmid expressing the PRH cDNA in frame with the GFP cDNA at the N-terminus of PRH cDNA. The plasmid contains an in-frame stop codon for PRH and also contains the PRH/HHEX 3'UTR. The pEGFP-PRH-Myc is derived from the pEGFP-PRH but the in-frame stop codon is removed and replaced

with the c-Myc epitope in frame with the C-terminus of the PRH cDNA followed by a stop codon. The 3' UTR region of the PRH cDNA was removed during the construction of this plasmid by Dr P S. Jayaraman (See **M&M section 2.1.12** for map and cloning details). pMUG1-Myc-PRH contains the Myc epitope fused in frame with the N-terminus of PRH and the sequence encoding this epitope is in frame with the PRH cDNA from amino acids 7-270 of PRH and retains the PRH stop codon. This plasmid also contains the 3'UTR for the *PRH/HHEX* cDNA. Quantitative PCR with *PRH/HHEX* primers shows that only cells transfected with GFP-PRH-Myc show mRNA expression of PRH after selection of the transfected cells with two weeks post transfection **(Figure 5.1A)**.

Following transient transfection with pEGFP-PRH Myc, cells were selected with G418 for 2 weeks to obtain a stable GFP-PRH-Myc overexpressing AKN-1 cell line. A GFP control cell line was created in parallel using pEGFP-empty plasmid and also selected with G418 for the same period of time. Western blotting with a GFP antibody was carried out to show that PRH is overexpressed following stable transfection and selection for the GFP-PRH-Myc plasmid **(Figure 5.1B)**. Multiple transfections with the GFP-PRH and GFP-PRH-Myc plasmids resulted in only the latter producing green colonies following selection. As the 3' Myc-tag in GFP-PRH Myc replaces the *PRH/HHEX* 3'UTR in this construct compared to the GFP-PRH construct which retains the 3' UTR, we infer that the 3' UTR of the PRH cDNA contains sequences that inhibits the expression of the PRH gene in AKN-1 cells.

The growth of the two stable cell lines AKN-1 GFP control and AKN-1 GFP-PRH-Myc was assessed by cell counting over 9 days using trypan blue staining to assess cell viability. **Figure 5.1C** shows the cumulative growth curves calculated from three different

passages of AKN-1 cells expressing GFP-PRH-Myc or a control cell line expressing GFP. The cumulative cell number of AKN-1 GFP-PRH-Myc is much higher than that of AKN-1 GFP control cells over 9 days. Moreover, **Figure 5.1D** shows the doubling time of the GFP-PRH-Myc cell line is considerably shorter than that of the GFP control AKN-1 cell line. Edu incorporation assays show that GFP-PRH-Myc overexpressing AKN-1 cells are more proliferative than the GFP control AKN-1 cells **(Figure 5.1E)**. Together, these results show that stable GFP-PRH-Myc overexpression at modest levels of expression promotes the proliferation of AKN-1 cells just as transient high levels of PRH expression does in CCLP and CCSW cells.

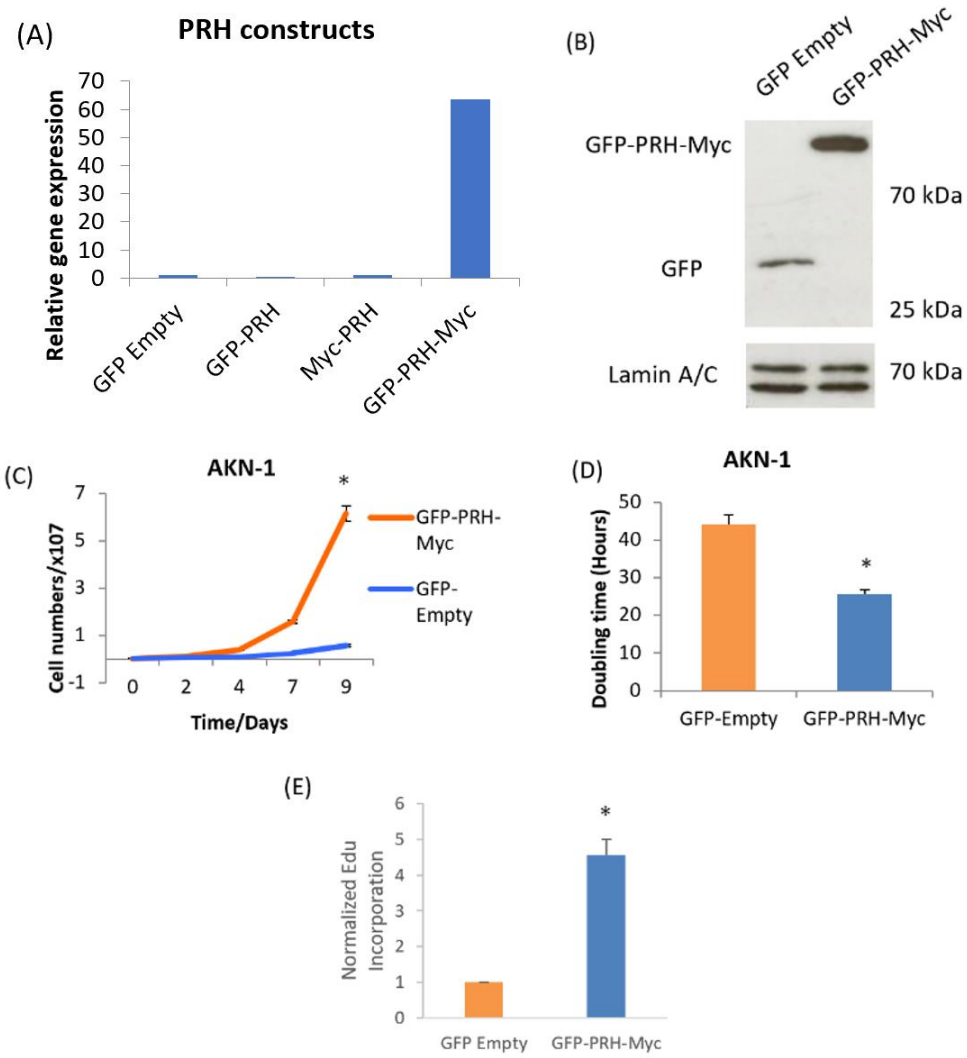

Figure 5.1 PRH OE increases cumulative cell number and change the cell morphology in AKN-1 cells. (A) qPCR for *PRH/HHEX* expression in AKN-1 cells transiently transfected with various plasmids encoding PRH cDNA in frame with cDNA-tags encoding different epitopes or GFP control plasmid normalized to β-actin. RNA obtained 48 hours post transfection. (n=1). (B) Representative western blots using an anti-mouse GFP antibody detecting exogenous GFP-PRH-Myc or GFP expression in the stable cell line. Lamin was used as loading control. 10 µg of protein was loaded into each lane. (n=3). Protein lysate produced 2 weeks after transfection. (C) AKN-1 cells were transfected with the GFP-PRH-Myc plasmid. Cells stably transfected were counted two weeks after transfection. Cells were trypsinized and counted in triplicate for each experimental repeat every 48 hours until Day 9. Error bars show the SD among the three experimental repeats. Statistical test: Two-tailed unpaired T-test (n=3; *p<0.05) (D) Doubling time of GFP-PRH-Myc and GFP control AKN-1 cells. Statistical test: Two-tailed unpaired T-test (n=3; *p<0.05) (E) Proliferative activity of GFP-PRH-Myc and GFP control AKN-1. Cells were incubated in Edu for 2 hours and click reaction was detected by an HRP-conjugated antibody and OPD was added and absorbance was measured at 450 nm. The signal was normalized to cell numbers. Statistical test: Two-tailed unpaired T-test (n=3; *p<0.05). The error bars show the SD of three experimental repeats.

Importantly, stable AKN-1 GFP-PRH-Myc cells show a morphological change compared to AKN-1 GFP control cells. Elevated PRH expression results in a change in the epithelial

morphology of AKN-1 cells to a more mesenchymal morphology **(Figure 5.2A)**. A significant decrease in E-cadherin expression was also observed in the AKN-1 GFP-PRH-Myc cells compared to AKN-1 GFP control cells and this was companied by increased Vimentin expression **(Figure 5.2B)**. The changes in the cell surface and cytoskeletal proteins are characteristic of EMT. PRH also increases Notch3 protein expression in the AKN-1 GFP-PRH-Myc cells.

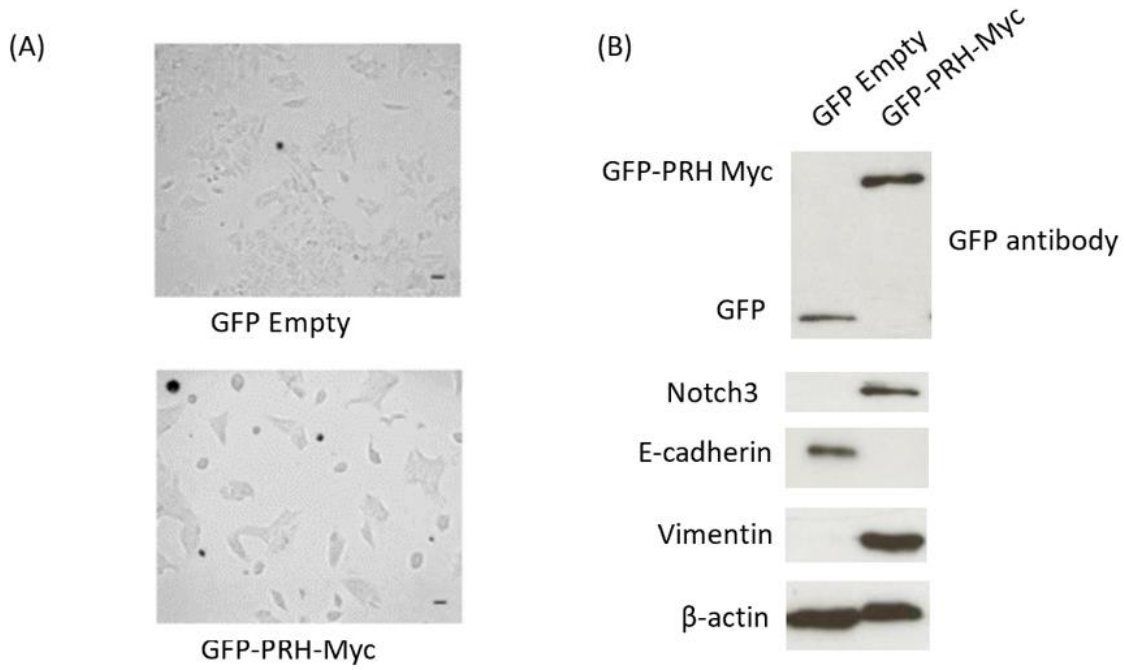

Figure 5.2 PRH OE leads to EMT and increases Notch expression. (A) Morphology of stably transfected PRH OE and control AKN-1 cells at same cell density. Image taken at 10x by light microscope. Scale bars represent 10 µm. (B) Representative Western blots for Notch3, E-cadherin and Vimentin expression in GFP-PRH-Myc and GFP control AKN-1 cells. 10 µg of protein was loaded into each lane. β-actin was used as a loading control. (n=3)

5.2 PRH overexpression increases migration, invasion and colony formation in AKN-1

Since PRH was shown to increase migration and invasion in CCLP and CCSW, similar effects were hypothesized to occur in the stable AKN-1 GFP-PRH-Myc cells. To assess

the effect of PRH expression in these cells, transwell migration assays and invasion assays were performed with AKN-1 GFP-PRH-Myc or GFP control cells. **Figure 5.3A** shows that GFP-PRH-Myc AKN-1 cells are more migratory and also more invasive compared to GFP control cells **(Figure 5.3B)**.

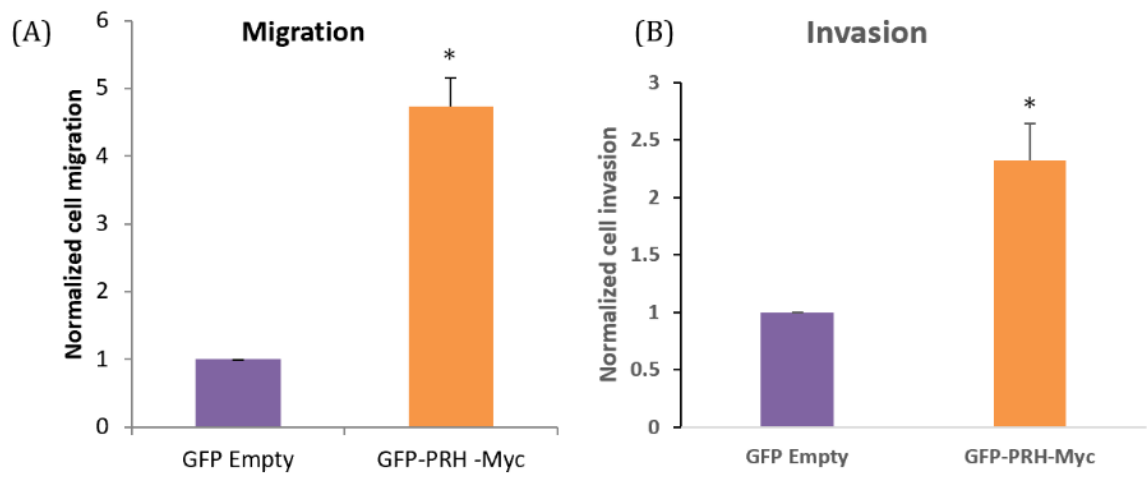

Figure 5.3 Stable PRH expression increases AKN-1 cell migration and invasion. (A) Cell migration of AKN1 GFP-PRH-Myc or GFP control through a transwell filter in a 2-t10% serum gradient for 72 hours. 1 mM hydroxyurea was added 24 hours before the migration assay and throughout the assay to inhibit proliferation. Statistical test: Two-tailed unpaired T-test (n=3; *p<0.05) (B) Cell invasion of AKN1 GFP-PRH-Myc or GFP control through a transwell filter coated with 10% Matrigel in a 2-10% serum gradient for 24 hours. 1 mM hydroxyurea was added 24 hours before the migration assay and throughout the assay to inhibit proliferation. Statistical test: Two-tailed unpaired T-test (n=3; *p<0.05). The error bars show the SD of three experimental repeats.

Colony formation assays were also performed to investigate whether PRH overexpression can increase the tumour forming properties of AKN-1 cells. Colony formation assays show that AKN-1 GFP-PRH-Myc cells form a greater number of colonies than the AKN-1 GFP control cells **(Figure 5.4Bi)**. Moreover, the size of the colonies formed by the GFP-PRH-Myc cells is also bigger than the control cells **(Figure 5.4Bii)**. A histogram was plotted to show the distribution of the number of colonies of different sizes for both AKN-1 GFP-PRH-Myc and GFP control AKN-1 cells **(Figure 5.4C)**. Thus, modestly but stably elevating PRH in spontaneously immortalized AKN-1 cells leads to increased proliferation, migration, invasion, induction of EMT and an increase in anoikis

resistance. These phenotypical changes are specific to transformed biliary epithelium as PRH acts as a tumour suppressor for other solid cancers.

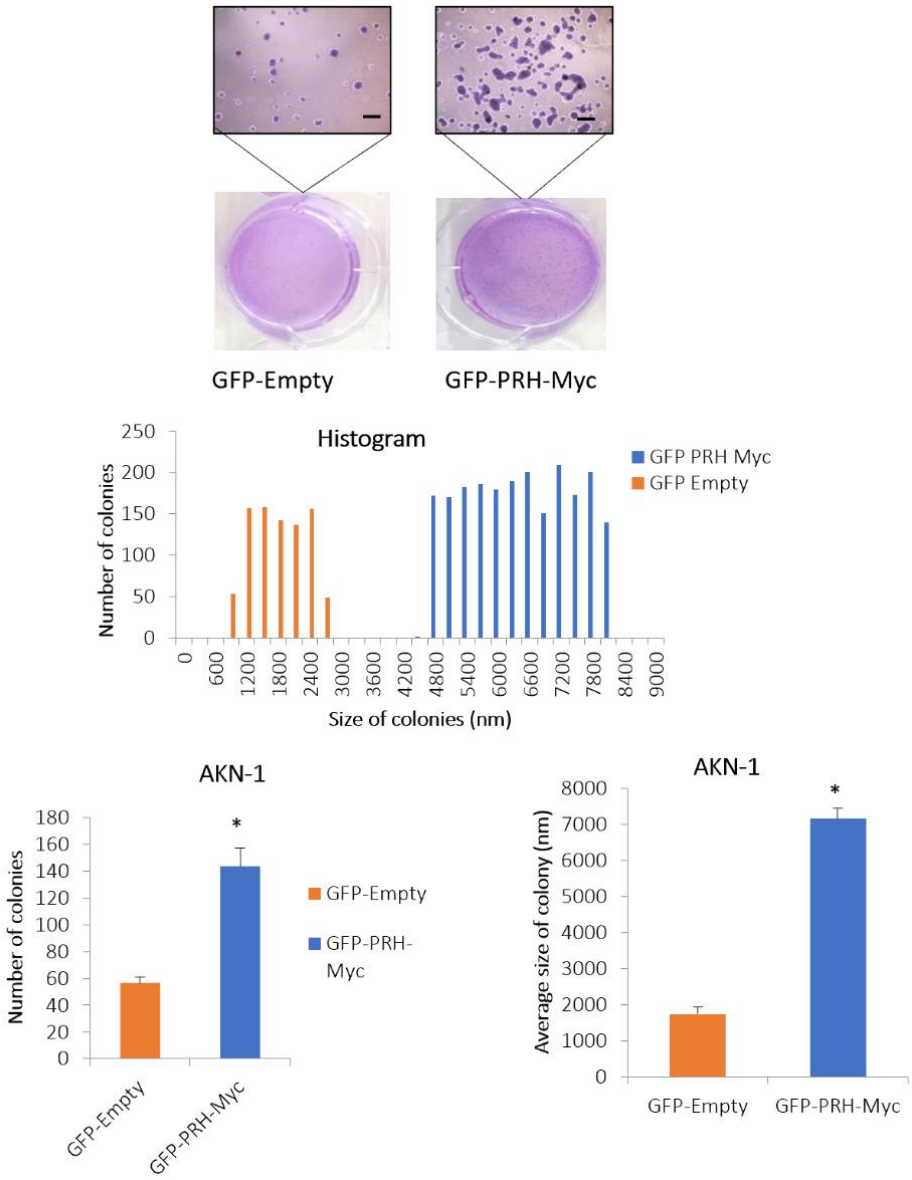

Figure 5.4 Stable PRH expression in AKN-1 promotes colony formation in soft agar. (A) 2 x 10^4 cells were plated on low melting agar (3%) in triplicate in a 6 well plate and incubated for 10 days. Cells were then stained with crystal violet blue and images were taken. Image of colony formed by AKN-1 GFP control cells or GFP- PRH-Myc cells under light microscope at magnification 10x. The scale bar represents 30 µm in length. (B) Image J was used to analyze the images to determine the number of colonies and size of each colony in each image. Histogram was plotted to show the number of colonies and size of colonies formed by GFP-PRH-Myc and GFP control cells. The histogram shows pooled data from 3 biological repeats of the colony formation assay with 5 images taken for each cell line. (Ci) Average size of the colonies formed by GFP-PRH-Myc and GFP control AKN-1 cells. Error bars show the SD among the three experimental repeats. (ii) Average number of the colonies formed by GFP-PRH-Myc and GFP control AKN-1 cells. Statistical test: Two-tailed unpaired T-test (n=3; *, $p<0.01$).

5.3 Identify differential gene expression in AKN-1 when PRH is overexpressed by RNA sequencing

To investigate the gene expression changes that underlie the observed changes in phenotype in AKN-1 GFP-PRH-Myc cells, RNA-seq experiments were conducted with AKN-1 GFP-PRH-Myc and AKN-1 GFP control. Two passages from the AKN-1 GFP-PRH-Myc and AKN-1 GFP control cells were used for RNA extraction and RNA-seq as described previously. Following bioinformatic analysis of the RNAseq data, massive changes in gene expression were identified; there are 5673 genes up-regulated and 5221 genes down-regulated. This represents more than 50% of the 20,000 genes in the genome. To validate the RNA-seq data from AKN-1 GFP-PRH-Myc, qPCR was conducted on the PRH target genes that we have previously investigated in CCLP and CCSW cells. A comparison of RNA-seq and qPCR data for selected genes is shown in **Figure 5.5A**. There is a substantial upregulation of *NOTCH3* gene and repression of *CDH1* (E-cadherin) gene expression in the GFP-PRH-Myc overexpressing AKN-1 cells as shown in the RNA-seq and qPCR data (**Figure 5.5A&5.5B)**. Moreover, the gene expression of mesenchymal marker genes including *VIM* (Vimentin) shows up-regulation by 4-fold. Furthermore, the expression of genes encoding other EMT transcription factors such as *ZEB1* and *TWIST1* are also significantly upregulated. These results are consistent with qPCR data and protein expression data for Notch3, E-cadherin and Vimentin. Although the cell cycle inhibitors *CDKN1B* and *CDKN2B* were not assessed by qPCR they are downregulated by 3-fold in the RNA-seq data **(Figure 5.5A)**. Surprisingly, there is no increase in the *CCND2* gene in the RNA-seq data and as assessed by qPCR and furthermore there is no increase

in Cyclin D2 protein expression in Western blotting in AKN-1 cells. Whereas in both CCLP and CCSW cells, *CCND2* expression is altered by PRH.

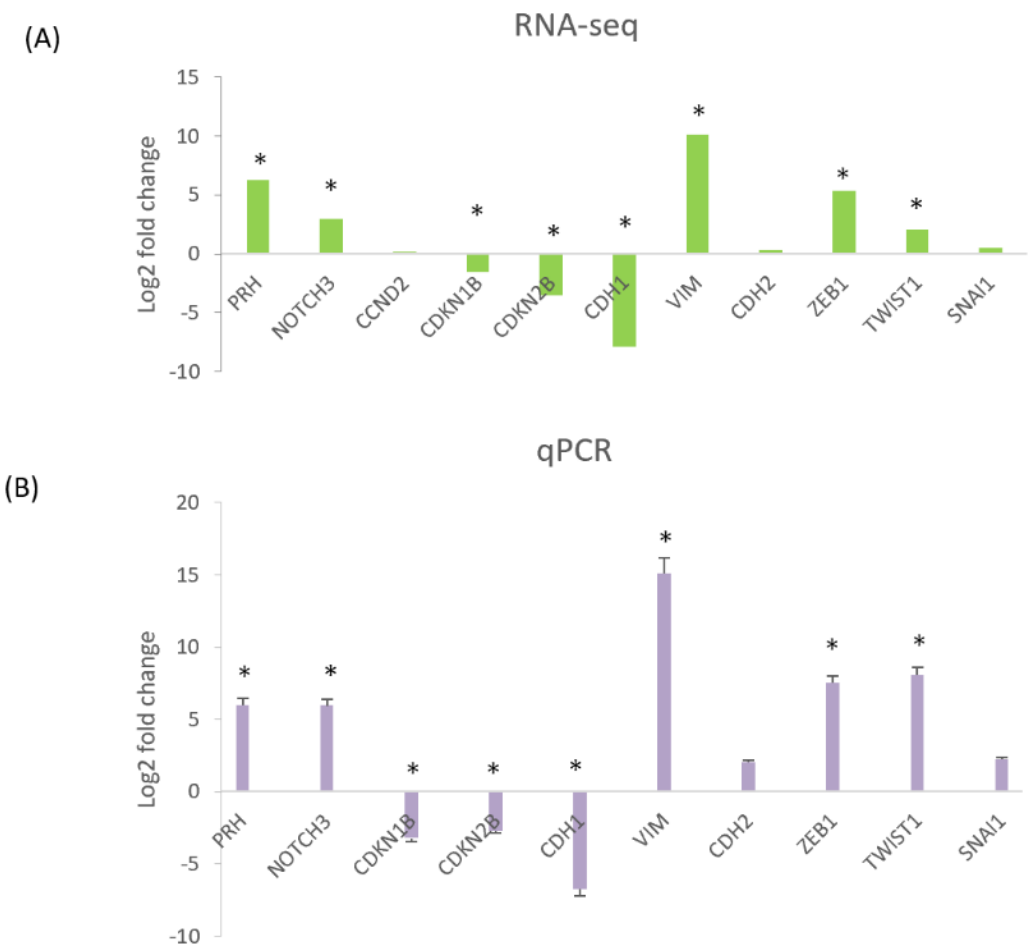

Figure 5.5 PRH OE upregulates Notch3 and modulates EMT genes expression in AKN-1 cells. (A) RNA-seq data of GFP-PRH-Myc AKN-1 cells and GFP control. The experiment was repeated twice. (n=2; *q<0.05) (B) qPCR showing the mRNA expression of *NOTCH3* and EMT genes in GFP-PRH-Myc AKN-1 cells and GFP control. The mRNA expression is normalized to β-actin. Statistical test: Two-tailed unpaired T-test (n=3; *p<0.05). The error bars show the SD of three experimental repeats.

Since RNA-seq data was shown to be verified by qPCR analysis and Western blotting data for several genes the data was further analyzed using GSEA hallmark geneset analysis **Figure 5.6A.** The EMT pathway is most strongly enriched in AKN-1 GFP-PRH -Myc cells. This is consistent with the morphological and phenotypical changes observed in the AKN-1 GFP-PRH -Myc. Ranked Enrichment plots were plotted using the GSEA software by inputting the DEG list and corresponding $\log_2$ fold change **(Figure 5.6B)**. The green

curves refer to the enrichment score curves. The plots show that the DEGs in EMT pathway of AKN-1 are mostly upregulated. A heatmap was generated for the full list of DEGs in the EMT pathway in AKN-1 cells **(Figure S4)** and Volcano plots were also generated for the genes in the GSEA EMT pathway using the DEG gene lists and the $\log_2$ fold change and the q-values (False Discovery Rate) in the GSEA analysis. The volcano plot shows some of the key genes that are differentially regulated by PRH related to EMT pathway including *VIM* **(Figure 5.6C)**. Strikingly in these cells the Notch pathway is also enriched. The GSEA Enrichment plot for the Notch pathway shows that the DEG are mostly upregulated by PRH **(Figure 5.6D)**. A heatmap was generated for the full list of DEGs in the Notch pathway in AKN-1 cells **(Figure S6).** As expected, *NOTCH3* is one of the DEGs in the AKN-1 gene set (**Figure 5.6E**). *PRKCA* encoding the protein kinase C alpha and *CCND1* are both a highly differentially expressed genes and in the hallmark set of DEGs in the Notch pathway as they are involved in the Notch signaling pathway. Surprisingly, C*CND2* is not altered by PRH in AKN-1 cells although Notch3 is elevated.

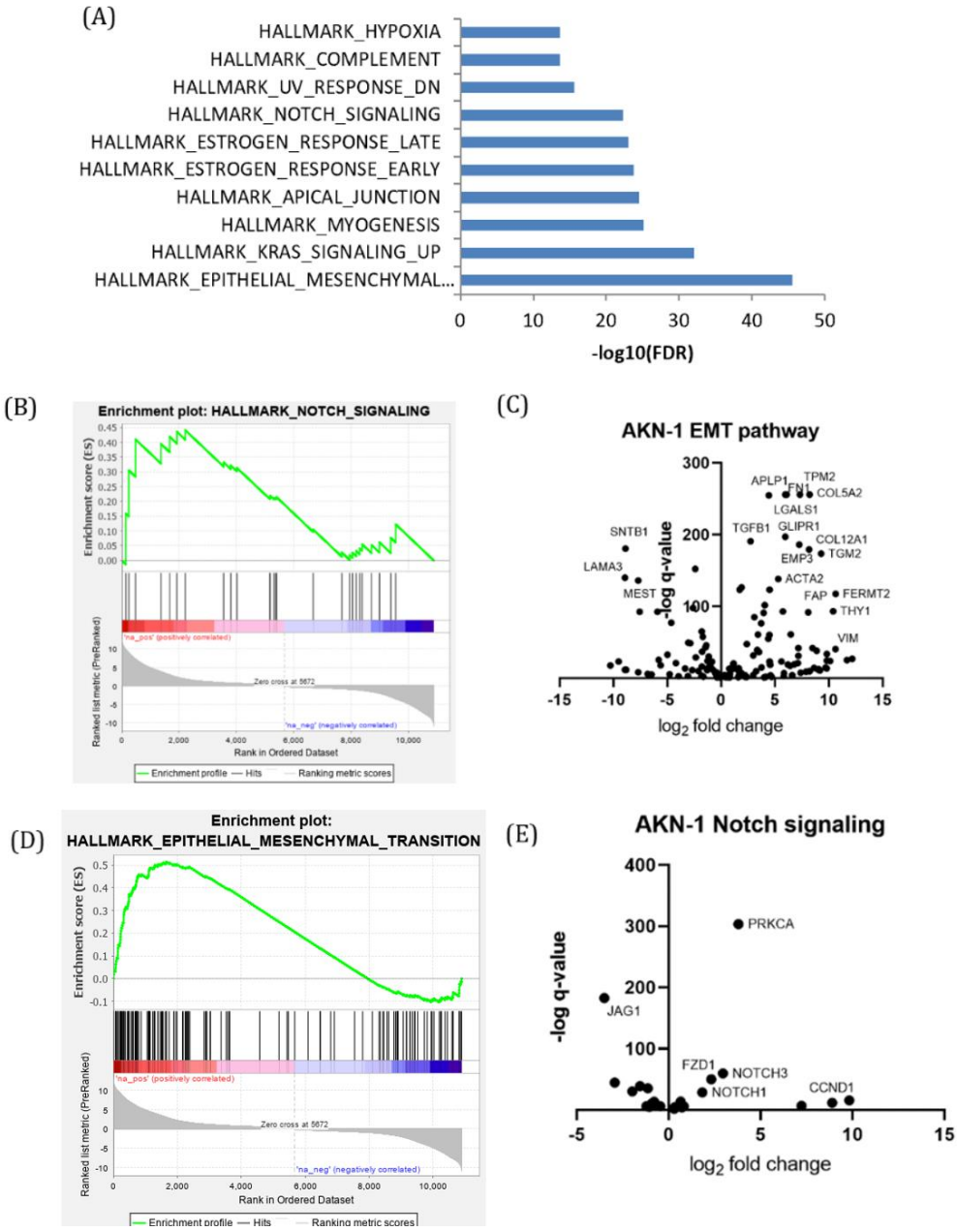

Figure 5.6 GSEA of RNA-seq data of PRH OE AKN-1. (A) Gene set enrichment analysis using Hallmark gene sets for PRH OE DEGs in AKN-1. (B) Enrichment plot for EMT pathway for RNA-seq data of AKN-1 cells. (C) Volcano plot of the DEG genes in EMT pathway of RNA-seq data of PRH overexpressing AKN-1 cells. (D) Enrichment plot for Notch pathway for RNA-seq data of AKN-1 cells. (E) Volcano plot of the DEGs in NOTCH pathway of RNA-seq data of PRH overexpressing AKN-1 cells.

The differentially expressed gene lists identified in the CCLP cells overexpressing PRH compared to controls and AKN-1 cells stably overexpressing GFP-PRH-Myc compared to GFP controls were examined to determine whether there are a set of genes that are

regulated by PRH in both cell types. **Figure 5.7** shows that 432 genes (8.6 %) are upregulated in both cell types whereas 440 genes (8.4 %) are downregulated by PRH in both cell lines.

A comparison of the GSEA analysis for the RNA-seq data from CCLP AdPRH and AKN-1 GFP-PRH-Myc cells revealed that the KRAS signaling pathway, apical junction and the estrogen response pathways are enriched in both cell lines. The EMT pathway however is only enriched in the AKN1 cell line. Presumably this is because CCLP cells are mesenchymal and cannot undergo EMT. CCLP1 cells however do become more invasive with PRH overexpression and many individual genes associated with invasion are differentially regulated. GSEA shows enrichment of the EMT pathway is when PRH is depleted in CCLP cells in the PRH KD RNA seq data set (**see Figure 3.13**) because the PRH KD cells undergo MET. PRH induces massive changes in gene expression in AKN-1 but only around 800 genes changes in CCLP by exogenous PRH. This can be explained by the fact that PRH is already highly expressed in CCLP cells whereas AKN-1 cells are not transformed CCA cell line that does not express PRH. Therefore, more gene expression changes are expected in AKN-1 cells than in CCLP cells.

Regarding the genes related to proliferation, *NOTCH3* is upregulated by PRH in AKN-1 cells just as it is in CCLP and CCSW cells. Cell cycle inhibitors *CDKN1B* and *CDKN2B* are inhibited by PRH in the AKN-1 cells and they are also decreased in the CCLP cells by exogenous PRH. Surprisingly, although *CCND2* is upregulated by AdPRH in the CCLP and CCSW cells, it is not altered in the AKN-1 cells. Instead, *CCND1* is upregulated by PRH in AKN-1 cells. Therefore, *CCND1* may be more important in driving cell cycle progression by PRH in the immortalized cells rather than *CCND2*. In CCLP cells, *CCND1* is already

highly expressed according to the RNA-seq normalized count data. We speculate that it could not be increased further by exogenous PRH.

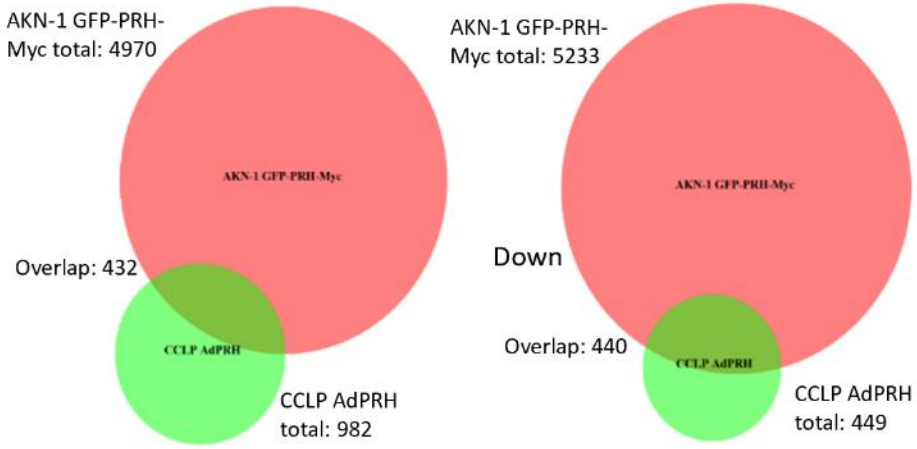

Figure 5.7 Overlap of genes regulated by PRH in CCA and cholangiocytes. Venn diagrams showing the set of differentially expressed genes that are either upregulated (left) or down regulated (right) in AKN-1-GFP-PRH-Myc stable cell line (red) and CCLP AdPRH cells (green). The number of genes in the overlap between the sets is shown.

5.4 PRH overexpression increases migration, invasion and colony formation in primary BECs

To determine if overexpression of PRH has the same effect in untransformed primary biliary epithelial cells (BECs) as the cholangiocyte cell line, BECs were isolated from donor livers that were rejected for liver transplantation (Details in **M&M section 2.1.5**). BECs were isolated from three patients diagnosed with alcoholic liver disease (ALD) using an Epcam antibody column based positive selection procedure (Verhulst et al., 2019). To prove that the isolated BECs retain biliary markers after isolation and passaging, two different passages from each BECs isolation were checked for expression of genes encoding bile duct marker proteins such as Keratin 7 (*KRT7*) and for the absence of genes encoding hepatic marker protein such as Albumin using either qPCR or by

Western blotting. **Figure 5.8Ai** shows that all isolated BECs samples have a high level of Keratin 7 protein expression and BECs donor 1 and donor 2 also express high levels of Keratin 7. Additionally, the gene encoding the hepatic marker albumin is not expressed in BECs at first isolation, demonstrating that the cells are not hepatocytes **(Figure 5.8Bi&Bii)**. Having verified that primary BECs had been successfully isolated from the liver donors, the first BEC sample (donor 1) was infected with AdPRH or AdEmpty at MOI 50. Western blotting was carried out to confirm PRH is overexpressed in the primary BECs in each experiment. The AdPRH and AdEmpty infection was repeated three times independently for each BEC donor and for each infection the cells were used for Edu experiments and the protein lysates produced were Western blotted to detect PRH expression. **(Figure 5.9A)**. Primary BECs (donor 1) that overexpress PRH are more proliferative compared to the controls **(Figure 5.9B)**.

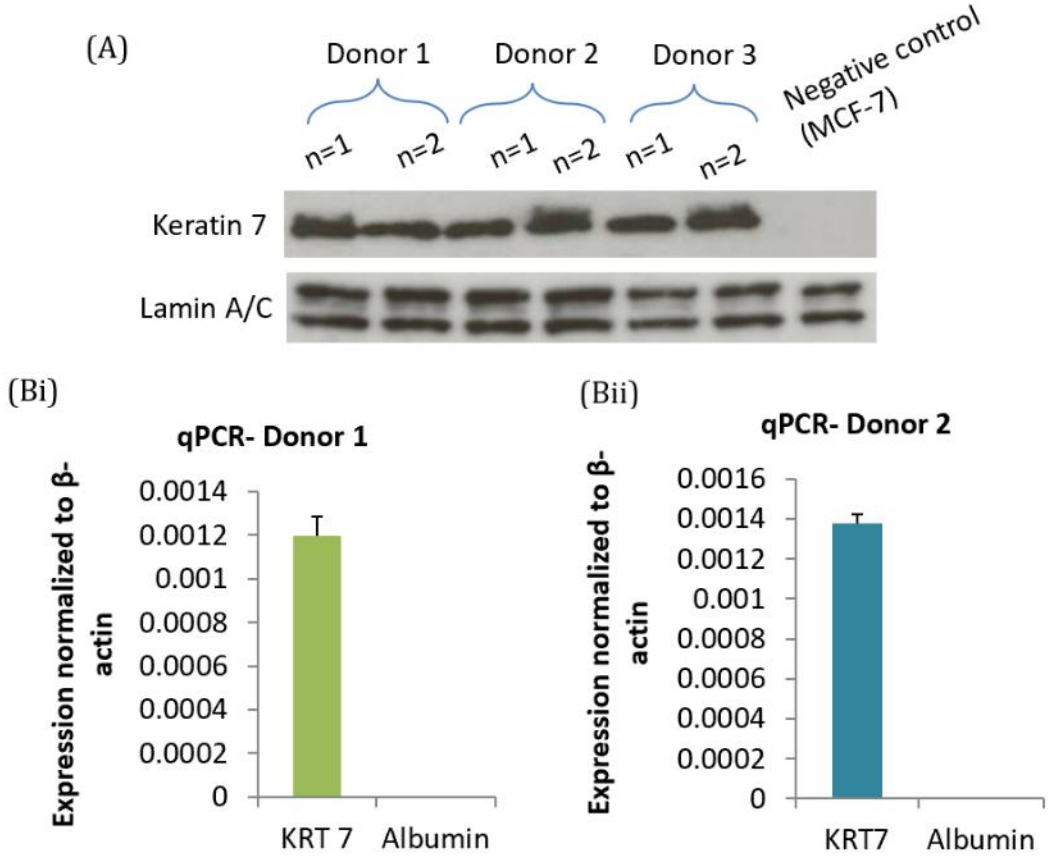

Figure 5.8 Characterization of primary BECs. (A) Western blots showing the expression of Keratin 7 using an anti-Keratin 7 antibody in three different BEC isolates donor 1, 2 and 3. Two passages from each isolate is shown on the blot. 10 µg of protein was loaded into each lane. Lamin A/C was used as loading control and cell lysate from MCF-7 breast cancer cell line was used as a negative control for Keratin 7 expression. (B) qPCR for *KRT7* and *ALB* expression in primary BECs isolated from (i) Donor 1 and (ii) Donor 2 The qPCR was performed for each donor three times from RNA produced from three different passages of each BEC isolate. The error bars show the SD of three experimental repeats.

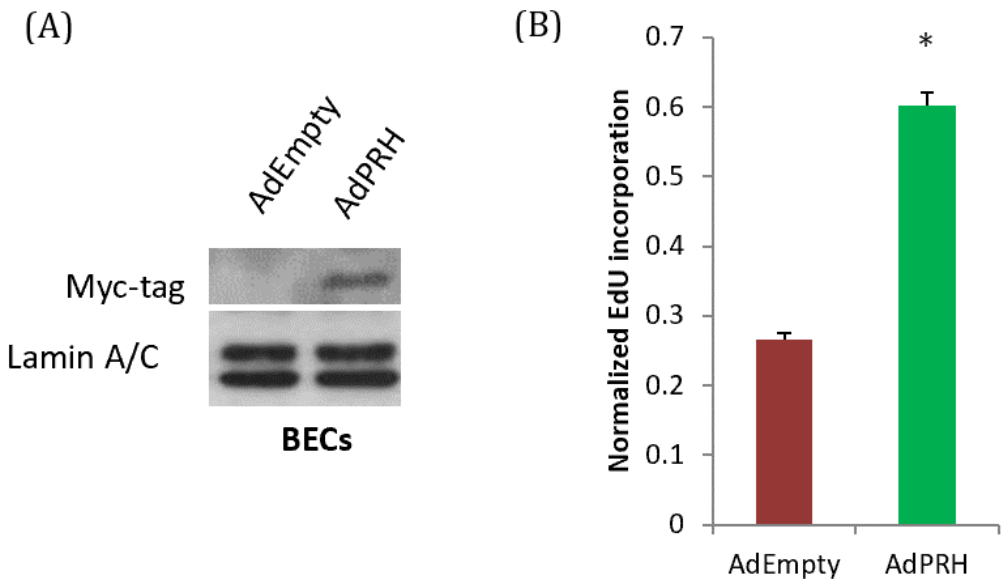

Figure 5.9 PRH OE increases proliferation in BECs. (A) Representative Western blotting using an anti-Myc-tag antibody showing PRH overexpression in primary BECs following infection with AdPRH but not AdEmpty, Lamin A/C was used as a loading control for the blot. 10 µg of protein was loaded into each lane. (B) Proliferative activity of AdPRH infected and AdEmpty infected control primary BECs. Cells were incubated in Edu for 4 hours and click reaction was detected by an HRP-conjugated antibody and OPD was added and absorbance was measured at 450 nm. Signal was normalized to cell numbers. Error bars show the SD among the three experimental repeats. Statistical test: Two-tailed unpaired T-test (n=3; *p<0.05).

5.5 PRH overexpression increases migration, invasion and colony formation in primary BECs

Since PRH was shown to increase migration and invasion in AKN-1, similar effects were hypothesized to occur in the BECs. To assess the effect of exogenous PRH expression in these cells, transwell migration assays and invasion assays were performed with AdPRH primary BECs donor 1 and AdEmpty control cells. BECs infected with AdPRH are also more migratory and invasive than AdEmpty infected control cells **(Figure 5.10)**. This is consistent with increased invasion and migration observed in AKN-1 cells when PRH is stably overexpressed. Colony formation assays were also performed to investigate whether PRH overexpression results in colony formation in primary BECs. Strikingly, PRH overexpressing primary BECs (Donor 1) are able to form colonies in soft agar whereas the BECs infected with empty adenovirus do not form colonies **(Figure 5.11)**.

According to the results of these functional assays, it can be concluded that PRH alone is sufficient to increase proliferation, invasion, migration and anoikis resistance in primary BECs.

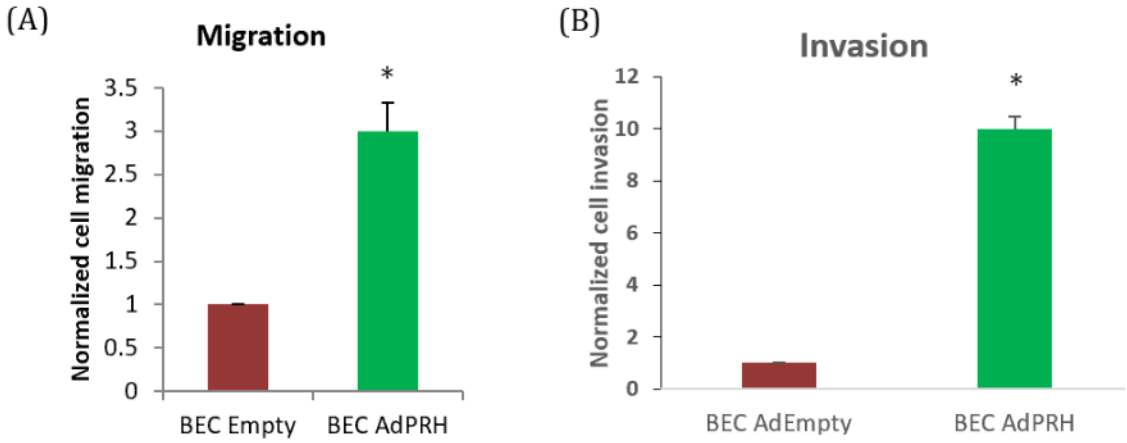

Figure 5.10 PRH OE increases cell migration and invasion in primary BECs (Donor 1). (A) Cell migration of AdPRH and AdEmpty BECs through transwell filter in a 2-10% serum gradient for 72 hours. 1 mM hydroxyurea was added 24 hours before the migration assay and throughout the assay to inhibit proliferation. Statistical test: Two-tailed unpaired T-test (n=3; *p<0.05) (B) Invasion AdPRH and AdEmpty BECs through transwell filter with 10 % matriel gel, 1 mM hydroxyurea was added 24 hours before the invasion assay to inhibit proliferation. Statistical test: Two-tailed unpaired T-test (n=3; *p<0.05). The error bars show the SD of three experimental repeats.

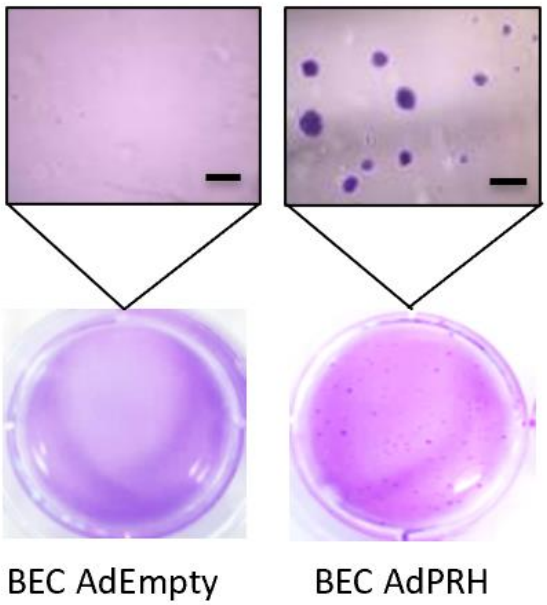

Figure 5.11 AdPRH in BECs (Donor 1) promotes colony formation in soft agar. Primary BECs were infected with AdPRH or AdEmpty at MOI50. Cells were plated with low melting agar on a 6 well plate and incubated for 10 days. Cells were then stained with crystal violet blue and images were taken under light microscope at magnification 10x. The scale bar represents 20 µm in length.

5.6 Identify differential gene expression in primary BECs when PRH is overexpressed by RNA sequencing

Phenotypical changes observed when PRH is overexpressed in AKN-1 cells were recapitulated when primary BECs (Donor 1) transiently overexpressed PRH using adenovirus. To investigate the gene expression changes that underlie the observed changes in phenotype, RNA-seq experiments were conducted on AdEmpty or AdPRH infected primary BECs (Donor 1). RNA was extracted from BECs sample 48 hours after AdPRH or AdEmpty infections. The adenoviral infection was repeated twice independently to allow DEG analysis. To validate the RNA-seq data from AdPRH BECs, qPCR was conducted on selected PRH target genes that we have previously investigated in AKN-1 cells. A comparison of RNA-seq and qPCR data for selected genes is shown in **Figure 5.12**. PRH overexpression in primary BECs donor 1 leads to the upregulation of *NOTCH3*, *CCND2* and *VIM* and downregulation of *CDH1* **Figures 5.12B**. *SNAI1* is the only

EMT transcription factor that is upregulated by PRH in BECs donor 1. The qPCR data is consistent with the RNA-seq data. Western blotting confirms the changes in Notch3, Cyclin D2, E-cadherin and Vimentin **(Figure 5.12C)**. Cyclin D2 is upregulated in PRH overexpressing primary BECs and CCLP cells but as mentioned earlier not in AKN-1 GFP-PRH-Myc cells. The RNA seq data, qPCR and protein data are consistent for Notch3, Cyclin D2, E-cadherin and Vimentin genes in BEC donor 1 and the changes are similar to those observed in GFP-PRH-Myc AKN-1 cells. As *SNAI1* is the only upregulated EMT transcription factor in AdPRH BECs donor1 we infer that Snail1 is important in driving EMT in the BECs and in promoting further invasive properties in CCLP cells.

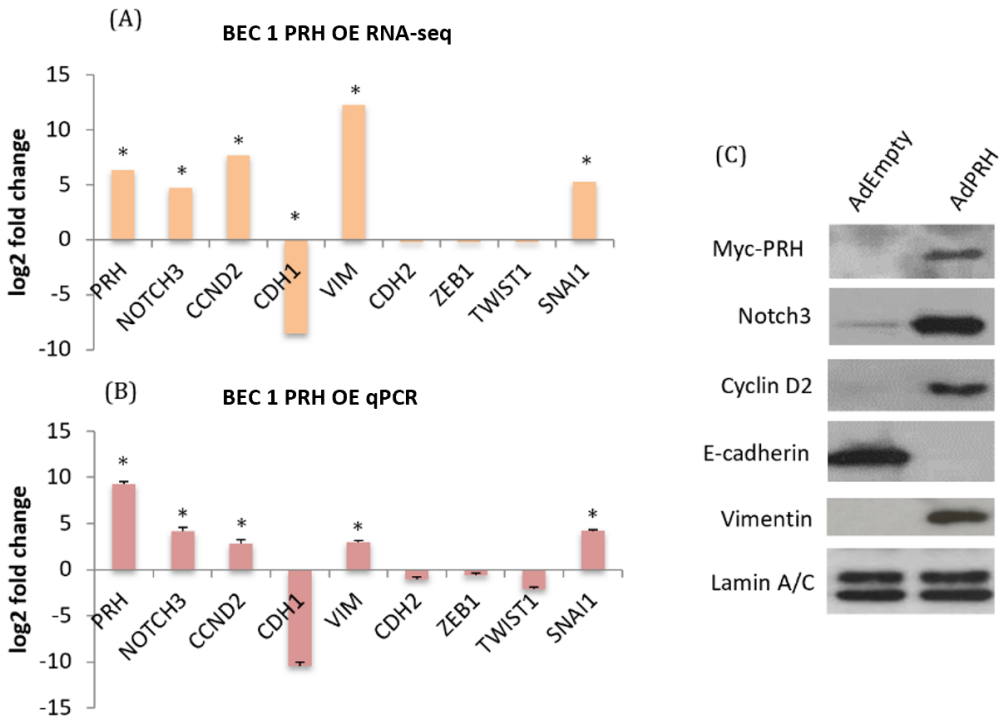

Figure 5.12 PRH OE upregulates Notch3 and modulates EMT genes expression in BECs donor 1. (A) The $\log_2$ fold change of gene expression for selected genes obtained from the RNA seq data. (B) qPCR showing the mRNA expression of *NOTCH3* and EMT genes in AdPRH and AdEmpty control primary BECs (Donor 1). The gene expression is normalized to β-actin. Statistical test: Two-tailed unpaired T-test (n=3; *$p<0.05$). The error bars show the SD of three experimental repeats. (C) Representative Western blots showing Notch3, Cyclin D2, E-cadherin and Vimentin protein expression in AdPRH and AdEmpty BECs donor 1. 10 µg of protein was loaded into each lane. Lamin was used as a loading control. The experiment was repeated in 3 different passages of primary BECs donor 1 and all show similar results.

GSEA hallmark gene set analysis was conducted with RNA-seq data from primary BECs donor 1 infected with AdPRH. The EMT pathway is most strongly enriched pathway in BECs donor 1 infected with AdPRH **(Figure 5.13A)**. This is consistent with the morphological and phenotypical changes observed in BECs AdPRH (donor 1). Ranked Enrichment plots were generated using the GSEA software by inputing the DEG list and corresponding $\log_2$ fold change. The graph shows that the DEGs in the EMT pathway are mostly upregulated **(Figure 5.13B)**. Volcano plots were plotted for the EMT pathway for the GSEA datasets of primary BECs donor 1 using the DEG and the $\log_2$ fold change obtained from the GSEA software and the q-values. The plot shows that multiple genes

encoding collagen component proteins are differentially regulated by PRH in primary BECs donor 1 and are genes in the hallmark EMT set/ Collagen proteins **(Figure 5.13C)**. This is consistent with PRH OE in CCLP and AKN-1 cells. Moreover, the mesenchymal marker *VIM* is also one of the key DEGs in the EMT pathway in primary BECs. For a full list of DEGs in the EMT pathway for BECs donor 1, see the heatmap in **figure S4**. The DEGs in the EMT pathway in primary BECs donor 1 are similar to those identified in AKN-1 cells. In fact, identification of genes present in both types AKN1 and primary BECs that are part of the EMT pathway using the 'BioVenn' software shows that 79% EMT genes are in common for BECs donor 1 and AKN-1 **(see Venn diagram Figure S5)**.

The Notch pathway is another enriched pathway in both BEC donor 1 and AKN1 cells (Figure 5.12D). A heatmap was generated for the full list of DEGs in the Notch pathway for BECs donor 1 **(Figure S6)**. *NOTCH3*, *NOTCH1, FZD1* and *CCND2* are the key DEGs in the Notch pathway that are regulated by PRH and this is consistent with the corresponding qPCR and Western blot data **(Figure 5.12)**. Notably, *CCND2* is regulated by PRH in CCLP, CCSW and primary BECs donor 1.

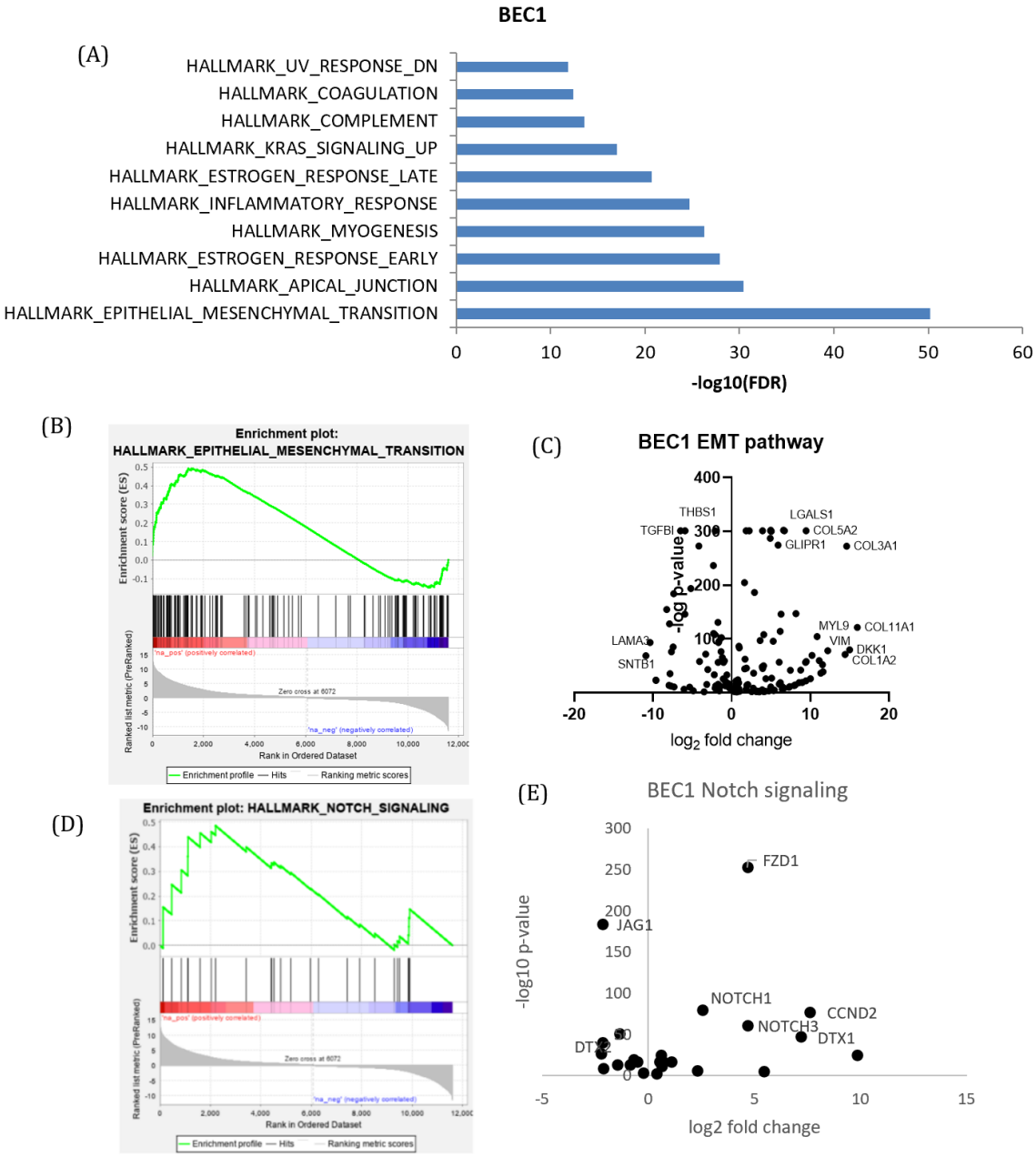

Figure 5.13 GSEA of RNA-seq data of PRH OE BECs donor 1. (A) Gene set enrichment analysis using Hallmark gene sets for PRH OE DEGs in BECs donor 1. (B) Enrichment plot for EMT pathway for RNA-seq data of BECs donor 1 cells. (C) Volcano plot of the DEGs in EMT pathway of RNA-seq data of PRH overexpressing BECs donor 1. (D) Enrichment plot for Notch pathway for RNA-seq data of BECs donor 1 cells. (E) Volcano plot of the DEG genes in NOTCH pathway of RNA-seq data of PRH overexpressing BECs donor 1.

In order to determine if the phenotypical changes and gene expression changes by PRH are reproducible in the primary BECs, BEC donor 2 and donor 3 were infected with AdPRH or AdEmpty as described previously. Western blot was carried out to confirm

exogenous Myc PRH expression in BECs donor 2 and BECs donor 3 after infection with AdPRH or AdEmpty **(Figure 5.14A)**. Edu proliferation experiments shows no change in proliferation in BECs isolated from donor 2 compared to its control. In contrast, Edu proliferation experiments of BECs donor 3 infected with AdPRH did show higher proliferation compared to the AdEmpty control **(Figure 5.14B)**. Furthermore, in migration assays, BECs from donor 3 are more migratory when PRH is overexpressed compared to the AdEmpty infected controls, whereas PRH overexpressing primary BECs from donor 2 shows no change in migration upon AdPRH infection compared to AdEmpty controls **(Figure 5.14C)**. As PRH is not expressed in all three BEC samples, this could indicate patient specific differences in response to AdPRH. The donors were from livers of patients with liver alcoholic disease and the genetic background might not be the same as a healthy donor. Therefore, PRH OE in the condition of liver alcoholic disease promotes CCA and further experiments are needed to confirm exogenous PRH initiate carcinogenesis in healthy donor sample.

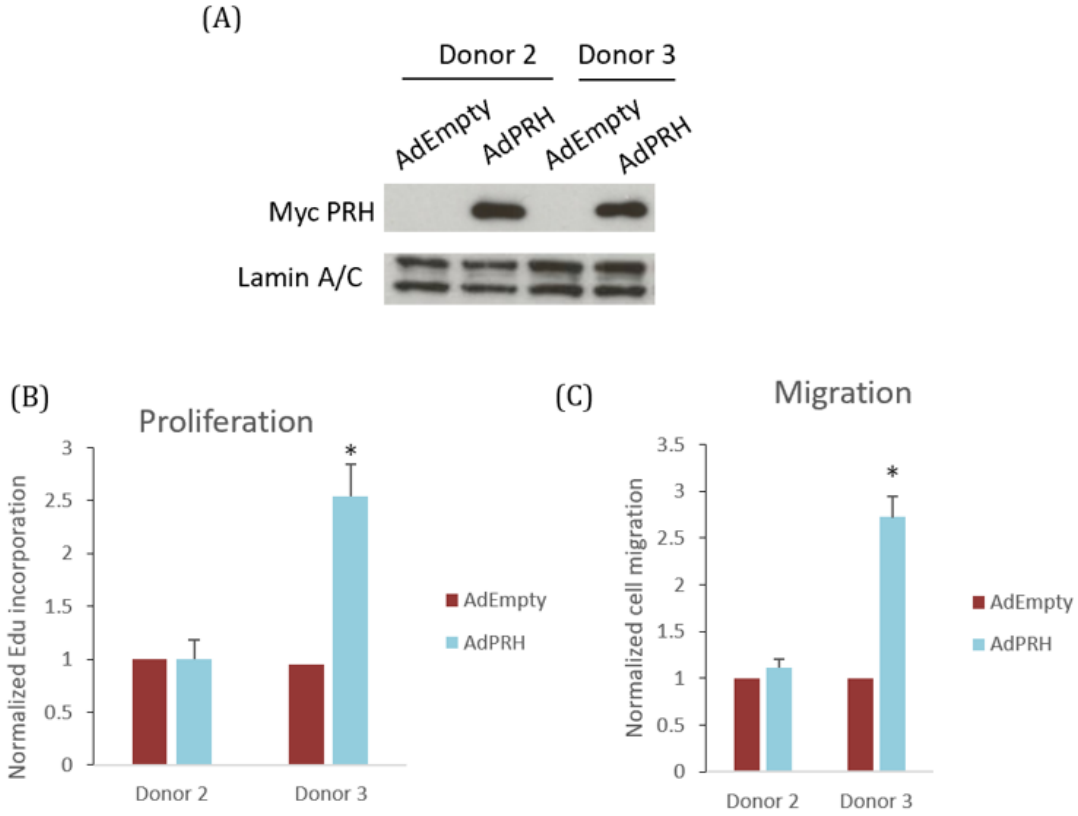

Figure 5.14 The effects of PRH OE in proliferation of primary BECs donor 2 and donor 3. (A) Representative Western blotting showing the exogenous Myc-PRH protein expression in Donor 2 and Donor 3 BECs. 10 µg of protein was loaded into each lane. (n=2) (B) Proliferative activity of AdPRH and AdEmpty infected primary BECs donor 2 and 3. Cells were incubated in Edu for 4 hours and click reaction was detected by an HRP-conjugated antibody and OPD was added and absorbance was measured at 450 nm. Error bars show the SEM among the two experimental repeats. Statistical test: Two-tailed unpaired T-test (n=3; *p<0.05). The error bars show the SD of three experimental repeats. (C) Cell migration of AdPRH and AdEmpty infected primary BECs donor 2 and donor 3 through transwell filter at 10% serum gradient. 1 mM hydroxyurea was added 24 hours before the migration assay to inhibit proliferation. Statistical test: Two-tailed unpaired T-test (n=3; *p<0.05).

5.7 Investigation of the differentially regulated genes and pathways in primary BECs donors

The phenotypical changes in AKN-1 GFP-PRH-Myc and BEC AdPRH donor 1 are recapitulated in BEC AdPRH donor 3 but not in donor 2. In order to investigate if the gene expression changes in BECs donor 2 is different from other BECs donors, RNA-seq was conducted on AdEmpty or AdPRH infected primary BECs donor 2 and donor 3. Two passages from the AdPRH and AdEmpty of donor 2 and donor 3 were used for RNA extraction and RNA-seq as described previously. For each donor, the adenoviral infection was repeated twice independently to allow DEG analysis. In the RNA-seq data, the number of genes that are regulated by AdPRH varies considerably between the three BECs donors. In each case, AdPRH is highly expressed in the cells. BECs (donor 3) RNA sample has the greatest number of genes being regulated by PRH and BECs (donor 2) RNA sample has the fewest regulated genes **(Table 8)**. Interestingly, there are only 18 genes upregulated in common between all the three primary BECs samples and there are only 2 genes downregulated in common among all three BECs samples. Donor 1 and donor 3 have similar phenotypical changes when AdPRH is highly expressed and these two BEC samples have many more differentially regulated genes in common, compared to BEC donor 1 and 2 or to BEC donor 2 and 3. This is consistent with the phenotypical changes in common between BECs (donor 1) and BECs (donor 3) and the absence of phenotypical changes seen in BECs (donor 2).

	PRH expression (Log_2 fold change)	Total number of DEGs	Number of upregulated DEGs	Number of downregulated genes
AKN-1	6.22	10894	5673	5221
BECs donor 1	6.34	11594	6072	5522
BECs donor 2	8.16	1735	1086	649
BECs donor 3	4.44	2280	632	1576

Table 8 PRH expression and the number of DEGs ($q<0.05$) from the RNA-seq data of AKN-1 and BECs donors.

qPCR was conducted to confirm the RNA-seq data for Donor 2 and Donor 3. RNA-seq in BEC donor 3 is very similar to the changes observed in BECs donor 1 upon AdPRH infection. BEC donor 3 also shows changes in *NOTCH3*, *CCND2*, *VIM* and CDH1 similar to changes in gene expression in BECs donor 1 **(Figure 5.15B)**.

AdPRH infection of BECs donor 2 did not lead to changes in the proliferative behaviour of these cells and we observe that in RNA-seq experiments and qPCR experiments only modest changes in *NOTCH3* and *CCND2* expression are seen. Both RNA-seq and qPCR show little change in gene expression of *CDH1* and *VIM* upon PRH overexpression. The lack of changes in very well established EMT markers is likely to underlie the inability of PRH to promote migration in this donor **(Figure 5.16B)**. The hallmark set of EMT genes includes *VCL*, *LOXL*, *SNAI1* and *MMP1* which were all differentially regulated in the RNA seq data and quantitative PCR was used to confirm these changes. *VCL* encodes Vinculin which is required for stablizing E-cadherin at the cell surface (Peng et al., 2010). *LOXL* encodes Lysyl oxidase 1 (LOXL1) is a repressor of E-cadherin and was found to associated

with cancer metastasis (Xiao and Ge, 2012). *MMP1* encodes Matrix Metallopeptidase 1, a protein involved in degrading extracellular matrix and facilitating cell invasion (Chen and Parks, 2009). **Figure 5.16** shows that AdPRH leads to 1.5 fold increase in *VCL* and *SNAI1* expressions and a 2-fold increase in *LOXL* expression and a 2-fold decrease in *MMP1.* This data reveals although PRH does not regulate EMT markers such as *VIM* or *CDH1*, it does regulate several other EMT pathway genes in this BEC donor. Despite this the modulation of these genes do not appear to be sufficient to lead to changes in migration in the transwell experiments. Intriguingly, the transcript level for Vimentin in the RNA seq data from sample 2 BEC infected with AdEmpty is relatively high compared to that found for Vimentin in donor 1 and donor 3. The high basal level of Vimentin expression in donor 2 AdEmpty infected cells could preclude further expression of Vimentin in the presence of elevated PRH levels in this donor.

In conclusion, PRH overexpression in primary BECs donor 1 and donor 3 recapitulates most changes observed in GFP-PRH Myc AKN-1 cells except that *CCND2* encoding Cyclin D2 is activated in BECs but not in AKN-1 cells. BECs donor 2 shows some gene expression changes that are associated with EMT but are not sufficient to cause EMT in these cells.

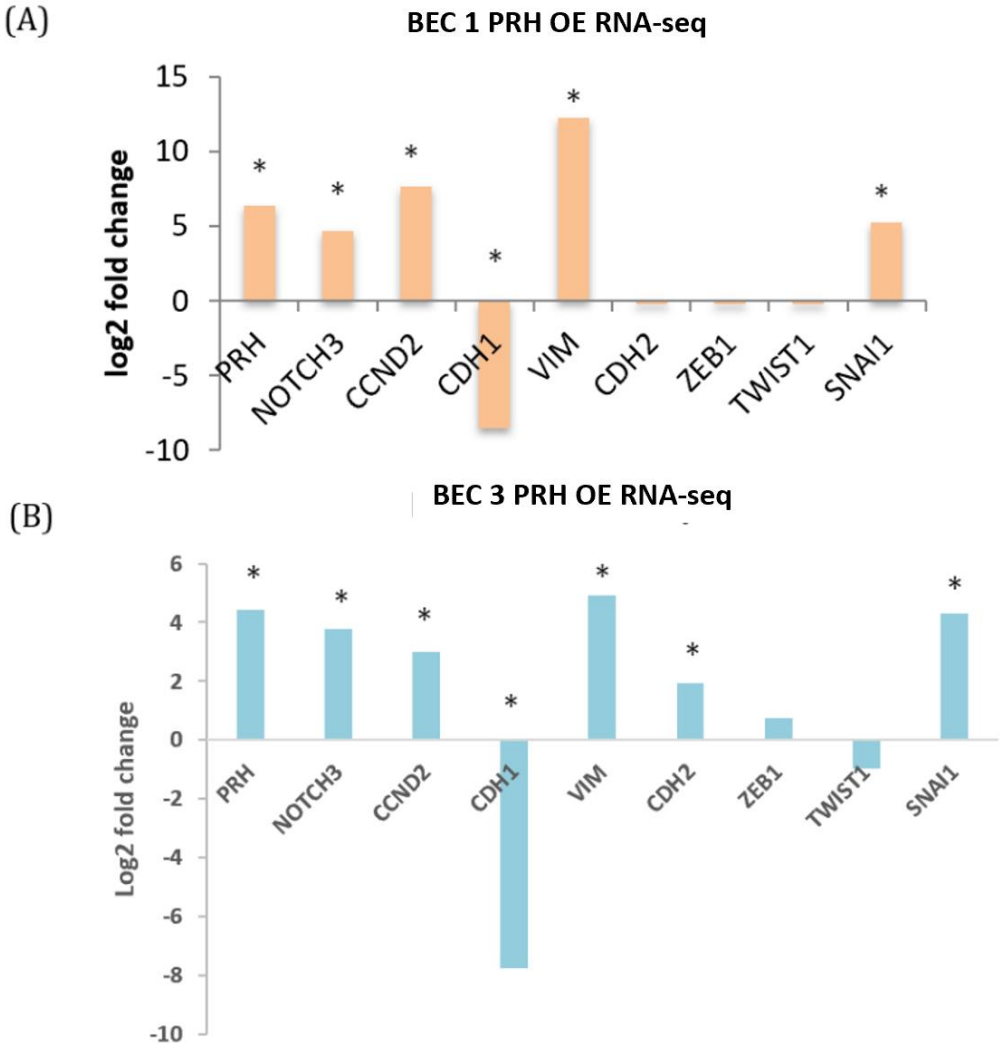

Figure 5.15 RNA seq data of BECs donor 3. (A) RNA-seq data of the AdPRH BECs donor 1. Statistical test: Two-tailed unpaired T-test. (n=2; *q<0.05) (B) RNA-seq data of the AdPRH BECs donor 1. Statistical test: Two-tailed unpaired T-test. (n=2; *q<0.05).

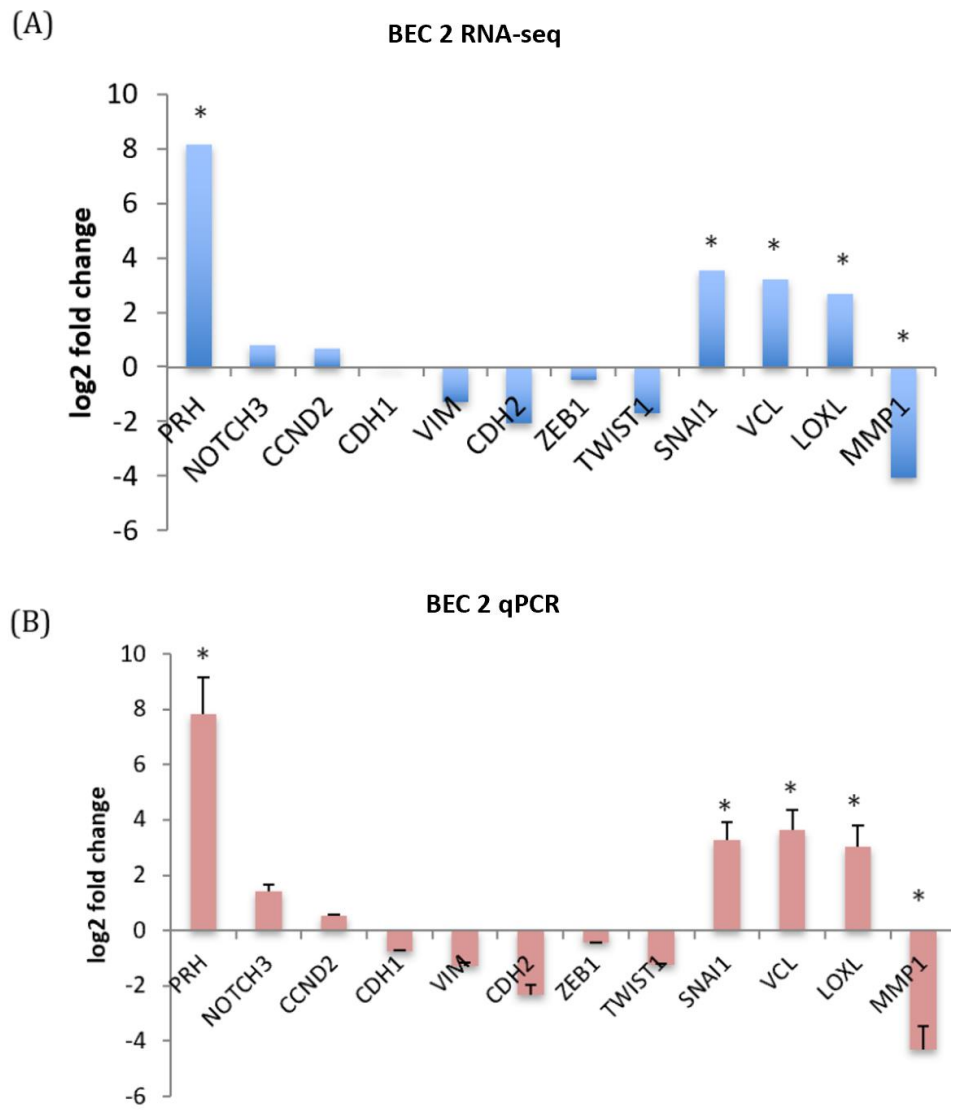

Figure 5.16 RNA seq and qPCR data from BECs donor 2. (A) RNA seq data showing the log2 fold change in gene expression for AdPRH infected BECs donor 2. Statistical test: Two-tailed unpaired T-test. (n=2; *q<0.05) (B) qPCR showing the mRNA expression (log2 fold change) for *NOTCH3* and EMT pathway genes in AdPRH and AdEmpty control primary BECs (Donor 2). Statistical test: Two-tailed unpaired T-test. (n=2; *p<0.05). The error bars show the SD of three experimental repeats.

GSEA hallmark geneset analysis was conducted with RNA-seq data from BECs donor 2 and donor 3 infected with AdPRH. Kras signaling is the most strongly enriched pathway in donor 2 and donor 3 BECs **(Figure 5.17)**. Full list of DEGs related to EMT pathway for BECs donor 2 and donor 3 is shown as a heatmap in **Figure S4.** Notably, all three primary BECs samples showed enrichment of EMT pathway, KRAS signaling pathway, estrogen

response and apical junction pathways. Enrichment plots show that the DEG in EMT pathway of AKN-1 and primary BECs donor 1 are mostly upregulated and for BECs donor 2 and 3 are mostly downregulated **(Figure 5.6, 5.13, 5.17 and 5.18)**. Volcano plots were plotted for the EMT pathway for the GSEA datasets of primary BECs donors 2 and 3 using the DEG and the $\log_2$ fold change obtained from the GSEA software and the q-values. The volcano plots show some of the key genes that are differentially regulated by PRH related to EMT pathway **(Figure 5.17&5.18)**. The plots show that at least one gene encoding collagen component proteins are differentially regulated by PRH in all differentially regulated genesets. Moreover, the gene encoding Laminin (*LAMA*) is differentially regulated by PRH in AKN-1 and BECs donor 1 and donor 3. Laminin is one of the best known biomarkers among the basement membrane constituents and it is downregulated during EMT in squamous cell carcinoma (Marinkovich, 2007).

In conclusion, PRH appears to regulate EMT pathway genes in all cell types but patient specific genetic differences determine whether the key markers of EMT are altered and hence whether the cells can become migratory.

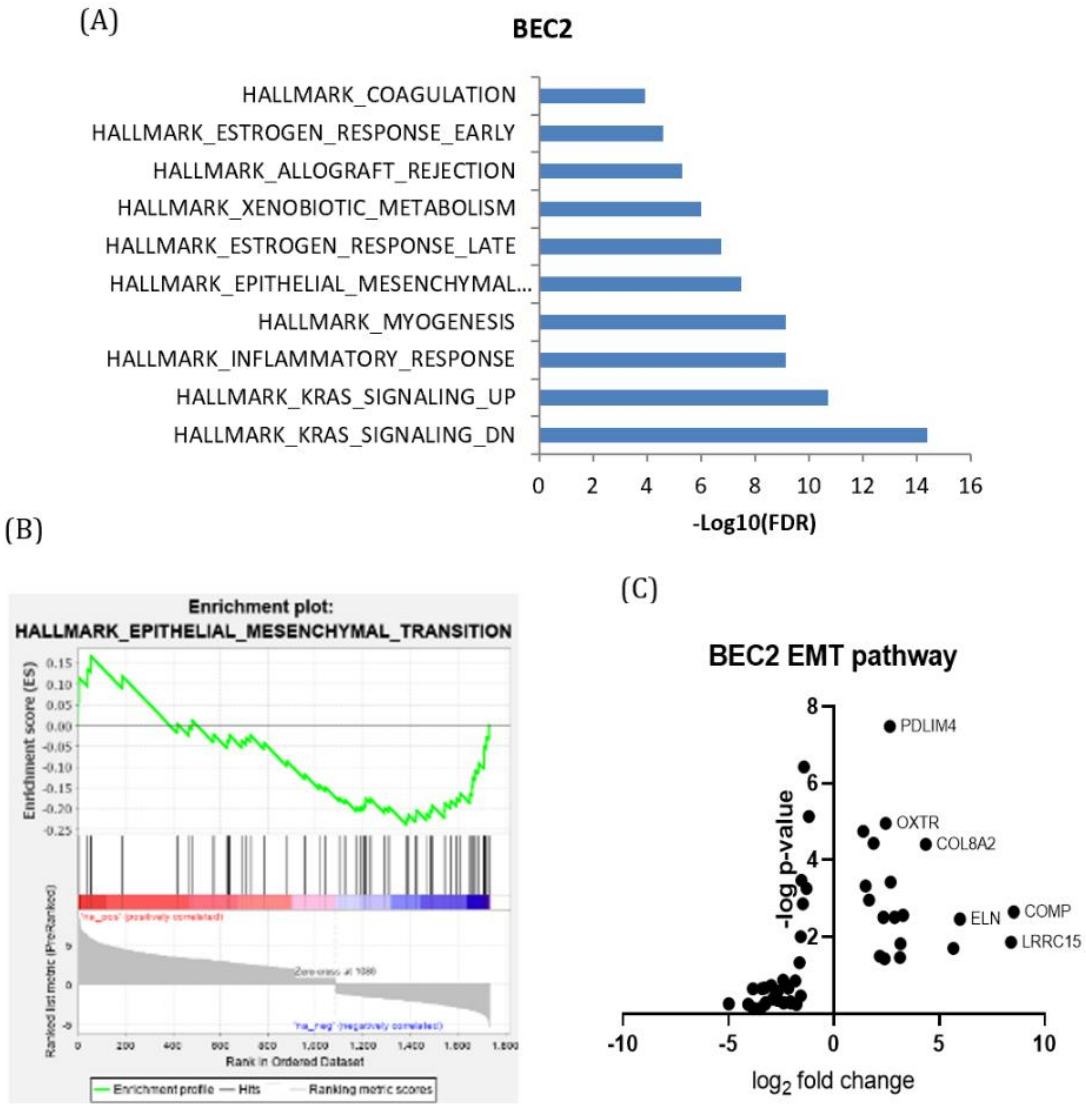

Figure 5.17 GSEA of RNA-seq data from PRH overexpression in BECs donor 2. (A) Gene set enrichment analysis using Hallmark gene sets for PRH OE DEGs in BECs donor 2. (B) Ranked Enrichment plot for EMT pathway for RNA-seq data of BECs donor 2 cells. (C) Volcano plot of the DEG genes in EMT pathway of RNA-seq data of PRH overexpressing BECs donor 2.

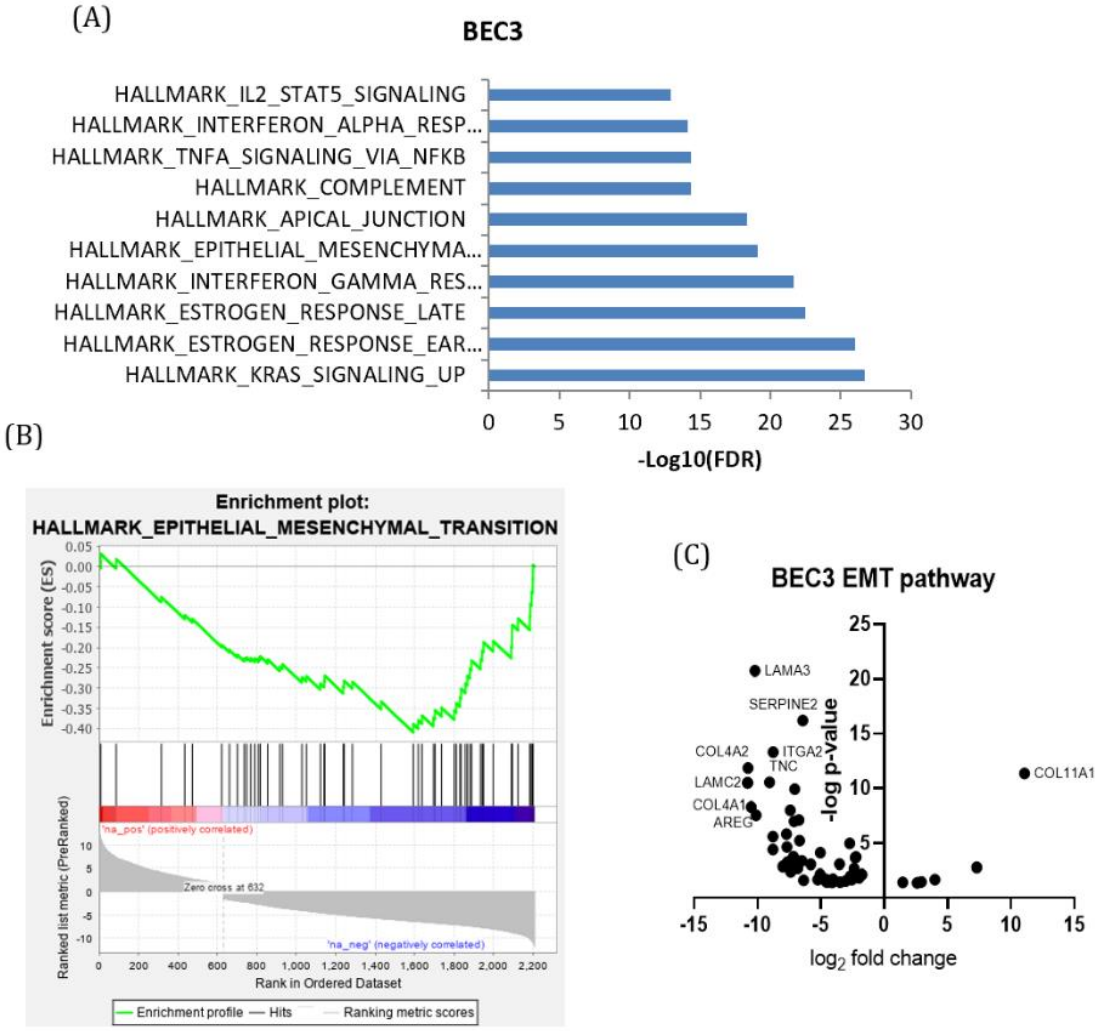

Figure 5.18 GSEA of RNA-seq data of PRH OE BECs donor 3. (A) Gene set enrichment analysis using Hallmark gene sets for PRH OE DEGs in BECs donor 3. (B) Enrichment plot for EMT pathway for RNA-seq data of BECs donor 3 cells. (C) Volcano plot of the DEG genes in EMT pathway of RNA-seq data of PRH overexpressing BECs donor 3.

CHAPTER 6

Novel drug treatments for CCA

6. Novel drug treatment for CCA

6.1 PRH overexpression increases sensitivity to Palbociclib

Palbociclib is one of the CDK4/6 inhibitors that is currently approved for clinical use (Bui et al., 2019). Palbociclib is used as treatment for estrogen receptor (ER)-positive breast cancer based on the results of clinical trials demonstrating improvements in progression-free survival when CDK4/6 inhibitors are used in anti-estrogen therapy (Malorni et al., 2016). The primary mechanism of CDK4/6 inhibitor activity is suppression of RB phosphorylation, enforcing G_1 cell cycle arrest, and thus inhibiting proliferation (Malorni et al., 2016).

Previous chapters in this thesis have shown that the activation of Notch pathway and genes involved in proliferation and EMT including *CDH1* and *VIM* and cell cycle genes, *CCND2, CDKN1B* and *CDKN2B* all have a common origin in the dysregulation of the transcription factor *PRH/HHEX*. CDK4/6 kinase activity is inhibited by p27 (*CDKN1B*) and p15 (*CDKN2B*) proteins and stimulated by the *CCND1* and *CCND2* gene products upon binding of Cyclin D molecules. It is expected that as the CDK4/6 kinase is important for cell cycle that this kinase would ultimately be activated by elevated PRH expression.

Thus, it is likely that in CCA cells where PRH is elevated, CDK4/6 kinase is hyperactive and the cells might be more sensitive to Palbociclib. In order to investigate whether there is a relationship between PRH expression levels and sensitivity towards Palbociclib, four CCA cell lines, CCLP, CCSW, KKU-100 and KKU213 were used for cell viability experiments. Dose response curves were obtained as follow: 1 million cells were infected with AdPRH or AdEmpty at MOI 50 for 24 hours in a 6-well plate. 5×10^4 infected cells were then counted and replated in each well of a 96-well plate in triplicate. Cells

were then incubated with Palbociclib serially diluted over a concentration range from 3 µm to 3 nM or with DMSO as vehicle control for 24 hours. In these assays, the effect of the drug on cell viability reflects drug toxicity as the cells are not expected to grow within 24 hours since the doubling time of all the cell lines tested is greater than 24 hours. In each cell line, the lethal dose (LD50) for Palbociclib (concentration at which 50% of cells are viable) was calculated from the dose response curves using Graph pad prism (See **M&M section 2.11**). Dose response curves were plotted using the MTT signal against the logarithm of drug concentration. The MTT signal is proportional to cell numbers within the linear range (See **M&M 2.11** for graph of cell number against MTT signal). The dose response curves were plotted both with or without PRH overexpression. In all MTT experiments with cells incubated with drug treatment, the MTT signal is normalized against cells treated with vehicle in parallel. **Figure 6.1** shows the dose response curves of the four CCA cell lines infected with AdPRH or AdEmpty incubated in Palbociclib for 24 hours. The LD50 for AdEmpty infected CCLP, CCSW and KKU-213 cells is 90 nM whereas the LD50 for KKU-100 is 150 nM. The LD50 for AdPRH infected CCLP, CCSW and KKU-213 cells is 46 nM whereas it is 100 nM for KKU-100 cells. Thus, all the cell lines are responsive to Palbociclib treatment but they become more sensitive to treatment when PRH is overexpressed. The dose response curves report on cell viability in the presence of drug and this is the outcome of changes in cell proliferation and cell death. To determine the effect of Palbociclib on cell proliferation, the four CCA cell lines were incubated with Palbociclib exactly as described above at each of their respective LD50 for 24 hours and Edu proliferation assays were performed**. Figure 6.2A** shows that as expected, 90nM Palbociclib inhibits the proliferation of CCLP, CCSW and KKU-213 cell

lines. However, it does not strongly inhibit the proliferation of the KKU-100 cell line. Interestingly this cell line has relatively low PRH protein expression levels **(Figure 6.2B)**.

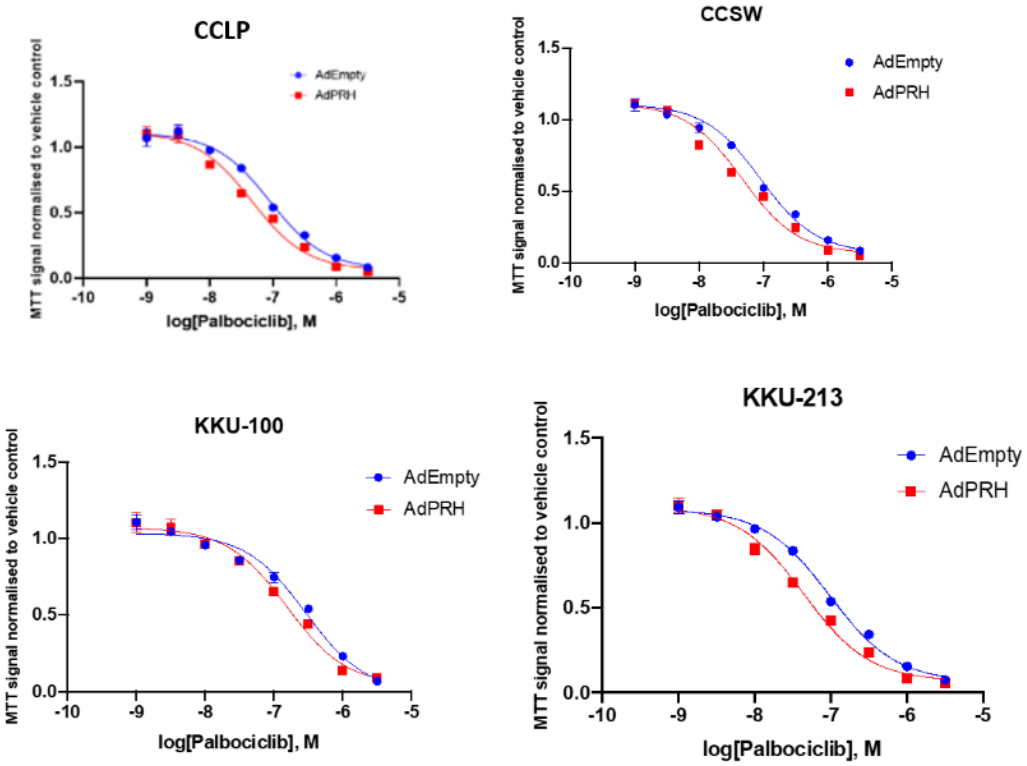

Figure 6.1 AdPRH expression increases sensitivity towards Palbociclib in the CCA cell lines. Dose response curves for CCA cell lines infected with AdEmpty or with AdPRH and treated with Palbociclib. LD50 for AdEmpty in CCLP, CCSW and KKU-213 = 90nM. LD50 for AdPRH in CCLP, CCSW and KKU213 =46nM. LD50 for AdEmpty in KKU-100 is 150 nM and for AdPRH in KKU-100 is 100 nM. MTT cell viability assays were performed at 24 hours and cell viability was normalized to vehicle treated controls. The error bars show the SD of three experimental repeats. Where errors bars cannot be seen they are smaller than the symbols (n=3).

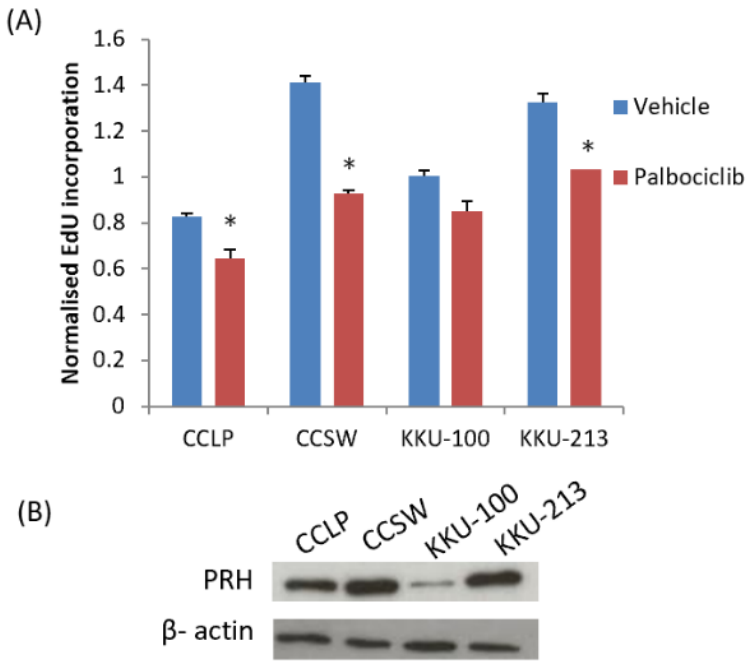

Figure 6.2 The effect of Palbociclib on CCA cell lines. (A) Edu proliferation assays were carried out on four CCA cell lines CCLP, CCSW, KKU-100 and KKU-213 with Palbociclib treatment or DMSO vehicle control at their LD50. Statistical test: Two-tailed unpair T-test (n=3; *p<0.05). The error bars show the SD of three experimental repeats. (B) Western blotting showing the endogenous PRH expression in CCA cell lines using M3 antibody. 10 µg of protein was loaded into each lane.

The effect of Palbociclib on cell proliferation is known to be dependent on the presence of phosphorylated retinoblastoma (Rb) tumour suppressor protein (Llovet et al., 2015). We therefore examined Rb and phosphorylated Rb (pRb) expression in the European and Thai CCA cell lines used in this study and also in primary BECs. Western blotting for Rb and Lamin A/C shows that RB protein expression is very low or undetectable in primary BECs although it is present in all the CCA cell lines **(Figure 6.3A)**. Phosphorylated Rb is also present in all four CCA cells lines previously tested in cell viability and proliferation assays **(Figure 6.3Bi)**. Moreover, treatment of these CCA cell lines with Palbociclib at their respective LD50 for 24 hours reduces the levels of phosphorylated pRb in all cell lines indicating that Palbociclib does inhibit CDK4/6 kinase phosphorylation of Rb in all cell lines. **(Figure 6.3Bi&6.3Bii)**. The expression of PRH is not affected by

Palbociclib treatment and the PRH expression is low in KKU-100 **(Figure 6.3Bi)**. Thus, the decreased sensitivity of KKU100 cells to Palbociclib is not through decreased Rb protein expression or phosphorylation. Presumably the reduced sensitivity is either because Palbociclib cannot inhibit the activity of CDK4/6 on other members of the Rb family of proteins (pocket protein) or because KKU-100 cells are less sensitive to Palbociclib due to low PRH expression.

To determine the importance of Rb to cell proliferation in Palbociclib sensitive CCLP cells, the Rb protein was depleted in CCLP cells by transient transfection with an siRNA against Rb (GS5925, Qiagen) for 24 hours. Western blotting with antibodies against Rb and ß-actin shows that Rb is reduced in cells transfected with siRb for 48 hours. To determine the effect of Palbociclib on Rb depleted cells, 24 hours after transfection with siRb, the CCLP cells were treated with 100 nM Palbociclib (LD50) or with DMSO vehicle control for a further 24 hours and then Edu proliferation assays were performed. Although the proliferation of the CCLP control cells is inhibited by Palbociclib treatment, siRB knockdown CCLP cells are far less sensitive to the effects of this drug. We infer that CDK4/6 dependent phosphorylation of Rb is of importance to cell cycle progression in these cells (**Figure 6.3D**). Interestingly, Palbociclib has almost no effect on the proliferation of the PRH KD CCLP cell line whereas it strongly inhibited in the paired control shRNA cell line (**Figure 6.3D**). It can be concluded that both Rb and PRH are important for the effect of Palbociclib as both Rb depleted and PRH depleted cells are less sensitive to Palbociclib. In KKU-100 cells, Rb and pRb protein levels are similar to that observed in KKU-213 cells but the cells are less sensitive to Palbociclib inhibition of proliferation. One explanation for this is that KKU-100 cells could express other pocket

proteins. Increased amount of Palbociclib would be required to inhibit proliferation in this case.

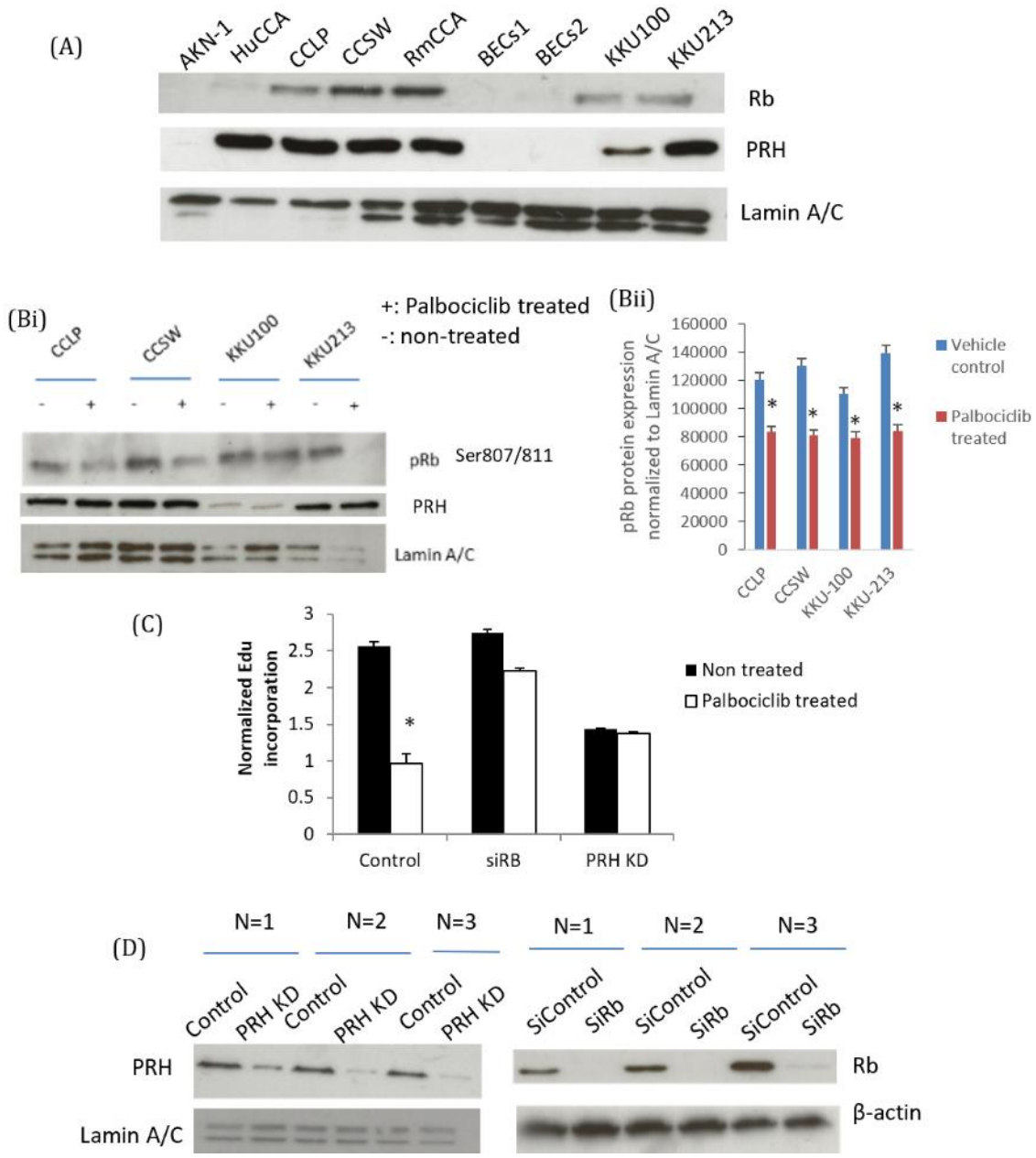

Figure 6.3 Effect of Palbociclib on Rb and phospho Rb. (A) Representative Western blot to show the expression of Rb and PRH in a panel of CCA cell lines using Rb and M3 antibody. 10 µg of protein was loaded into each lane. (n=3) (Bi) Representative Western blotting showing the expression of pRb and PRH in four CCA cell lines with Palbociclib treatment or with DMSO vehicle control using pRb Ser807/811 and M3 antibody. 10 µg of protein was loaded into each lane. (n=3) (Bii) Quantification of the pRb protein levels by image J normalized against the loading control, Lamin A/C. Statistical test: Two-tailed unpaired T-test (n=3; *p<0.05). (C) Edu proliferation assay showing the proliferation activity of sIRb and PRH KD in CCLP with Palbociclib treatment or with DMSO vehicle control. Statistical test: Two-tailed unpaired T-test (n=3; *p<0.05). The error bars show the SD of three experimental repeats. (D) Representative Western blot to show Rb and PRH protein expression in CCLP cells (n=3). 10 µg of protein was loaded into each lane.

In order to further investigate whether PRH expression is important for cell sensitivity towards Palbociclib, PRH was overexpressed by adenoviral infection in the four CCA cell lines (as described in M&M 2.1.8). 24 hours following infection, cells were treated with Palbociclib at their respective LD50 for 24 hours followed by Edu proliferation assays. In all cell lines, the presence of exogenous PRH increases sensitivity to Palbociclib (**Figure 6.4)**. Collectively, these results suggest that the ability of Palbociclib to inhibit cell proliferation is at least partially PRH dependent.

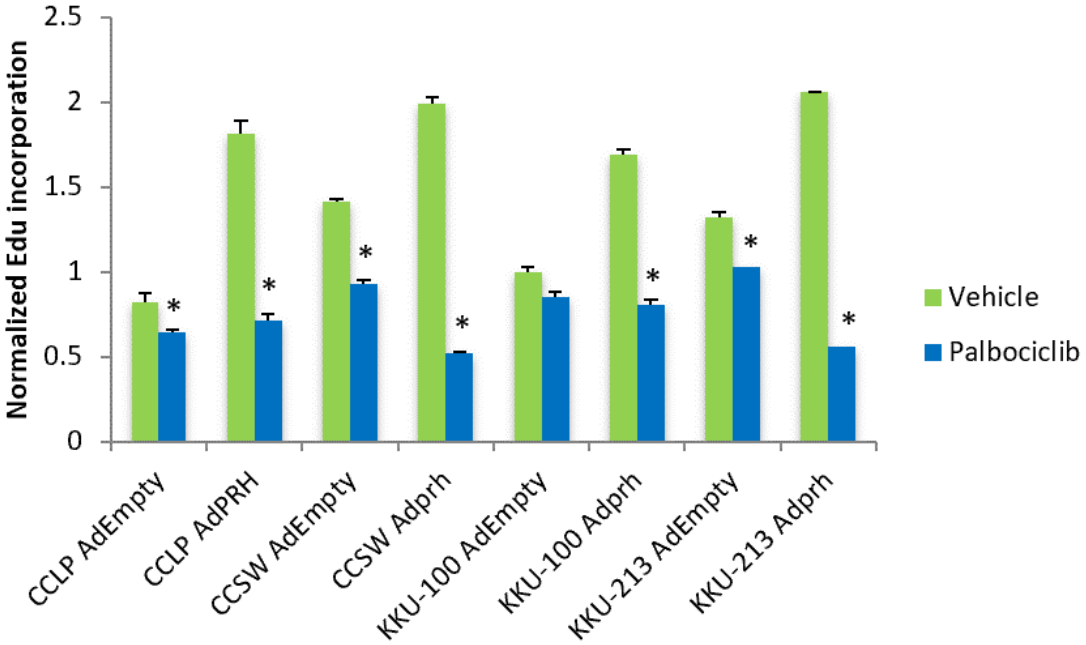

Figure 6.4 The effect of Palbociclib in PRH OE and KD CCLP cells. Edu proliferation assay was carried out on four PRH overexpressed CCA cell lines CCLP, CCSW, KKU-100 and KKU-213 with Palbociclib treatment or with DMSO vehicle control at their ED50. Statistical test: Two-tailed unpaired T-test (n=3; *p<0.05). The error bars show the SD of three experimental repeats.

Palbociclib has been shown to promote apoptosis in bladder tumour cells (G. Zhang et al., 2019). Although the mechanism by which Palbociclib inhibits cell proliferation is well established, its effect on apoptosis has not been intensively studied. To determine whether Palbociclib induces apoptosis in CCA cell lines, the CCA cell lines (1 x 10^6 / 6 well) were treated with Palbociclib or with DMSO vehicle control for 24 hours and then

cells were washed with PBS and centrifuged to form cell pellets. Caspase-3 apoptosis assays were performed on the cell pellet **(See M&M section 2.7.2)**. **Figure 6.5A** shows that Palbociclib increases Caspase-3 activity in all the CCA cell lines. Caspase-3 apoptosis assays were also performed in each cell line following AdEmpty or AdPRH infection of cells for 24 hours and then treatment with Palbociclib at the respective LD50 or with DMSO vehicle control for 24 hours. The setup of the experiment is very similar to that used for Edu proliferation assays following adenoviral infection but the treated cells (1 x 10^6) are pelleted for the apoptosis assay. The AdPRH infected cells show increased Caspase-3 activity compared to AdEmpty infected controls upon Palbociclib treatment (**Figure 6.5A)**. The experiment was repeated but cells were stained with Annexin/PI staining and staining was measured by FACs. The FACs data shows that there are more apoptotic cells in AdPRH infected cells compared to AdEmpty infected control cells with Palbociclib treatment at their LD50 for each cell line **(Figure 6.5Bii)**. Thus, in all cell lines, exogenous PRH expression increases the apoptotic effect of Palbociclib. The effect of 100 nM Palbociclib treatment for 24 hours was also assessed on PRH KD and control CCLP cells using the Caspase-3 assay. **Figure 6.5C** shows that Palbociclib does not increase Caspase-3 activity in PRH KD cells. Collectively, these results indicate that PRH increases the sensitivity towards Palbociclib by increasing the apoptotic effect of Palbociclib.

(A)

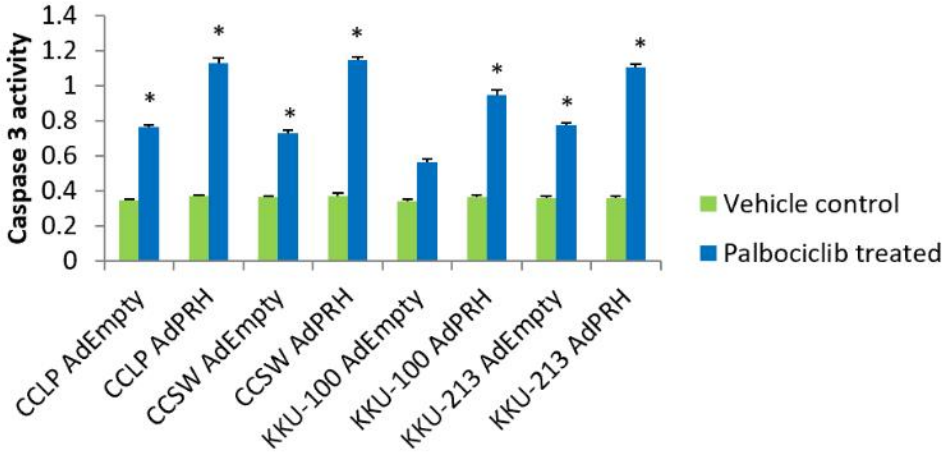

(Bi)

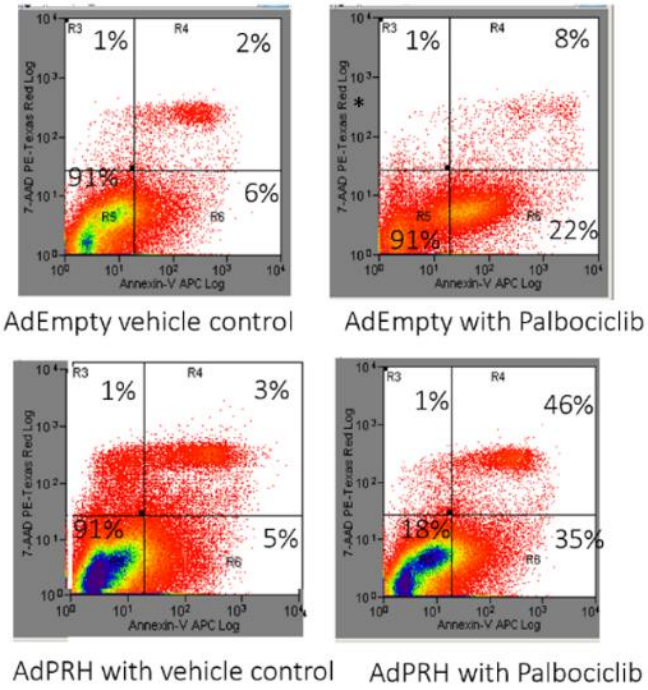

R3	Necrosis
R4	Late apoptosis
R5	Live cells
R6	Early apoptosis

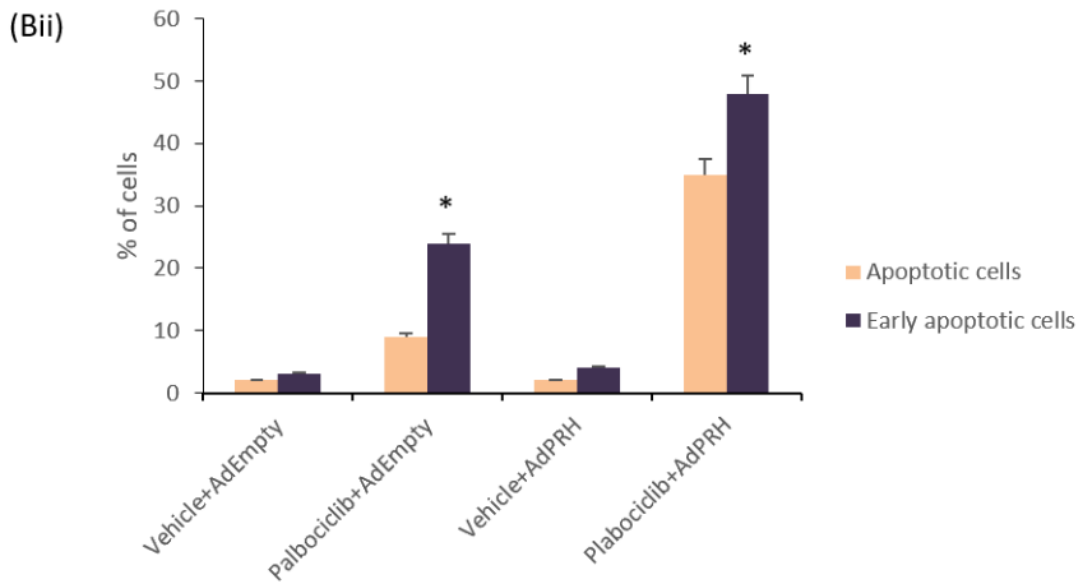

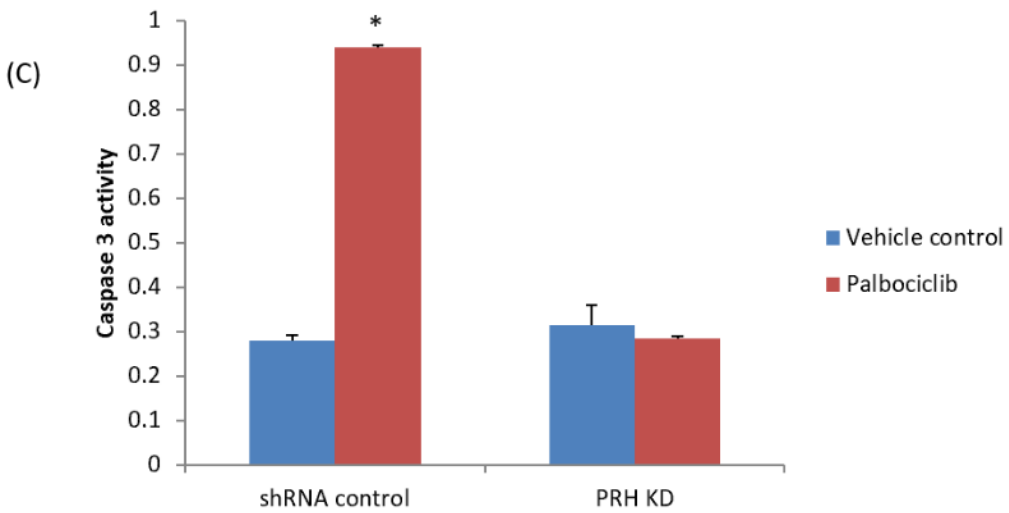

Figure 6.5 Palbociclib has pro-apoptotic effect on CCA cell lines. (A) Caspase-3 assays were carried out on four CCA cell lines with AdPRH overexpression or Empty virus control AdEmpty with Palbociclib treatment or with DMSO vehicle control. Statistical test: Two-tailed unpaired T-test (n=3; *p<0.05) (Bi) FACs followed by Annexin V staining on AdPRH and AdEmpty CCLP cells with Palbociclib treatment or with DMSO vehicle control. (Bii) Quantification of the FACs data showing the early apoptotic cells and apoptotic cells in AdPRH or AdEmpty CCLP with Palbociclib treatment or with DMSO vehicle control. Statistical test: Two-tailed unpaired T-test (n=3; *p<0.05) (C) Caspase-3 assays were carried out on PRH KD CCLP and controls with Palbociclib treatment or with DMSO vehicle control. Statistical test: Two-tailed unpair T-test (n=3; *p<0.05; #>0.05). The error bars show the SD of three experimental repeats.

In summary, KKU-100 cells with low PRH protein expression are less sensitive to Palbociclib although Palbociclib is able to inhibit phosphorylation of Rb in these cells. The Rb protein expression in KKU-100 cells is similar to KKU-213 cells indicating that the difference in sensitivity is not simply related to Rb expression levels. Exogenous PRH

expression in KKU-100 increases the inhibitory effects of Palbociclib on cell proliferation and the pro-apoptotic effects of Palbociclib underscoring the PRH dependent effects of Palbociclib inhibition. In CCLP cells, which are more sensitive to Palbociclib than KKU-100, both Rb and PRH are involved in Palbociclib sensitivity. Palbociclib also increases apoptosis in CCA cell lines and exogenous PRH increases apoptotic effect of Palbociclib in CCA cell lines. In conclusion, PRH promotes dose dependent sensitivity to Palbociclib in multiple cell lines. The sensitivity is likely dependent on the intrinsic apoptotic pathway in each cell line and the ability of PRH to modulate these pathways. Key proteins that are involved in apoptosis and proliferation are likely to be regulated by PRH.

6.2 Drug repurposing screen to determine novel drug treatment for CCA

The prognosis for CCA is very poor and current treatments, chemotherapy and surgery are not very successful. Although Palbociclib treatment is a promising new approach, it is costly and drug resistance is a common problem for drug treatment. Combination drug approaches for treatment of cancers are more successful for long-term remission (Mokhtari et al., 2017). Drug repurposing provides a new and pragmatic approach for treatments as it holds the promise of rapid clinical impact at a lower cost than de novo drug treatment (Corsello et al., 2017). Therefore, to determine whether there are any other compounds that can affect cell viability in CCA cell lines, a drug screen was performed. The drug screen was performed blind by Ms G. Kaur using a library of 104 off-patent drugs (provided by Dr Farhat Khanim, University of Birmingham), at clinically relevant peak serum concentrations. The drug library was compiled by selecting oral, off-patent drugs of low toxicity from all fifteen chapters of the British National

Formulary (Khanim et al., 2011). In multiple myeloma cell lines, 72 hours incubation was the optimal time point for drug screening experiments using the drug library (Khanim et al., 2011). The cell lines used for screening the drug library included two CCA cell lines (CCLP and CCSW) and an immortalized cholangiocyte cell line (AKN-1). For each cell line, 5 x 10^4 cells were treated with the 104 compounds for 72 hours using the maximum peak serum concentrations achieved as reported in the literature following use for standard clinical indications and MTT assays were used to examine cell viability (5 x 10^4 cells) following drug treatment (Khanim et al., 2011). However, when CCLP cells were treated for 72 hours, their viability did not significantly decrease **(Figure 6.6)**. In contrast at 96 hours incubation treatment with the same drugs led to a decrease in cell viability in MTT assays. Therefore, cell viability was measured after 96 hours using the MTT cell viability assay for each of the drugs in the drug screen. Cell viability with drug treatment cells was normalized to the cells treated with corresponding vehicle control for each of the 104 drugs. (**Fig. 6.7A-6.7D**). The experiment was repeated in three different cell lines three times independently and statistical analysis was carried out using a paired, two-tailed T-test followed by Benjamini-Hochberg multiple corrections to determine which compounds had a reproducible decrease in viability (n=3). **Table 9** shows all the drug in the screen and p-values. Ascorbic acid, Imatinib, Zinc acetate, Itraconazole, Prochlorperazine, Niclosamide, Mebendazole, Deferrioxamine mesilate, Colchicine, methotrexate and Carvedilol p-values (<0.05) are shown in red indicating that these compounds have a reproducible and statistically significant effect on cell viability in all cell lines **Fig. 6.7A-D.**

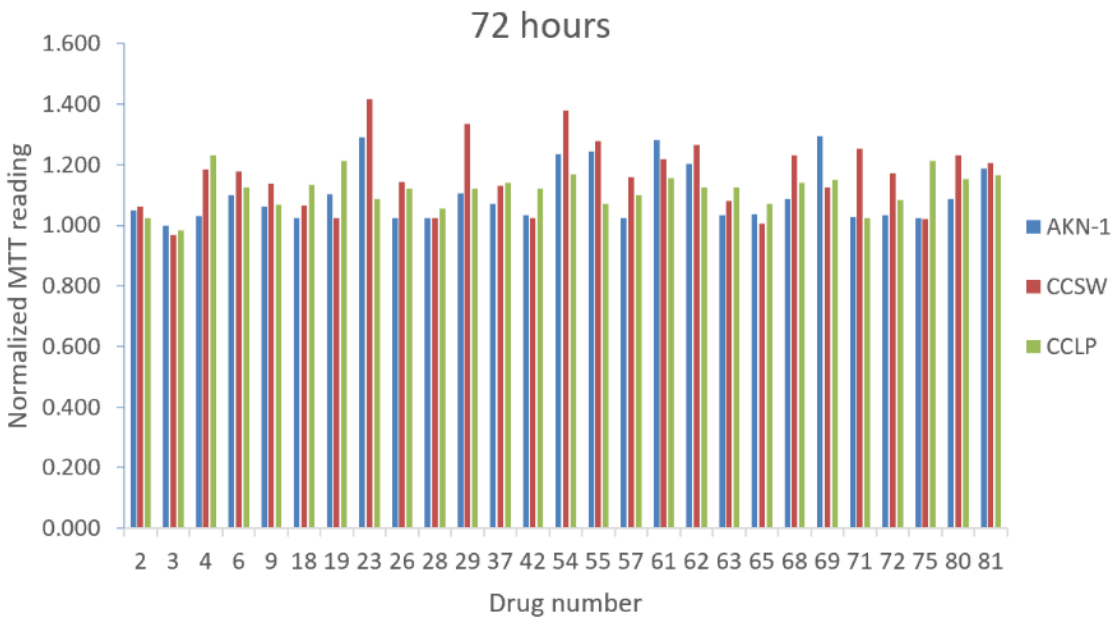

Figure 6.6 Repurposing drug screening by MTT assay. Drug screenings were carried out 3 times using MTT assay on CCLP, CCSW and AKN-1 cells. Cells were incubated with the drugs for 72 hours.

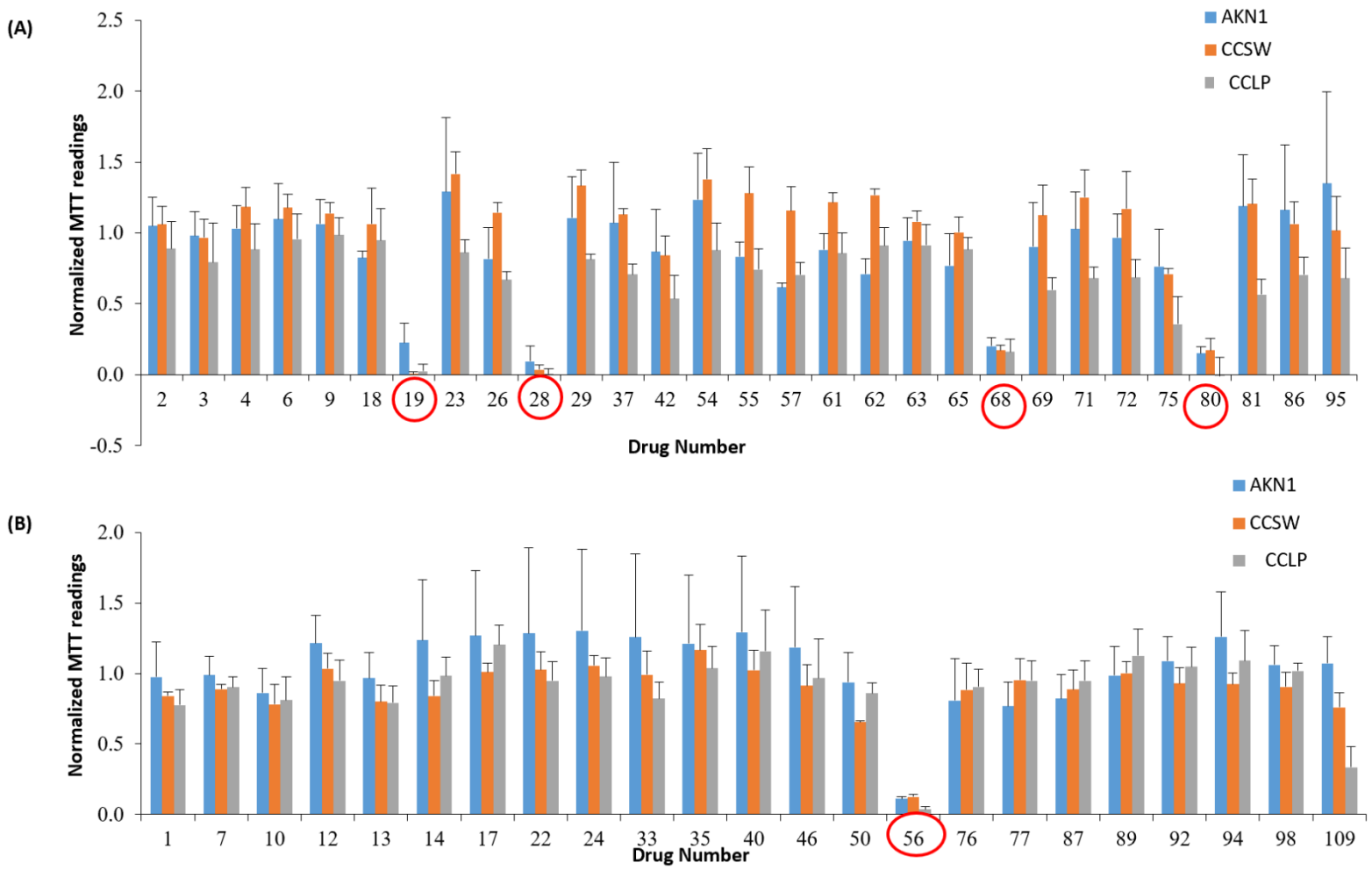
(A)
AKN1
CCSW
CCLP
Normalized MTT readings
2.5
2.0
1.5
1.0
0.5
0.0
-0.5
2 3 4 6 9 18 19 23 26 28 29 37 42 54 55 57 61 62 63 65 68 69 71 72 75 80 81 86 95
Drug Number
(B)
AKN1
CCSW
CCLP
Normalized MTT readings
2.0
1.5
1.0
0.5
0.0
1 7 10 12 13 14 17 22 24 33 35 40 46 50 56 76 77 87 89 92 94 98 109
Drug Number

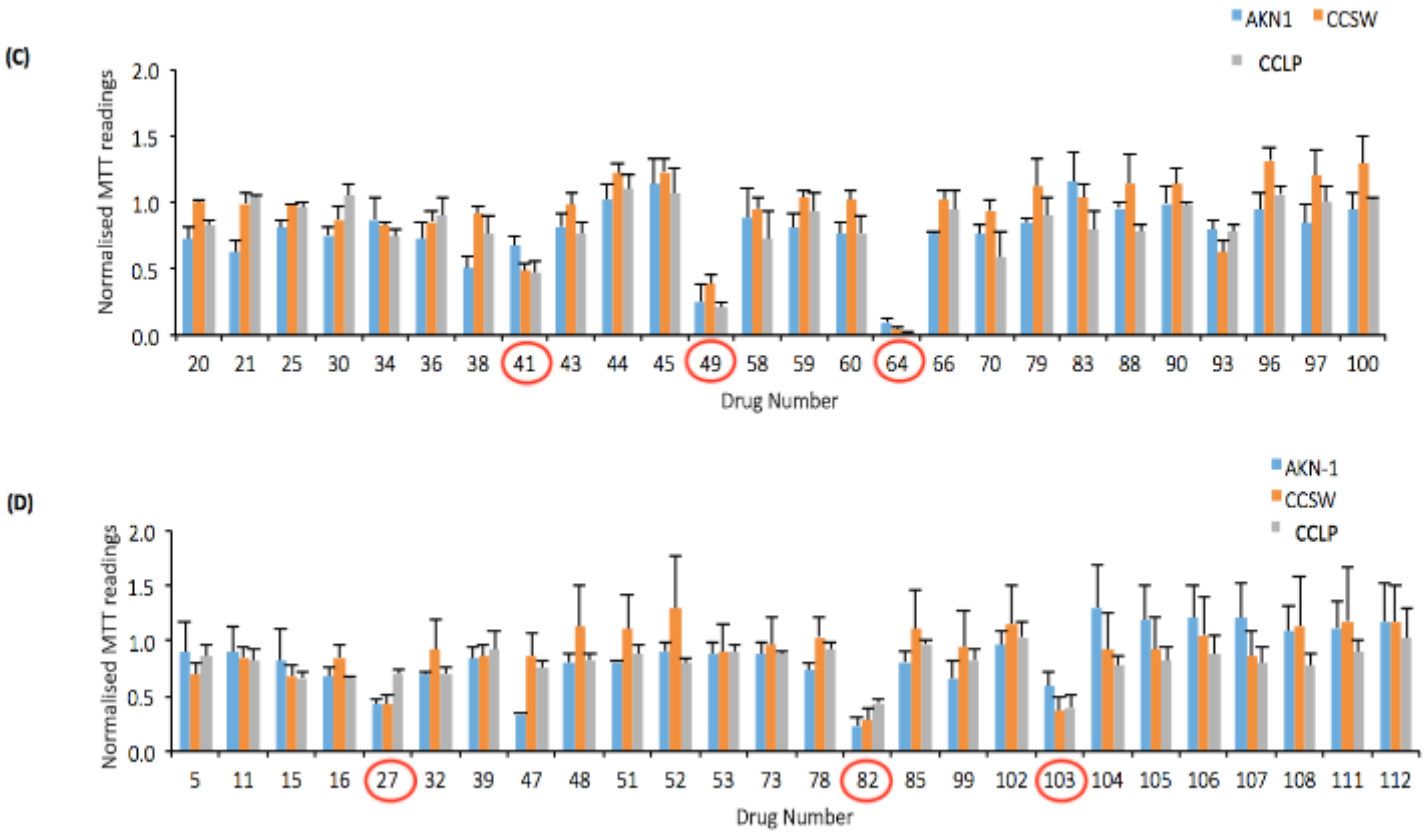

Figure 6.7 Repurposing drug screening by MTT assay. Drug screenings were carried out 3 times using MTT assay on CCLP, CCSW and AKN-1 cells. Cells were incubated with the drugs for 96 hours. Red circle indicates drug candidates selected for further experiments.

Drug Number	Drug Name	AKN-1 p-value	CCSW p-value	CCLP p-value
1	Prednisolone	0.501	0.063	0.189
2	Amantidine hydrochloride	0.538	0.516	0.474
3	Folic acid	0.884	0.825	0.333
4	Thiamine HCl	0.587	0.370	0.361
5	Ranitidine/zantac	0.670	0.113	0.314
6	Fluoxetine	0.657	0.321	0.858
7	Dexamethasone	0.607	0.100	0.282
9	Phytomenadione/ vitamin K1	0.772	0.280	0.609
10	Carbamazepine	0.302	0.270	0.376
11	Propanolol hydrochloride	0.624	0.316	0.218
12	Erythromycin	0.335	0.949	0.654
13	Retinol	0.713	0.212	0.218
14	Bendroflumethiazide	0.939	0.254	0.785
15	Propylthiouracil	0.537	0.134	0.041
16	Nicotinic acid	0.126	0.262	0.002
17	Theophylline	0.943	0.929	0.234
18	Nicotinamide	0.163	0.508	0.758
19	Ascorbic acid	0.131	0.099	0.059
20	Acyclovir	0.064	0.858	0.111
21	Allopurinol	0.032	0.902	0.140
22	Chlorpheniramine disodium salt	0.919	0.948	0.636
23	Neostigmine	0.845	0.113	0.307
24	Alpha tocopheryl acetate	0.991	0.617	0.772
25	2-bromo-a-ergocryptine methanesulfonate salt/ bromocriptine	0.085	0.202	0.432
26	Cyclophosphamide	0.256	0.151	0.029
27	Imatinib	0.028	0.089	0.015
28	Zinc acetate	0.179	0.019	0.062
29	Valproic acid	0.630	0.096	0.049
30	Rifampicin	0.084	0.383	0.582
32	Praziquantel	0.035	0.487	0.052
33	Flutamide	0.917	0.751	0.254
34	Clomipramine	0.497	0.004	0.013
35	Testosterone	0.895	0.478	0.907
36	Calciferol/ergocalciferol	0.108	0.185	0.490
37	Doxycycline	0.515	0.215	0.067
38	Tetracycline	0.030	0.314	0.239
39	Ibuprofen	0.285	0.250	0.600
40	Norethisterone	0.968	0.935	0.698
41	Itraconazole	0.080	0.008	0.009
42	Methyldopa	0.335	0.261	0.143
43	Fenofibrate	0.222	0.957	0.075

44	Clofibric acid	0.955	0.155	0.477
45	Clobetasol propionate	0.583	0.161	0.617
46	Paracetamol (acetaminophen)	0.930	0.495	0.798
47	Alverine citrate	0.016	0.365	0.077
48	Mefenamic acid	0.177	0.888	0.120
49	Prochlorperazine	0.054	0.001	0.012
50	Chlorambucil	0.437	0.018	0.222
51	Metoclopromide HCL	0.044	0.893	0.237
52	Domperidone	0.379	0.809	0.069
53	Thalidomide	0.395	0.444	0.212
54	Chloroquine	0.912	0.223	0.339
55	Metformin hydrochloride	0.220	0.293	0.188
56	Niclosamide	0.178	0.020	0.006
57	Pravastatin sodium	0.112	0.443	0.134
58	Nortryptyline	0.715	0.558	0.261
59	Dantrolene sodium	0.211	0.760	0.787
60	Omeprazole	0.109	0.964	0.187
61	Diclofenac sodium	0.273	0.170	0.267
62	Ritodrine hydrochloride	0.100	0.112	0.355
63	Selegiline hydrochloride / deprenyl HCl	0.377	0.422	0.343
64	Mebendazole	0.050	0.020	0.018
65	Flupentixol	0.258	0.672	0.224
66	Acipimox	0.002	0.813	0.728
68	Desferrioxamine mesilate	0.117	0.080	0.041
69	Imipramine	0.337	0.584	0.093
70	Artemisinin	0.123	0.453	0.163
71	Propantheline bromide	0.711	0.211	0.086
72	Diltiazem hydrochloride	0.717	0.566	0.169
73	Ampicillin sodium salt	0.394	0.542	0.016
75	Amphotericin b	0.246	0.043	0.002
76	Danazol	0.326	0.536	0.509
77	Phenoxymethyl penicillin**	0.228	0.751	0.648
78	5'aminosalicyclic acid/ mesalazine	0.079	0.796	0.350
79	Finasteride	0.024	0.561	0.533
80	Colchicine	0.111	0.050	0.034
81	Levothyroxine sodium	0.795	0.300	0.009
82	Methotrexate	0.024	0.095	0.009
83	Mifepristone	0.525	0.739	0.262
85	Cefaclor	0.248	0.867	0.467
86	Cyanocobalamin (vitamin B12)	0.622	0.634	0.065
87	Medroxyprogesterone acetate	0.273	0.530	0.753
88	Bezafibrate	0.371	0.668	0.134
89	Paroxetine	0.550	0.907	0.602

90	**Trimethoprim**	0.984	0.439	0.600
92	**Naloxone hydrochloride**	0.812	0.677	0.820
93	**Simvastatin**	0.080	0.109	0.112
94	**Flecainide acetate**	0.588	0.345	0.764
95	**Pilocarpine HCl**	0.803	0.777	0.351
96	**Fluconazole**	0.787	0.043	0.487
97	**Acitretin**	0.428	0.491	0.830
98	**Chloramphenicol**	0.892	0.370	0.878
99	**Bortezamib**	0.150	0.541	0.232
100	**Phenelzine**	0.854	0.323	0.489
102	**Clomiphene citrate**	0.684	0.983	0.912
103	**Carvedilol**	0.019	0.098	0.063
104	**Amidorone**	0.561	0.509	0.152
105	**Methylphenidate**	0.667	0.489	0.293
106	**Selenium**	0.659	0.748	0.494
107	**Merperidine phenidate**	0.659	0.373	0.337
108	**ABT-199**	0.853	0.874	0.162
109	**Riboflavin**	0.951	0.159	0.071
111	**Memantine**	0.784	0.952	0.402
112	**Magesium Sulfate**	0.738	0.861	0.977

Table 9 Effect of various compounds on CCLP, CCSW and immortalised cell line AKN-1. Statistical analysis performed using a paired, two-tailed t-test followed by Benjamini-Hochberg multiple corrections to identify compounds of interest. Drugs highlighted in red represent significant values for the compounds that resulted in a significant decrease in cell viability ($p<0.05$).

We ideally would like to identify drugs that have a much greater effect on highly tumourigenic cells compared to immortalized and normal cells. Therefore, 6 of the 104 drugs were picked for further analysis because they appeared to show a weaker inhibition in AKN-1 immortalized bile duct cells compared to the cytotoxic inhibition in CCLP and CCSW tumour cell lines in the screen. The six drugs chosen were Ascorbic acid, Zinc acetate, Niclosamide, Mebendazol, Deferrioxamine mesilate and Colchicine.

Ascorbic acid (Vitamin C) is a dietary supplement that has previously been demonstrated to induce a cytotoxic effect on CCA cells (Wang et al., 2017). Zinc acetate is a drug that is currently used for patients with Zinc deficiency (Hosui et al., 2018). Both Niclosamide and Mebendazol are antiparasitic drugs for tapeworm infestation and Niclosamide has recently been investigated and shown to have antitumour effect in multiple cancer types

such as leukaemia through the Notch and Wnt signaling pathways (Sawanyawisuth et al., 2014). Mebendazol is proposed to have both pro-apoptotic effects and an inhibitory effect on proliferation in CCA cell lines (Sawanyawisuth et al., 2014). Colchicine has anti-mitotic effects on lung and gastric cancer cells (Lin et al., 2016). Deferioxamine mesylate is an iron chelator that is used to treat iron overload and it is shown to induce apoptosis in a breast cancer cell line (Jiang et al., 2002).

In order to determine the dose at which 50% of cells remain viable after 96 hours of treatment (Effective dose 50), MTT assays were carried out following treatment with serial logarithmic dilution of the drug from the peak value used in serum. This generated dose response curves for these drugs candidates in four different cell lines CCLP, CCSW, KKU100 and KKU213. The experimental setup for the dose response curves is the same as described for Palbociclib dose response curves except that the cells were incubated with the drugs for 96 hours instead of 24 hours **(Figure 6.8)**. As the cells were incubated with the drug for 96 hours, the MTT reading (cell viability) reports on the combination of cell growth over 96 hours and the inhibitory effect of the drug. Thus, the effective dose 50 (ED50) at 96 hours is calculated instead of LD50 from each of the response curves for each drug in each cell line reported in **Figure 6.8**.

To determine the effects of each drug on proliferation in CCLP cells, Edu proliferation assays were performed after 96 hours incubation of the cells with each of the 6 drug candidates at their ED50 concentration in CCLP cells. **Figure 6.9Ai** shows how the experiment was organized and the timeline of the setup. **Figure 6.9Aii** shows that Mebendozole, Niclosamide and Cochicine can inhibit the proliferation of CCLP cells compared to cells treated with vehicle controls.

In order to investigate whether the six drug candidates induce apoptosis in CCLP cells, Caspase-3 apoptosis assays were performed. The timeline of the experiment setup is shown in **Figure 6.9Bi**. All six of the drug candidates have a significant stimulatory effect on promoting apoptosis levels in CCLP cells (**Figure 6.9Bii)**.

Finally, invasion assays were carried out to investigate whether the drug candidates can inhibit the invasion of CCLP cells. CCLP cells were treated with each drug or vehicle control at their ED50 for 96 hours in a 6-well plate. At 48 hours following drug incubation, 1 mM hydroxyurea was added to inhibit proliferation. At 72 hours, 5 x 10^4 cells were replated and grown in the presence of hydroxyurea and drug in 24-well plates containing transwell filter inserts. At 96 hours, the invading cells were measured (See **M&M section 2.9.2**). The experimental details and timeline are shown in **Figure 6.9Ci**. None of the drug candidates successfully inhibit the invasion of CCLP cells, rather, Niclosamide and Deferrioxamine mesilate increased their invasive capacity under the conditions tested **(Figure 6.9Cii)**.

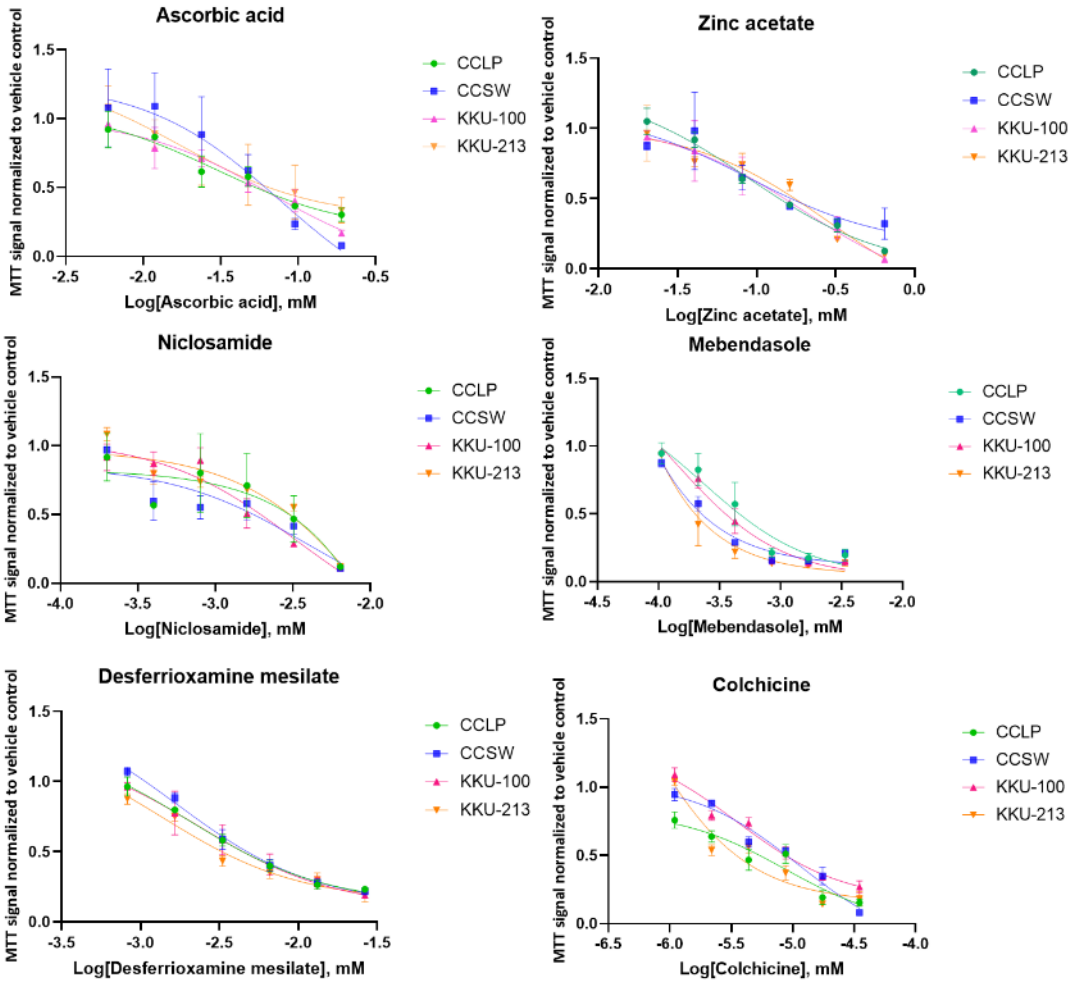

Figure 6.8 Dose response curves for selected drug candidates. CCLP, CCSW, KKU-100 and KKU-213 cell lines were treated with 6 drug candidates or with vehicle control for 96 hours. MTT assays were then performed in triplicate for each cell lines and the experiment were repeated 3 times for 3 different passages. The error bars show the SD of three experimental repeats.

ED50 of drugs (µM)	CCLP	CCSW	KKU-100	KKU-213	Peak concentration in serum
Ascrobic acid	73.41	53.21	42.63	55.24	95 (Lykkesfeldt and Tveden-Nyborg, 2019)
Zinc Acetate	327.79	327.46	397.13	396.77	323.4 (Katayama et al., 2020)
Niclosamide	2.52	1.55	2.03	2.3	3.2 (Schweizer et al., 2018)
Mebendazole	0.58	0.41	0.36	0.38	1.7 (Bekhti, 1985)
Desferrioxamine mesilate	11.92	10.83	9.86	10.8	13.2 (Gomez et al., 1997)
Colchicine	0.013	0.014	0.018	0.012	0.018 (Berkun et al., 2012)

Table 10 Dose response curves for selected drug candidates. CCLP, CCSW, KKU-100 and KKU-213 cell lines were treated with 6 drug candidates or with vehicle control for 96 hours. MTT assays were then performed in triplicate for each cell lines and the experiment were repeated 3 times for 3 different passages. The error bars show the SD of three experimental repeats.

Edu proliferation assay

(Ai)

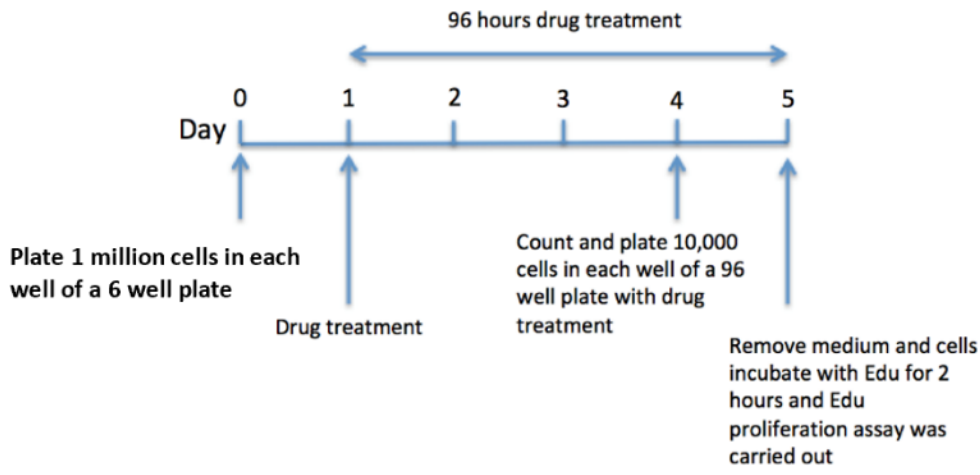

(Aii)

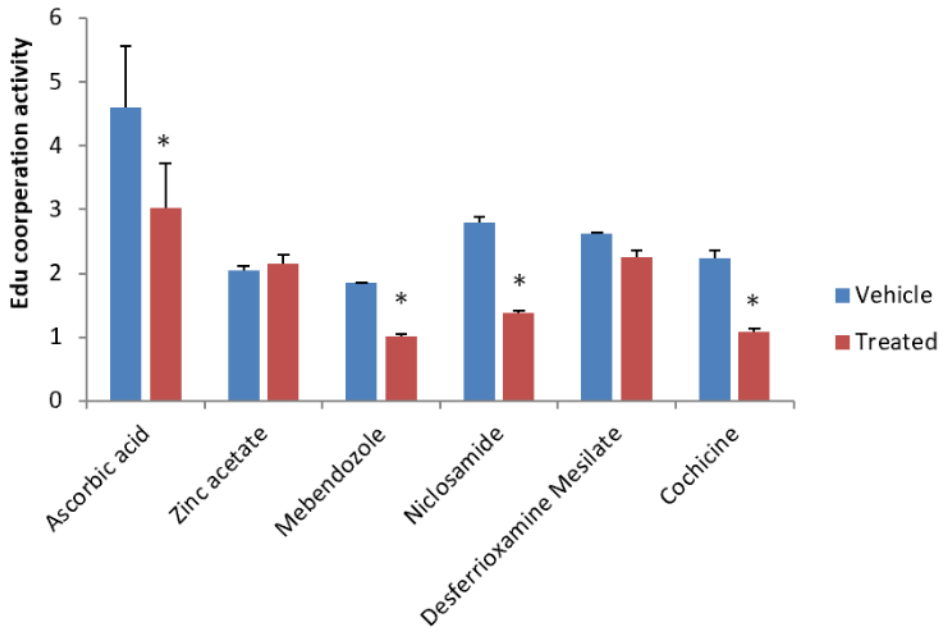

Caspase-3 apoptosis assay

(Bi)

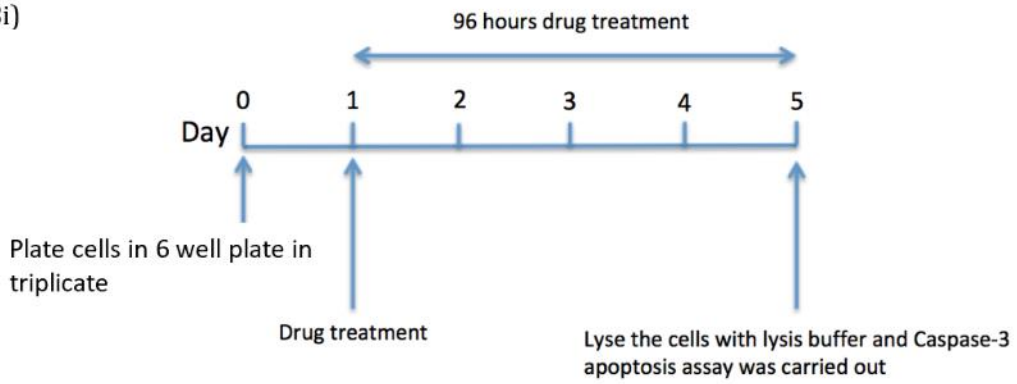

(Bii)

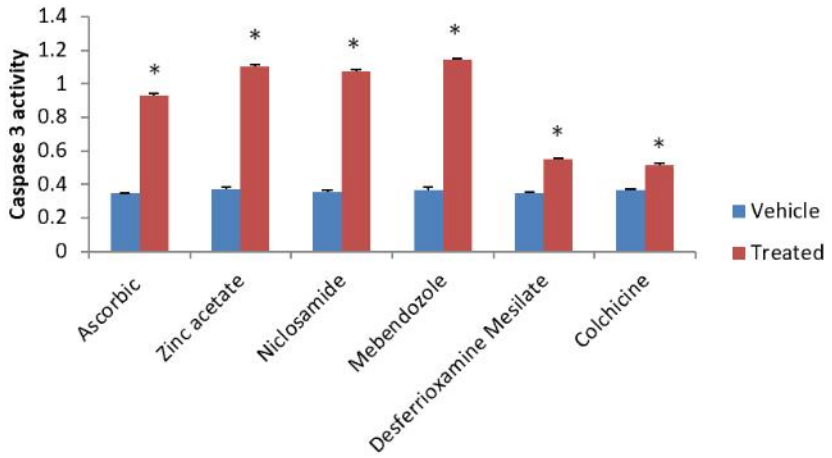

Transwell invasion assay

(Ci)

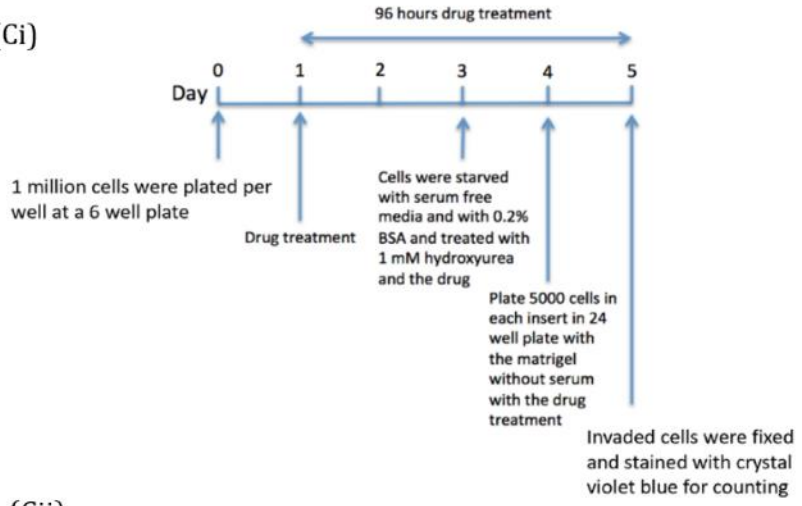

(Cii)

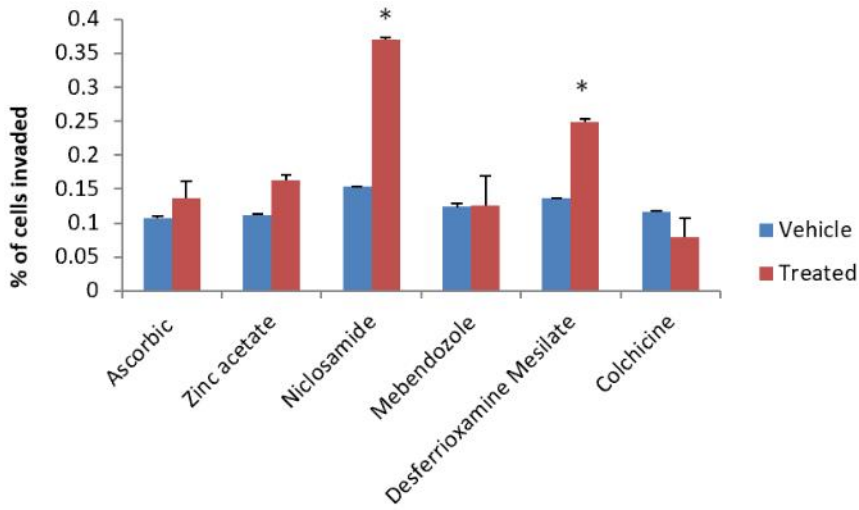

Figure 6.9 Effect of drug candidates on CCLP cells. (A) Edu proliferation assays on CCLP cells treated with drug candidates at their LD50 with corresponding vehicle controls. Statistical test: Two-tailed unpair T-test (n=3; *p<0.05) (B) Caspase-3 apoptosis assays on CCLP cells treated with drug candidates at their ED50 with corresponding vehicle controls. Statistical test: Two-tailed unpair T-test (n=3; *p<0.05) (C) Invasion assays on CCLP cells treated with drug candidates at their ED50 with corresponding vehicle controls. Statistical test: Two-tailed unpair T-test (n=3; *p<0.05). The error bars show the SD of three experimental repeats.

Suliman et al. showed that Niclosamide decreases Notch3 protein expression in colon cancer and that the decrease of Notch3 protein expression level by Niclosamide is part

of the mechanism by which Niclosamide inhibits colon cancer progression (Suliman et al., 2016). As previously we have shown that Notch3 activates PRH protein expression in CCA cell lines, we investigated whether Niclosamide treatment alters Notch3 and PRH levels in CCLP cells. CCLP cells (1×10^6) were treated with Niclosamide at its ED50 or with vehicle control for 96 hours in one well of a 6 well plate and protein was extracted. Western blotting was then performed with the extracted protein lysate using Notch3, PRH and ß-actin antibodies. **Figure 6.10** shows that Niclosamide downregulates both Notch3 and PRH expression in CCLP, CCSW and KKU-213 cells. Moreover, Niclosamide also decreases Notch3 expression. These findings are in agreement with the known inhibitory effects of Niclosamide on Notch3 expression in colon cancer (Suliman et al., 2016). The effect of Niclosamide on PRH has not previously been described but decreased Notch3 and PRH could be part of the mechanism underlying the Niclosamide-dependent inhibition of cell viability in CCLP cells.

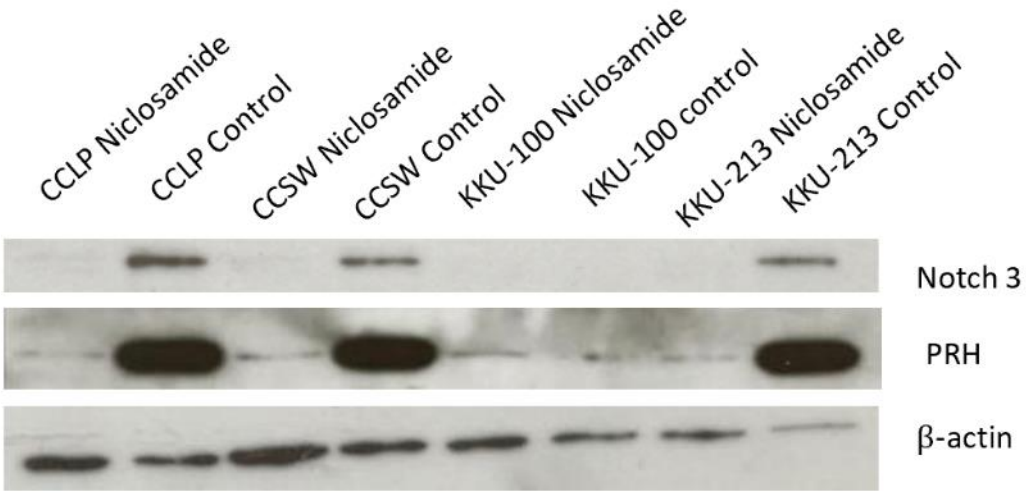

Figure 6.10 Niclosamide treatment (2.5 µM) downregulate PRH expression in CCA cell lines. Representative Western blotting showing Niclosamide treatment downregulates PRH expression and Notch3 expression in three CCA cell lines including CCLP, CCSW and KKU-213. 10 µg of protein was loaded into each lane. (n=3)

6.3 Drug combination

CCLP cells were treated with combinations of any 2 of the 6 drug candidates chosen in the screen to identify combinations that increase cytotoxicity. Additionally, the effect of Palbociclib treatment for 96 hours was also examined in combination with the six drugs from the screen. MTT assays were performed on CCLP cells treated with different concentrations of Palbociclib for 96 hours to generate a dose response curve and the ED50 for Palbociclib treatment alone was calculated exactly as described previously **(Figure 6.11)**. For combination assay, CCLP cells were incubated with each drug alone at their ED50 concentration or in pairwise combinations with each drug incubated at its ED50. After incubating cells for 96 hours MTT assays were performed. **Figure 6.12A** shows the MTT assay readings for the cells at 96 hours with each combination or with each drug alone. As expected, incubation with single drug alone in each case results in a vehicle normalized MTT reading of approximately 0.5 indicating that 50% cells are

viable (right hand ED50 column in **Figure 6.12A)**. The drug combinations that resulted in a cell viability 10 times lower than expected for the ED50 for each drug alone are highlighted in yellow **(Figure 6.12A)**. To determine whether the combination effects on cell viability are reproducible in another cell line, the experiments were repeated in CCSW cells. A dose response curve for CCSW cells treated with Palbociclib for 96 hours were obtained from performing MTT assays as described above **(Figure 6.12)**. **Figure 6.12B** shows that the same combination had similar effects in CCSW cells. **Table 11** shows the list of drug combinations in CCLP and CCSW cells that results in a much greater reduction in cell viability than each drug alone. In order to determine if similar effects on cell viability can be observed in the Thai CCA cell lines, these combinations were used in MTT assays with KKU-100 and KKU-213 cell lines as described above. The dose response curve for KKU-100 and KKU-213 treated with Palbociclib for 96 hours are shown in **Figure 6.11** and the ED50 is calculated for Palbociclib in each cell line. **Figure 6.13** showed that the drug combinations have similar effects on KKU-213 and KKU-100 cell lines.

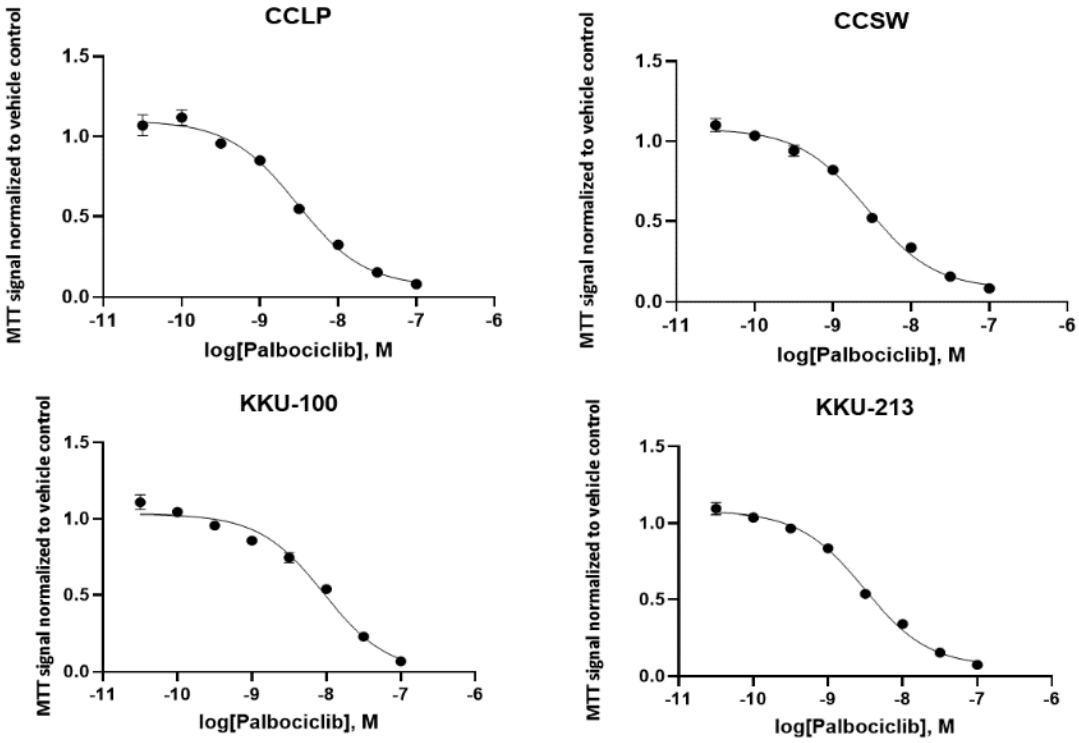

Figure 6.11 Dose response curve of Palbociclib for CCA cell lines. Cells were incubated with Palbociclib for 96 hours at concentration ranging from 0.03 nM to 100 nM. MTT assays were then carried out in triplicate. The ED50 of CCLP, CCSW and KKU-214 with Palbociclib treatment for 96 hours is 80 nM and 65 nM for KKU-100. The assays were repeated 3 times with different passages of the cells. The error bars show the SD of three experimental repeats.

(A)

Average	Ascorbic acid	Zinc acetate	Niclosamide	Mebendozole	Desferrioxamine Mesilate	Colchicine	Palbociclib	ED50
Ascorbic acid	0.18							0.49
Zinc acetate	0.34	0.14						0.43
Niclosamide	0.49	0.015	0.124					0.509
Mebendozole	0.15	0.012	0.208	0.12				0.48
Desferrioxamine Mesilate	0.44	0.015	0.46	0.19	0.37			0.54
Colchicine	0.38	0.017	0.32	0.094	0.51	0.37		0.506
Palbociclib	0.014	0.015	0.014	0.13	0.14	0.086	0.046	0.43

(B)

Average	Ascorbic acid	Zinc acetate	Niclosamide	Mebendozole	Desferrioxamine Mesilate	Colchicine	Palbociclib	ED50
Ascorbic	0.19							0.47
Zinc acetate	0.34	0.12						0.47
Niclosamide	0.45	0.016	0.099					0.49
Mebendozole	0.16	0.027	0.32	0.13				0.48
Desferrioxamine Mesilate	0.36	0.017	0.407	0.12	0.401			0.50 3
Colchicine	0.37	0.013	0.33	0.11	0.46	0.34		0.52
Palbociclib	0.015	0.015	0.018	0.16	0.15	0.21	0.12	0.47

Figure 6.12 The survival rate of the drug combination treatment. (A) MTT assays were carried out on the drug combination at the ED50 on both drugs on (A) CCLP and (B) CCSW. The numbers are the MTT signal of the average of the triplicate on 96 well plates. Numbers highlighted in colors indicated the drug effect on the cells are 10 times higher than the single drug treatment at ED50. (n=3)

Selected Drug combination from CCLP and CCSW
Zinc acetate and Niclosamide
Zinc acetate and Mebendazole
Zinc acetate and Desferrioxamine Mesilate
Zinc acetate and Colchicine
Palbociclib and Ascorbic acid
Palbociclib and Zinc acetate
Palbociclib and Niclosamide

Table 11 List of drug combinations that are shown to be 10 times more effective than single drug treatment in CCLP and CCSW cells.

(A)

Average	Ascorbic acid	zinc acetate	Niclosamide	Mebendozole	Desferrio xamine Mesilate	Colchicine	Palbociclib	ED50
Ascorbic acid								0.44
Zinc acetate								0.47
Niclosamide		0.021						0.52
Mebendozole		0.16						0.48
Desferrioxam ine Mesilate		0.16						0.53
Colchicine		0.56						0.5
Palbociclib	0.14	0.014	0.019					0.48

(B)

Average	Ascorbic acid	Zinc acetate	Niclosamide	Mebendozole	Desferrio xamine Mesilate	Colchicine	Palbociclib	ED50
Ascorbic acid								0.46
Zinc acetate								0.52
Niclosamide		0.0209						0.49
Mebendozole		0.095						0.51
Desferrioxam ine Mesilate		0.129						0.47
Colchicine		0.52						0.48
Palbociclib	0.16	0.015	0.018					0.48

Figure 6.13 The survival rate of selected drug combination treatment. (A) MTT assays were carried out on the drug combination at the ED50 on both drugs on (A) KKU-100 and (B) KKU-213. The numbers are the MTT signal of the average of the three wells on 96 well plates. Numbers highlighted in colors indicated the drug effect on the cells are 10 times higher than the single drug treatment at ED50. (n=3)

In order to examine whether the increased effect of the drug combinations on cell viability of the CCA cell lines is synergistic or additive, the Chou Talalay method was used. The Chou-Talalay method for drug combination is based on the median-effect equation. The resulting Combination Index (CI) theorem of Chou-Talalay offers quantitative definition for additive effect (CI = 1), synergism (CI < 1), and antagonism (CI > 1) in drug combinations. The drug combination that was further investigated was Palbociclib with Niclosamide. The experimental design is shown in **Figure 6.14A**. MTT assays were performed on CCLP cells treated with Palbociclib or Niclosamide at concentrations ranging from 0.125 times of their ED50 to 8 times their ED50 at a constant ratio. The MTT reading is proportional to cell viability and the MTT reading was converted to drug effect by calculating one minus the MTT signal for each combination. The drug effect for each combination was then inserted into Compusyn software which calculated the CI for the combination. The experiment was repeated three times independently in all four cell lines. **Figure 6.14** shows the CI for the drug combinations in all cell lines: CCLP, CCSW, KKU-100 and KKU-213 respectively. The selected drug combinations show CI with less than 1 in all cell lines indicating a synergistic effect of Palbociclib with Niclosamide in all four cell lines.

A Vimentin inhibitor, FiVE1 was also investigated in combination with Niclosamide using the Chou Talalay method. A dose response curve for FiVE1 on CCLP cells was generated as described previously and the ED50 calculated **(Figure 6.15A)**. The two drugs were incubated for 96 hours with CCLP cells at their respective ED50 as described above. **Figure 6.15B** shows that this drug combination in contrast to Palbociclib with

Niclosamide, has antagonistic effects as the CI is above 1. To conclude, the combination of Palbociclib and Niclosamide on CCLP cells has a synergistic effect while the combination of FiVE1 with Niclosamide has an antagonistic effect on CCLP cells. Palbociclib and Niclosamide could be an interesting new combination whereby lower doses of both drugs could be used to provide a potent cytotoxic effect. Future work on toxicity in non-tumour cells will need to be assessed.

(A)

X= ED50	0.125x	0.25x	0.5x	x	2x	4x	8x
Palbociclib (nM)	10	20	40	80	160	320	640
Niclosamide (nM)	315	630	1260	2520	5040	10080	20160
Palbociclib + Niclosamide	Combine both drugs at their ED50 ratio Eg: 0.125x = Palbociclib 10 nM + Niclosamide 315 nM						

(B)

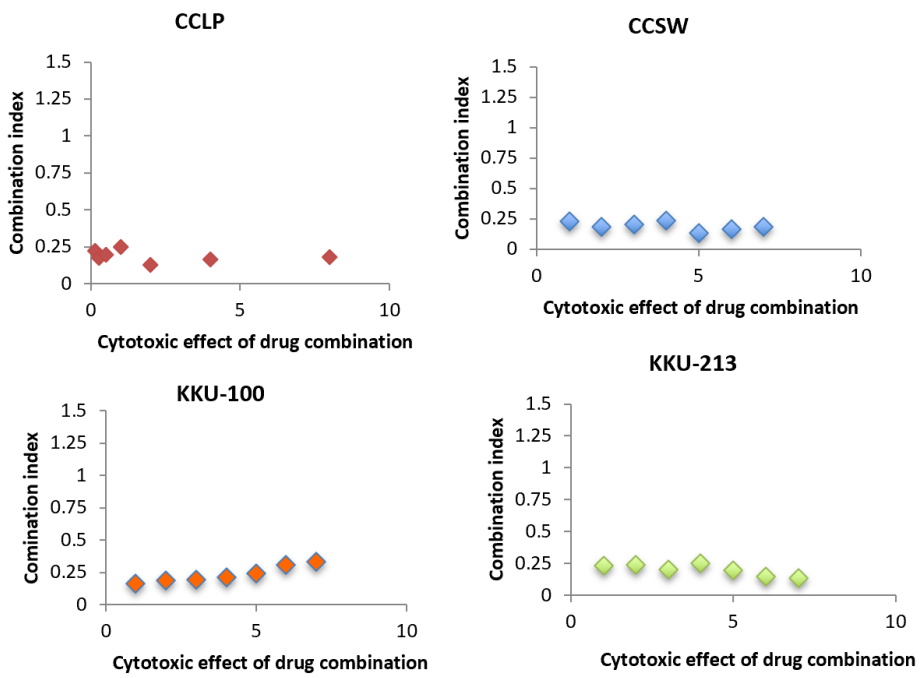

Figure 6.14 Synergism of drug combination Niclosamide with Palbociclib in CCA cell lines. (A) Setup of the drug synergism experiment. (B) MTT assays were carried out on four CCA cell lines with the drug combination Niclosamide and Palbociclib and the concentration range of 0.125x the ED50 to 8x the ED50 of the drugs were used. The combination index was calculated using the Compusyn software by inputing the data obtained from MTT assays.

(A)

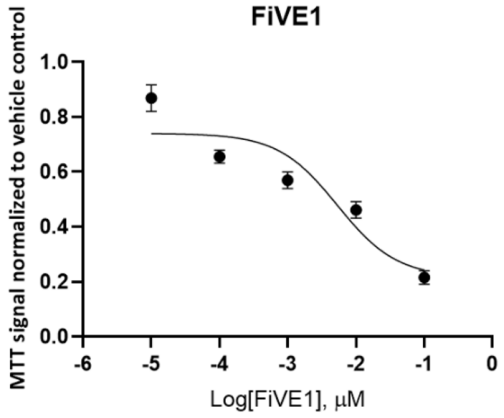

(B)

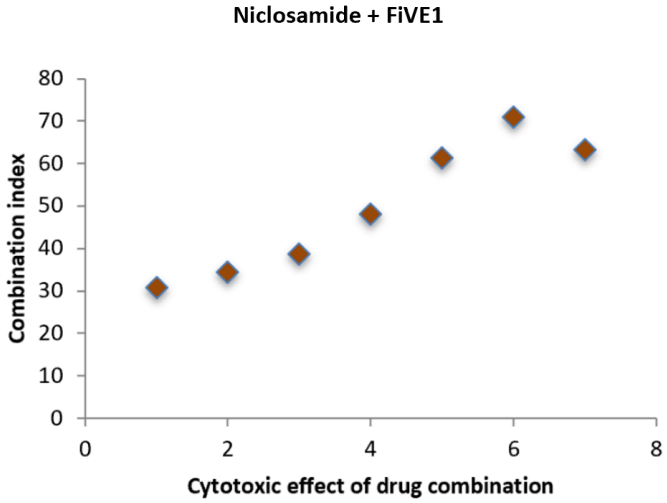

Figure 6.15 Synergism of drug combination FiVE1 with Niclosamide in CCA cell lines. (A) Dose response curve of FiVE1 in CCLP cells treated for 96 hours. The ED50 for CCLP with FiVE treatment for 96 hours is 349 nM. (B) MTT assays were carried out on CCLP with the drug combination Niclosamide and FiVE1 and the concentration range of 0.125x the ED50 to 8x the ED50 of the drugs were used. The combination index was calculated using the Compusyn software by inputing the data obtained from MTT assays.

CHAPTER 7

Discussion

7. Discussion

The experiments described in this thesis demonstrates that the *PRH/HHEX* gene and PRH/Hhex protein are highly expressed in CCA and that the PRH protein promotes cell proliferation, migration and invasion in CCA cell lines. Genome-wide analysis reveals that PRH regulates many signaling pathways and key genes involved in proliferation, cell cycle and in the Epithelial-mesenchymal transition (EMT). This thesis also examines the mechanisms underlying PRH regulation of some of these key gene and shows that Notch3 and PRH are in a regulatory loop and these factors co-regulate genes required for proliferation and EMT. Furthermore, this thesis shows that PRH regulates expression of the *VIM* gene which encodes Vimentin, a key marker of mesenchymal morphology. Vimentin is able to regulate cell proliferation of CCA cells and this thesis demonstrates the novel finding that specific cell cycle genes are regulated by Vimentin working in concert with PRH to control expression. Regarding therapeutic agents, this thesis demonstrates that PRH expression increases the sensitivity of CCA tumour cells towards Palbociclib. Furthermore, a drug repurposing screen identifies multiple compounds that are effective in reducing CCA proliferation *in vitro* when used both as single agents and in combination with Palbociclib.

7.1 PRH is an oncoprotein in CCA

The public RNA-seq data in the TCGA database shows that *PRH/HHEX* gene is not mutated or amplified in CCA. This is consistent with current literature as *PRH/HHEX* mutation is not reported in the literature in other cancer types. Instead we found that the *PRH/HHEX* gene is highly upregulated in CCA compared to its expression in other

cancer cohorts in the database. Although, *PRH/HHEX* does have oncogenic activity in some subtypes of leukemia, for example, *PRH/HHEX* mRNA expression is elevated in AML (McCormack et al., 2010) and *PRH/HHEX* is also an oncogene in a subtype of T-cell acute lymphoblastic leukemia known as early T-cell precursor-like ALL (ETP-ALL) (George et al., 2003; Smith et al., 2014). It was not expected that *PRH/HHEX* would be highly expressed in solid tumour cells, indeed *PRH/HHEX* has been shown to exhibit low expression in solid tumours in previous studies in breast cancer, prostate cancer and hepatocellular carcinoma (reviewed in Gaston et al., 2016). However *in vitro* experiments and xenograft experiments (performed by colleagues) using CCA cell lines produced in this study showed that PRH depletion leads to a reduction in the number of tumours and in tumour size (Kitchen et al., 2019). These results together with expression data in primary CCA tumours show that PRH plays an important role in promoting CCA *in vivo*.

Recent studies have identified different mutational signatures between liver fluke associated and non-fluke associated CCA (Jusakul et al., 2017). For example, *TP53* mutation is most frequent in the non-fluke associated CCA and *IDH1/2* is frequently associated with liver fluke related CCA (Jusakul et al., 2017). To further investigate the role of PRH in the etiology of CCA, PRH expression was examined in several cell lines mainly from Europe and Thailand with the Thai cell lines being associated with liver fluke infection. Since all of the CCA cell lines (Thai and European) show high PRH mRNA and protein expression compared with primary BECs (UK) and the immortalized AKN-1 cell line (European), regardless of the geographic region/liver fluke infection, we conclude that dysregulation of PRH is not specifically associated with liver fluke infection in the

cell lines studied. For future investigation, to examine whether PRH dysregulation is a common feature of CCA initiation and progression and independent of etiology, additional CCA lines, immortalized cells and primary BECs from patients who are known to have been previously infected with liver flukes should also be examined for PRH protein expression.

7.2 PRH increases tumour cell number and anoikis resistance in CCA

In our studies in CCA cell lines, PRH overexpression increased cell number and knockdown of PRH decreased cell number. Edu assays and apoptosis assays further showed that the changes in cell number are due to changes in proliferation rather than apoptosis. Alterations in PRH levels also affect anoikis resistance and tumour cell survival. Similar findings in PRH overexpressing AKN-1 cells and at least some primary BEC isolates support the idea that PRH regulates proliferation. It is noteworthy that BEC sample 2 did not respond in the same way as the other two isolates in all assays, presumably because of patient specific differences in the genetic background. However, in at least two of the BEC isolates elevated PRH confers increased proliferation and also tumour related properties such as anoikis resistance. The induction of anoikis resistance is unexpected and may be of great significance to tumour initiation as it shows that high PRH expression alone can confer some tumour properties on otherwise untransformed cells. The proliferation, anoikis resistance and survival properties of PRH in CCA contribute to its role as an oncoprotein. This is the first report of PRH as an oncoprotein in a solid cancer (Kitchen et al., 2019). PRH plays a similar role in MLL-ENL fusion protein driven AML; in a mouse model of MLL-ENL AML, PRH contributes to AML initiation as well as AML maintenance (Jackson et al., 2018; Shields et al., 2016b).

GSEA data from RNA seq experiments with PRH KD and PRH overexpressing CCLP cells reveal multiple signaling pathways that are regulated by PRH. Although the same genes are not regulated in both PRH KD and PRH overexpression conditions the same pathways are controlled by PRH through the regulation of a different set of genes under each experimental condition. These include gene sets that are known to regulate proliferation (G2M genes and cell cycle genes), cause cell morphological change or changes in apical junctions. The EMT and Notch pathways are also significantly enriched in conditions of PRH overexpression and are discussed in detail below. Several additional key pathways that were not intensively investigated in this thesis but are enriched in the GSEA of the RNA seq data include the estrogen signaling pathway (Sritana et al., 2018), p53 pathway (Maroni et al., 2012), TNFα pathway (Itatsu et al., 2009), Ras pathway and Wnt pathway. Each of these pathways could contribute to increased proliferation and/or anoikis resistance with PRH overexpression. However, the Ras pathway and the Wnt pathway require specific mention as they are well known to play an important role in the development of CCA. Gain of function *KRAS* gene mutation occurs in 25% of CCA patients and this results in activation of KRAS signaling and in turn activation of cell proliferation (Ahrendt et al., 2000; Eso et al., 2017). Activation of liver specific *KRAS* alone induces HCC but not CCA, however, activation of *KRAS* combined with *PTEN* deletion together in mice leads to both HCC and CCA (Ikenoue et al., 2016). *PTEN* is an inhibitor of the PI3K-Akt pathway, therefore, deletion of *PTEN* leads to activation of the PI3K-Akt pathway. The RNA-seq data shows that PRH inhibits *PTEN* expression in both AKN-1 cells and in at least some primary BEC cells (BECs donor 1). The KRAS signaling pathway is also strongly enriched in AKN-1 and primary BECs cell types. It can be hypothesized that initiation of

tumour formation occurs through PRH regulation of both the KRAS pathway and the PI3K pathway via PTEN in these cell types. In CCLP cells, the KRAS pathway is activated but, in these cells, PTEN expression is not altered; instead the PI3K pathway genes, *MYD88* and *AKT1* are upregulated in both CCLP and AKN-1 cells which is another way that PI3K pathway can be activated. Thus, in CCLP, the activation of PI3K/Akt signaling together with the KRAS pathway may be contributing to tumourigenesis. Further investigation is needed to understand the importance of the regulation of KRAS signaling pathway genes by PRH and the interaction of the Ras pathway and PI3K pathway.

In this study we noted that genes in the Wnt signaling pathway are regulated by PRH in CCLP, BECs donor 1 and 3 and AKN-1 cells. RNA-seq data shows differential expression of multiple Wnt genes including *WNT11*, *WNT16* and *TCF7L1* and ChIP-seq data shows that PRH binds near to the *WNT11*, *WNT16* and *TCF7L1* genes demonstrating that PRH directly regulates genes in the Wnt pathway. Additional reporter gene assays and sub-cellular localization studies for ß-catenin and E-cadherin performed by Dr. P Kitchen in the Jayaraman laboratory have suggested that PRH can drive autocrine Wnt signaling (Kitchen et al., 2019). Boulter et al. showed that macrophages provide a source of Wnt ligand and account for the aberrant Wnt signaling in CCA (Boulter et al., 2015; Loilome et al., 2014). Therefore, the aberrant Wnt signaling is not solely triggered by macrophages or macrophages are involved in the mechanism underlying how PRH directly regulates Wnt ligands.

7.3 PRH regulates cell proliferation through Notch signaling

Several studies have demonstrated the importance of Notch signaling in CCA development. In particular it was demonstrated *in vivo* that Notch signaling can promote CCA development through transforming hepatocytes into biliary cells (Fan et al., 2012; Sekiya and Suzuki, 2012). In this thesis we have focused on the PRH dependent regulation of the Notch signaling pathway, on the regulation of Notch3 in particular and the role of elevated Notch3 expression on the proliferation of both untransformed cells and tumour cells. We showed that PRH regulates the *NOTCH3* gene in CCLP cells and also in all other cell types. In fact, *NOTCH3* is one of the small number of genes (53 genes) differentially regulated by PRH in both PRH KD cells and PRH overexpressing CCLP cells suggesting that this gene is tightly controlled by PRH. Quantitative PCR and Western blotting further confirm that PRH positively regulates both *NOTCH3* transcription and Notch3/Notch3 ICD protein levels in CCLP and CCSW cells as well as in AKN1 and primary BECs (donor 1 and 3).

Unexpectedly, *PRH/HHEX* gene and protein expression is itself downregulated upon depletion of Notch3 demonstrating that PRH and Notch3 form a positive feedback loop. As PRH overexpression in Notch3 depleted CCLP cells results in no statistically significant changes in proliferation we conclude that the effects of PRH on proliferation are dependent on the activity of Notch3. Moreover, the expression of key genes required for proliferation such as *CCND2* (Cyclin D2) and genes required for epithelial to mesenchymal transition such as *CDH1* (E-cadherin) were also dependent on Notch3 expression indicating that they are co-regulated by both PRH and Notch3. The implication of a positive feedback loop between PRH and Notch3 is that changes in

either Notch3 or PRH would leads to activation of each other and thereby the expression of both PRH and Notch3 once initiated are maintained throughout the development of CCA. As mentioned above PRH regulates genes in the *PI3K/AKT* pathway including *MYD88* and *AKT1*. Deletion of Notch3 in mice significantly reduces CCA tumour growth and the mechanism through which Notch3 regulates tumour formation is through regulation of Notch3 target genes, such as the PI3K pathway genes, independently of its DNA binding partner RBPJ/CSL (Guest et al., 2016). It is possible that PRH and Notch3 also co-regulate PI3K pathway genes independently of RBPJ. Further investigation is required to test this possibility.

We investigated the mechanism by which PRH regulates *NOTCH3.* We have shown that PRH is unlikely to directly regulate *NOTCH3* through DNA binding as ChIP-seq experiments do not show PRH binding within 100kb of the *NOTCH3* gene. PRH overexpression experiments using wild type PRH and the PRH DNA binding mutant PRH N187A show that when this mutant protein is overexpressed, Notch3 protein levels remain unchanged. Since the regulation of Notch3 by PRH requires an intact PRH homeodomain this suggests that either DNA binding by PRH or interaction of PRH with other proteins through its homeodomain are required for regulation. Although PRH does not bind near the *NOTCH3* gene*,* the RNA-seq and ChIP-seq data shows that PRH regulates and binds within 30 kb of the 3' UTR of one of the key Notch3 target genes, *HES1.* We speculate that regulation of *HES1* by PRH is important for *NOTCH3* expression because Hes1 protein has many regulatory roles including regulation of the Notch proteins. Hes1 is a member of the hairy and enhancer of split (*HES*) family and it is one of the Notch signaling pathway canonical downstream effectors that repress

subsequent target genes that regulate differentiation, such as *MASH1* (Kageyama et al., 2007). It has been demonstrated that Hes1 is highly expressed in several CCA cell lines. Moreover, γ-secretase inhibitor treatment resulting in decreased Notch ICD on the CCA cell lines inhibit cell proliferation (Khatib et al., 2013). Hes1 can regulate Notch signaling and hence Notch1/3 ICD activity and both Notch3 ICD and Notch1 ICD can regulate the expression of *NOTCH3* gene (Zhang et al., 2019). Thus, the regulation of *NOTCH3* by PRH might be through the binding of PRH at the *HES1* gene.

In neural progenitor cell line, Hes1 interacts with Groucho/TLE protein to mediate transcriptional repression through chromatin remodeling and also interacts with protein kinase CK2 (Nuthall et al., 2002). PRH also interacts with both Groucho/TLE and CK2 (Noy et al., 2012; Soufi et al., 2009; Swingler et al., 2004b). We speculate that in addition to regulation of *HES1* transcription PRH could also regulate Hes1 post-translationally in CCA to impact Notch3 expression.

7.3.1 PRH regulates cell cycle genes independently and together with Notch3

The RNA-seq data from AKN1 cells overexpressing PRH shows that PRH increases *CCND1* gene expression in AKN1 cells. Similarly, PRH overexpression in primary BECs samples (donor 1 and 3) also regulated *CCND1* but this was not observed in the other primary BECs samples or in CCLP cells. Dysregulation of the genes regulating the cell cycle frequently occurs in cancer. In CCA, several studies have reported that the expression of cell cycle modulating proteins including Cyclin D1 are associated with CCA progression (Kang et al., 2002; Sugimachi et al., 2001). *CCND1* is known as one of the downstream targets of Notch signaling pathway in multiple cancer types. For example, in breast cancer, *CCND1* is a direct target of the Notch pathway mediated by *JAG1* (Cohen et al.,

2010). Notch3 promotes cell proliferation, migration and invasion through Cyclin D1 in glioma (Alqudah et al., 2013). The ability of PRH to regulate *CCND1* expression has been previously reported in different cell types. For example, PRH is capable of inhibiting *CCND1* mRNA transport in U937 leukemic cells post transcriptionally through binding to eIF4E (Topisirovic et al., 2003a). However PRH also activates *CCND1* expression in embryonic stem cell derived hematopoietic colonies (Paz et al., 2010) and in early lymphoid development (Goodings et al., 2015; Jackson et al., 2015). One reason for PRH not activating *CCND1* expression in CCLP cells is that *CCND1* expression could be already high in these cells. Indeed, high *CCND1* expression (in the absence of PRH overexpression) is observed in the RNA-seq normalized count data from CCLP cells. Instead the tumour cell lines CCLP and CCSW both show *CCND2* activation by PRH overexpression and *CCND2* is also activated when PRH is overexpressed in primary BEC donor 1 and 3 cells. Conversely, *CCND2* gene expression is downregulated when PRH is depleted in CCLP PRH KD cells. In Notch3 depleted cells, neither *CCND2* mRNA or protein can be increased upon PRH overexpression indicating that Notch3 is required together with PRH for the regulation of both the *CCND2* gene and Cyclin D2 protein. Again, this regulation requires the PRH homeodomain as *CCND2* gene expression remains unchanged in both CCLP and CCSW cells when PRH-N187A is expressed. We conclude that one of the mechanisms underlying the increase in proliferation by Notch3 and PRH is very likely to be through changes in expression of Cyclin D2. It should be noted that the primary BEC sample (donor 2) that shows no change of Cyclin D1 and Cyclin D2 expression, also shows no proliferation changes and no changes in Notch3 expression.

This reinforces the importance of the regulation of Cyclin D1 and Cyclin D2 expression by PRH and Notch3 on cell proliferation.

The majority of studies focus on the role of Cyclin D1 in the progression of CCA therefore, little is known about Cyclin D2 in CCA. However, Cyclin D2 has been found to be overexpressed in gastric cancer and colon cancer (Takano et al., 2000). Cyclin D2 also plays an important role in RUNX-ETO driven AML; Cyclin D2 activates CDK4/6 to stimulate the cell cycle and drive leukemia (Martinez-Soria et al., 2018). It can be concluded that PRH regulates *CCND1* and *CCND2* in different contexts. Regulation of *CCND1* might be more important in initiating CCA malignancy as it is increased by PRH in AKN-1 and BECs donors 1 and 3 cells whereas *CCND2* might be more important in CCA progression as this gene and protein becomes elevated in aggressive CCLP and CCSW.

In addition to co-regulation of Cyclin D proteins by Notch3 and PRH, the PRH protein also regulates cell cycle inhibitor genes. In CCA, there is insufficient expression of cell cycle inhibitors, for example, there is frequent loss of p16 and p27 in CCA patient samples (Kang et al., 2002). Here, we showed using RNA-seq, qPCR and a combination of ChIP-seq and ChIP-qPCR that PRH represses *CDKN1B* (p27) and *CDKN2B* (p15) genes and also directly binds to these genes in CCLP cells. p27 and p15 are both cyclin-dependent kinase inhibitors and they are known to be tumour suppressors that regulate the progression of G_1 phase (Choi and Anders, 2014). Repression of the cell cycle inhibitors to promote cell proliferation is consistent with the cell cycle analyses showing that the G_1 phase is altered in both PRH KD and PRH overexpressing CCLP cells.

It should be noted that besides decreasing G_1 in CCLP cells, exogenous PRH causes more cells to be held in G_2M phase. In addition, in RNA-seq experiments, PRH overexpression

leads to enrichment of a G_2M geneset. It is therefore possible that PRH decreases G1 and S through repression of cell cycle genes *CDKN1B* and *CDKN2B* (p27 and p15) and also modestly lengthens G_2/M through regulation of genes associated with G_2M such as *SMAD3* and *TGFB1* (Iordanskaia and Nawshad, 2011). However more analysis is required to determine the importance of the effects of PRH on the G_2M phase to cell division.

In other cell types PRH is known to repress genes encoding other cell cycle inhibitors such as *CDKN2A* (p16 and p19Arf proteins) and *CDKN1A* (p21). For example, in the MLL-ENL AML mouse model, loss of PRH leads to expression of *CDKN2A* (p16 and p19Arf proteins) and PRH overexpression causes repression of *CDKN2A* through recruitment of Polycomb repressor proteins (Shields et al., 2016b). Although *CDKN1A* (p16) was not altered in CCLP cells PRH did unexpectedly increase the expression of *CDKN2A* (p21). In some tumour types elevated expression of p21 occurs in the cytoplasm and this is related to tumour formation (Shamloo and Usluer, 2019). It is not known whether p21 is pro-oncogenic in CCA cells but this will be of value to investigate in the future. Figure 7.1 summarizes the effect of PRH on the cell cycle.

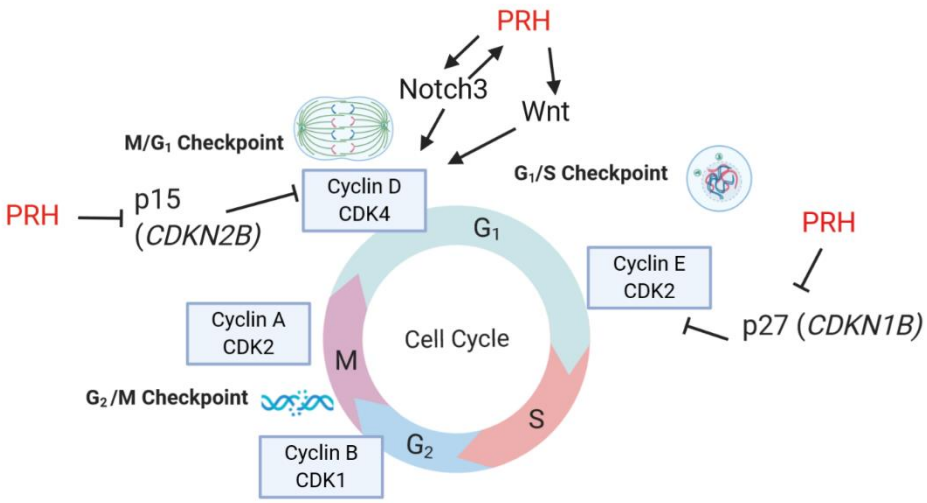

Figure 7.1 Regulation of cell cycle by PRH. PRH directly represses p15 and p27 and hence causes cell arrest in G1 phase and S phase.

7.3.2 PRH does not alter basal apoptosis in CCLP cells

PRH overexpression in CCLP cells does not increase basal apoptosis of the cells as measured by Annexin staining, however there is a small but reproducible increase in Caspase-3 activity in the cells. RNA-seq data shows that PRH does increase some genes associated with apoptosis including Baculoviral IAP Repeat Containing 3 (*BIRC3*) and Tumour necrosis factor super family member 15 (*TNFSF15)*. *BIRC3* is known to be an inhibitor of apoptosis and is highly expressed in HCC (Cao et al., 2018). *BIRC3* is downregulated by PRH OE CCLP cells. *TNFSF15* is an inducer of apoptosis in endothelial cells but little is known about its association with tumourigenesis (Xu et al., 2014). *TNFSF15* is upregulated in PRH overexpressing CCLP cells. The regulation of *BIRC3* and *TNFSF15* by PRH is consistent with the increase in Caspase-3 activity observed. We propose the presence of specific apoptotic inducers can increase apoptosis of CCLP cells when the apoptotic pathways are primed by high PRH expression but that the changes in gene expression (priming) brought about by PRH are insufficient to alter basal apoptosis of the CCLP cell line in the absence of additional inducers. It should be noted that the p53 protein in CCLP cells contains the p53R306 mutation that would remove the entirety of the p53 C-terminal tetramerization domain that is required for p53-mediated apoptosis (Chen et al., 1996). This mutation may make cells resistant to intrinsic apoptosis.

7.3.3 PRH regulates migration, invasion and EMT in CCA

PRH is able to increase the migration and invasion of all cell types investigated. GSEA of the RNA-seq data from CCLP tumour cells, AKN1 cells and BECs show that genes in the EMT hallmark pathway gene set are strongly enriched in every cell type. Thus, regulation of EMT pathway genes is clearly of importance to tumour initiation and also to tumour progression. The EMT hallmark set includes genes that are involved in EMT and also genes associated with migration and invasion. Interestingly genes encoding Collagens (present in the EMT hallmark set) are strongly differentially regulated across several cell types. For example, in BECs from donor 1, *COL1A1* is upregulated by PRH. Additionally, *COL11A1* and *COL5A2* are differentially regulated by PRH in tumour cells and untransformed cells. Collagen is reported as a prognostic factor associated with cancer invasion, cancer differentiation and cancer stages in various cancer types including breast cancer, prostate cancer, HCC and colorectal cancer (Xu et al., 2019). Collagen is the most abundant matrix protein polymer that plays an important role in the formation of the tumour microenvironment (Yamauchi et al., 2018). Deposition of collagen is one of the pathological characteristics of cancers including pancreatic cancer (Whatcott et al., 2015). The architecture of collagen can be altered by tumour suppressors or oncogenes. In breast cancer, mutated p53 alters the collagen bundle related to the cancer border and this results in increased proliferation and invasion of cancer (Kenny et al., 2017). Moreover, alteration in collagen along with oncogenes contributes to cancer progression. In pancreatic cells, Snail protein expression together with mutated *KRAS* leads to increased production of collagen and also deposition of collagen (Shields et al., 2013). Similarly in CCA, it was reported that in mice with p53 mutation, type I and

type III collagens are increased and stimulate biliary hyperplasia resulting in CCA progression (Farazi et al., 2006). Furthermore several genes encoding collagen were the top 10 significantly upregulated genes in a genome-wide integrative analysis of CCA associated genes including *COL1A1*, *COL4A1*, *COL10A1* and *COL4A2* (Zhong et al., 2018). Thus, the upregulation of collagens by PRH is likely to be of significance with regard to increased invasive capacity of all three cell types.

7.4 PRH regulates EMT pathway

7.4.1 PRH regulates epithelial cell marker, E-cadherin

It has long been considered in cancer that one of the mechanisms for epithelial cells to become migratory and invasive is to undergo epithelial-mesenchymal transition (EMT) (Thiery et al., 2009). It is widely considered that repression of E-cadherin is a landmark and crucial step for EMT and it is also known that repression of E-cadherin is associated with anoikis resistance (Derksen et al., 2006). In CCA, the loss of E-cadherin is commonly observed (Vaquero et al., 2017). Several oncogenes are known to regulate E-cadherin in CCA. Notch1 was shown to regulate EMT in CCA by inhibiting E-cadherin expression (Zhou et al., 2013). Sonic Hedgehog (Shh) was also reported to modulate E-cadherin expression in CCA and activates EMT (Khatib et al., 2013). In several tumour types, it has been shown that PRH is an inhibitor of EMT. For example, PRH directly represses the Goosecoid gene which is an inducer of EMT in breast cells (Brickman et al., 2000; Hartwell et al., 2006; Williams et al., 2008). It has also been shown that PRH can inhibit migration and EMT by activating the TGF-β co-receptor, Endoglin and this can occur in breast and prostate cancer cells (Kershaw et al., 2014).

In this thesis we show that PRH promotes EMT in keeping with its role as an oncoprotein. E-cadherin is expressed in untransformed cells and is repressed by elevated PRH in AKN-1 cells and BECs. Stable PRH overexpression causes AKN1 cells to undergo EMT and change their morphology and increase anoikis resistance. Transient expression of PRH in BECs is not sufficient to elicit morphological changes although it does induce anoikis resistance of cells that are normally dependent on cell-cell contacts. Many EMT markers are altered in both BECs and in AKN1 cells and PRH is also involved in regulating the process of migration and invasion in the normal and immortalized cells. In CCLP tumour cells the regulation of E-cadherin depends on both PRH and Notch3 because depletion of Notch3 prevents E-cadherin expression and this cannot be reinstated by elevated PRH expression alone. PRH can promote tumour invasion and further promote anoikis resistance in CCLP1 cells but morphological changes are not observed as the cells are already mesenchymal. Strikingly, in PRH depleted CCLP tumour cells, E-cadherin is restored and they appear epithelial as they undergo MET and become less migratory and invasive. In both overexpression and PRH KD conditions the EMT pathway is regulated.

The changes in E-cadherin brought about by PRH and the changes in invasion and migration are consistent with the idea that EMT and invasion are linked. However, it is still under debate whether there is a direct relationship between the loss of E-cadherin and the formation of mesenchymal cells. For example, overexpressing E-cadherin is not sufficient to block EMT in MDCK cells (Batlle et al., 2000). Recently, a study observed that loss of E-cadherin is needed for local invasion but that E-cadherin is required in cells for metastasis where it acts as a survival factor (Padmanaban et al., 2019b). Therefore,

during invasion and metastasis the cells may co-express epithelial and mesenchymal markers to exhibit a hybrid epithelial/mesenchymal phenotype (Chin and Lim, 2019). This might also occur during anoikis resistance to allow maintenance of the cell colonies (survival). The main signaling pathways that regulate EMT plasticity are Notch, Wnt and TGF-β signaling. For example, an inhibitor of the Notch pathway, Numb, is capable of preventing cells from fully transforming into the mesenchymal phenotype (Bocci et al., 2017). As PRH regulates both Notch and Wnt signaling pathways and also both epithelial and mesenchymal marker proteins such as E-cadherin and Vimentin, it is highly likely that PRH has a role in EMT plasticity.

In this study, it is shown using ChIP-seq data from CCLP cells overexpressing PRH that the regulation of E-cadherin by PRH does not appear to be through direct DNA binding close to the gene (less than 100kb). The results in CCLP cells are in contrast with previous data in prostate tumours where PRH inhibits EMT and also E-cadherin in prostate cancer in a tumour suppressive manner (Siddiqui et al., 2017). PRH was shown to regulate the E-cadherin (*CDH1*) gene and bind to the promoter in ChIP-seq experiments (Marcolino et al., 2020). The absence of PRH binding at the E-cadherin gene in CCLP cells could be a result of the absence of specific co-repressor proteins or altered accessibility to chromatin near the *CDH1* gene in CCLP cells. Although the regulation of E-cadherin by PRH is indirect, experiments using the PRH mutant (N187A) that lacks the ability to bind DNA show that the regulation of E-cadherin by PRH still requires an intact homeodomain and DNA binding. This implies that there is another gene or transcript involved in the regulation. The additional gene could be associated with other EMT TFs or indeed with the Notch pathway.

7.4.2 PRH regulates EMT-related junction proteins

A major finding in this thesis is that PRH is an inducer of EMT in BECs and an inducer of invasion in CCA. Of greatest significance, PRH can directly regulate the EMT marker protein Vimentin (discussed further below) as well as indirectly regulating not only the expression of E-cadherin but also the expression of multiple other cell surface receptors or junction proteins and additional EMT transcription factors.

For example, in both RNA-seq and Western blot data exogenous PRH represses Claudin1 in CCLP cells. Additionally RNA-seq data shows that multiple Claudins including *CLDN3, CLDN4, CLDN7* and *CLDN9* are repressed by PRH in AKN-1 cells and *CLDN4* is repressed BECs donors 1 and 3. Claudins are a family of transmembrane proteins that are important in tight junction maintenance (Tabariès and Siegel, 2017). The destruction of the integrity of tight junctions occurs in tumour development to allow tumour extravasation across the endothelial barrier (Tabariès and Siegel, 2017). Claudins are dysregulated in numerous cancer types as key components in tight junctions and Claudin 1, 3, 4 and 7 are the most commonly dysregulated Claudins in cancer (Singh et al., 2010). In CCA, Claudin4 was reported overexpressed and Claudin4 depletion resulted in reduced migration and invasion (Bunthot et al., 2012). However another study using IHC shows that Claudin1 expression is lower in poorly differentiated bile duct cancer and gall bladder cancer compared to moderately or well differentiated bile duct and gall bladder cancers (Németh et al., 2009). Further investigation needs to be carried out on more cell lines to investigate if the regulation of Claudin by PRH is important in causing EMT in CCA or simply a consequence of EMT.

7.4.3 PRH regulates EMT-related Transcription Factors

Although the expression of multiple EMT inducing transcription factors are shown to correlate with CCA, Snail is the most studied EMT transcription factor in CCA (Vaquero et al., 2017). High expression of Snail was shown to correlate with metastasis in CCA and can serve as a prognostic factor for patients with CCA (Techasen et al., 2012b). Consistent with the role of Snail as a direct repressor of E-cadherin, the expression of Snail is negatively correlated with E-cadherin in CCA (Huang et al., 2014). Of note, Snail is upregulated in both transcript and protein levels when PRH is overexpressed in CCLP cells implicating Snail expression in the increased invasive behavior of CCLP cells. In AKN-1 cells, *SNAI1* is upregulated by exogenous PRH. Additionally, in all PRH overexpressing BECs donors, the transcription of *SNAI1* is upregulated but not the transcription of other genes encoding EMT TFs such as *ZEB1* and *TWIST1*. We infer that Snail is both an important inducer of EMT and invasion in normal bile duct epithelial cells and a promoter of invasion in CCLP tumour cells. Interestingly, RNA-seq data produced by Dr P. Kitchen on the CCLP Notch3 KD cells overexpressing PRH showed the regulation of *SNAI1* by PRH is independent of Notch3 expression (P.K. /PSJ personal communication). Thus, in contrast to the regulation of E-cadherin by PRH the regulation of *SNAI1* is not Notch3 dependent.

The interplay of the microenvironment and the tumour epithelia is very important in CCA. Regarding the Notch signaling cascade, activation of Notch signaling is known to lead to EMT and inhibition of Notch1 leads to reduced Snail and Vimentin expression and results in reduced invasion and migration of CCA cells (Khatib et al., 2013). PRH is

clearly another important element in the signaling that leads to alterations in morphology and also in the signaling that leads to increased invasion.

7.4.4 PRH regulates mesenchymal marker, Vimentin

Apart from E-cadherin and EMT related transcription factors, the regulation of EMT by PRH also involves the key mesenchymal marker, Vimentin. Vimentin is a well-established mesenchymal marker and it plays a vital role in cancer progression through EMT and is responsible for cancer migration and invasion in colorectal cancer (Du et al., 2018).

GEPIA data in Chapter 3 shows that there is a correlation between the expression of PRH and Vimentin in patients with CCA. It was also shown in Chapter 5 that PRH activates *VIM* gene expression and protein expression in AKN1 cells and in BECs (donor 1). In Chapter 3 we also showed that PRH regulates Vimentin protein expression in CCLP cells. Surprisingly, neither the depletion of PRH nor the overexpression of PRH in CCLP tumour cells resulted in changes in regulation of the Vimentin gene in these cells. In Chapter 4, it was shown that this discrepancy is possible to be explained by the effects of cell confluency/density on the *VIM* gene. In growth conditions of low cell density, the CCLP tumour cells express less Vimentin compared to growth conditions of high cell density. When *VIM* is highly expressed in CCLP cells grown at high cell density, PRH is not able to increase the Vimentin mRNA expression further. The expression of *VIM* depending on the cell density was first demonstrated by A Ben Ze'ev using Madin-Darby bovine epithelial cells (MDBK) (Ben-Ze'ev, 1984). The study demonstrates that Vimentin synthesis is low in sparse cell culture and the expression of Vimentin is altered by cell-cell interaction (Ben-Ze'ev, 1984). Another study also shows that the expression of Vimentin depends on cell density in glioblastoma cells (Trog et al., 2008) and that the

expression of Vimentin is lower in low cell density (Trog et al., 2008). A similar trend of Vimentin expression was observed in the CCLP cells.

In breast cancer cells it was found that Vimentin can regulate cell migration in high cell density but not in low cell density (Messica et al., 2017). It is not known if the regulation of CCLP cell migration by Vimentin is affected by cell density but it can be hypothesized that cells grown at high cell density that express high Vimentin are likely to be more migratory compared to low cell density cells. Interestingly, cell density also affects expression of the endogenous *PRH/HHEX* gene in CCLP cells. It is likely that expression of genes encoding both Vimentin and PRH proteins are dependent on cell-cell interactions. In angiogenesis, Vimentin is able to regulate Notch ligands (Antfolk et al., 2017). Similarly, interactions involving Notch ligands with Notch receptors might also impact both *PRH/HHEX* and *VIM* gene expression and thereby influence cell motility. As the cell density affects experiment results, this highlights the limitation ofusing cell lines as a model system as cell lines do not necessary represent the tumour microenvironment *in vivo*. Further investigation is to conduct experiments using mouse model to validate results observed in cell lines.

7.4.5 PRH directly binds and interact with Vimentin

Although Vimentin is considered to be a cytoskeletal protein and is detected in the cell cytoplasm to control cell morphology and cell adhesion, recent studies revealed Vimentin is able to interact with the genome and is a potential regulator of gene expression (Yang et al., 2005). Vimentin is also known be highly phosphorylated and regulated by phosphorylation throughout mitosis (Duarte et al., 2019) and the phosphorylation is essential for normal mitosis to occur. It was shown that Vimentin

interacts with p53 in the cytosol in Rheumatoid Arthritis Synovial Fibroblasts (RASF). The studies together suggest that the interaction of Vimentin with genomic DNA is due to the fact that the Vimentin filament is tightly associated with nuclei and mitochondria (Tolstonog et al., 2000). The same research team also identified the N-terminus of Vimentin serves as a DNA binding site (Wang et al., 2000).

ChIP-seq data produced by Dr. P Kitchen was interrogated for binding of PRH near the Vimentin gene. ChIP-seq data shows that the regulation of Vimentin expression by PRH is through direct DNA binding of *PRH/HHEX* at the *VIM* gene at several positions across the gene including the 5' promoter region and across the last intron and 3' UTR region. Additionally, co-IP experiments demonstrate that Vimentin also interacts with PRH in the nucleus and the cytoplasm in both CCLP and AKN1 cells. The interaction between the proteins could be indirect and mediated in the nucleus through other nuclear proteins such as nuclear lamins or through binding to DNA. Co-IP experiments show that Vimentin interacts with the N-terminal region of PRH between amino acid 50 and 132; the PRH homeodomain also seems to be crucial for interacting with Vimentin protein as the PRH-N187A mutation at its homeodomain impairs but does not eliminate its ability to interact with Vimentin. A PRH chicken homologue bearing the equivalent mutation retains the ability to repress transcription when fused to the GAL4 DNA binding domain in luciferase reporter experiments demonstrating that the mutant protein is not completely misfolded (Muriel Guiral et al., 2001). The homeodomain of PRH does not only function by binding to DNA to repress transcription but interacts with other transcription factors to achieve transcriptional repression. For example, PRH interacts with the transcription factor AP-1 (Activator protein-1) using its homeodomain and

inhibits Fos/Jun heterodimerization (Schaefer et al., 2001). In the case of Vimentin in CCLP cells, the interaction of Vimentin with PRH requires both the N-terminus and the PRH homeodomain. It is possible that in order for Vimentin to interact with PRH, the PRH protein needs to be able to bind to Vimentin directly though the homeodomain. On the other hand, it is also possible that the mutation of the homeodomain of PRH causes an indirect effect, for example a change in the conformation of PRH resulting in Vimentin being not able to access and bind the N-terminus of PRH. The N-terminus of PRH amino acid 50-136 is known to contain a region that can mediate oligomerization through the homeodomain whereas the first 50 amino acids of N-terminus contain a dimerization region (reviewed in Soufi and Jayaraman, 2008). This oligomeric PRH protein is able to bind to DNA sequences with multiple PRH binding sites with high affinity compared to the full length PRH (Soufi and Jayaraman, 2008). Therefore, it is possible that the oligomerization of PRH is involved in the interaction between PRH and Vimentin and that Vimentin binding influences both the oligomerization and DNA binding properties of PRH. In support of the idea that Vimentin can influence DNA binding by PRH we showed in ChIP-qPCR experiments that Vimentin increases the binding of PRH at the *CDKN1B* gene. Furthermore, we showed that Vimentin regulates p27 expression in CCLP cells at gene and protein level.

Future experiments to substantiate these findings would be to carry out ChIP experiments with the Myc-PRH protein followed by re-ChIP of associated DNA with Vimentin antibodies. This experiment would be useful to confirm that binding of PRH to the *CDKN1B* gene also involves Vimentin binding. Additionally, direct ChIP of Vimentin

using Vimentin antibodies at the *CDKN1B* gene would also show whether Vimentin binds to additional regions at the *CDKN1B* gene.

Since the *VIM* gene is also a direct DNA binding target of PRH, it is possible that Vimentin could also influence its own expression through PRH. Direct Vimentin ChIP-qPCR using Vimentin antibodies and PCR at regions where PRH has been shown to bind, (for example within the last intron) would also be useful to confirm that Vimentin is interacting with chromatin at the same regions that PRH binds to the *VIM* gene.

Vimentin has previously been identified as a regulator of proliferation through its ability to regulate the expression of the p21 cell cycle protein in the nucleus (Mergui et al., 2010). This thesis shows that depletion of PRH or Vimentin has an additive effect on proliferation as both SiRNAVIM transfected into CCLP cells and the PRH KD CCLP cells are less proliferative than control cells. Moreover, the proliferation of the PRH depleted cells is further decreased when Vimentin is also depleted. These experiments are interpreted to indicate that PRH and Vimentin both have independent effects on proliferation. However, it is likely that there are also be some overlapping effects on proliferation presumably through the co-regulation of genes such as *CDKN1B.*

To sum up, we have shown PRH is involved in at least four aspects of the ten hallmarks of cancer shown in Figure 7.2. PRH regulates the Notch3 oncoprotein and together they regulate Cyclin D proteins and E-cadherin. PRH can directly regulate cell cycle inhibitor proteins and Vimentin. The regulation of these genes is involved in sustaining proliferation and promoting EMT and invasion. (Figure 7.2). Elevation of PRH can activate many of the same mechanisms in primary cells and in transformed cells.

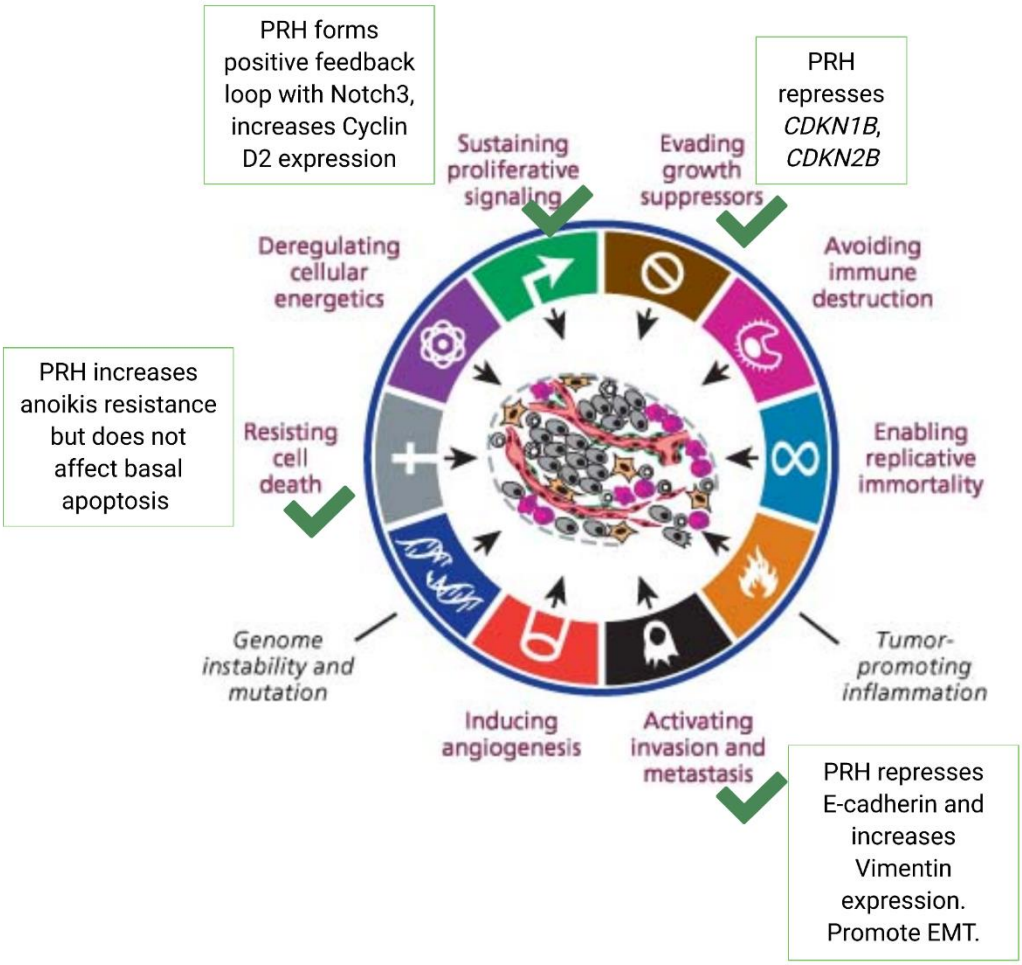

Figure 7.2 The overview of PRH in cancer hallmarks in CCA. PRH was investigated in four aspects of cancer hallmarks. Sustaining proliferative signaling: PRH activates Notch signaling and forms a positive feedback loop with Notch3. PRH also increases Cyclin D1, Cyclin D2 and activates the Wnt and KRAS signaling pathway. Evading growth suppressors: PRH directly represses cell dependent kinase inhibitors p15 and p27. Activating invasion and metastasis: PRH promotes EMT in both tumour and primary BECs. PRH represses E-cadherin and directly increases Vimentin expression and regulates the EMT transcription factor Snail and the junction protein, Claudin1. Resisting cell death: Although PRH does not regulate basal apoptosis in tumour cell lines, it increases anoikis resistance in tumour cell lines and also in primary BECs.

7.5 Novel therapeutic agents for CCA

CCA is a rare and highly aggressive malignancy and surgery is the only curative treatment option. However, the malignancy is often detected at inoperable stage and with poor prognosis. A standard first-line treatment for patients with inoperable CCA is chemotherapy with Gemcitabine and Cisplatin (Valle et al., 2010). Novel targeted therapies for CCA have recently been identified using genomic sequencing technology (Xue et al., 2019) including inhibitors for Fibroblast growth factor receptor 2 (*FGFR2*) gene fusions and the epigenetic regulator and enzyme Isocitrate dehydrogenase *IDH1/2. FGFR2* translocations were identified in around 13 % to 17 % of patients. Multiple inhibitors targeting FGFR pathway are now in phase 2 or phase 3 clinical trials. The clinical trials show promising results towards patients with *FGFR2* fusion (Javle et al., 2018). Pemigatinib is useful and has been licenced for treatment of FGF fusion driven CCA (Abou-Alfa et al., 2020). Apart from *FGFR*, *IDH1/2* is also mutated in approximately 20 % of patients with CCA. *IDH* mutation results in accumulation of 2-hydroxyglutarate that interferes with the function of DNA regulators and histone demethylation (Farshidfar et al., 2017b). Inhibitors of mutated *IDH1* are currently under phase III clinical trial and the survival outcome is significantly improved with good tolerance (Abou-Alfa et al., 2020a). Despite these promising avenues new treatments for the majority of patients without these mutations is still urgently needed.

7.5.1 PRH increases CCLP cells sensitivity towards Palbociclib

Genomic studies have identified activation of the cell cycle kinase CDK4/6 to commonly occur (20%) in CCA due to the mutation of *CDKN2A* gene encoding p16 p14Arf cell cycle inhibitory proteins. Palbociclib, an inhibitor for CDK4/6, is best known for its effect on

reducing proliferation in breast cancer and also glioma (Liu et al., 2018). In oncology clinics, Palbociclib is a current treatment for HER2+ ER- breast cancer (Serra et al., 2019). Recently, Palbociclib has also been shown to inhibit proliferation and promote apoptosis in bladder cancer cells in xenograft experiments (Zhang et al., 2019). Despite these promising studies, a recent small basket clinical trial for biliary and pancreatic cancers showed that Palbociclib had no significant effect on 10 patients with *CDKN2A* mutation and advanced CCA (Al Baghdadi et al., 2019). It is possible that the patients participate in this clinical trial do not have high PRH expression. However, it is also possible that PRH is highly expressed in these patients as suggested by the TCGA data and cells with high PRH level are not sensitive towards Palbociclib in clinical setting.

We showed that in multiple tumour cells lines (CCLP, CCSW, KKU-100 and KKU-213), Palbociclib is able to reduce both proliferation and increase apoptosis. Moreover, we showed that the effect of Palbociclib on proliferation and apoptosis increases with PRH expression although as expected the inhibitory effect of Palbociclib on proliferation is also dependent on Rb. A recent study investigating the effect of Palbociclib on CCA identified that the sensitivity of CCA towards Palbociclib is related to the activation of KRAS signaling (Sittithumcharee et al., 2019). In our RNA-seq data, GSEA using Hallmark gene-set shows that genes in the KRAS signaling pathway are enriched, such that PRH regulates multiple genes in this pathway in CCLP, AKN-1 and all the primary BECs samples. The regulation of KRAS signaling by PRH might be an explanation for the sensitivity of CCA cell lines showing high PRH expression. Therefore, instead of using Palbociclib for CCA patients with *CDKN2A* mutation, selection of patients with high PRH expression or with altered KRAS signaling pathway may result in a more successful

clinical outcome. However, more experiments are needed to investigate whether the sensitivity of cells towards Palbociclib is dependent on the regulation of KRAS signaling by PRH. Experiments that could be performed to investigate this is Palbociclib treatment of CCLP cells with KRAS knockdown or the use of Ras inhibitors with Palbociclib in CCLP cells. We showed that high PRH in cells can increase the cytotoxic effect of Palbociclib potentially by increasing Caspase-3 activity and promoting the apoptosis initiated by Palbociclib in CCLP cells. It is also worth investigating whether PRH regulated genes such as *BIRC3 and TNFSF15* are involved in the pro-apoptotic effects of Palbociclib potentiated by PRH.

7.5.2 Drug screening

In breast cancer, one study suggested combining Palbociclib with an mTOR inhibitor (Michaloglou et al., 2018). The combination of mTOR and Palbociclib prolonged regression in breast cancer cell lines and xenografts. It was also demonstrated in cell lines resistant to Palbociclib that the cells are sensitive towards mTOR inhibitor and the addition of mTOR inhibitors provide treatment options for patients relapsing on Palbociclib treatment (Michaloglou et al., 2018). An alternative to mTOR inhibitors is to find new combination therapies to increase the efficacy of Palbociclib. Drug repurposing screening has been performed to identify new relatively safe off patent drugs for CCA treatment. In our drug repurposing screen Ascorbic acid, Zinc acetate, Niclosamide, Mebendazol, Deferrioxamine mesilate and Colchicine were all identified as compounds that can significantly reduce the viability of CCA cell lines. Further functional assays including proliferation assays, Caspase-3 apoptosis assays and invasion assays were performed using these drug candidates to assess their effect on the CCA cell lines.

Among the drug candidates, Ascorbic acid was previously demonstrated to have a potential therapeutic effect on CCA cells (Wang et al., 2017). Ascorbic acid induces the cytotoxic effect on CCA cells through producing intracellular reactive oxygen species resulting in DNA damage and mTOR pathway inhibition (Wang et al., 2017). Ascorbic acid is able to reduce CCA cell proliferation and induce apoptosis by modulating the expression of apoptosis regulators Bcl-2 and Bax (Somparn et al., 2018). Here, we also show that Ascorbic acid decreases proliferation and increases apoptosis in CCLP cells at its ED50 and this is consistent with the literature.

Mebendazole is an antiparasitic drug that has anti-cancer effect in in various cancers by inhibiting tubulin polymerization resulting in apoptosis (Sawanyawisuth et al., 2014). In Chapter 6, it was shown to inhibit proliferation and increase Caspase-3 activity in CCLP cells. This is consistent with a study demonstrating that Mebendazole increases the activity of Caspase-3 and also inhibits proliferation in KKU-213 cells and also *in vivo* (Sawanyawisuth et al., 2014). However, it should be noted that Mebendazole was shown to be more effective in the initial stage of cancer in nude mice when the tumours are at minimal size, therefore, further investigation of the effect of Mebendazole in CCA is needed to know if this drug is feasible for treating CCA.

Zinc acetate, Niclosamide, Deferrioxamine mesilate and Colchicine all indicate a pro-apoptotic effect on CCLP cells in Caspase-3 assays and these are novel findings as the effect of these drug candidates on CCA cells have not been investigated previously.

Zinc is known to be a co-factor for various enzymatic activities involved in anti-inflammatory and pro-apoptotic responses. The liver is crucial for maintaining systemic zinc homeostasis (Hosui et al., 2018). The level of Zinc is lower in liver tissue from HCC

patients compared to normal liver tissue. Low Zinc levels are thought to be associated with the development of HCC as a reduction in cellular Zinc causes p53 to take a mutant form that has decreased DNA binding ability (Reaves et al., 2000). Zinc causes apoptosis by facilitating Cytochrome-C to interact with caspases (Costello and Franklin, 2014). Since we showed that Zinc acetate increases Caspase-3 activity and has no effect on proliferation in CCLP cells. It is highly likely that Zinc acetate is also promoting apoptosis in CCA.

Desferrioxamine mesilate serves as an iron chelator that is currently used to treat iron overload in thalassemia patients. It is not being investigated as a treatment for cancer but a number of iron chelators were shown to inhibit proliferation in HCC (Kicic et al., 2001). We showed however that although Desferrioxamine mesylate does not have effect on proliferation in CCLP cells, it does increase Caspase-3 activity in CCLP cells. A similar effect was demonstrated in breast cancer where it was shown that iron depletion leads to apoptosis in breast cancer (Jiang et al., 2002). Further investigation is needed to determine whether iron depletion can be a potential therapy for CCA.

Colchicine is another drug candidate that was shown to increase Caspase-3 activity in CCLP cells and it was also shown to reduce proliferation in CCLP cells. Colchicine has been shown to cause apoptosis in various cancer types including breast, lung, liver and gastric cancer (Lin et al., 2016). It is established that Colchicine induces apoptosis in cancer cells by preventing tublin incorporation into microtubules to disrupt cell division (Lin et al., 2016).

Niclosamide is also an anthelmintic drug that has been demonstrated to have potential anticancer effect in a wide range of cancers including leukemia, breast cancer, prostate

cancer, hepatocellular carcinoma and glioblastoma (Hamdoun et al., 2017). Niclosamide was shown to inhibit Wnt and Notch signaling pathways, and it targets mitochondria in cancer cells to induce cell cycle arrest and apoptosis (Li et al., 2014). Niclosamide has been shown to inhibit the Wnt pathway using multiple mechanisms in human osteosarcoma U2OS cells (Chen et al., 2009). Niclosamide has also been reported to inhibit the Notch3 pathway, in leukemia K562 cells (Wang et al., 2009). We showed in Chapter 6, that Niclosamide decreases proliferation and increases Caspase-3 activity in CCLP cells. We also demonstrated that Niclosamide decreases the expression of both Notch3 and also PRH proteins in CCLP cells. Therefore, it can be inferred that one mechanism for the anti-proliferative effect of Niclosamide in CCLP cells could be through decreasing Notch3 and PRH protein expression thereby decreasing proliferation. Xenograft *in vivo* experiments are needed to confirm the anti-cancer effect of Niclosamide in CCA.

Notably, CCLP cells treated with Niclosamide show decreased proliferation and viability but increased invasion. This is unexpected as CCLP cells with depleted PRH expression show decreased invasion. Therefore, it is likely that Niclosamide has effects on invasion by CCLP cells unrelated to PRH protein levels. Further investigation is needed on the effect of Niclosamide in invasion.

7.5.3 Drug combination experiments

Drug combination experiments showed that drug combinations with the compounds described above and including either Palbociclib or Zinc acetate showed much greater inhibition of cell viability compared to other combinations of drugs identified in the screen. The drug combination of Zinc acetate with other therapeutic agents is currently

not being investigated and the data presented in this thesis suggests that it could be further examined as a treatment for CCA either as a single agent or in combination with Palbociclib. As exogenous Zinc acetate exerts an apoptotic effect in CCA cell lines and also show toxic effects on cell viability when combined with other drugs, the apoptotic effect of Zinc might amplify with the effect of other drug candidates including Palbociclib and Niclosamide. However, the level of Zinc in CCA patients is not known and further investigation on the pathways or genes that are related to Zinc is needed.

The drug combination of Palbociclib with other drug candidates such as Ascorbic acid, Niclosamide and Zinc acetate were also shown to be 10 times more effective compared to single drug treatment on multiple CCA cell lines. Since Palbociclib itself has both an anti-proliferative effect and also a pro-apoptotic effect on CCA cell lines, these effects may be amplified when treating the cells with Ascorbic acid and Zinc acetate as each of these single agents from the drug screen were also shown to promote increased Caspase-3 activity in CCA cell lines. It is interesting that Palbociclib and Niclosamide used in combination are 10 times more effective than treating the cells with single drug. By using the Chou Talalay method for examining drug synergy, Niclosamide and Palbociclib were found to have synergistic effects on CCA cell lines. This is counter intuitive as Niclosamide was shown to decrease PRH expression and cells with lower PRH expression were shown to have decreased sensitivity towards Palbociclib. However, the synergistic effects observed may be because both drugs have independent pro-apoptotic effects which exert their effects more rapidly in cells than any effects obtained through a change in the expression of the Notch3 and PRH protein. Long term exposure to the

drug combination is required to determine whether down regulation of PRH will eventually prevent the synergism observed.

New potential combination therapies with Palbociclib have been identified. The repurposed drugs are all used at concentrations lower than the maximum serum level known to be tolerated in man and hence these novel drug combinations may be more rapidly transferred to the clinic. However, both single drug and drug combination experiments need to be repeated in primary BECs to determine the level of cytotoxicity of the drugs in untransformed cells before treatments in xenograft models and patients can commence.

7.6 Conclusion

To conclude, this thesis shows that *PRH/HHEX* transcription factor is an oncoprotein and of great importance in the development of CCA. Notably exogenous expression of PRH in immortalized AKN-1 cell line and primary BECs is sufficient to initiate many tumour related phenotypes and promote invasion; exogenous expression of PRH in CCLP tumour cells further promotes proliferative and invasive properties. PRH regulates genes and pathways that are related to proliferation, cell cycle and EMT. The positive regulation of Notch3 oncoprotein by PRH was shown to be of central importance to the phenotype of proliferation and the regulation of the Vimentin protein important for cell proliferation and EMT. The mechanisms underlying PRH regulates gene expression and signalling pathways were studied and used to identify the cell cycle kinase inhibitor Palbociclib as a useful therapeutic in PRH elevated tumours. Additional compounds from repurposed drug screening experiments were identified to decrease cell viability and show that

some of these agents can act in combination with Palbociclib to decrease cell viability synergistically.

8. References

Abou-Alfa, G.K., Macarulla, T., Javle, M.M., Kelley, R.K., Lubner, S.J., Adeva, J., Cleary, J.M., Catenacci, D.V., Borad, M.J., Bridgewater, J., Harris, W.P., Murphy, A.G., Oh, D.-Y., Whisenant, J., Lowery, M.A., Goyal, L., Shroff, R.T., El-Khoueiry, A.B., Fan, B., Wu, B., Chamberlain, C.X., Jiang, L., Gliser, C., Pandya, S.S., Valle, J.W., Zhu, A.X., 2020. Ivosidenib in IDH1-mutant, chemotherapy-refractory cholangiocarcinoma (ClarIDHy): a multicentre, randomised, double-blind, placebo-controlled, phase 3 study. Lancet Oncol. 21, 796–807. https://doi.org/10.1016/S1470-2045(20)30157-1

Ae, S., Z, Z., Gh, L., T, A., Xn, S., Dj, W., A, M., Jl, D., 2008. A novel "patient-like" model of cholangiocarcinoma progression based on bile duct inoculation of tumourigenic rat cholangiocyte cell lines. Hepatology 47, 1178–1190. https://doi.org/10.1002/hep.22088

Ahrendt, S.A., Rashid, A., Chow, J.T., Eisenberger, C.F., Pitt, H.A., Sidransky, D., 2000. p53 overexpression and K-ras gene mutations in primary sclerosing cholangitis-associated biliary tract cancer. J Hepatobiliary Pancreat Surg 7, 426–431. https://doi.org/10.1007/s005340070039

Al Baghdadi, T., Halabi, S., Garrett-Mayer, E., Mangat, P.K., Ahn, E.R., Sahai, V., Alvarez, R.H., Kim, E.S., Yost, K.J., Rygiel, A.L., Antonelli, K.R., Butler, N.L., Bruinooge, S.S., Schilsky, R.L., 2019. Palbociclib in Patients With Pancreatic and Biliary Cancer With CDKN2A Alterations: Results From the Targeted Agent and Profiling Utilization Registry Study. JCO Precision Oncology 1–8. https://doi.org/10.1200/PO.19.00124

Alenzi, F.Q.B., 2004. Links between apoptosis, proliferation and the cell cycle. Br. J. Biomed. Sci. 61, 99–102. https://doi.org/10.1080/09674845.2004.11732652

Alqudah, M.A.Y., Agarwal, S., Al-Keilani, M.S., Sibenaller, Z.A., Ryken, T.C., Assem, M., 2013. NOTCH3 Is a Prognostic Factor That Promotes Glioma Cell Proliferation, Migration and Invasion via Activation of CCND1 and EGFR. PLOS ONE 8, e77299. https://doi.org/10.1371/journal.pone.0077299

Antoniou, A., Raynaud, P., Cordi, S., Zong, Y., Tronche, F., Stanger, B.Z., Jacquemin, P., Pierreux, C.E., Clotman, F., Lemaigre, F.P., 2009. Intrahepatic bile ducts develop according to a new mode of tubulogenesis regulated by the transcription factor SOX9. Gastroenterology 136, 2325–2333. https://doi.org/10.1053/j.gastro.2009.02.051

Apte, U., Zeng, G., Muller, P., Tan, X., Micsenyi, A., Cieply, B., Dai, C., Liu, Y., Kaestner, K.H., Monga, S.P.S., 2006. Activation of Wnt/beta-catenin pathway during hepatocyte growth factor-induced hepatomegaly in mice. Hepatology 44, 992–1002. https://doi.org/10.1002/hep.21317

Arellano, M., Moreno, S., 1997. Regulation of CDK/cyclin complexes during the cell cycle. Int. J. Biochem. Cell Biol. 29, 559–573. https://doi.org/10.1016/s1357-2725(96)00178-1

Arterbery, A.S., Bogue, C.W., 2016. Hhex Is Necessary for the Hepatic Differentiation of Mouse ES Cells and Acts via Vegf Signaling. PLoS One 11. https://doi.org/10.1371/journal.pone.0146806

Ashkenazi, A., Dixit, V.M., 1998. Death receptors: signaling and modulation. Science 281, 1305–1308. https://doi.org/10.1126/science.281.5381.1305

Balcazar, N., Sathyamurthy, A., Elghazi, L., Gould, A., Weiss, A., Shiojima, I., Walsh, K., Bernal-Mizrachi, E., 2009. mTORC1 Activation Regulates β-Cell Mass and Proliferation by Modulation of Cyclin D2 Synthesis and Stability. J Biol Chem 284, 7832–7842. https://doi.org/10.1074/jbc.M807458200

Banales, J.M., Cardinale, V., Carpino, G., Marzioni, M., Andersen, J.B., Invernizzi, P., Lind, G.E., Folseraas, T., Forbes, S.J., Fouassier, L., Geier, A., Calvisi, D.F., Mertens, J.C., Trauner, M., Benedetti, A., Maroni, L., Vaquero, J., Macias, R.I.R., Raggi, C., Perugorria, M.J., Gaudio, E., Boberg, K.M., Marin, J.J.G., Alvaro, D., 2016. Cholangiocarcinoma: current knowledge and future perspectives

consensus statement from the European Network for the Study of Cholangiocarcinoma (ENS-CCA). Nat Rev Gastroenterol Hepatol 13, 261–280. https://doi.org/10.1038/nrgastro.2016.51
Baron, M., 2003. An overview of the Notch signalling pathway. Semin. Cell Dev. Biol. 14, 113–119.
Barrallo-Gimeno, A., Nieto, M.A., 2005. The Snail genes as inducers of cell movement and survival: implications in development and cancer. Development 132, 3151–3161. https://doi.org/10.1242/dev.01907
Batlle, E., Sancho, E., Francí, C., Domínguez, D., Monfar, M., Baulida, J., García De Herreros, A., 2000. The transcription factor snail is a repressor of E-cadherin gene expression in epithelial tumour cells. Nat. Cell Biol. 2, 84–89. https://doi.org/10.1038/35000034
Bekaii-Saab, T., Phelps, M.A., Li, X., Saji, M., Goff, L., Kauh, J.S.W., O'Neil, B.H., Balsom, S., Balint, C., Liersemann, R., Vasko, V.V., Bloomston, M., Marsh, W., Doyle, L.A., Ellison, G., Grever, M., Ringel, M.D., Villalona-Calero, M.A., 2011. Multi-Institutional Phase II Study of Selumetinib in Patients With Metastatic Biliary Cancers. J Clin Oncol 29, 2357–2363. https://doi.org/10.1200/JCO.2010.33.9473
Bekhti, A., 1985. Serum concentrations of mebendazole in patients with hydatid disease. Int J Clin Pharmacol Ther Toxicol 23, 633–641.
Belmokhtar, C.A., Hillion, J., Ségal-Bendirdjian, E., 2001. Staurosporine induces apoptosis through both caspase-dependent and caspase-independent mechanisms. Oncogene 20, 3354–3362. https://doi.org/10.1038/sj.onc.1204436
Ben-Ze'ev, A., 1984. Differential control of cytokeratins and vimentin synthesis by cell-cell contact and cell spreading in cultured epithelial cells. The Journal of Cell Biology 99, 1424–1433. https://doi.org/10.1083/jcb.99.4.1424
Berkun, Y., Wason, S., Brik, R., Butbul, Y., Ben-Chetrit, E., Hashkes, P.J., Livneh, A., Ozen, S., Ozdogan, H., Faulkner, R., Davis, M.W., 2012. Pharmacokinetics of colchicine in pediatric and adult patients with familial Mediterranean fever. Int J Immunopathol Pharmacol 25, 1121–1130. https://doi.org/10.1177/039463201202500429
Bess, K.L., Swingler, T.E., Rivett, A.J., Gaston, K., Jayaraman, P.-S., 2003a. The transcriptional repressor protein PRH interacts with the proteasome. Biochem. J. 374, 667–675. https://doi.org/10.1042/BJ20030769
Bess, K.L., Swingler, T.E., Rivett, A.J., Gaston, K., Jayaraman, P.-S., 2003b. The transcriptional repressor protein PRH interacts with the proteasome. Biochemical Journal 374, 667–675. https://doi.org/10.1042/bj20030769
Biswas, S., Rao, C.M., 2018. Epigenetic tools (The Writers, The Readers and The Erasers) and their implications in cancer therapy. European Journal of Pharmacology 837, 8–24. https://doi.org/10.1016/j.ejphar.2018.08.021
Blechacz, B., 2017. Cholangiocarcinoma: Current Knowledge and New Developments. Gut Liver 11, 13–26. https://doi.org/10.5009/gnl15568
Blokzijl, A., Dahlqvist, C., Reissmann, E., Falk, A., Moliner, A., Lendahl, U., Ibáñez, C.F., 2003. Cross-talk between the Notch and TGF-β signaling pathways mediated by interaction of the Notch intracellular domain with Smad3. J Cell Biol 163, 723–728. https://doi.org/10.1083/jcb.200305112
Bocci, F., Jolly, M.K., Tripathi, S.C., Aguilar, M., Hanash, S.M., Levine, H., Onuchic, J.N., 2017. Numb prevents a complete epithelial-mesenchymal transition by modulating Notch signalling. J R Soc Interface 14. https://doi.org/10.1098/rsif.2017.0512
Bonato, G., Cristoferi, L., Strazzabosco, M., Fabris, L., 2015. Malignancies in Primary Sclerosing Cholangitis – A Continuing Threat. Digestive diseases (Basel, Switzerland) 33, 140. https://doi.org/10.1159/000440826
Borggrefe, T., Oswald, F., 2009. The Notch signaling pathway: transcriptional regulation at Notch target genes. Cell. Mol. Life Sci. 66, 1631–1646. https://doi.org/10.1007/s00018-009-8668-7
Bort, R., Martinez-Barbera, J.P., Beddington, R.S.P., Zaret, K.S., 2004. Hex homeobox gene-dependent tissue positioning is required for organogenesis of the ventral pancreas. Development 131, 797–806. https://doi.org/10.1242/dev.00965
Boulter, L., Guest, R.V., Kendall, T.J., Wilson, D.H., Wojtacha, D., Robson, A.J., Ridgway, R.A., Samuel, K., Van Rooijen, N., Barry, S.T., Wigmore, S.J., Sansom, O.J., Forbes, S.J., 2015a. WNT signaling drives

cholangiocarcinoma growth and can be pharmacologically inhibited. J Clin Invest 125, 1269–1285. https://doi.org/10.1172/JCI76452

Boulter, L., Guest, R.V., Kendall, T.J., Wilson, D.H., Wojtacha, D., Robson, A.J., Ridgway, R.A., Samuel, K., Van Rooijen, N., Barry, S.T., Wigmore, S.J., Sansom, O.J., Forbes, S.J., 2015b. WNT signaling drives cholangiocarcinoma growth and can be pharmacologically inhibited. J Clin Invest 125, 1269–1285. https://doi.org/10.1172/JCI76452

Brickman, J.M., Jones, C.M., Clements, M., Smith, J.C., Beddington, R.S., 2000. Hex is a transcriptional repressor that contributes to anterior identity and suppresses Spemann organiser function. Development 127, 2303–2315.

Bui, T.B.V., Burgers, D.M., Agterof, M.J., van de Garde, E.M., 2019. Real-World Effectiveness of Palbociclib Versus Clinical Trial Results in Patients With Advanced/Metastatic Breast Cancer That Progressed on Previous Endocrine Therapy. Breast Cancer (Auckl) 13, 1178223418823238. https://doi.org/10.1177/1178223418823238

Bunthot, S., Obchoei, S., Kraiklang, R., Pirojkul, C., Wongkham, S., Wongkham, C., 2012. Overexpression of claudin-4 in cholangiocarcinoma tissues and its possible role in tumour metastasis. Asian Pac. J. Cancer Prev. 13 Suppl, 71–76.

Burak, K., Angulo, P., Pasha, T., Egan, K., Petz, J., Lindor, K., 2004. Incidence and Risk Factors for Cholangiocarcinoma in Primary Sclerosing Cholangitis. American Journal of Gastroenterology 99, 523–526.

Cadamuro, M., Nardo, G., Indraccolo, S., Dall'olmo, L., Sambado, L., Moserle, L., Franceschet, I., Colledan, M., Massani, M., Stecca, T., Bassi, N., Morton, S., Spirli, C., Fiorotto, R., Fabris, L., Strazzabosco, M., 2013. Platelet-derived growth factor-D and Rho GTPases regulate recruitment of cancer-associated fibroblasts in cholangiocarcinoma. Hepatology 58, 1042–1053. https://doi.org/10.1002/hep.26384

Cancer Statistics for the UK [WWW Document], 2015. . Cancer Research UK. URL https://www.cancerresearchuk.org/health-professional/cancer-statistics-for-the-uk (accessed 11.3.19).

Cao, J., Qiu, J., Wang, X., Lu, Z., Wang, D., Feng, H., Li, X., Liu, Q., Pan, H., Han, X., Wei, J., Liu, S., Wang, L., 2018. Identification of microRNA-124 in regulation of Hepatocellular carcinoma through BIRC3 and the NF-κB pathway. J Cancer 9, 3006–3015. https://doi.org/10.7150/jca.25956

Cardinale, V., Renzi, A., Carpino, G., Torrice, A., Bragazzi, M.C., Giuliante, F., De Rose, A.M., Fraveto, A., Onori, P., Napoletano, C., Franchitto, A., Cantafora, A., Grazi, G., Caporaso, N., D'Argenio, G., Alpini, G., Reid, L.M., Gaudio, E., Alvaro, D., 2015. Profiles of Cancer Stem Cell Subpopulations in Cholangiocarcinomas. The American Journal of Pathology 185, 1724–1739. https://doi.org/10.1016/j.ajpath.2015.02.010

Chen, M., Wang, J., Lu, J., Bond, M.C., Ren, X.-R., Lyerly, H.K., Barak, L.S., Chen, W., 2009. The Anti-Helminthic Niclosamide Inhibits Wnt/Frizzled1 Signaling. Biochemistry 48, 10267–10274. https://doi.org/10.1021/bi9009677

Chen, P., Parks, W.C., 2009. Role of Matrix Metalloproteinases in Epithelial Migration. J Cell Biochem 108, 1233–1243. https://doi.org/10.1002/jcb.22363

Chen, X., Ko, L.J., Jayaraman, L., Prives, C., 1996. p53 levels, functional domains, and DNA damage determine the extent of the apoptotic response of tumour cells. Genes Dev. 10, 2438–2451. https://doi.org/10.1101/gad.10.19.2438

Chin, V.L., Lim, C.L., 2019. Epithelial-mesenchymal plasticity—engaging stemness in an interplay of phenotypes. Stem Cell Investig 6. https://doi.org/10.21037/sci.2019.08.08

Choi, Y.J., Anders, L., 2014. Signaling through cyclin D-dependent kinases. Oncogene 33, 1890–1903. https://doi.org/10.1038/onc.2013.137

Chua, M.M.J., Ortega, C.E., Sheikh, A., Lee, M., Abdul-Rassoul, H., Hartshorn, K.L., Dominguez, I., 2017. CK2 in Cancer: Cellular and Biochemical Mechanisms and Potential Therapeutic Target. Pharmaceuticals (Basel) 10. https://doi.org/10.3390/ph10010018

Churi, C.R., Shroff, R., Wang, Y., Rashid, A., Kang, H.C., Weatherly, J., Zuo, M., Zinner, R., Hong, D., Meric-Bernstam, F., Janku, F., Crane, C.H., Mishra, L., Vauthey, J.-N., Wolff, R.A., Mills, G., Javle, M., 2014. Mutation Profiling in Cholangiocarcinoma: Prognostic and Therapeutic Implications. PLoS One 9. https://doi.org/10.1371/journal.pone.0115383

Cillo, U., Fondevila, C., Donadon, M., Gringeri, E., Mocchegiani, F., Schlitt, H.J., Ijzermans, J.N.M., Vivarelli, M., Zieniewicz, K., Damink, S.W.M.O., Koerkamp, B.G., 2019. Surgery for cholangiocarcinoma. Liver International 39, 143. https://doi.org/10.1111/liv.14089

Ciombor, K.K., Goff, L.W., 2013. Advances in the Management of Biliary Tract Cancers. Clin Adv Hematol Oncol 11, 28–34.

Clapéron, A., Mergey, M., Ho-Bouldoires, T.H.N., Vignjevic, D., Wendum, D., Chrétien, Y., Merabtene, F., Frazao, A., Paradis, V., Housset, C., Guedj, N., Fouassier, L., 2014. EGF/EGFR axis contributes to the progression of cholangiocarcinoma through the induction of an epithelial-mesenchymal transition. Journal of Hepatology 61, 325–332. https://doi.org/10.1016/j.jhep.2014.03.033

Clotman, F., Lemaigre, F.P., 2006. Control of hepatic differentiation by activin/TGFbeta signaling. Cell Cycle 5, 168–171. https://doi.org/10.4161/cc.5.2.2341

Cohen, B., Shimizu, M., Izrailit, J., Ng, N.F.L., Buchman, Y., Pan, J.G., Dering, J., Reedijk, M., 2010. Cyclin D1 is a direct target of JAG1-mediated Notch signaling in breast cancer. Breast Cancer Res. Treat. 123, 113–124. https://doi.org/10.1007/s10549-009-0621-9

Collas, P., Dahl, J.A., 2008. Chop it, ChIP it, check it: the current status of chromatin immunoprecipitation. Front. Biosci. 13, 929–943. https://doi.org/10.2741/2733

Conacci-Sorrell, M., Simcha, I., Ben-Yedidia, T., Blechman, J., Savagner, P., Ben-Ze'ev, A., 2003. Autoregulation of E-cadherin expression by cadherin-cadherin interactions: the roles of beta-catenin signaling, Slug, and MAPK. J. Cell Biol. 163, 847–857. https://doi.org/10.1083/jcb.200308162

Cong, R., Jiang, X., Wilson, C.M., Hunter, M.P., Vasavada, H., Bogue, C.W., 2006. Hhex is a direct repressor of endothelial cell-specific molecule 1 (ESM-1). Biochem. Biophys. Res. Commun. 346, 535–545. https://doi.org/10.1016/j.bbrc.2006.05.153

Cooper, G.M., 2000. Signaling in Development and Differentiation. The Cell: A Molecular Approach. 2nd edition.

Costello, L.C., Franklin, R.B., 2014. The status of zinc in the development of hepatocellular cancer. Cancer Biol Ther 15, 353–360. https://doi.org/10.4161/cbt.27633

Costello, L.C., Franklin, R.B., 2012. Cytotoxic/tumour suppressor role of zinc for the treatment of cancer: an enigma and an opportunity. Expert Rev Anticancer Ther 12, 121–128. https://doi.org/10.1586/era.11.190

Crompton, M.R., Bartlett, T.J., MacGregor, A.D., Manfioletti, G., Buratti, E., Giancotti, V., Goodwin, G.H., 1992. Identification of a novel vertebrate homeobox gene expressed in haematopoietic cells. Nucleic Acids Res. 20, 5661–5667. https://doi.org/10.1093/nar/20.21.5661

Cutter, A., Hayes, J.J., 2015. A Brief Review of Nucleosome Structure. FEBS Lett 589, 2914–2922. https://doi.org/10.1016/j.febslet.2015.05.016

Dalmer, T.R.A., Clugston, R.D., 2019. Gene ontology enrichment analysis of congenital diaphragmatic hernia-associated genes. Pediatr Res 85, 13–19. https://doi.org/10.1038/s41390-018-0192-8

Danial, N.N., Korsmeyer, S.J., 2004. Cell death: critical control points. Cell 116, 205–219. https://doi.org/10.1016/s0092-8674(04)00046-7

Danielsson, F., Peterson, M.K., Caldeira Araújo, H., Lautenschläger, F., Gad, A.K.B., 2018. Vimentin Diversity in Health and Disease. Cells 7. https://doi.org/10.3390/cells7100147

Das, C., Tyler, J.K., 2013. Histone exchange and histone modifications during transcription and aging. Biochim Biophys Acta 1819, 332–342.

Daya-Makin, M., Sanghera, J.S., Mogentale, T.L., Lipp, M., Parchomchuk, J., Hogg, J.C., Pelech, S.L., 1994. Activation of a tumour-associated protein kinase (p40TAK) and casein kinase 2 in human squamous cell carcinomas and adenocarcinomas of the lung. Cancer Res. 54, 2262–2268.

De Assis Jr, E.M., Siddiqui, Y.H., Van Den Bosch, M., Poole, A.W., Jayaraman, P.-S., Gaston, K., 2020. Blood platelets stimulate cancer extravasation through TGFβ-mediated down-regulation of PRH/HHEX. Oncogenesis.

de Sousa Mesquita, A.P., de Araújo Lopes, S., Pernambuco Filho, P.C.A., Nader, H.B., Lopes, C.C., 2017. Acquisition of anoikis resistance promotes alterations in the Ras/ERK and PI3K/Akt signaling pathways and matrix remodeling in endothelial cells. Apoptosis 22, 1116–1137. https://doi.org/10.1007/s10495-017-1392-0

Denson, L.A., McClure, M.H., Bogue, C.W., Karpen, S.J., Jacobs, H.C., 2000. HNF3beta and GATA-4 transactivate the liver-enriched homeobox gene, Hex. Gene 246, 311–320. https://doi.org/10.1016/s0378-1119(00)00082-2

Derksen, P.W.B., Liu, X., Saridin, F., van der Gulden, H., Zevenhoven, J., Evers, B., van Beijnum, J.R., Griffioen, A.W., Vink, J., Krimpenfort, P., Peterse, J.L., Cardiff, R.D., Berns, A., Jonkers, J., 2006. Somatic inactivation of E-cadherin and p53 in mice leads to metastatic lobular mammary carcinoma through induction of anoikis resistance and angiogenesis. Cancer Cell 10, 437–449. https://doi.org/10.1016/j.ccr.2006.09.013

Derynck, R., Akhurst, R.J., Balmain, A., 2001. TGF-beta signaling in tumour suppression and cancer progression. Nat. Genet. 29, 117–129. https://doi.org/10.1038/ng1001-117

Deshpande, A., Sicinski, P., Hinds, P.W., 2005. Cyclins and cdks in development and cancer: a perspective. Oncogene 24, 2909–2915. https://doi.org/10.1038/sj.onc.1208618

Desjobert, C., Noy, P., Swingler, T., Williams, H., Gaston, K., Jayaraman, P.-S., 2009. The PRH/Hex repressor protein causes nuclear retention of Groucho/TLE co-repressors. Biochem. J. 417, 121–132. https://doi.org/10.1042/BJ20080872

Di Domenico, M., Giordano, A., 2017. Signal transduction growth factors: the effective governance of transcription and cellular adhesion in cancer invasion. Oncotarget 8, 36869–36884. https://doi.org/10.18632/oncotarget.16300

Djavani, M., Topisirovic, I., Zapata, J.C., Sadowska, M., Yang, Y., Rodas, J., Lukashevich, I.S., Bogue, C.W., Pauza, C.D., Borden, K.L.B., Salvato, M.S., 2005. The Proline-Rich Homeodomain (PRH/HEX) Protein Is Down-Regulated in Liver during Infection with Lymphocytic Choriomeningitis Virus. J Virol 79, 2461–2473. https://doi.org/10.1128/JVI.79.4.2461-2473.2005

Du, L., Li, J., Lei, L., He, H., Chen, E., Dong, J., Yang, J., 2018. High Vimentin Expression Predicts a Poor Prognosis and Progression in Colorectal Cancer: A Study with Meta-Analysis and TCGA Database. Biomed Res Int 2018. https://doi.org/10.1155/2018/6387810

Du, W., Searle, J.S., 2009. The Rb Pathway and Cancer Therapeutics. Curr Drug Targets 10, 581–589.

Duangkumpha, K., Techasen, A., Loilome, W., Namwat, N., Thanan, R., Khuntikeo, N., Yongvanit, P., 2014. BMP-7 blocks the effects of TGF-β-induced EMT in cholangiocarcinoma. Tumour Biol. 35, 9667–9676. https://doi.org/10.1007/s13277-014-2246-9

el-Deiry, W.S., Tokino, T., Velculescu, V.E., Levy, D.B., Parsons, R., Trent, J.M., Lin, D., Mercer, W.E., Kinzler, K.W., Vogelstein, B., 1993. WAF1, a potential mediator of p53 tumour suppression. Cell 75, 817–825. https://doi.org/10.1016/0092-8674(93)90500-p

Eso, Y., Uza, N., Yamagishi, H., Imada, K., Kimura, Y., Masui, T., Kodama, Y., Seno, H., 2017. Utility of KRAS mutational analysis in the preoperative diagnosis of synchronous pancreatic cancer and intrahepatic cholangiocarcinoma. Medicine (Baltimore) 96. https://doi.org/10.1097/MD.0000000000009217

Espinosa, L., Cathelin, S., D'Altri, T., Trimarchi, T., Statnikov, A., Guiu, J., Rodilla, V., Inglés-Esteve, J., Nomdedeu, J., Bellosillo, B., Besses, C., Abdel-Wahab, O., Kucine, N., Sun, S.-C., Song, G., Mullighan, C.C., Levine, R.L., Rajewsky, K., Aifantis, I., Bigas, A., 2010. The Notch/Hes1 pathway sustains NF-κB activation through CYLD repression in T cell leukemia. Cancer Cell 18, 268–281. https://doi.org/10.1016/j.ccr.2010.08.006

Falix, F.A., Weeda, V.B., Labruyere, W.T., Poncy, A., de Waart, D.R., Hakvoort, T.B.M., Lemaigre, F., Gaemers, I.C., Aronson, D.C., Lamers, W.H., 2014. Hepatic Notch2 deficiency leads to bile duct agenesis perinatally and secondary bile duct formation after weaning. Developmental Biology 396, 201–213. https://doi.org/10.1016/j.ydbio.2014.10.002

Fan, B., Malato, Y., Calvisi, D.F., Naqvi, S., Razumilava, N., Ribback, S., Gores, G.J., Dombrowski, F., Evert, M., Chen, X., Willenbring, H., 2012. Cholangiocarcinomas can originate from hepatocytes in mice. J Clin Invest 122, 2911–2915. https://doi.org/10.1172/JCI63212

Farazi, P.A., Zeisberg, M., Glickman, J., Zhang, Y., Kalluri, R., DePinho, R.A., 2006. Chronic Bile Duct Injury Associated with Fibrotic Matrix Microenvironment Provokes Cholangiocarcinoma in p53-Deficient Mice. Cancer Res 66, 6622–6627. https://doi.org/10.1158/0008-5472.CAN-05-4609

Farshidfar, F., Zheng, S., Gingras, M.-C., Newton, Y., Shih, J., Robertson, A.G., Hinoue, T., Hoadley, K.A., Gibb, E.A., Roszik, J., Covington, K.R., Wu, C.-C., Shinbrot, E., Stransky, N., Hegde, A., Yang, J.D., Reznik, E., Sadeghi, S., Pedamallu, C.S., Ojesina, A.I., Hess, J.M., Auman, J.T., Rhie, S.K., Bowlby, R., Borad, M.J., Zhu, A.X., Stuart, J.M., Sander, C., Akbani, R., Cherniack, A.D., Deshpande, V.,

Mounajjed, T., Foo, W.C., Torbenson, M.S., Kleiner, D.E., Laird, P.W., Wheeler, D.A., McRee, A.J., Bathe, O.F., Andersen, J.B., Bardeesy, N., Roberts, L.R., Kwong, L.N., 2017a. Integrative Genomic Analysis of Cholangiocarcinoma Identifies Distinct IDH-Mutant Molecular Profiles. Cell Rep 18, 2780–2794. https://doi.org/10.1016/j.celrep.2017.02.033

Farshidfar, F., Zheng, S., Gingras, M.-C., Newton, Y., Shih, J., Robertson, A.G., Hinoue, T., Hoadley, K.A., Gibb, E.A., Roszik, J., Covington, K.R., Wu, C.-C., Shinbrot, E., Stransky, N., Hegde, A., Yang, J.D., Reznik, E., Sadeghi, S., Pedamallu, C.S., Ojesina, A.I., Hess, J.M., Auman, J.T., Rhie, S.K., Bowlby, R., Borad, M.J., Zhu, A.X., Stuart, J.M., Sander, C., Akbani, R., Cherniack, A.D., Deshpande, V., Mounajjed, T., Foo, W.C., Torbenson, M.S., Kleiner, D.E., Laird, P.W., Wheeler, D.A., McRee, A.J., Bathe, O.F., Andersen, J.B., Bardeesy, N., Roberts, L.R., Kwong, L.N., 2017b. Integrative Genomic Analysis of Cholangiocarcinoma Identifies Distinct IDH-Mutant Molecular Profiles. Cell Rep 18, 2780–2794. https://doi.org/10.1016/j.celrep.2017.02.033

Feitelson, M.A., Arzumanyan, A., Kulathinal, R.J., Blain, S.W., Holcombe, R.F., Mahajna, J., Marino, M., Martinez-Chantar, M.L., Nawroth, R., Sanchez-Garcia, I., Sharma, D., Saxena, N.K., Singh, N., Vlachostergios, P.J., Guo, S., Honoki, K., Fujii, H., Georgakilas, A.G., Amedei, A., Niccolai, E., Amin, A., Ashraf, S.S., Boosani, C.S., Guha, G., Ciriolo, M.R., Aquilano, K., Chen, S., Mohammed, S.I., Azmi, A.S., Bhakta, D., Halicka, D., Nowsheen, S., 2015. Sustained proliferation in cancer: mechanisms and novel therapeutic targets. Semin Cancer Biol 35, S25–S54. https://doi.org/10.1016/j.semcancer.2015.02.006

Frampton, G., Invernizzi, P., Bernuzzi, F., Pae, H.Y., Quinn, M., Horvat, D., Galindo, C., Huang, L., McMillin, M., Cooper, B., Rimassa, L., DeMorrow, S., 2012. Interleukin-6-driven progranulin expression increases cholangiocarcinoma growth by an Akt-dependent mechanism. Gut 61, 268–277. https://doi.org/10.1136/gutjnl-2011-300643

Franklin, R.B., Costello, L.C., 2009. The Important Role of the Apoptotic Effects of Zinc in the Development of Cancers. J Cell Biochem 106, 750–757. https://doi.org/10.1002/jcb.22049

Frisch, S.M., Francis, H., 1994. Disruption of epithelial cell-matrix interactions induces apoptosis. J. Cell Biol. 124, 619–626. https://doi.org/10.1083/jcb.124.4.619

Fruman, D.A., Meyers, R.E., Cantley, L.C., 1998. Phosphoinositide kinases. Annu. Rev. Biochem. 67, 481–507. https://doi.org/10.1146/annurev.biochem.67.1.481

Furubo, S., Harada, K., Shimonishi, T., Katayanagi, K., Tsui, W., Nakanuma, Y., 1999. Protein expression and genetic alterations of p53 and ras in intrahepatic cholangiocarcinoma. Histopathology 35, 230–240. https://doi.org/10.1046/j.1365-2559.1999.00705.x

Gartel, A.L., Tyner, A.L., 2002. The Role of the Cyclin-dependent Kinase Inhibitor p21 in Apoptosis 1 Supported in part by NIH Grant R01 DK56283 (to A. L. T.) for the p21 research and Campus Research Board and Illinois Department of Public Health Penny Severns Breast and Cervical Cancer grants (to A. L. G.).1. Mol Cancer Ther 1, 639–649.

Gasior, K., Wagner, N.J., Cores, J., Caspar, R., Wilson, A., Bhattacharya, S., Hauck, M.L., 2019. The role of cellular contact and TGF-beta signaling in the activation of the epithelial mesenchymal transition (EMT). Cell Adhesion & Migration 13, 63–75. https://doi.org/10.1080/19336918.2018.1526597

Gaston, K., Tsitsilianos, M.-A., Wadey, K., Jayaraman, P.-S., 2016. Misregulation of the proline rich homeodomain (PRH/HHEX) protein in cancer cells and its consequences for tumour growth and invasion. Cell Biosci 6, 12. https://doi.org/10.1186/s13578-016-0077-7

Gauvrit, S., Villasenor, A., Strilic, B., Kitchen, P., Collins, M.M., Marín-Juez, R., Guenther, S., Maischein, H.-M., Fukuda, N., Canham, M.A., Brickman, J.M., Bogue, C.W., Jayaraman, P.-S., Stainier, D.Y.R., 2018. HHEX is a transcriptional regulator of the VEGFC/FLT4/PROX1 signaling axis during vascular development. Nat Commun 9, 1–14. https://doi.org/10.1038/s41467-018-05039-1

George, A., Morse, H.C., Justice, M.J., 2003. The homeobox gene Hex induces T-cell-derived lymphomas when overexpressed in hematopoietic precursor cells. Oncogene 22, 6764–6773. https://doi.org/10.1038/sj.onc.1206822

Gire, V., Dulić, V., 2015. Senescence from G2 arrest, revisited. Cell Cycle 14, 297–304. https://doi.org/10.1080/15384101.2014.1000134

Go, M.J., Eastman, D.S., Artavanis-Tsakonas, S., 1998. Cell proliferation control by Notch signaling in Drosophila development. Development 125, 2031–2040.

Golabi, P., Fazel, S., Otgonsuren, M., Sayiner, M., Locklear, C.T., Younossi, Z.M., 2017. Mortality assessment of patients with hepatocellular carcinoma according to underlying disease and

treatment modalities. Medicine (Baltimore) 96. https://doi.org/10.1097/MD.0000000000005904

Gomez, H.F., McClafferty, H.H., Flory, D., Brent, J., Dart, R.C., 1997. Prevention of gastrointestinal iron absorption by chelation from an orally administered premixed deferoxamine/charcoal slurry. Ann Emerg Med 30, 587–592. https://doi.org/10.1016/s0196-0644(97)70073-8

Goodings, C., Smith, E., Mathias, E., Elliott, N., Cleveland, S.M., Tripathi, R.M., Layer, J.H., Chen, X., Guo, Y., Shyr, Y., Hamid, R., Du, Y., Davé, U.P., 2015. Hhex is Required at Multiple Stages of Adult Hematopoietic Stem and Progenitor Cell Differentiation. STEM CELLS 33, 2628–2641. https://doi.org/10.1002/stem.2049

Goossens, N., Sun, X., Hoshida, Y., 2015. Molecular classification of hepatocellular carcinoma: potential therapeutic implications. Hepat Oncol 2, 371–379. https://doi.org/10.2217/hep.15.26

Guest, R.V., Boulter, L., Dwyer, B.J., Kendall, T.J., Man, T.-Y., Minnis-Lyons, S.E., Lu, W.-Y., Robson, A.J., Gonzalez, S.F., Raven, A., Wojtacha, D., Morton, J.P., Komuta, M., Roskams, T., Wigmore, S.J., Sansom, O.J., Forbes, S.J., 2016. Notch3 drives development and progression of cholangiocarcinoma. Proc. Natl. Acad. Sci. U.S.A. 113, 12250–12255. https://doi.org/10.1073/pnas.1600067113

Guiral, M., Bess, K., Goodwin, G., Jayaraman, P.S., 2001. PRH represses transcription in hematopoietic cells by at least two independent mechanisms. J. Biol. Chem. 276, 2961–2970. https://doi.org/10.1074/jbc.M004948200

Guiral, Muriel, Bess, K., Goodwin, G., Jayaraman, P.-S., 2001. PRH Represses Transcription in Hematopoietic Cells by at Least Two Independent Mechanisms. J. Biol. Chem. 276, 2961–2970. https://doi.org/10.1074/jbc.M004948200

Hallaq, H., Pinter, E., Enciso, J., McGrath, J., Zeiss, C., Brueckner, M., Madri, J., Jacobs, H.C., Wilson, C.M., Vasavada, H., Jiang, X., Bogue, C.W., 2004. A null mutation of Hhex results in abnormal cardiac development, defective vasculogenesis and elevated Vegfa levels. Development 131, 5197–5209. https://doi.org/10.1242/dev.01393

Hanahan, D., Weinberg, R.A., 2011. Hallmarks of cancer: the next generation. Cell 144, 646–674. https://doi.org/10.1016/j.cell.2011.02.013

Hartwell, K.A., Muir, B., Reinhardt, F., Carpenter, A.E., Sgroi, D.C., Weinberg, R.A., 2006. The Spemann organizer gene, Goosecoid, promotes tumour metastasis. Proc. Natl. Acad. Sci. U.S.A. 103, 18969–18974. https://doi.org/10.1073/pnas.0608636103

Hengartner, M.O., 2000. The biochemistry of apoptosis. Nature 407, 770–776. https://doi.org/10.1038/35037710

Hinds, P.W., Mittnacht, S., Dulic, V., Arnold, A., Reed, S.I., Weinberg, R.A., 1992. Regulation of retinoblastoma protein functions by ectopic expression of human cyclins. Cell 70, 993–1006. https://doi.org/10.1016/0092-8674(92)90249-c

Hirata, H., Yoshiura, S., Ohtsuka, T., Bessho, Y., Harada, T., Yoshikawa, K., Kageyama, R., 2002. Oscillatory expression of the bHLH factor Hes1 regulated by a negative feedback loop. Science 298, 840–843. https://doi.org/10.1126/science.1074560

Hofmann, J.J., Zovein, A.C., Koh, H., Radtke, F., Weinmaster, G., Iruela-Arispe, M.L., 2010. Jagged1 in the portal vein mesenchyme regulates intrahepatic bile duct development: insights into Alagille syndrome. Development 137, 4061–4072. https://doi.org/10.1242/dev.052118

Honey, K., 2005. Notch balances self-renewal and differentiation. Nat Rev Immunol 5, 184–184. https://doi.org/10.1038/nri1585

Hosokawa, S., Furuyama, K., Horiguchi, M., Aoyama, Y., Tsuboi, K., Sakikubo, M., Goto, T., Hirata, K., Tanabe, W., Nakano, Y., Akiyama, H., Kageyama, R., Uemoto, S., Kawaguchi, Y., 2015. Impact of Sox9 Dosage and Hes1-mediated Notch Signaling in Controlling the Plasticity of Adult Pancreatic Duct Cells in Mice. Scientific Reports 5, 8518. https://doi.org/10.1038/srep08518

Hosui, A., Kimura, E., Abe, S., Tanimoto, T., Onishi, K., Kusumoto, Y., Sueyoshi, Y., Matsumoto, K., Hirao, M., Yamada, T., Hiramatsu, N., 2018. Long-Term Zinc Supplementation Improves Liver Function and Decreases the Risk of Developing Hepatocellular Carcinoma. Nutrients 10. https://doi.org/10.3390/nu10121955

Hu, W., Fu, J., Lu, S.-X., Liu, L.-L., Luo, R.-Z., Yun, J.-P., Zhang, C.Z., 2015. Decrease of Bcl-xL/Bcl-2-associated death promoter in hepatocellular carcinoma indicates poor prognosis. Am J Cancer Res 5, 1805–1813.

Huang, Q., Li, J., Zheng, J., Wei, A., 2019. The Carcinogenic Role of the Notch Signaling Pathway in the Development of Hepatocellular Carcinoma. J Cancer 10, 1570–1579. https://doi.org/10.7150/jca.26847

Huang, X.-Y., Zhang, C., Cai, J.-B., Shi, G.-M., Ke, A.-W., Dong, Z.-R., Zhang, P.-F., Fan, J., Peng, B.-G., Zhou, J., 2014. Comprehensive Multiple Molecular Profile of Epithelial Mesenchymal Transition in Intrahepatic Cholangiocarcinoma Patients. PLOS ONE 9, e96860. https://doi.org/10.1371/journal.pone.0096860

Hunter, M.P., Wilson, C.M., Jiang, X., Cong, R., Vasavada, H., Kaestner, K.H., Bogue, C.W., 2007. The homeobox gene Hhex is essential for proper hepatoblast differentiation and bile duct morphogenesis. Dev. Biol. 308, 355–367. https://doi.org/10.1016/j.ydbio.2007.05.028

Huntzicker, E.G., Hötzel, K., Choy, L., Che, L., Ross, J., Pau, G., Sharma, N., Siebel, C.W., Chen, X., French, D.M., 2015. Differential effects of targeting Notch receptors in a mouse model of liver cancer. Hepatology 61, 942–952. https://doi.org/10.1002/hep.27566

Ikenoue, T., Terakado, Y., Nakagawa, H., Hikiba, Y., Fujii, T., Matsubara, D., Noguchi, R., Zhu, C., Yamamoto, K., Kudo, Y., Asaoka, Y., Yamaguchi, K., Ijichi, H., Tateishi, K., Fukushima, N., Maeda, S., Koike, K., Furukawa, Y., 2016. A novel mouse model of intrahepatic cholangiocarcinoma induced by liver-specific Kras activation and Pten deletion. Sci Rep 6. https://doi.org/10.1038/srep23899

Inoki, K., Ouyang, H., Zhu, T., Lindvall, C., Wang, Y., Zhang, X., Yang, Q., Bennett, C., Harada, Y., Stankunas, K., Wang, C.-Y., He, X., MacDougald, O.A., You, M., Williams, B.O., Guan, K.-L., 2006. TSC2 integrates Wnt and energy signals via a coordinated phosphorylation by AMPK and GSK3 to regulate cell growth. Cell 126, 955–968. https://doi.org/10.1016/j.cell.2006.06.055

Itatsu, K., Sasaki, M., Yamaguchi, J., Ohira, S., Ishikawa, A., Ikeda, H., Sato, Y., Harada, K., Zen, Y., Sato, H., Ohta, T., Nagino, M., Nimura, Y., Nakanuma, Y., 2009. Cyclooxygenase-2 is involved in the up-regulation of matrix metalloproteinase-9 in cholangiocarcinoma induced by tumour necrosis factor-alpha. Am. J. Pathol. 174, 829–841. https://doi.org/10.2353/ajpath.2009.080012

Jackson, J.T., Nasa, C., Shi, W., Huntington, N.D., Bogue, C.W., Alexander, W.S., McCormack, M.P., 2015. A crucial role for the homeodomain transcription factor Hhex in lymphopoiesis. Blood 125, 803–814. https://doi.org/10.1182/blood-2014-06-579813

Jackson, J.T., Ng, A.P., Shields, B.J., Haupt, S., Haupt, Y., McCormack, M.P., 2018. Hhex induces promyelocyte self-renewal and cooperates with growth factor independence to cause myeloid leukemia in mice. Blood Adv 2, 347–360. https://doi.org/10.1182/bloodadvances.2017013243

Jang, S.W., Hwang, S.S., Kim, H.S., Kim, M.K., Lee, W.H., Hwang, S.U., Gwak, J., Yew, S.K., Flavell, R.A., Lee, G.R., 2019. Homeobox protein Hhex negatively regulates Treg cells by inhibiting Foxp3 expression and function. PNAS 116, 25790–25799. https://doi.org/10.1073/pnas.1907224116

Jansen, P.L.M., 2007. Endogenous bile acids as carcinogens. Journal of Hepatology 47, 434–435. https://doi.org/10.1016/j.jhep.2007.06.001

Javle, M., Lowery, M., Shroff, R.T., Weiss, K.H., Springfeld, C., Borad, M.J., Ramanathan, R.K., Goyal, L., Sadeghi, S., Macarulla, T., El-Khoueiry, A., Kelley, R.K., Borbath, I., Choo, S.P., Oh, D.-Y., Philip, P.A., Chen, L.-T., Reungwetwattana, T., Van Cutsem, E., Yeh, K.-H., Ciombor, K., Finn, R.S., Patel, A., Sen, S., Porter, D., Isaacs, R., Zhu, A.X., Abou-Alfa, G.K., Bekaii-Saab, T., 2018. Phase II Study of BGJ398 in Patients With FGFR-Altered Advanced Cholangiocarcinoma. J. Clin. Oncol. 36, 276–282. https://doi.org/10.1200/JCO.2017.75.5009

Jeong, W.-J., Ro, E.J., Choi, K.-Y., 2018. Interaction between Wnt/β-catenin and RAS-ERK pathways and an anti-cancer strategy via degradations of β-catenin and RAS by targeting the Wnt/β-catenin pathway. npj Precision Onc 2, 1–10. https://doi.org/10.1038/s41698-018-0049-y

Jiang, X.P., Wang, F., Yang, D.C., Elliott, R.L., Head, J.F., 2002. Induction of apoptosis by iron depletion in the human breast cancer MCF-7 cell line and the 13762NF rat mammary adenocarcinoma in vivo. Anticancer Res. 22, 2685–2692.

Jiao, Y., Huang, B., Chen, Y., Hong, G., Xu, J., Hu, C., Wang, C., 2018. Integrated Analyses Reveal Overexpressed Notch1 Promoting Porcine Satellite Cells' Proliferation through Regulating the Cell Cycle. Int J Mol Sci 19. https://doi.org/10.3390/ijms19010271

Jusakul, A., Cutcutache, I., Yong, C.H., Lim, J.Q., Huang, M.N., Padmanabhan, N., Nellore, V., Kongpetch, S., Ng, A.W.T., Ng, L.M., Choo, S.P., Myint, S.S., Thanan, R., Nagarajan, S., Lim, W.K., Ng, C.C.Y., Boot, A., Liu, M., Ong, C.K., Rajasegaran, V., Lie, S., Lim, A.S.T., Lim, T.H., Tan, J., Loh, J.L., McPherson, J.R., Khuntikeo, N., Bhudhisawasdi, V., Yongvanit, P., Wongkham, S., Totoki, Y.,

Nakamura, H., Arai, Y., Yamasaki, S., Chow, P.K.-H., Chung, A.Y.F., Ooi, L.L.P.J., Lim, K.H., Dima, S., Duda, D.G., Popescu, I., Broet, P., Hsieh, S.-Y., Yu, M.-C., Scarpa, A., Lai, J., Luo, D.-X., Carvalho, A.L., Vettore, A.L., Rhee, H., Park, Y.N., Alexandrov, L.B., Gordân, R., Rozen, S.G., Shibata, T., Pairojkul, C., Teh, B.T., Tan, P., 2017. Whole-Genome and Epigenomic Landscapes of Etiologically Distinct Subtypes of Cholangiocarcinoma. Cancer Discov 7, 1116–1135. https://doi.org/10.1158/2159-8290.CD-17-0368

Kageyama, R., Ohtsuka, T., Kobayashi, T., 2007. The Hes gene family: repressors and oscillators that orchestrate embryogenesis. Development 134, 1243–1251. https://doi.org/10.1242/dev.000786

Kamikawa, T., Amenomori, M., Itoh, T., Momoi, H., Hiai, H., Machinami, R., Ishikawa, Y., Mori, T., Shimahara, Y., Yamaoka, Y., Fukumoto, M., 1999. Analysis of genetic changes in intrahepatic cholangiocarcinoma induced by thorotrast. Radiat. Res. 152, S118-124.

Kang, Y.K., Kim, W.H., Jang, J.J., 2002. Expression of G1-S modulators (p53, p16, p27, cyclin D1, Rb) and Smad4/Dpc4 in intrahepatic cholangiocarcinoma. Hum. Pathol. 33, 877–883. https://doi.org/10.1053/hupa.2002.127444

Karp, G., 2009. Cell and Molecular Biology: Concepts and Experiments. John Wiley & Sons.

Kasamatsu, S., Sato, A., Yamamoto, T., Keng, V.W., Yoshida, H., Yamazaki, Y., Shimoda, M., Miyazaki, J., Noguchi, T., 2004. Identification of the transactivating region of the homeodomain protein, hex. J. Biochem. 135, 217–223. https://doi.org/10.1093/jb/mvh025

Katayama, K., Hosui, A., Sakai, Y., Itou, M., Matsuzaki, Y., Takamori, Y., Hosho, K., Tsuru, T., Takikawa, Y., Michitaka, K., Ogawa, E., Miyoshi, Y., Ito, T., Ida, S., Hamada, I., Miyoshi, K., Kodama, H., Takehara, T., 2020. Effects of Zinc Acetate on Serum Zinc Concentrations in Chronic Liver Diseases: a Multicenter, Double-Blind, Randomized, Placebo-Controlled Trial and a Dose Adjustment Trial. Biol Trace Elem Res 195, 71–81. https://doi.org/10.1007/s12011-019-01851-y

Kaul, A., Schuster, E., Jennings, B.H., 2014. The Groucho Co-repressor Is Primarily Recruited to Local Target Sites in Active Chromatin to Attenuate Transcription. PLOS Genetics 10, e1004595. https://doi.org/10.1371/journal.pgen.1004595

Kenny, T.C., Schmidt, H., Adelson, K., Hoshida, Y., Koh, A.P., Shah, N., Mandeli, J., Ting, J., Germain, D., 2017. Patient-derived Interstitial Fluids and Predisposition to Aggressive Sporadic Breast Cancer through Collagen Remodeling and Inactivation of p53. Clin. Cancer Res. 23, 5446–5459. https://doi.org/10.1158/1078-0432.CCR-17-0342

Kershaw, R. M., Roberts, D., Wragg, J., Shaaban, A.M., Humphreys, E., Halsall, J., Price, L., Bicknell, R., Gaston, K., Jayaraman, P.-S., 2017. Proline-Rich Homeodomain protein (PRH/HHEX) is a suppressor of breast tumour growth. Oncogenesis 6, e346. https://doi.org/10.1038/oncsis.2017.42

Kershaw, R M, Roberts, D., Wragg, J., Shaaban, A.M., Humphreys, E., Halsall, J., Price, L., Bicknell, R., Gaston, K., Jayaraman, P.-S., 2017. Proline-Rich Homeodomain protein (PRH/HHEX) is a suppressor of breast tumour growth. Oncogenesis 6, e346. https://doi.org/10.1038/oncsis.2017.42

Kershaw, R.M., Siddiqui, Y.H., Roberts, D., Jayaraman, P.-S., Gaston, K., 2014. PRH/HHex inhibits the migration of breast and prostate epithelial cells through direct transcriptional regulation of Endoglin. Oncogene 33, 5592–5600. https://doi.org/10.1038/onc.2013.496

Khalaf, A.M., Fuentes, D., Morshid, A.I., Burke, M.R., Kaseb, A.O., Hassan, M., Hazle, J.D., Elsayes, K.M., 2018. Role of Wnt/β-catenin signaling in hepatocellular carcinoma, pathogenesis, and clinical significance. J Hepatocell Carcinoma 5, 61–73. https://doi.org/10.2147/JHC.S156701

Khan, S.A., Thomas, H.C., Toledano, M.B., Cox, I.J., Taylor-Robinson, S.D., 2005. p53 mutations in human cholangiocarcinoma: a review. Liver International 25, 704–716. https://doi.org/10.1111/j.1478-3231.2005.01106.x

Khanim, F.L., Merrick, B. a. M.E., Giles, H.V., Jankute, M., Jackson, J.B., Giles, L.J., Birtwistle, J., Bunce, C.M., Drayson, M.T., 2011. Redeployment-based drug screening identifies the anti-helminthic niclosamide as anti-myeloma therapy that also reduces free light chain production. Blood Cancer Journal 1, e39–e39. https://doi.org/10.1038/bcj.2011.38

Khatib, M.E., Bozko, P., Palagani, V., Malek, N.P., Wilkens, L., Plentz, R.R., 2013a. Activation of Notch Signaling Is Required for Cholangiocarcinoma Progression and Is Enhanced by Inactivation of p53 In Vivo. PLOS ONE 8, e77433. https://doi.org/10.1371/journal.pone.0077433

Khatib, M.E., Kalnytska, A., Palagani, V., Kossatz, U., Manns, M.P., Malek, N.P., Wilkens, L., Plentz, R.R., 2013b. Inhibition of hedgehog signaling attenuates carcinogenesis in vitro and increases necrosis of cholangiocellular carcinoma. Hepatology 57, 1035–1045. https://doi.org/10.1002/hep.26147

Khorasanizadeh, S., 2004. The nucleosome: from genomic organization to genomic regulation. Cell 116, 259–272. https://doi.org/10.1016/s0092-8674(04)00044-3

Kicic, A., Chua, A.C., Baker, E., 2001. Effect of iron chelators on proliferation and iron uptake in hepatoma cells. Cancer 92, 3093–3110. https://doi.org/10.1002/1097-0142(20011215)92:12<3093::aid-cncr10107>3.0.co;2-b

Kitchen, P., Lee, K.Y., Clark, D., Lau, N., Lertsuwan, J., Sawasdichai, A., Satayavivad, J., Oltean, S., Afford, S., Gaston, K., Jayaraman, P.-S., 2019. A runaway PRH/HHEX-Notch3 positive feedback loop drives cholangiocarcinoma and determines response to CDK4/6 inhibition. Cancer Res. https://doi.org/10.1158/0008-5472.CAN-19-0942

Kim, E., Lisby, A., Ma, C., Lo, N., Ehmer, U., Hayer, K.E., Furth, E.E., Viatour, P., 2019. Promotion of growth factor signaling as a critical function of β-catenin during HCC progression. Nat Commun 10, 1–17. https://doi.org/10.1038/s41467-019-09780-z

Klenova, E., Chernukhin, I., Inoue, T., Shamsuddin, S., Norton, J., 2002. Immunoprecipitation techniques for the analysis of transcription factor complexes. Methods 26, 254–259. https://doi.org/10.1016/S1046-2023(02)00029-4

Knudsen, E.S., Knudsen, K.E., 2008. Tailoring to RB: tumour suppressor status and therapeutic response. Nat Rev Cancer 8, 714–724. https://doi.org/10.1038/nrc2401

Kobayashi, S., Werneburg, N.W., Bronk, S.F., Kaufmann, S.H., Gores, G.J., 2005. Interleukin-6 contributes to Mcl-1 up-regulation and TRAIL resistance via an Akt-signaling pathway in cholangiocarcinoma cells. Gastroenterology 128, 2054–2065. https://doi.org/10.1053/j.gastro.2005.03.010

Kodama, Y., Hijikata, M., Kageyama, R., Shimotohno, K., Chiba, T., 2004. The role of notch signaling in the development of intrahepatic bile ducts. Gastroenterology 127, 1775–1786. https://doi.org/10.1053/j.gastro.2004.09.004

Kopan, R., Ilagan, Ma.X.G., 2009. The Canonical Notch Signaling Pathway: Unfolding the Activation Mechanism. Cell 137, 216–233. https://doi.org/10.1016/j.cell.2009.03.045

Kreis, N.-N., Louwen, F., Yuan, J., 2019. The Multifaceted p21 (Cip1/Waf1/CDKN1A) in Cell Differentiation, Migration and Cancer Therapy. Cancers (Basel) 11. https://doi.org/10.3390/cancers11091220

Kroemer, G., Galluzzi, L., Brenner, C., 2007. Mitochondrial membrane permeabilization in cell death. Physiol. Rev. 87, 99–163. https://doi.org/10.1152/physrev.00013.2006

Kühl, S.J., Kühl, M., 2013. On the role of Wnt/β-catenin signaling in stem cells. Biochim. Biophys. Acta 1830, 2297–2306. https://doi.org/10.1016/j.bbagen.2012.08.010

Landesman-Bollag, E., Romieu-Mourez, R., Song, D.H., Sonenshein, G.E., Cardiff, R.D., Seldin, D.C., 2001. Protein kinase CK2 in mammary gland tumourigenesis. Oncogene 20, 3247–3257. https://doi.org/10.1038/sj.onc.1204411

Lee, T.I., Young, R.A., 2013. Transcriptional Regulation and Its Misregulation in Disease. Cell 152, 1237–1251. https://doi.org/10.1016/j.cell.2013.02.014

Lefebvre, P., Cariou, B., Lien, F., Kuipers, F., Staels, B., 2009. Role of bile acids and bile acid receptors in metabolic regulation. Physiol. Rev. 89, 147–191. https://doi.org/10.1152/physrev.00010.2008

Leone, F., Cavalloni, G., Pignochino, Y., Sarotto, I., Ferraris, R., Piacibello, W., Venesio, T., Capussotti, L., Risio, M., Aglietta, M., 2006. Somatic mutations of epidermal growth factor receptor in bile duct and gallbladder carcinoma. Clin. Cancer Res. 12, 1680–1685. https://doi.org/10.1158/1078-0432.CCR-05-1692

Leong, K.G., Niessen, K., Kulic, I., Raouf, A., Eaves, C., Pollet, I., Karsan, A., 2007. Jagged1-mediated Notch activation induces epithelial-to-mesenchymal transition through Slug-induced repression of E-cadherin. J. Exp. Med. 204, 2935–2948. https://doi.org/10.1084/jem.20071082

Li, Y., Li, P.-K., Roberts, M.J., Arend, R.C., Samant, R.S., Buchsbaum, D.J., 2014. Multi-targeted therapy of cancer by niclosamide: A new application for an old drug. Cancer Lett. 349, 8–14. https://doi.org/10.1016/j.canlet.2014.04.003

Liberzon, A., Birger, C., Thorvaldsdóttir, H., Ghandi, M., Mesirov, J.P., Tamayo, P., 2015. The Molecular Signatures Database Hallmark Gene Set Collection. cels 1, 417–425. https://doi.org/10.1016/j.cels.2015.12.004

Lin, H.-Y., Liang, Y.-K., Dou, X.-W., Chen, C.-F., Wei, X.-L., Zeng, D., Bai, J.-W., Guo, Y.-X., Lin, F.-F., Huang, W.-H., Du, C.-W., Li, Y.-C., Chen, M., Zhang, G.-J., 2018. Notch3 inhibits epithelial–mesenchymal transition in breast cancer via a novel mechanism, upregulation of GATA-3 expression. Oncogenesis 7, 1–15. https://doi.org/10.1038/s41389-018-0069-z

Lin, Z.-Y., Kuo, C.-H., Wu, D.-C., Chuang, W.-L., 2016. Anticancer effects of clinically acceptable colchicine concentrations on human gastric cancer cell lines. The Kaohsiung Journal of Medical Sciences 32, 68–73. https://doi.org/10.1016/j.kjms.2015.12.006

Litchfield, D.W., 2003. Protein kinase CK2: structure, regulation and role in cellular decisions of life and death. Biochem. J. 369, 1–15. https://doi.org/10.1042/BJ20021469

Liu, M., Liu, H., Chen, J., 2018. Mechanisms of the CDK4/6 inhibitor palbociclib (PD 0332991) and its future application in cancer treatment (Review). Oncology Reports 39, 901–911. https://doi.org/10.3892/or.2018.6221

Llovet, J.M., Villanueva, A., Lachenmayer, A., Finn, R.S., 2015. Advances in targeted therapies for hepatocellular carcinoma in the genomic era. Nat Rev Clin Oncol 12, 408–424. https://doi.org/10.1038/nrclinonc.2015.103

Lobry, C., Oh, P., Aifantis, I., 2011. Oncogenic and tumour suppressor functions of Notch in cancer: it's NOTCH what you think. J Exp Med 208, 1931–1935. https://doi.org/10.1084/jem.20111855

Loilome, W., Bungkanjana, P., Techasen, A., Namwat, N., Yongvanit, P., Puapairoj, A., Khuntikeo, N., Riggins, G.J., 2014. Activated macrophages promote Wnt/β-catenin signaling in cholangiocarcinoma cells. Tumour Biol 35, 5357–5367. https://doi.org/10.1007/s13277-014-1698-2

Lozier, J., McCright, B., Gridley, T., 2008. Notch signaling regulates bile duct morphogenesis in mice. PLoS ONE 3, e1851. https://doi.org/10.1371/journal.pone.0001851

LU, J., XIA, Y., CHEN, K., ZHENG, Y., WANG, J., LU, W., YIN, Q., WANG, F., ZHOU, Y., GUO, C., 2016. Oncogenic role of the Notch pathway in primary liver cancer. Oncol Lett 12, 3–10. https://doi.org/10.3892/ol.2016.4609

Lu, J., Zhou, Y., Hu, T., Zhang, Hui, Shen, M., Cheng, P., Dai, W., Wang, F., Chen, K., Zhang, Y., Wang, C., Li, J., Zheng, Y., Yang, J., Zhu, R., Wang, Jianrong, Lu, W., Zhang, Huawei, Wang, Junshan, Xia, Y., Assuncao, T.M.D., Jalan-Sakrikar, N., Huebert, R.C., Zhou, B., Guo, C., 2016. Notch Signaling Coordinates Progenitor Cell-Mediated Biliary Regeneration Following Partial Hepatectomy. Sci Rep 6, 1–16. https://doi.org/10.1038/srep22754

Lundell, M.J., Lee, H.-K., Pérez, E., Chadwell, L., 2003. The regulation of apoptosis by Numb/Notch signaling in the serotonin lineage of Drosophila. Development 130, 4109–4121. https://doi.org/10.1242/dev.00593

Lykkesfeldt, J., Tveden-Nyborg, P., 2019. The Pharmacokinetics of Vitamin C. Nutrients 11, 2412. https://doi.org/10.3390/nu11102412

MacDonald, B.T., Tamai, K., He, X., 2009. Wnt/beta-catenin signaling: components, mechanisms, and diseases. Dev. Cell 17, 9–26. https://doi.org/10.1016/j.devcel.2009.06.016

Majidinia, M., Darband, S.G., Kaviani, M., Nabavi, S.M., Jahanban-Esfahlan, R., Yousefi, B., 2018. Cross-regulation between Notch signaling pathway and miRNA machinery in cancer. DNA Repair 66–67, 30–41. https://doi.org/10.1016/j.dnarep.2018.04.002

Malorni, L., Piazza, S., Ciani, Y., Guarducci, C., Bonechi, M., Biagioni, C., Hart, C.D., Verardo, R., Di Leo, A., Migliaccio, I., 2016. A gene expression signature of retinoblastoma loss-of-function is a predictive biomarker of resistance to palbociclib in breast cancer cell lines and is prognostic in patients with ER positive early breast cancer. Oncotarget 7, 68012–68022. https://doi.org/10.18632/oncotarget.12010

Manfioletti, G., Gattei, V., Buratti, E., Rustighi, A., De Iuliis, A., Aldinucci, D., Goodwin, G.H., Pinto, A., 1995. Differential expression of a novel proline-rich homeobox gene (Prh) in human hematolymphopoietic cells. Blood 85, 1237–1245.

Mao, Y., Keller, E.T., Garfield, D.H., Shen, K., Wang, J., 2013. Stromal cells in tumour microenvironment and breast cancer. Cancer Metastasis Rev. 32, 303–315. https://doi.org/10.1007/s10555-012-9415-3

Marcolino, E., Siddiqui, Y.H., van den Bosch, M., Poole, A.W., Jayaraman, P.-S., Gaston, K., 2020. Blood platelets stimulate cancer extravasation through TGFβ-mediated downregulation of PRH/HHEX. Oncogenesis 9, 1–12. https://doi.org/10.1038/s41389-020-0189-0

Marfil, V., Blazquez, M., Serrano, F., Castell, J.V., Bort, R., 2015. Growth-promoting and tumourigenic activity of c-Myc is suppressed by Hhex. Oncogene 34, 3011–3022. https://doi.org/10.1038/onc.2014.240

Margagliotti, S., Clotman, F., Pierreux, C.E., Beaudry, J.-B., Jacquemin, P., Rousseau, G.G., Lemaigre, F.P., 2007. The Onecut transcription factors HNF-6/OC-1 and OC-2 regulate early liver expansion by controlling hepatoblast migration. Dev. Biol. 311, 579–589. https://doi.org/10.1016/j.ydbio.2007.09.013

Marinkovich, M.P., 2007. Laminin 332 in squamous-cell carcinoma. Nature Reviews Cancer 7, 370–380. https://doi.org/10.1038/nrc2089

Maroni, L., Pierantonelli, I., Banales, J.M., Benedetti, A., Marzioni, M., 2012. The significance of genetics for cholangiocarcinoma development. Annals of Translational Medicine 1, 7. https://doi.org/10.3978/j.issn.2305-5839.2012.10.04

Martinez Barbera, J.P., Clements, M., Thomas, P., Rodriguez, T., Meloy, D., Kioussis, D., Beddington, R.S., 2000. The homeobox gene Hex is required in definitive endodermal tissues for normal forebrain, liver and thyroid formation. Development 127, 2433–2445.

Martinez-Soria, N., McKenzie, L., Draper, J., Ptasinska, A., Issa, H., Potluri, S., Blair, H.J., Pickin, A., Isa, A., Chin, P.S., Tirtakusuma, R., Coleman, D., Nakjang, S., Assi, S., Forster, V., Reza, M., Law, E., Berry, P., Mueller, D., Elder, A., Bomken, S.N., Pal, D., Allan, J.M., Veal, G.J., Cockerill, P.N., Wichmann, C., Vormoor, J., Lacaud, G., Bonifer, C., Heidenreich, O., 2018. The Oncogenic Transcription Factor RUNX1/ETO Corrupts Cell Cycle Regulation to Drive Leukemic Transformation. Cancer Cell 34, 626-642.e8. https://doi.org/10.1016/j.ccell.2018.08.015

McCormack, M.P., Young, L.F., Vasudevan, S., Graaf, C.A. de, Codrington, R., Rabbitts, T.H., Jane, S.M., Curtis, D.J., 2010. The Lmo2 Oncogene Initiates Leukemia in Mice by Inducing Thymocyte Self-Renewal. Science 327, 879–883. https://doi.org/10.1126/science.1182378

McLin, V.A., Rankin, S.A., Zorn, A.M., 2007. Repression of Wnt/β-catenin signaling in the anterior endoderm is essential for liver and pancreas development. Development 134, 2207–2217. https://doi.org/10.1242/dev.001230

Meng, X., Franklin, D.A., Dong, J., Zhang, Y., 2014. MDM2-p53 Pathway in Hepatocellular Carcinoma. Cancer Res 74, 7161–7167. https://doi.org/10.1158/0008-5472.CAN-14-1446

Mergui, X., Puiffe, M.-L., Valteau-Couanet, D., Lipinski, M., Bénard, J., Amor-Guéret, M., 2010. p21Waf1 expression is regulated by nuclear intermediate filament vimentin in neuroblastoma. BMC Cancer 10, 473. https://doi.org/10.1186/1471-2407-10-473

Messica, Y., Laser-Azogui, A., Volberg, T., Elisha, Y., Lysakovskaia, K., Eils, R., Gladilin, E., Geiger, B., Beck, R., 2017. The role of Vimentin in Regulating Cell Invasive Migration in Dense Cultures of Breast Carcinoma Cells. Nano Lett. 17, 6941–6948. https://doi.org/10.1021/acs.nanolett.7b03358

Metcalfe, C., Mendoza-Topaz, C., Mieszczanek, J., Bienz, M., 2010. Stability elements in the LRP6 cytoplasmic tail confer efficient signalling upon DIX-dependent polymerization. J Cell Sci 123, 1588–1599. https://doi.org/10.1242/jcs.067546

Michaloglou, C., Crafter, C., Siersbaek, R., Delpuech, O., Curwen, J.O., Carnevalli, L.S., Staniszewska, A.D., Polanska, U.M., Cheraghchi-Bashi, A., Lawson, M., Chernukhin, I., McEwen, R., Carroll, J.S., Cosulich, S.C., 2018. Combined Inhibition of mTOR and CDK4/6 Is Required for Optimal Blockade of E2F Function and Long-term Growth Inhibition in Estrogen Receptor–positive Breast Cancer. Mol Cancer Ther 17, 908–920. https://doi.org/10.1158/1535-7163.MCT-17-0537

Minami, T., Murakami, T., Horiuchi, K., Miura, M., Noguchi, T., Miyazaki, J., Hamakubo, T., Aird, W.C., Kodama, T., 2004. Interaction between hex and GATA transcription factors in vascular endothelial cells inhibits flk-1/KDR-mediated vascular endothelial growth factor signaling. J. Biol. Chem. 279, 20626–20635. https://doi.org/10.1074/jbc.M308730200

Miwa, M., Stuehr, D.J., Marletta, M.A., Wishnok, J.S., Tannenbaum, S.R., 1987. Nitromation of amines by stimulated macrophages. Carcinogenesis 8, 955–958. https://doi.org/10.1093/carcin/8.7.955

Miyaki, M., Kuroki, T., 2003. Role of Smad4 (DPC4) inactivation in human cancer. Biochem. Biophys. Res. Commun. 306, 799–804. https://doi.org/10.1016/s0006-291x(03)01066-0

Mokhtari, R.B., Homayouni, T.S., Baluch, N., Morgatskaya, E., Kumar, S., Das, B., Yeger, H., 2017. Combination therapy in combating cancer. Oncotarget 8, 38022–38043. https://doi.org/10.18632/oncotarget.16723

Morin, P.J., 2005. Claudin proteins in human cancer: promising new targets for diagnosis and therapy. Cancer Res. 65, 9603–9606. https://doi.org/10.1158/0008-5472.CAN-05-2782

Nakagawa, T., Abe, M., Yamazaki, T., Miyashita, H., Niwa, H., Kokubun, S., Sato, Y., 2003. HEX acts as a negative regulator of angiogenesis by modulating the expression of angiogenesis-related gene in endothelial cells in vitro. Arterioscler. Thromb. Vasc. Biol. 23, 231–237. https://doi.org/10.1161/01.atv.0000052670.55321.87

Nebert, D.W., 2002. Transcription factors and cancer: an overview. Toxicology 181–182, 131–141. https://doi.org/10.1016/S0300-483X(02)00269-X

Nejak-Bowen, K., Monga, S.P., 2008. Wnt/β-catenin signaling in hepatic organogenesis. Organogenesis 4, 92–99.

Németh, Z., Szász, A.M., Somorácz, Á., Tátrai, P., Németh, J., Győrffy, H., Szíjártó, A., Kupcsulik, P., Kiss, A., Schaff, Z., 2009a. Zonula Occludens-1, Occludin, and E-cadherin Protein Expression in Biliary Tract Cancers. Pathol. Oncol. Res. 15, 533. https://doi.org/10.1007/s12253-009-9150-4

Németh, Z., Szász, A.M., Tátrai, P., Németh, J., Györffy, H., Somorácz, Á., Szíjártó, A., Kupcsulik, P., Kiss, A., Schaff, Z., 2009b. Claudin-1, −2, −3, −4, −7, −8, and −10 Protein Expression in Biliary Tract Cancers. J Histochem Cytochem. 57, 113–121. https://doi.org/10.1369/jhc.2008.952291

Nguyen, T., Brunson, D.K., Crespi, C.L., Penman, B.W., Wishnok, J.S., Tannenbaum, S.R., 1992. DNA damage and mutation in human cells exposed to nitric oxide in vitro. Proceedings of the National Academy of Sciences of the United States of America 89, 3030–3034. https://doi.org/10.1073/pnas.89.7.3030

Nieto, M.A., 2002. The snail superfamily of zinc-finger transcription factors. Nat. Rev. Mol. Cell Biol. 3, 155–166. https://doi.org/10.1038/nrm757

Nonomura, A., Ohta, G., Nakanuma, Y., Izumi, R., Mizukami, Y., Matsubara, F., Hayashi, M., Watanabe, K., Takayanagi, N., 1988. Simultaneous detection of epidermal growth factor receptor (EGF-R), epidermal growth factor (EGF) and ras p21 in cholangiocarcinoma by an immunocytochemical method. Liver 8, 157–166. https://doi.org/10.1111/j.1600-0676.1988.tb00985.x

Nowell, C.S., Radtke, F., 2017. Notch as a tumour suppressor. Nature Reviews Cancer 17, 145–159. https://doi.org/10.1038/nrc.2016.145

Noy, P., Sawasdichai, A., Jayaraman, P.-S., Gaston, K., 2012. Protein kinase CK2 inactivates PRH/Hhex using multiple mechanisms to de-repress VEGF-signalling genes and promote cell survival. Nucleic Acids Res. 40, 9008–9020. https://doi.org/10.1093/nar/gks687

Noy, P., Williams, H., Sawasdichai, A., Gaston, K., Jayaraman, P.-S., 2010. PRH/Hhex controls cell survival through coordinate transcriptional regulation of vascular endothelial growth factor signaling. Mol. Cell. Biol. 30, 2120–2134. https://doi.org/10.1128/MCB.01511-09

Nussler, A.K., Vergani, G., Gollin, S.M., Dorko, K., Gansauge, S., Morris, S.M., Demetris, A.J., Nomoto, M., Beger, H.G., Strom, S.C., 1999. Isolation and Characterization of a Human Hepatic Epithelial-like Cell Line (AKN-1) from a Normal Liver. In Vitro Cellular & Developmental Biology. Animal 35, 190–197.

Nuthall, H.N., Husain, J., McLarren, K.W., Stifani, S., 2002. Role for Hes1-Induced Phosphorylation in Groucho-Mediated Transcriptional Repression. Mol Cell Biol 22, 389–399. https://doi.org/10.1128/MCB.22.2.389-399.2002

O'Brien, M.A., Kirby, R., 2008. Apoptosis: A review of pro-apoptotic and anti-apoptotic pathways and dysregulation in disease. Journal of Veterinary Emergency and Critical Care 18, 572–585. https://doi.org/10.1111/j.1476-4431.2008.00363.x

Oda, K., Matsuoka, Y., Funahashi, A., Kitano, H., 2005. A comprehensive pathway map of epidermal growth factor receptor signaling. Mol Syst Biol 1, 2005.0010. https://doi.org/10.1038/msb4100014

Ohtsubo, M., Theodoras, A.M., Schumacher, J., Roberts, J.M., Pagano, M., 1995. Human cyclin E, a nuclear protein essential for the G1-to-S phase transition. Mol. Cell. Biol. 15, 2612–2624. https://doi.org/10.1128/mcb.15.5.2612

Oliva-González, C., Uresti-Rivera, E.E., Galicia-Cruz, O.G., Jasso-Robles, F.I., Gandolfi, A.J., Escudero-Lourdes, C., 2017. The tumour suppressor phosphatase and tensin homolog protein (PTEN) is negatively regulated by NF-κb p50 homodimers and involves histone 3 methylation/deacetylation in UROtsa cells chronically exposed to monomethylarsonous acid. Toxicol. Lett. 280, 92–98. https://doi.org/10.1016/j.toxlet.2017.08.013

Ono, Y., Hiratsuka, Y., Murata, M., Takasawa, A., Fukuda, R., Nojima, M., Tanaka, S., Osanai, M., Hirata, K., Sawada, N., 2016. Claudins-4 and -7 might be valuable markers to distinguish hepatocellular carcinoma from cholangiocarcinoma. Virchows Arch. 469, 417–426. https://doi.org/10.1007/s00428-016-1984-z

Oshi, M., Takahashi, H., Tokumaru, Y., Yan, L., Rashid, O.M., Matsuyama, R., Endo, I., Takabe, K., 2020. G2M Cell Cycle Pathway Score as a Prognostic Biomarker of Metastasis in Estrogen Receptor (ER)-Positive Breast Cancer. International Journal of Molecular Sciences 21, 2921. https://doi.org/10.3390/ijms21082921

Padmanaban, V., Krol, I., Suhail, Y., Szczerba, B.M., Aceto, N., Bader, J.S., Ewald, A.J., 2019a. E-cadherin is required for metastasis in multiple models of breast cancer. Nature 573, 439–444. https://doi.org/10.1038/s41586-019-1526-3

Padmanaban, V., Krol, I., Suhail, Y., Szczerba, B.M., Aceto, N., Bader, J.S., Ewald, A.J., 2019b. E-cadherin is required for metastasis in multiple models of breast cancer. Nature 573, 439–444. https://doi.org/10.1038/s41586-019-1526-3

Palmer, D.J., Ng, P., 2008. Methods for the production of first generation adenoviral vectors. Methods Mol. Biol. 433, 55–78. https://doi.org/10.1007/978-1-59745-237-3_4

Paoli, P., Giannoni, E., Chiarugi, P., 2013. Anoikis molecular pathways and its role in cancer progression. Biochimica et Biophysica Acta (BBA) - Molecular Cell Research 1833, 3481–3498. https://doi.org/10.1016/j.bbamcr.2013.06.026

Parks, D.J., Blanchard, S.G., Bledsoe, R.K., Chandra, G., Consler, T.G., Kliewer, S.A., Stimmel, J.B., Willson, T.M., Zavacki, A.M., Moore, D.D., Lehmann, J.M., 1999. Bile acids: natural ligands for an orphan nuclear receptor. Science 284, 1365–1368. https://doi.org/10.1126/science.284.5418.1365

Paternot, S., Bockstaele, L., Bisteau, X., Kooken, H., Coulonval, K., Roger, P.P., 2010. Rb inactivation in cell cycle and cancer: the puzzle of highly regulated activating phosphorylation of CDK4 versus constitutively active CDK-activating kinase. Cell Cycle 9, 689–699. https://doi.org/10.4161/cc.9.4.10611

Paz, H., Lynch, M.R., Bogue, C.W., Gasson, J.C., 2010. The homeobox gene Hhex regulates the earliest stages of definitive hematopoiesis. Blood 116, 1254–1262. https://doi.org/10.1182/blood-2009-11-254383

Peinado, H., Portillo, F., Cano, A., 2004. Transcriptional regulation of cadherins during development and carcinogenesis. Int. J. Dev. Biol. 48, 365–375. https://doi.org/10.1387/ijdb.041794hp

Pellizzari, L., D'Elia, A., Rustighi, A., Manfioletti, G., Tell, G., Damante, G., 2000. Expression and function of the homeodomain-containing protein Hex in thyroid cells. Nucleic Acids Res 28, 2503–2511.

Peng, X., Cuff, L.E., Lawton, C.D., DeMali, K.A., 2010. Vinculin regulates cell-surface E-cadherin expression by binding to beta-catenin. J. Cell. Sci. 123, 567–577. https://doi.org/10.1242/jcs.056432

Peruzzi, B., Bottaro, D.P., 2006. Targeting the c-Met signaling pathway in cancer. Clin. Cancer Res. 12, 3657–3660. https://doi.org/10.1158/1078-0432.CCR-06-0818

Pfaffl, M.W., 2001. A new mathematical model for relative quantification in real-time RT–PCR. Nucleic Acids Res 29, e45.

Pinlaor, S., Hiraku, Y., Ma, N., Yongvanit, P., Semba, R., Oikawa, S., Murata, M., Sripa, B., Sithithaworn, P., Kawanishi, S., 2004. Mechanism of NO-mediated oxidative and nitrative DNA damage in hamsters infected with Opisthorchis viverrini: a model of inflammation-mediated carcinogenesis. Nitric Oxide 11, 175–183. https://doi.org/10.1016/j.niox.2004.08.004

Pinlaor, S., Onsurathum, S., Boonmars, T., Pinlaor, P., Hongsrichan, N., Chaidee, A., Haonon, O., Limviroj, W., Tesana, S., Kaewkes, S., Sithithaworn, P., 2013. Distribution and Abundance of Opisthorchis viverrini Metacercariae in Cyprinid Fish in Northeastern Thailand. The Korean Journal of Parasitology 51, 703. https://doi.org/10.3347/kjp.2013.51.6.703

Polakis, P., 2012. Wnt signaling in cancer. Cold Spring Harb Perspect Biol 4. https://doi.org/10.1101/cshperspect.a008052

Porta, C., Paglino, C., Mosca, A., 2014. Targeting PI3K/Akt/mTOR Signaling in Cancer. Front Oncol 4. https://doi.org/10.3389/fonc.2014.00064

pubmeddev, al, Z.S., et, n.d. Liver fluke infection and cholangiocarcinoma: a review. - PubMed - NCBI [WWW Document]. URL https://www.ncbi.nlm.nih.gov/pubmed/27718017 (accessed 11.14.19).

Puppin, C., D'Elia, A.V., Pellizzari, L., Russo, D., Arturi, F., Presta, I., Filetti, S., Bogue, C.W., Denson, L.A., Damante, G., 2003. Thyroid-specific transcription factors control Hex promoter activity. Nucleic Acids Res 31, 1845–1852.

Puppin, C., Presta, I., D'Elia, A.V., Tell, G., Arturi, F., Russo, D., Filetti, S., Damante, G., 2004. Functional interaction among thyroid-specific transcription factors: Pax8 regulates the activity of Hex promoter. Mol. Cell. Endocrinol. 214, 117–125. https://doi.org/10.1016/j.mce.2003.10.061

Puppin, C., Puglisi, F., Pellizzari, L., Manfioletti, G., Pestrin, M., Pandolfi, M., Piga, A., Di Loreto, C., Damante, G., 2006. HEX expression and localization in normal mammary gland and breast carcinoma. BMC Cancer 6, 192. https://doi.org/10.1186/1471-2407-6-192

Qin, Y., Yu, J., Zhang, M., Qin, F., Lan, X., 2019. ZEB1 promotes tumourigenesis and metastasis in hepatocellular carcinoma by regulating the expression of vimentin. Mol Med Rep 19, 2297–2306. https://doi.org/10.3892/mmr.2019.9866

Rattanasinganchan, P., Leelawat, K., Treepongkaruna, S., Tocharoentanaphol, C., Subwongcharoen, S., Suthiphongchai, T., Tohtong, R., 2006. Establishment and characterization of a cholangiocarcinoma cell line (RMCCA-1) from a Thai patient. World J. Gastroenterol. 12, 6500–6506. https://doi.org/10.3748/wjg.v12.i40.6500

Razumilava, N., Gores, G.J., 2013. Classification, Diagnosis, and Management of Cholangiocarcinoma. Clinical gastroenterology and hepatology : the official clinical practice journal of the American Gastroenterological Association 11, 13. https://doi.org/10.1016/j.cgh.2012.09.009

Reaves, S.K., Fanzo, J.C., Arima, K., Wu, J.Y., Wang, Y.R., Lei, K.Y., 2000. Expression of the p53 tumour suppressor gene is up-regulated by depletion of intracellular zinc in HepG2 cells. J. Nutr. 130, 1688–1694. https://doi.org/10.1093/jn/130.7.1688

Reed, J.C., 1997. Bcl-2 family proteins: regulators of apoptosis and chemoresistance in hematologic malignancies. Semin. Hematol. 34, 9–19.

Reitman, Z.J., Yan, H., 2010. Isocitrate dehydrogenase 1 and 2 mutations in cancer: alterations at a crossroads of cellular metabolism. J. Natl. Cancer Inst. 102, 932–941. https://doi.org/10.1093/jnci/djq187

Reynolds, A.B., Carnahan, R.H., 2004. Regulation of cadherin stability and turnover by p120ctn: implications in disease and cancer. Semin. Cell Dev. Biol. 15, 657–663. https://doi.org/10.1016/j.semcdb.2004.09.003

Rizvi, S., Khan, S.A., Hallemeier, C.L., Kelley, R.K., Gores, G.J., 2018. Cholangiocarcinoma — evolving concepts and therapeutic strategies. Nat Rev Clin Oncol 15, 95–111. https://doi.org/10.1038/nrclinonc.2017.157

Roberts, P.J., Der, C.J., 2007. Targeting the Raf-MEK-ERK mitogen-activated protein kinase cascade for the treatment of cancer. Oncogene 26, 3291–3310. https://doi.org/10.1038/sj.onc.1210422

Roderick, J.E., Tesell, J., Shultz, L.D., Brehm, M.A., Greiner, D.L., Harris, M.H., Silverman, L.B., Sallan, S.E., Gutierrez, A., Look, A.T., Qi, J., Bradner, J.E., Kelliher, M.A., 2014. c-Myc inhibition prevents leukemia initiation in mice and impairs the growth of relapsed and induction failure pediatric T-ALL cells. Blood 123, 1040–1050. https://doi.org/10.1182/blood-2013-08-522698

Rossi, J.M., Dunn, N.R., Hogan, B.L., Zaret, K.S., 2001. Distinct mesodermal signals, including BMPs from the septum transversum mesenchyme, are required in combination for hepatogenesis from the endoderm. Genes Dev. 15, 1998–2009. https://doi.org/10.1101/gad.904601

Ruebner, B.H., Blankenberg, T.A., Burrows, D.A., SooHoo, W., Lund, J.K., 1990. Development and transformation of the ductal plate in the developing human liver. Pediatr Pathol 10, 55–68. https://doi.org/10.3109/15513819009067096

Saentaweesuk, W., Araki, N., Vaeteewoottacharn, K., Silsirivanit, A., Seubwai, W., Talabnin, C., Muisuk, K., Sripa, B., Wongkham, S., Okada, S., Wongkham, C., 2018a. Activation of Vimentin Is Critical to Promote a Metastatic Potential of Cholangiocarcinoma Cells. Oncol. Res. 26, 605–616. https://doi.org/10.3727/096504017X15009778205068

Saentaweesuk, W., Araki, N., Vaeteewoottacharn, K., Silsirivanit, A., Seubwai, W., Talabnin, C., Muisuk, K., Sripa, B., Wongkham, S., Okada, S., Wongkham, C., 2018b. Activation of Vimentin Is Critical to Promote a Metastatic Potential of Cholangiocarcinoma Cells. Oncol. Res. 26, 605–616. https://doi.org/10.3727/096504017X15009778205068

Saitoh, M., Shirakihara, T., Miyazono, K., 2009. Regulation of the stability of cell surface E-cadherin by the proteasome. Biochem. Biophys. Res. Commun. 381, 560–565. https://doi.org/10.1016/j.bbrc.2009.02.098

Sakahira, H., Enari, M., Nagata, S., 1998. Cleavage of CAD inhibitor in CAD activation and DNA degradation during apoptosis. Nature 391, 96–99. https://doi.org/10.1038/34214

Santibañez, J.F., Quintanilla, M., Bernabeu, C., 2011. TGF-β/TGF-β receptor system and its role in physiological and pathological conditions. Clin. Sci. 121, 233–251. https://doi.org/10.1042/CS20110086

Satelli, A., Li, S., 2011. Vimentin as a potential molecular target in cancer therapy Or Vimentin, an overview and its potential as a molecular target for cancer therapy. Cell Mol Life Sci 68, 3033–3046. https://doi.org/10.1007/s00018-011-0735-1

Sawanyawisuth, K., Williamson, T., Wongkham, S., Riggins, G.J., 2014. Effect of the antiparasitic drug mebendazole on cholangiocarcinoma growth. The Southeast Asian journal of tropical medicine and public health 45, 1264–1270.

Scaffidi, C., Schmitz, I., Krammer, P.H., Peter, M.E., 1999. The role of c-FLIP in modulation of CD95-induced apoptosis. J. Biol. Chem. 274, 1541–1548. https://doi.org/10.1074/jbc.274.3.1541

Scaltriti, M., Baselga, J., 2006. The Epidermal Growth Factor Receptor Pathway: A Model for Targeted Therapy. Clin Cancer Res 12, 5268–5272. https://doi.org/10.1158/1078-0432.CCR-05-1554

Schaefer, L.K., Wang, S., Schaefer, T.S., 2001. Functional Interaction of Jun and Homeodomain Proteins. J. Biol. Chem. 276, 43074–43082. https://doi.org/10.1074/jbc.M102552200

Schweizer, M.T., Haugk, K., McKiernan, J.S., Gulati, R., Cheng, H.H., Maes, J.L., Dumpit, R.F., Nelson, P.S., Montgomery, B., McCune, J.S., Plymate, S.R., Yu, E.Y., 2018. A phase I study of niclosamide in combination with enzalutamide in men with castration-resistant prostate cancer. PLoS One 13, e0198389–e0198389. https://doi.org/10.1371/journal.pone.0198389

Sekiya, S., Suzuki, A., 2012. Intrahepatic cholangiocarcinoma can arise from Notch-mediated conversion of hepatocytes. J Clin Invest 122, 3914–3918. https://doi.org/10.1172/JCI63065

Serra, F., Lapidari, P., Quaquarini, E., Tagliaferri, B., Sottotetti, F., Palumbo, R., 2019. Palbociclib in metastatic breast cancer: current evidence and real-life data. Drugs Context 8. https://doi.org/10.7573/dic.212579

Sethi, S., Macoska, J., Chen, W., Sarkar, F.H., 2010. Molecular signature of epithelial-mesenchymal transition (EMT) in human prostate cancer bone metastasis. Am J Transl Res 3, 90–99.

Settakorn, J., Kaewpila, N., Burns, G.F., Leong, A.S.-Y., 2005. FAT, E-cadherin, β catenin, HER 2/neu, Ki67 immunoexpression, and histological grade in intrahepatic cholangiocarcinoma. Journal of Clinical Pathology 58, 1249–1254. https://doi.org/10.1136/jcp.2005.026575

Severn, C.B., 1971. A morphological study of the development of the human liver. I. Development of the hepatic diverticulum. Am. J. Anat. 131, 133–158. https://doi.org/10.1002/aja.1001310202

Shaw, R.J., Cantley, L.C., 2006. Ras, PI(3)K and mTOR signalling controls tumour cell growth. Nature 441, 424–430. https://doi.org/10.1038/nature04869

Sherr, C.J., Roberts, J.M., 1995. Inhibitors of mammalian G1 cyclin-dependent kinases. Genes Dev. 9, 1149–1163. https://doi.org/10.1101/gad.9.10.1149

Shields, B.J., Jackson, J.T., Metcalf, D., Shi, W., Huang, Q., Garnham, A.L., Glaser, S.P., Beck, D., Pimanda, J.E., Bogue, C.W., Smyth, G.K., Alexander, W.S., McCormack, M.P., 2016a. Acute myeloid leukemia requires Hhex to enable PRC2-mediated epigenetic repression of Cdkn2a. Genes Dev 30, 78–91. https://doi.org/10.1101/gad.268425.115

Shields, B.J., Jackson, J.T., Metcalf, D., Shi, W., Huang, Q., Garnham, A.L., Glaser, S.P., Beck, D., Pimanda, J.E., Bogue, C.W., Smyth, G.K., Alexander, W.S., McCormack, M.P., 2016b. Acute myeloid leukemia requires Hhex to enable PRC2-mediated epigenetic repression of *Cdkn2a*. Genes Dev. 30, 78–91. https://doi.org/10.1101/gad.268425.115

Shields, M.A., Ebine, K., Sahai, V., Kumar, K., Siddiqui, K., Hwang, R.F., Grippo, P.J., Munshi, H.G., 2013. Snail cooperates with KrasG12D to promote pancreatic fibrosis. Mol. Cancer Res. 11, 1078–1087. https://doi.org/10.1158/1541-7786.MCR-12-0637

Siddiqui, Y.H., Kershaw, R.M., Humphreys, E.H., Assis Junior, E.M., Chaudhri, S., Jayaraman, P.-S., Gaston, K., 2017. CK2 abrogates the inhibitory effects of PRH/HHEX on prostate cancer cell migration and invasion and acts through PRH to control cell proliferation. Oncogenesis 6, e293. https://doi.org/10.1038/oncsis.2016.82

Singh, A.B., Sharma, A., Dhawan, P., 2010. Claudin Family of Proteins and Cancer: An Overview [WWW Document]. Journal of Oncology. https://doi.org/10.1155/2010/541957

Sirisinha, S., Tengchaisri, T., Boonpucknavig, S., Prempracha, N., Ratanarapee, S., Pausawasdi, A., 1991. Establishment and characterization of a cholangiocarcinoma cell line from a Thai patient with intrahepatic bile duct cancer. Asian Pac. J. Allergy Immunol. 9, 153–157.

Sittithumcharee, G., Suppramote, O., Vaeteewoottacharn, K., Sirisuksakun, C., Jamnongsong, S., Laphanuwat, P., Suntiparpluacha, M., Matha, A., Chusorn, P., Buraphat, P., Kakanaporn, C., Charngkaew, K., Silsirivanit, A., Korphaisarn, K., Limsrichamrern, S., Tripatara, P., Pairojkul, C., Wongkham, S., Sampattavanich, S., Okada, S., Jirawatnotai, S., 2019. Dependency of Cholangiocarcinoma on Cyclin D–Dependent Kinase Activity. Hepatology 70, 1614–1630. https://doi.org/10.1002/hep.30704

Smith, S., Tripathi, R., Goodings, C., Cleveland, S., Mathias, E., Hardaway, J.A., Elliott, N., Yi, Y., Chen, X., Downing, J., Mullighan, C., Swing, D.A., Tessarollo, L., Li, L., Love, P., Jenkins, N.A., Copeland, N.G., Thompson, M.A., Du, Y., Davé, U.P., 2014. LIM Domain Only-2 (LMO2) Induces T-Cell Leukemia by Two Distinct Pathways. PLOS ONE 9, e85883. https://doi.org/10.1371/journal.pone.0085883

Somparn, N., Kukongviriyapan, V., Saenthaweesuk, S., 2018. Antiproliferative and apoptotic effects of high-dose vitamin C in cholangiocarcinoma cell line. Tropical Journal of Pharmaceutical Research 17, 1043–1048. https://doi.org/10.4314/tjpr.v17i6.9

Soufi, A., Jayaraman, P.-S., 2008a. PRH/Hex: an oligomeric transcription factor and multifunctional regulator of cell fate. Biochem. J. 412, 399–413. https://doi.org/10.1042/BJ20080035

Soufi, A., Jayaraman, P.-S., 2008b. PRH/Hex: an oligomeric transcription factor and multifunctional regulator of cell fate. Biochem J 412, 399–413. https://doi.org/10.1042/BJ20080035

Soufi, A., Noy, P., Buckle, M., Sawasdichai, A., Gaston, K., Jayaraman, P.-S., 2009. CK2 phosphorylation of the PRH/Hex homeodomain functions as a reversible switch for DNA binding. Nucleic Acids Res. 37, 3288–3300. https://doi.org/10.1093/nar/gkp197

Soufi, A., Smith, C., Clarke, A.R., Gaston, K., Jayaraman, P.-S., 2006. Oligomerisation of the developmental regulator proline rich homeodomain (PRH/Hex) is mediated by a novel proline-rich dimerisation domain. J. Mol. Biol. 358, 943–962. https://doi.org/10.1016/j.jmb.2006.02.020

Sparks, E.E., Huppert, K.A., Brown, M.A., Washington, M.K., Huppert, S.S., 2010. Notch signaling regulates formation of the three-dimensional architecture of intrahepatic bile ducts in mice. Hepatology 51, 1391–1400. https://doi.org/10.1002/hep.23431

Sripa, B., Kaewkes, S., 2000. Localisation of parasite antigens and inflammatory responses in experimental opisthorchiasis. International Journal for Parasitology 30, 735–740. https://doi.org/10.1016/S0020-7519(00)00054-0

Sripa, B., Leungwattanawanit, S., Nitta, T., Wongkham, C., Bhudhisawasdi, V., Puapairoj, A., Sripa, C., Miwa, M., 2005. Establishment and characterization of an opisthorchiasis-associated cholangiocarcinoma cell line (KKU-100). World J Gastroenterol 11, 3392–3397. https://doi.org/10.3748/wjg.v11.i22.3392

Sripa, B., Thinkhamrop, B., Mairiang, E., Laha, T., Kaewkes, S., Sithithaworn, P., Periago, M.V., Bhudhisawasdi, V., Yonglitthipagon, P., Mulvenna, J., Brindley, P.J., Loukas, A., Bethony, J.M., 2012. Elevated plasma IL-6 associates with increased risk of advanced fibrosis and cholangiocarcinoma in individuals infected by Opisthorchis viverrini. PLoS Negl Trop Dis 6, e1654. https://doi.org/10.1371/journal.pntd.0001654

Su, J., You, P., Zhao, J.-P., Zhang, S.-L., Song, S.-H., Fu, Z.-R., Ye, L.-W., Zi, X.-Y., Xie, D.-F., Zhu, M.-H., Hu, Y.-P., 2012. A potential role for the homeoprotein Hhex in hepatocellular carcinoma progression. Med. Oncol. 29, 1059–1067. https://doi.org/10.1007/s12032-011-9989-6

Sugimachi, K., Aishima, S., Taguchi, K., Tanaka, S., Shimada, M., Kajiyama, K., Sugimachi, K., Tsuneyoshi, M., 2001. The role of overexpression and gene amplification of cyclin D1 in intrahepatic cholangiocarcinoma. J. Hepatol. 35, 74–79. https://doi.org/10.1016/s0168-8278(01)00079-4

Suliman, M.A., Zhang, Z., Na, H., Ribeiro, A.L.L., Zhang, Y., Niang, B., Hamid, A.S., Zhang, H., Xu, L., Zuo, Y., 2016. Niclosamide inhibits colon cancer progression through downregulation of the Notch pathway and upregulation of the tumour suppressor miR-200 family. Int J Mol Med 38, 776–784. https://doi.org/10.3892/ijmm.2016.2689

Suzuki, A., Ito, T., Kawano, H., Hayashida, M., Hayasaki, Y., Tsutomi, Y., Akahane, K., Nakano, T., Miura, M., Shiraki, K., 2000. Survivin initiates procaspase 3/p21 complex formation as a result of

interaction with Cdk4 to resist Fas-mediated cell death. Oncogene 19, 1346–1353. https://doi.org/10.1038/sj.onc.1203429

Swingler, T.E., Bess, K.L., Yao, J., Stifani, S., Jayaraman, P.-S., 2004a. The proline-rich homeodomain protein recruits members of the Groucho/Transducin-like enhancer of split protein family to co-repress transcription in hematopoietic cells. J. Biol. Chem. 279, 34938–34947. https://doi.org/10.1074/jbc.M404488200

Swingler, T.E., Bess, K.L., Yao, J., Stifani, S., Jayaraman, P.-S., 2004b. The proline-rich homeodomain protein recruits members of the Groucho/Transducin-like enhancer of split protein family to co-repress transcription in hematopoietic cells. J. Biol. Chem. 279, 34938–34947. https://doi.org/10.1074/jbc.M404488200

Swinstead, E.E., Paakinaho, V., Presman, D.M., Hager, G.L., 2016. Pioneer factors and ATP-dependent chromatin remodeling factors interact dynamically: A new perspective. Bioessays 38, 1150–1157. https://doi.org/10.1002/bies.201600137

Tabariès, S., Siegel, P.M., 2017. The role of claudins in cancer metastasis. Oncogene 36, 1176–1190. https://doi.org/10.1038/onc.2016.289

Takaku, M., Grimm, S.A., Shimbo, T., Perera, L., Menafra, R., Stunnenberg, H.G., Archer, T.K., Machida, S., Kurumizaka, H., Wade, P.A., 2016. GATA3-dependent cellular reprogramming requires activation-domain dependent recruitment of a chromatin remodeler. Genome Biology 17, 36. https://doi.org/10.1186/s13059-016-0897-0

Takano, Y., Kato, Y., van Diest, P.J., Masuda, M., Mitomi, H., Okayasu, I., 2000. Cyclin D2 Overexpression and Lack of p27 Correlate Positively and Cyclin E Inversely with a Poor Prognosis in Gastric Cancer Cases. Am J Pathol 156, 585–594.

Tan, X., Yuan, Y., Zeng, G., Apte, U., Thompson, M.D., Cieply, B., Stolz, D.B., Michalopoulos, G.K., Kaestner, K.H., Monga, S.P.S., 2008. Beta-catenin deletion in hepatoblasts disrupts hepatic morphogenesis and survival during mouse development. Hepatology 47, 1667–1679. https://doi.org/10.1002/hep.22225

Tanaka, H., Yamamoto, T., Ban, T., Satoh, S., Tanaka, T., Shimoda, M., Miyazaki, J., Noguchi, T., 2005. Hex stimulates the hepatocyte nuclear factor 1alpha-mediated activation of transcription. Arch. Biochem. Biophys. 442, 117–124. https://doi.org/10.1016/j.abb.2005.08.001

Tchorz, J.S., Kinter, J., Müller, M., Tornillo, L., Heim, M.H., Bettler, B., 2009. Notch2 signaling promotes biliary epithelial cell fate specification and tubulogenesis during bile duct development in mice. Hepatology 50, 871–879. https://doi.org/10.1002/hep.23048

Techasen, A., Namwat, N., Loilome, W., Bungkanjana, P., Khuntikeo, N., Puapairoj, A., Jearanaikoon, P., Saya, H., Yongvanit, P., 2012a. Tumour necrosis factor-α (TNF-α) stimulates the epithelial–mesenchymal transition regulator Snail in cholangiocarcinoma. Med Oncol 29, 3083–3091. https://doi.org/10.1007/s12032-012-0305-x

Techasen, A., Namwat, N., Loilome, W., Bungkanjana, P., Khuntikeo, N., Puapairoj, A., Jearanaikoon, P., Saya, H., Yongvanit, P., 2012b. Tumour necrosis factor-α (TNF-α) stimulates the epithelial–mesenchymal transition regulator Snail in cholangiocarcinoma. Med Oncol 29, 3083–3091. https://doi.org/10.1007/s12032-012-0305-x

Techasen, A., Namwat, N., Loilome, W., Duangkumpha, K., Puapairoj, A., Saya, H., Yongvanit, P., 2014. Tumour necrosis factor-α modulates epithelial mesenchymal transition mediators ZEB2 and S100A4 to promote cholangiocarcinoma progression. Journal of Hepato-Biliary-Pancreatic Sciences 21, 703–711. https://doi.org/10.1002/jhbp.125

Testa, J.R., Bellacosa, A., 2001. AKT plays a central role in tumourigenesis. Proc Natl Acad Sci U S A 98, 10983–10985. https://doi.org/10.1073/pnas.211430998

Thibodeau, A., Márquez, E.J., Shin, D.-G., Vera-Licona, P., Ucar, D., 2017. Chromatin interaction networks revealed unique connectivity patterns of broad H3K4me3 domains and super enhancers in 3D chromatin. Sci Rep 7, 1–12. https://doi.org/10.1038/s41598-017-14389-7

Thiery, J.P., Acloque, H., Huang, R.Y.J., Nieto, M.A., 2009. Epithelial-mesenchymal transitions in development and disease. Cell 139, 871–890. https://doi.org/10.1016/j.cell.2009.11.007

Thompson, M., Nejak-Bowen, K., Monga, S.P.S., 2011. Crosstalk of the Wnt Signaling Pathway, in: Goss, K.H., Kahn, M. (Eds.), Targeting the Wnt Pathway in Cancer. Springer, New York, NY, pp. 51–80. https://doi.org/10.1007/978-1-4419-8023-6_4

Tian, X., Cao, Z., Ding, Q., Li, Z., Zhang, C., 2019. Prognostic value of multiple epithelial mesenchymal transition-associated proteins in intrahepatic cholangiocarcinoma. Oncol Lett 18, 2059–2065. https://doi.org/10.3892/ol.2019.10522

Timmerman, L.A., Grego-Bessa, J., Raya, A., Bertrán, E., Pérez-Pomares, J.M., Díez, J., Aranda, S., Palomo, S., McCormick, F., Izpisúa-Belmonte, J.C., de la Pompa, J.L., 2004. Notch promotes epithelial-mesenchymal transition during cardiac development and oncogenic transformation. Genes Dev. 18, 99–115. https://doi.org/10.1101/gad.276304

Tolstonog, G.V., Mothes, E., Shoeman, R.L., Traub, P., 2001. Isolation of SDS-stable complexes of the intermediate filament protein vimentin with repetitive, mobile, nuclear matrix attachment region, and mitochondrial DNA sequence elements from cultured mouse and human fibroblasts. DNA Cell Biol. 20, 531–554. https://doi.org/10.1089/104454901317094954

Tolstonog, G.V., Wang, X., Shoeman, R., Traub, P., 2000. Intermediate filaments reconstituted from vimentin, desmin, and glial fibrillary acidic protein selectively bind repetitive and mobile DNA sequences from a mixture of mouse genomic DNA fragments. DNA Cell Biol. 19, 647–677. https://doi.org/10.1089/10445490050199054

Topcu, Z., Mack, D.L., Hromas, R.A., Borden, K.L., 1999. The promyelocytic leukemia protein PML interacts with the proline-rich homeodomain protein PRH: a RING may link hematopoiesis and growth control. Oncogene 18, 7091–7100. https://doi.org/10.1038/sj.onc.1203201

Topisirovic, I., Culjkovic, B., Cohen, N., Perez, J.M., Skrabanek, L., Borden, K.L.B., 2003a. The proline-rich homeodomain protein, PRH, is a tissue-specific inhibitor of eIF4E-dependent cyclin D1 mRNA transport and growth. EMBO J 22, 689–703. https://doi.org/10.1093/emboj/cdg069

Topisirovic, I., Guzman, M.L., McConnell, M.J., Licht, J.D., Culjkovic, B., Neering, S.J., Jordan, C.T., Borden, K.L.B., 2003b. Aberrant eukaryotic translation initiation factor 4E-dependent mRNA transport impedes hematopoietic differentiation and contributes to leukemogenesis. Mol. Cell. Biol. 23, 8992–9002. https://doi.org/10.1128/mcb.23.24.8992-9002.2003

Triezenberg, S.J., 1995. Structure and function of transcriptional activation domains. Curr. Opin. Genet. Dev. 5, 190–196. https://doi.org/10.1016/0959-437x(95)80007-7

Trog, D., Yeghiazaryan, K., Schild, H.H., Golubnitschaja, O., 2008. Up-regulation of vimentin expression in low-density malignant glioma cells as immediate and late effects under irradiation and temozolomide treatment. Amino Acids 34, 539–545. https://doi.org/10.1007/s00726-007-0007-4

Tyagi, M., Imam, N., Verma, K., Patel, A.K., 2016. Chromatin remodelers: We are the drivers!! Nucleus 7, 388–404. https://doi.org/10.1080/19491034.2016.1211217

Valentijn, A.J., Metcalfe, A.D., Kott, J., Streuli, C.H., Gilmore, A.P., 2003. Spatial and temporal changes in Bax subcellular localization during anoikis. J. Cell Biol. 162, 599–612. https://doi.org/10.1083/jcb.200302154

Vaquero, J., Guedj, N., Clapéron, A., Nguyen Ho-Bouldoires, T.H., Paradis, V., Fouassier, L., 2017a. Epithelial-mesenchymal transition in cholangiocarcinoma: From clinical evidence to regulatory networks. Journal of Hepatology 66, 424–441. https://doi.org/10.1016/j.jhep.2016.09.010

Vaquero, J., Guedj, N., Clapéron, A., Nguyen Ho-Bouldoires, T.H., Paradis, V., Fouassier, L., 2017b. Epithelial-mesenchymal transition in cholangiocarcinoma: From clinical evidence to regulatory networks. Journal of Hepatology 66, 424–441. https://doi.org/10.1016/j.jhep.2016.09.010

Verhulst, S., Roskams, T., Sancho-Bru, P., van Grunsven, L.A., 2019. Meta-Analysis of Human and Mouse Biliary Epithelial Cell Gene Profiles. Cells 8. https://doi.org/10.3390/cells8101117

Vermeulen, K., Bockstaele, D.R.V., Berneman, Z.N., 2003. The cell cycle: a review of regulation, deregulation and therapeutic targets in cancer. Cell Proliferation 36, 131–149. https://doi.org/10.1046/j.1365-2184.2003.00266.x

Villanueva, A., Alsinet, C., Yanger, K., Hoshida, Y., Zong, Y., Toffanin, S., Rodriguez-Carunchio, L., Solé, M., Thung, S., Stanger, B.Z., Llovet, J.M., 2012. Notch signaling is activated in human hepatocellular carcinoma and induces tumour formation in mice. Gastroenterology 143, 1660-1669.e7. https://doi.org/10.1053/j.gastro.2012.09.002

Vinay, D.S., Ryan, E.P., Pawelec, G., Talib, W.H., Stagg, J., Elkord, E., Lichtor, T., Decker, W.K., Whelan, R.L., Kumara, H.M.C.S., Signori, E., Honoki, K., Georgakilas, A.G., Amin, A., Helferich, W.G., Boosani, C.S., Guha, G., Ciriolo, M.R., Chen, S., Mohammed, S.I., Azmi, A.S., Keith, W.N., Bilsland, A., Bhakta, D., Halicka, D., Fujii, H., Aquilano, K., Ashraf, S.S., Nowsheen, S., Yang, X., Choi, B.K., Kwon,

B.S., 2015. Immune evasion in cancer: Mechanistic basis and therapeutic strategies. Semin. Cancer Biol. 35 Suppl, S185–S198. https://doi.org/10.1016/j.semcancer.2015.03.004

Wang, A.-M., Ku, H.-H., Liang, Y.-C., Chen, Y.-C., Hwu, Y.-M., Yeh, T.-S., 2009. The autonomous notch signal pathway is activated by baicalin and baicalein but is suppressed by niclosamide in K562 cells. J. Cell. Biochem. 106, 682–692. https://doi.org/10.1002/jcb.22065

Wang, C., Lv, H., Yang, W., Li, T., Fang, T., Lv, G., Han, Q., Dong, L., Jiang, T., Jiang, B., Yang, G., Wang, H., 2017. SVCT-2 determines the sensitivity to ascorbate-induced cell death in cholangiocarcinoma cell lines and patient derived xenografts. Cancer Lett. 398, 1–11. https://doi.org/10.1016/j.canlet.2017.03.039

Wang, J., Dong, M., Xu, Z., Song, X., Zhang, S., Qiao, Y., Che, L., Gordan, J., Hu, K., Liu, Y., Calvisi, D.F., Chen, X., 2018. Notch2 controls hepatocyte-derived cholangiocarcinoma formation in mice. Oncogene 37, 3229–3242. https://doi.org/10.1038/s41388-018-0188-1

Wang, J., Xing, X., Li, Q., Zhang, G., Wang, T., Pan, H., Li, D., 2020. Targeting the FGFR signaling pathway in cholangiocarcinoma: promise or delusion? Ther Adv Med Oncol 12. https://doi.org/10.1177/1758835920940948

Wang, Q., Shoeman, R., Traub, P., 2000. Identification of the amino acid residues of the amino terminus of vimentin responsible for DNA binding by enzymatic and chemical sequencing and analysis by MALDI-TOF. Biochemistry 39, 6645–6651. https://doi.org/10.1021/bi000199s

Watanabe, H., Takayama, K., Inamura, M., Tachibana, M., Mimura, N., Katayama, K., Tashiro, K., Nagamoto, Y., Sakurai, F., Kawabata, K., Furue, M.K., Mizuguchi, H., 2014. HHEX Promotes Hepatic-Lineage Specification through the Negative Regulation of Eomesodermin. PLOS ONE 9, e90791. https://doi.org/10.1371/journal.pone.0090791

Whatcott, C.J., Diep, C.H., Jiang, P., Watanabe, A., LoBello, J., Sima, C., Hostetter, G., Shepard, H.M., Von Hoff, D.D., Han, H., 2015. Desmoplasia in Primary Tumours and Metastatic Lesions of Pancreatic Cancer. Clin. Cancer Res. 21, 3561–3568. https://doi.org/10.1158/1078-0432.CCR-14-1051

Williams, H., Jayaraman, P.-S., Gaston, K., 2008. DNA Wrapping and Distortion by an Oligomeric Homeodomain Protein. Journal of Molecular Biology 383, 10–23. https://doi.org/10.1016/j.jmb.2008.08.004

Wu, C.-E., Chen, M.-H., Yeh, C.-N., 2019. mTOR Inhibitors in Advanced Biliary Tract Cancers. Int J Mol Sci 20. https://doi.org/10.3390/ijms20030500

Wu, M., Bai, X., Xu, G., Wei, J., Zhu, T., Zhang, Y., Li, Q., Liu, P., Song, A., Zhao, L., Gang, C., Han, Z., Wang, S., Zhou, J., Lu, Y., Ma, D., 2007. Proteome analysis of human androgen-independent prostate cancer cell lines: variable metastatic potentials correlated with vimentin expression. Proteomics 7, 1973–1983. https://doi.org/10.1002/pmic.200600643

Wu, W.-R., Shi, X.-D., Zhang, R., Zhu, M.-S., Xu, L.-B., Yu, X.-H., Zeng, H., Wang, J., Liu, C., 2014. Clinicopathological significance of aberrant Notch receptors in intrahepatic cholangiocarcinoma. Int J Clin Exp Pathol 7, 3272–3279.

Wyatt, L.A., Filbin, M.T., Keirstead, H.S., 2014. PTEN inhibition enhances neurite outgrowth in human embryonic stem cell-derived neuronal progenitor cells. J. Comp. Neurol. 522, 2741–2755. https://doi.org/10.1002/cne.23580

Xiao, Q., Ge, G., 2012. Lysyl Oxidase, Extracellular Matrix Remodeling and Cancer Metastasis. Cancer Microenviron 5, 261–273. https://doi.org/10.1007/s12307-012-0105-z

Xing, X., Burgermeister, E., Geisler, F., Einwächter, H., Fan, L., Hiber, M., Rauser, S., Walch, A., Röcken, C., Ebeling, M., Wright, M.B., Schmid, R.M., Ebert, M.P.A., 2009. Hematopoietically expressed homeobox is a target gene of farnesoid X receptor in chenodeoxycholic acid–induced liver hypertrophy. Hepatology 49, 979–988. https://doi.org/10.1002/hep.22712

Xu, C.-R., Cole, P.A., Meyers, D.J., Kormish, J., Dent, S., Zaret, K.S., 2011. Chromatin “prepattern” and histone modifiers in a fate choice for liver and pancreas. Science 332, 963–966. https://doi.org/10.1126/science.1202845

Xu, L.-X., Grimaldo, S., Qi, J.-W., Yang, G.-L., Qin, T.-T., Xiao, H.-Y., Xiang, R., Xiao, Z., Li, L.-Y., Zhang, Z.-S., 2014. Death receptor 3 mediates TNFSF15- and TNFα-induced endothelial cell apoptosis. Int. J. Biochem. Cell Biol. 55, 109–118. https://doi.org/10.1016/j.biocel.2014.08.015

Xu, S., Xu, H., Wang, W., Li, S., Li, H., Li, T., Zhang, W., Yu, X., Liu, L., 2019. The role of collagen in cancer: from bench to bedside. Journal of Translational Medicine 17, 309. https://doi.org/10.1186/s12967-019-2058-1

Xu, X., Choi, S.H., Hu, T., Tiyanont, K., Habets, R., Groot, A.J., Vooijs, M., Aster, J.C., Chopra, R., Fryer, C., Blacklow, S.C., 2015. Insights into Autoregulation of Notch3 from Structural and Functional Studies of Its Negative Regulatory Region. Structure 23, 1227–1235. https://doi.org/10.1016/j.str.2015.05.001

Xue, L., Guo, C., Zhang, K., Jiang, H., Pang, F., Dou, Y., Liu, X., Lin, H., Dong, X., Zhao, S., Yao, M., Wang, K., Feng, Y., Gu, W., 2019. Comprehensive molecular profiling of extrahepatic cholangiocarcinoma in Chinese population and potential targets for clinical practice. Hepatobiliary Surg Nutr 8, 615–622. https://doi.org/10.21037/hbsn.2019.08.05

Yamauchi, M., Barker, T.H., Gibbons, D.L., Kurie, J.M., 2018. The fibrotic tumour stroma. J. Clin. Invest. 128, 16–25. https://doi.org/10.1172/JCI93554

Yang, M.-H., Chen, C.-L., Chau, G.-Y., Chiou, S.-H., Su, C.-W., Chou, T.-Y., Peng, W.-L., Wu, J.-C., 2009. Comprehensive analysis of the independent effect of twist and snail in promoting metastasis of hepatocellular carcinoma. Hepatology 50, 1464–1474. https://doi.org/10.1002/hep.23221

Yang, X., Wang, J., Liu, C., Grizzle, W.E., Yu, S., Zhang, S., Barnes, S., Koopman, W.J., Mountz, J.D., Kimberly, R.P., Zhang, H.-G., 2005. Cleavage of p53-Vimentin Complex Enhances Tumour Necrosis Factor-Related Apoptosis-Inducing Ligand-Mediated Apoptosis of Rheumatoid Arthritis Synovial Fibroblasts. Am J Pathol 167, 705–719.

Yenice, S., Davis, A.T., Goueli, S.A., Akdas, A., Limas, C., Ahmed, K., 1994. Nuclear casein kinase 2 (CK-2) activity in human normal, benign hyperplastic, and cancerous prostate. Prostate 24, 11–16. https://doi.org/10.1002/pros.2990240105

Yook, J.I., Li, X.-Y., Ota, I., Hu, C., Kim, H.S., Kim, N.H., Cha, S.Y., Ryu, J.K., Choi, Y.J., Kim, J., Fearon, E.R., Weiss, S.J., 2006. A Wnt-Axin2-GSK3beta cascade regulates Snail1 activity in breast cancer cells. Nat. Cell Biol. 8, 1398–1406. https://doi.org/10.1038/ncb1508

Zaret, K.S., Grompe, M., 2008. Generation and regeneration of cells of the liver and pancreas. Science 322, 1490–1494. https://doi.org/10.1126/science.1161431

Zender, S., Nickeleit, I., Wuestefeld, T., Sörensen, I., Dauch, D., Bozko, P., El-Khatib, M., Geffers, R., Bektas, H., Manns, M.P., Gossler, A., Wilkens, L., Plentz, R., Zender, L., Malek, N.P., 2013. A Critical Role for Notch Signaling in the Formation of Cholangiocellular Carcinomas. Cancer Cell 23, 784–795. https://doi.org/10.1016/j.ccr.2013.04.019

Zhan, T., Rindtorff, N., Boutros, M., 2017. Wnt signaling in cancer. Oncogene 36, 1461–1473. https://doi.org/10.1038/onc.2016.304

Zhang, G., Ma, F., Li, L., Li, J., Li, P., Zeng, S., Sun, H., Li, E., 2019. Palbociclib triggers apoptosis in bladder cancer cells by Cdk2-induced Rad9-mediated reorganization of the Bak.Bcl-xl complex. Biochemical Pharmacology 163, 133–141. https://doi.org/10.1016/j.bcp.2019.02.017

Zhang, K., Wang, D., Zhang, S., Jiao, X., Li, C., Wang, X., Yu, Q., Cui, H., 2010. The E-cadherin repressor slug and progression of human extrahepatic hilar cholangiocarcinoma. J. Exp. Clin. Cancer Res. 29, 88. https://doi.org/10.1186/1756-9966-29-88

Zhang, K.-J., Zhang, B.-Y., Zhang, K.-P., Tang, L.-M., Liu, S.-S., Zhu, D.-M., Zhang, D.-L., 2010. Clinicopathologic significance of slug expression in human intrahepatic cholangiocarcinoma. World Journal of Gastroenterology 16, 2554–2557. https://doi.org/10.3748/wjg.v16.i20.2554

Zhang, L., Zhou, F., ten Dijke, P., 2013. Signaling interplay between transforming growth factor-β receptor and PI3K/AKT pathways in cancer. Trends in Biochemical Sciences 38, 612–620. https://doi.org/10.1016/j.tibs.2013.10.001

Zhang, W., Yatskievych, T.A., Baker, R.K., Antin, P.B., 2004. Regulation of Hex gene expression and initial stages of avian hepatogenesis by Bmp and Fgf signaling. Developmental Biology 268, 312–326. https://doi.org/10.1016/j.ydbio.2004.01.019

Zhang, Y., Xie, Z.-Y., Guo, X.-T., Xiao, X.-H., Xiong, L.-X., 2019. Notch and breast cancer metastasis: Current knowledge, new sights and targeted therapy. Oncol Lett 18, 2743–2755. https://doi.org/10.3892/ol.2019.10653

Zhang, Y.E., 2017. Non-Smad Signaling Pathways of the TGF-β Family. Cold Spring Harb Perspect Biol 9. https://doi.org/10.1101/cshperspect.a022129

Zhao, R., Watt, A.J., Li, J., Luebke-Wheeler, J., Morrisey, E.E., Duncan, S.A., 2005. GATA6 is essential for embryonic development of the liver but dispensable for early heart formation. Mol. Cell. Biol. 25, 2622–2631. https://doi.org/10.1128/MCB.25.7.2622-2631.2005

Zhong, W., Dai, L., Liu, J., Zhou, S., 2018. Cholangiocarcinoma-associated genes identified by integrative analysis of gene expression data. Mol Med Rep 17, 5744–5753. https://doi.org/10.3892/mmr.2018.8594

Zhou, Q., Wang, Y., Peng, B., Liang, L., Li, J., 2013. The roles of Notch1 expression in the migration of intrahepatic cholangiocarcinoma. BMC Cancer 13, 244. https://doi.org/10.1186/1471-2407-13-244

Zong, Y., Panikkar, A., Xu, J., Antoniou, A., Raynaud, P., Lemaigre, F., Stanger, B.Z., 2009. Notch signaling controls liver development by regulating biliary differentiation. Development 136, 1727–1739. https://doi.org/10.1242/dev.029140

Zorn, A.M., Butler, K., Gurdon, J.B., 1999. Anterior endomesoderm specification in Xenopus by Wnt/beta-catenin and TGF-beta signalling pathways. Dev. Biol. 209, 282–297. https://doi.org/10.1006/dbio.1999.9257

ADDIN ZOTERO_BIBL {"uncited":[],"omitted":[],"custom":[]} CSL_BIBLIOGRAPHY

9. Appendices (Supplementary figures)

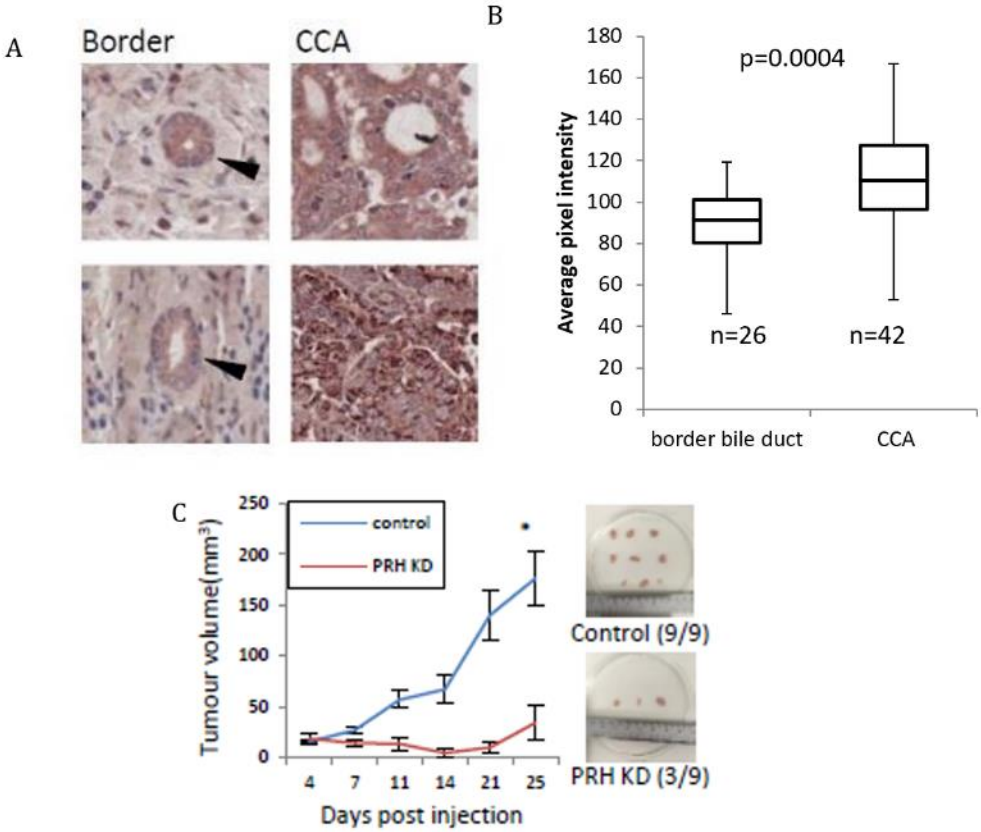

Figure S1 CCA tissues express high level of PRH. (A) Representative immunostaining of PRH in CCA tissue microarray using in-house polyclonal anti-PRH antibody. The arrows point to the biliary epithelial border tissue. (B) Quantification of the immunostaining by PRH antibody in CCA tissue compared to the border bile duct tissue by image J. (C) Tumour growth of CCLP control (34±17 mm^3) and PRH knockdown cells (176±27 mm^2) in nude mouse xenografts, n=9 per group, p=0.0006 at day 25.

Accession	Description	Score	Coverage	# Proteins	# Unique Peptides	# Peptides	# PSMs	# AAs	MW [kDa]	calc. pI
P04264	Keratin, type II cytoskeletal 1 OS=Homo sapiens GN=KRT1 PE=1 SV=6 - [K2C1_HUMAN]	14.96	8.54	1	3	3	4	644	66.0	8.12
P35527	Keratin, type I cytoskeletal 9 OS=Homo sapiens GN=KRT9 PE=1 SV=3 - [K1C9_HUMAN]	10.62	8.03	1	3	3	3	623	62.0	5.24
P02768	Serum albumin OS=Homo sapiens GN=ALB PE=1 SV=2 - [ALBU_HUMAN]	6.58	4.43	1	2	2	2	609	69.3	6.28
Q03014	Hematopoietically-expressed homeobox protein HHEX OS=Homo sapiens GN=HHEX PE=1 SV=1 - [HHEX_HUMAN]	6.46	9.26	1	2	2	2	270	30.0	7.24
P10809	60 kDa heat shock protein, mitochondrial OS=Homo sapiens GN=HSPD1 PE=1 SV=2 - [CH60_HUMAN]	3.26	4.36	1	1	1	1	573	61.0	5.87
P35908	Keratin, type II cytoskeletal 2 epidermal OS=Homo sapiens GN=KRT2 PE=1 SV=2 - [K22E_HUMAN]	2.95	1.88	1	1	1	1	639	65.4	8.00
P13645	Keratin, type I cytoskeletal 10 OS=Homo sapiens GN=KRT10 PE=1 SV=6 - [K1C10_HUMAN]	2.95	1.54	1	1	1	1	584	58.8	5.21
Q04695	Keratin, type I cytoskeletal 17 OS=Homo sapiens GN=KRT17 PE=1 SV=2 - [K1C17_HUMAN]	2.95	3.01	2	1	1	1	432	48.1	5.02

Accession	Description	Score	Coverage	# Proteins	# Unique Peptides	# Peptides	# PSMs	# AAs	MW [kDa]	calc. pI
P10809	60 kDa heat shock protein, mitochondrial OS=Homo sapiens GN=HSPD1 PE=1 SV=2 - [CH60_HUMAN]	17.64	6.46	1	2	2	7	573	61.0	5.87
P35527	Keratin, type I cytoskeletal 9 OS=Homo sapiens GN=KRT9 PE=1 SV=3 - [K1C9_HUMAN]	8.69	6.26	1	2	2	2	623	62.0	5.24
P04264	Keratin, type II cytoskeletal 1 OS=Homo sapiens GN=KRT1 PE=1 SV=6 - [K2C1_HUMAN]	4.70	4.81	1	1	1	1	644	66.0	8.12
P35908	Keratin, type II cytoskeletal 2 epidermal OS=Homo sapiens GN=KRT2 PE=1 SV=2 - [K22E_HUMAN]	3.63	1.88	1	1	1	1	639	65.4	8.00

Accession	Description	Score	Coverage	# Proteins	# Unique Peptides	# Peptides	# PSMs	# AAs	MW [kDa]	calc. pI
P35527	Keratin, type I cytoskeletal 9 OS=Homo sapiens GN=KRT9 PE=1 SV=3 - [K1C9_HUMAN]	8.70	6.26	1	2	2	2	623	62.0	5.24
P04264	Keratin, type II cytoskeletal 1 OS=Homo sapiens GN=KRT1 PE=1 SV=6 - [K2C1_HUMAN]	5.62	4.81	1	1	1	1	644	66.0	8.12
P02768	Serum albumin OS=Homo sapiens GN=ALB PE=1 SV=2 - [ALBU_HUMAN]	3.38	1.97	1	1	1	1	609	69.3	6.28
P35908	Keratin, type II cytoskeletal 2 epidermal OS=Homo sapiens GN=KRT2 PE=1 SV=2 - [K22E_HUMAN]	3.30	1.88	1	1	1	1	639	65.4	8.00

Figure S2 Mass spectrometry on Myc-PRH IP of CCLP. Mass spectrometry result on the corresponding gel band #1, band #3 and band #4.

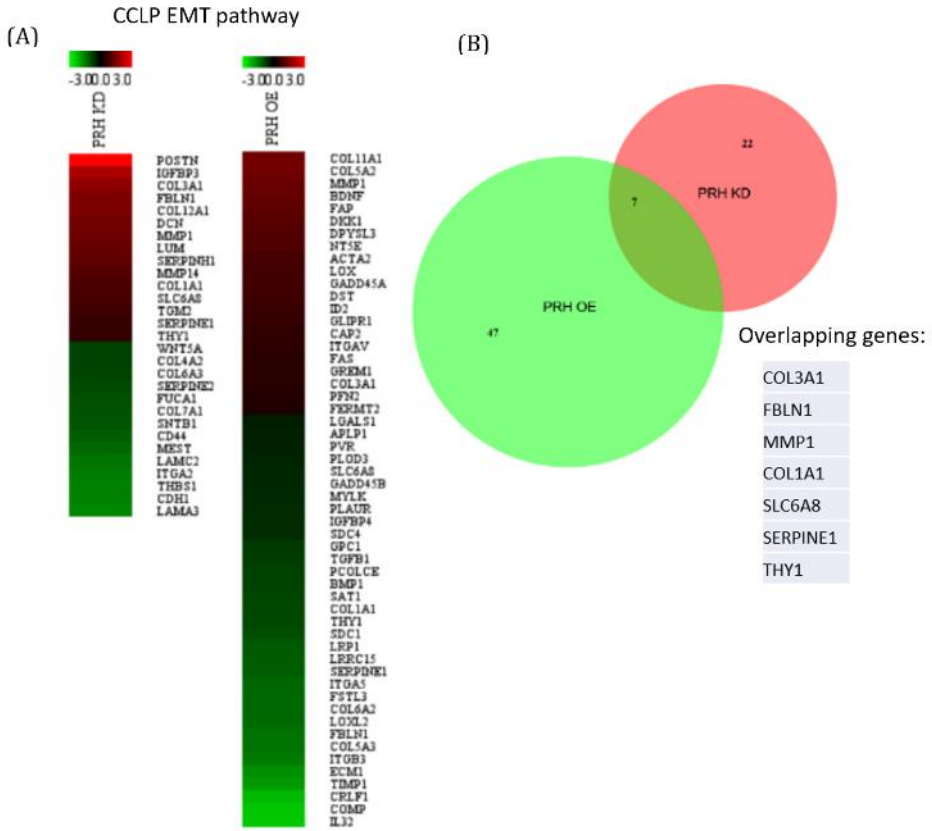

Figure S3 Differentially regulated EMT related genes by PRH in PRH KD and OE CCLP cells. (A) Heatmaps showing full list of EMT related DEGs in PRH KD and PRH OE CCLP cells (B) Venn diagram plotted using BioVenn software showing the overlapping EMT related DEGs between PRH KD and PRH OE CCLP cells.

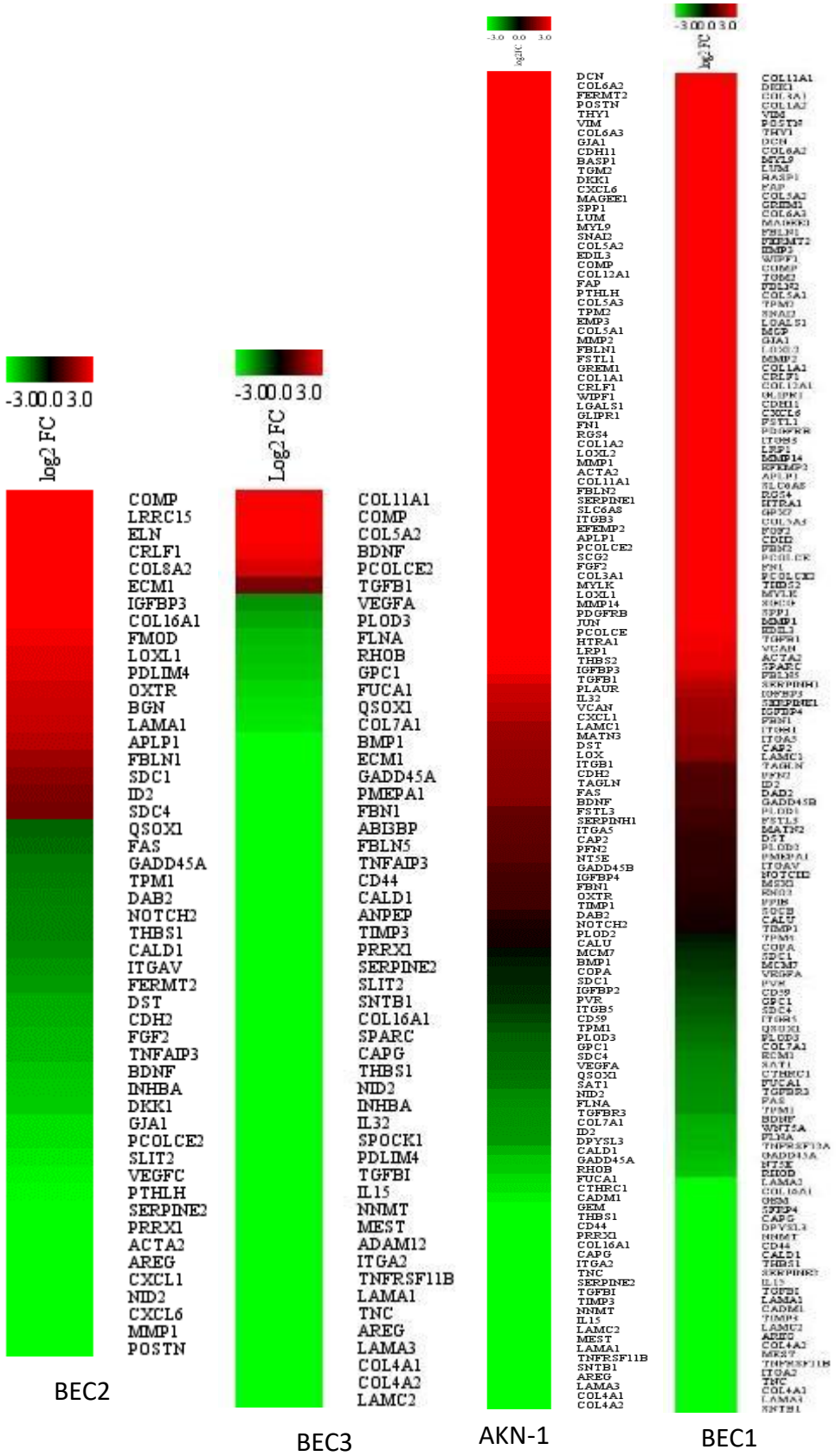

Figure S4 Differentially regulated EMT related genes by PRH in AdPRH overexpressed AKN-1 and BECs donors. Heatmaps showing full list of EMT related DEGs in AdPRH overexpressed AKN-1 and BECs from three donors.

(A)

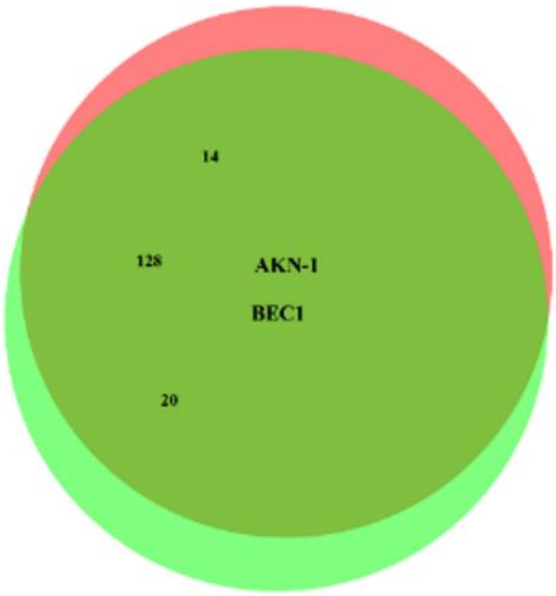

(B)

EMT Overlapping genes:

COL5A2	TIMP3	GJA1	SERPINE2	CTHRC1	CDH2
TPM2	LAMC2	TNC	COL4A2	VEGFA	DPYSL3
LGALS1	FAP	IGFBP3	CRLF1	DKK1	COL1A2
FN1	MYLK	COL5A1	TPM1	CALD1	THBS1
APLP1	LRP1	PLOD3	COL7A1	EDIL3	CALU
GLIPR1	CAPG	GADD45A	PFN2	COMP	PLOD2
TGFB1	MMP14	DCN	BASP1	TAGLN	COL11A1
EMP3	ID2	TGFBI	GPC1	HTRA1	SDC1
SNTB1	COL1A1	COL6A2	NT5E	LAMA1	FBN1
COL12A1	EFEMP2	COL6A3	MYL9	COPA	BDNF
TGM2	FLNA	VIM	FAS	COL5A3	DAB2
RHOB	PCOLCE2	SDC4	SERPINH1	RGS4	COL3A1
LAMA3	GEM	ITGB3	CDH11	PVR	MCM7
ACTA2	CADM1	MMP1	CD44	IGFBP4	
MEST	QSOX1	COL4A1	FSTL3	DST	
LAMC1	SAT1	CD59	TIMP1	IL15	
ITGB1	MMP2	FBLN1	MAGEE1	ITGA2	
SLC6A8	SNAI2	COL16A1	SPP1	NNMT	
FERMT2	POSTN	ITGA5	CXCL6	THBS2	
FGF2	PCOLCE	FSTL1	GADD45B	NOTCH2	
FUCA1	LUM	CAP2	AREG	VCAN	
THY1	TGFBR3	WIPF1	TNFRSF11B	GREM1	
LOXL2	PDGFRB	SERPINE1	ITGB5	FBLN2	

Figure S5 Common EMT pathway related DEGs from RNA-seq data for AKN-1 cells and BECs. (A) Venn diagram showing the EMT related DEGs in AKN-1 overlapping with BECs donor1. (B) The list of EMT related DEGs that are in common for AKN-1 and BECs.

(A)

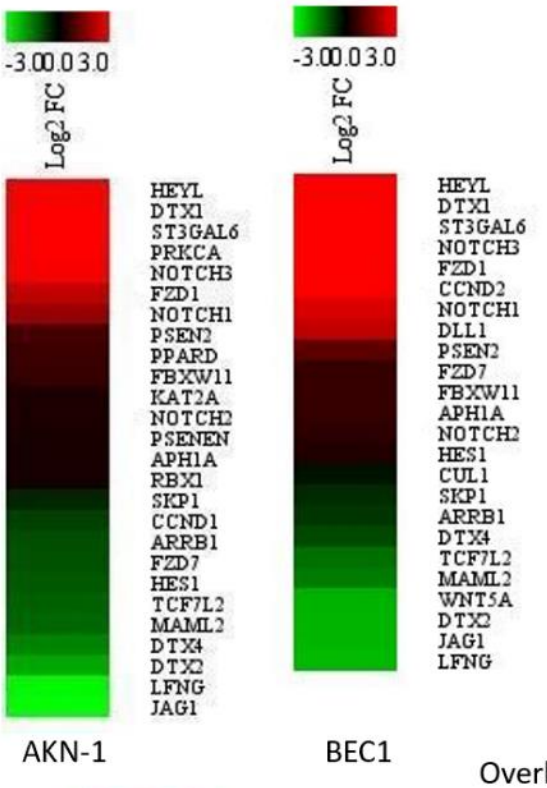

(B)

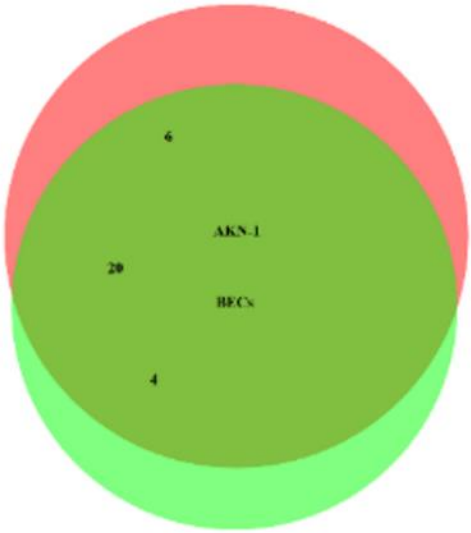

Overlapping genes:

HEYL
DTX1
ST3GAL6
NOTCH3
FZD1
NOTCH1
PSEN2
FBXW11
NOTCH2
APH1A
SKP1
ARRB1
FZD7
HES1
TCF7L2
MAML2
DTX4
DTX2
LFNG
JAG1

Figure S6 List of Notch related DEGs from RNA-seq in AKN-1 and BECs donor 1. (A) Heatmaps showing the DEGs in Notch pathway in AKN-1 and BECs donor1. (B) Venn diagram showing the common Notch related DEGs in AKN-1 and BECs donor 1.